METHODS FOR STRENGTHENING FLEXURAL STEEL DETAILS IN REINFORCED CONCRETE BRIDGE GIRDERS USING A NEAR-SURFACE MOUNTED RETROFITTING TECHNIQUE

DEANNA AMNEUS

M.S.

OREGON STATE UNIVERSITY

AN ABSTRACT OF THE THESIS OF

Deanna Amneus for the degree of Master of Science in Civil Engineering presented on August 22, 2014.

Title: Methods for Strengthening Flexural Steel Details in Reinforced Concrete Bridge Girders using a Near-Surface Mounted Retrofitting Technique.

Abstract approved: _____

Christopher C. Higgins

Many older reinforced concrete deck girder (RCDG) bridges contain straight bar terminations of flexural reinforcement. Common bridge design practice of the 1950s did not consider the additional demands on the terminated bars from shear and flexure. Moreover, more stringent code specifications and heavier permit trucks contribute to the insufficient ratings and presence of diagonal cracks in RCDG bridges. Replacement of these bridges is not economically feasible and thus strengthening methods are necessary.

The goal of this research was to investigate anchorage strengthening methods using full-scale vintage girder specimens. The specimens were constructed with a flexural anchorage

deficiency by terminating two flexural bars that extended only one-third of their development length past a 45° preformed diagonal crack.

A common flexural strengthening technique called near-surface mounting (NSM) was applied to T-specimens. Two metallic materials were selected for the NSM reinforcement: titanium and stainless steel. These materials were chosen because of their high strength, ductility, environmental durability, and ability to fabricate mechanical anchorages. This study found that the NSM strengthening technique with metallic materials increased the midspan displacement by at least 85%, and load capacity by at least 31% for each specimen. In addition, a case study was performed to simulate the positive moment anchorage strengthening of the Mosier Bridge in Oregon.

METHODS FOR STRENGTHENING FLEXURAL STEEL DETAILS IN REINFORCED CONCRETE BRIDGE GIRDERS USING A NEAR-SURFACE MOUNTED RETROFITTING TECHNIQUE

by
Deanna Amneus

A THESIS

submitted to

Oregon State University

in partial fulfillment of
the requirements for the
degree of

Master of Science

Presented August 22, 2014
Commencement June 2015

Master of Science thesis of Deanna Amneus presented on August 22, 2014

APPROVED:

Major Professor, representing Civil Engineering

Head of the School of Civil and Construction Engineering

Dean of the Graduate School

I understand that my thesis will become part of the permanent collection of Oregon State University libraries. My signature below authorizes release of my thesis to any reader upon request.

Deanna Amneus, Author

ACKNOWLEDGEMENTS

I would like to thank Dr. Christopher Higgins for his guidance in and out of country throughout this project. His patience, knowledge, and wisdom are what led to the success of this project.

I would like to thank the Oregon Department of Transportation for their funding, support, and genuine interest of this project.

I am appreciative of the feedback provided by my committee members Dr. Tucker, Dr. Miller, and Dr. Ideker.

Undergraduate research assistants Kyle England, Brandon Zaikoski, and Caleb Lennon were integral in the laboratory construction of the specimens. I thank them for their enthusiasm throughout this process.

I would like to acknowledge the support of my friends and family who encouraged me throughout this program.

Lastly, I would like to sincerely thank my research partner Laura Barker. She has challenged, encouraged, and walked along side me throughout my graduate program.

TABLE OF CONTENTS

TABLE OF CONTENTS (Continued)

Page

TABLE OF CONTENTS (Continued)

Page

TABLE OF CONTENTS (Continued)

Page

LIST OF FIGURES

Figure Page

LIST OF FIGURES (Continued)

Figure Page

LIST OF FIGURES (Continued)

Figure Page

LIST OF FIGURES (Continued)

Figure Page

LIST OF FIGURES (Continued)

Figure Page

LIST OF FIGURES (Continued)

Figure Page

LIST OF TABLES

Table Page

LIST OF TABLES (Continued)

Table Page

LIST OF APPENDICES

Page

METHODS FOR STRENGTHENING FLEXURAL STEEL DETAILS IN REINFORCED CONCRETE BRIDGE GIRDERS USING A NEAR-SURFACE MOUNTED RETROFITTING TECHNIQUE

1 INTRODUCTION

The Federal-Aid Highway Acts of the 1950s expanded the interstate highway system. As a part of this program, hundreds of conventional reinforced concrete deck girder (RCDG) bridges were designed and constructed. Common bridge design practices of the 1950s did not consider the demands from both shear and flexure on anchorages. Furthermore, proprietary bars used before the 1950s often required the use of hooked and extended terminations to account for variability in surface deformations. After the advent of the standardized deformations on reinforcing steel in the 1950s, designers detailed straight-bar terminations of flexural steel where they were no longer required by calculation. Present day design specifications extend terminations past the theoretical cutoff location and consider the increased tension on flexural steel from shear across a diagonal crack. Currently, inspectors have noted diagonal cracks in many RCDG bridges which place higher demands on the flexural steel. Today, many vintage RCDGs exhibit insufficient ratings due to inadequate anchorage details. Replacements of these deficient bridges are not economically feasible and thus strengthening methods are necessary.

There is limited information available on anchorage failures in RCDG T girders except for those tested in the early 2000s at Oregon State University. These specimens were designed to investigate diagonal cracking with fully anchored bars (Higgins *et al*., 2004). A second study was conducted on full-scale specimens with a preformed diagonal crack adjacent to an inadequate anchorage detail (Triska, 2010). After characterizing behavior of inadequate details, the need to develop strengthening methods was realized.

The goal of this research was to investigate anchorage strengthening methods on full-scale RCDG girder specimens with vintage details. The T-specimens were constructed, instrumented, and tested similar to the previous studies at Oregon State University. These T-specimens were 26 ft (7.92 m) long and 48 in. (1219 mm) tall with a 36 in. (914 mm) wide flange and 14 in. (356 mm) wide web. Two of the five flexural bars had straight-bar terminations in the flexural tension zone.

A common flexural strengthening technique called near-surface mounting (NSM) was used. Typically, this technique consists of epoxying a carbon fiber reinforced polymer (CFRP) rod in a groove cut into the concrete cover. Instead, the present work proposed two metallic materials selected for the NSM reinforcement: titanium and stainless steel. These materials were chosen because of their high strength, ductility, environmental durability, and ability to fabricate mechanical anchorages.

In this research, the following tasks were performed: 1) A review of the literature was conducted. 2) Laboratory tests of the retrofitted T-specimens were performed with instrumentation at critical sections to enable evaluation of strength and behavior. 3) Analytical prediction methods were compared to experimental values. 4) A case study on an existing bridge was performed. The strengthening techniques successfully increased the capacity of the specimen, leading directly a field application. Ultimately, this retrofitting technique could help maintain and improve the operational safety and mobility of the transportation system.

2 BACKGROUND

This chapter surveys archival literature on anchorage and bond stress in steel reinforcing and fiber reinforced polymer (FRP) bars. First, a generalized bond stress equation has been derived. Then, a review of the literature has been performed summarizing literature describing the behavior of steel reinforcing bars in concrete. Next, a review of NSM bars in epoxy has been summarized. Lastly, changes in code specifications are explained with correlations to the literature.

2.1 Anchorage Concerns

Adequate anchorage is essential to obtain the full strength of a reinforcing steel bar embedded in concrete. Bridge designers prior to the 1950s commonly detailed hooked bar terminations to ensure adequate anchorage on proprietary reinforcing steel bars. This practice of ceased after experimental testing on standardized deformations on reinforcing bars indicated an greatly improved bond strength. Over the past 66 years, designers and scholars have found that straight bar terminations in the flexural tension zone can result in cracking and premature loss of anchorage. Evidence of these early terminations can be seen from web cracking in vintage RCDG bridges.

Originally, to attain adequate anchorage of reinforcing steel, designers limited bond stress. Bond stress, μ, is the stress transferred between the reinforcing bar and the concrete and must account for the change in tension along the bar as illustrated Fig. 2.1.

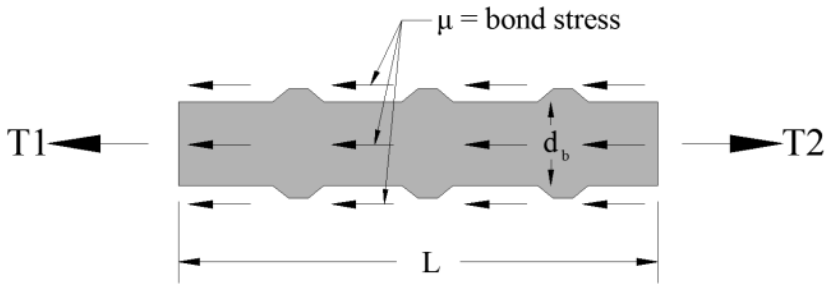

Fig. 2.1-Bond stress in bar

Bond stress is a function of the surface area and the length of bar embedded. Actual bond stress is variable over the length of the bar so μ, is typically specified as μ_{avg}. The bond stress of a bar is computed as:

$$\mu_{avg} = \frac{\Delta f_s d_b}{4L} \quad [2.1]$$

where Δf_s is the change in stress over the segment, d_b is the nominal bar diameter, and L is the embedded length.

To design for bond stress in a full-scale beam, early literature depended on basic beam mechanics. The average bond stress in the flexural steel is found by dividing the applied shear by the area of steel multiplied by the lever arm as:

$$\mu_{avg} = \frac{V}{jd\Sigma o} \quad [2.2]$$

where V is the applied shear, jd is the effective distance from the centroids of the compression and tension zones, and Σo is the perimeter of the bar. This approach is reflected in early design specifications when detailing anchorages.

More modern research has found there are additional factors that exacerbate anchorage demands in flexural tension zones. The presence of a diagonal crack in a section with shear and flexure can place additional demands on the tension steel, as illustrated in Fig. 2.2.

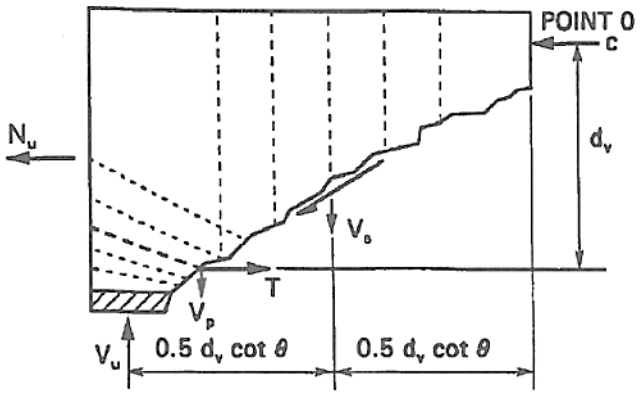

Fig. 2.2 - Internal forces at a diagonally cracked section (AASHTO LRFD, 2007)

If summed about Point 0, the tensile demand, *T*, is expressed in English units as:

$$T = \frac{M_u}{d_v} + 0.5N_u + \left(V_u - 0.5V_s - V_p\right) * cot\theta \qquad \text{AASHTO Eq. 5.8.3.5-1 [2.3]}$$

where M_u is the factored moment demand taken where the crack crosses the flexural steel, d_v is the distance from the center of the compression block to the centroid of steel, N_u is the applied factored axial force, V_u is the applied factored shear demand, V_s is the shear resistance provided by the transverse reinforcement, V_p is the shear carried by the prestressing strands, and θ is the crack angle. For conventionally reinforced beams, N_u and V_p are not applicable. If a diagonal crack propagates in the region where the reinforcing steel bar is not fully developed, the additional demands could produce an anchorage failure.

Anchorage failures fall into two categories: slipping and splitting failures. Slipping anchorage failures usually occur if there is transverse reinforcement present to confine the flexural reinforcing steel and prevent concrete splitting. Once the bar initiates slip, the deformations of the bar are engage and crush the concrete locally. The bar slowly slips through the concrete, creating a ductile response (Triska, 2010). Splitting anchorage failures occur when the reinforcing bar deformations engage the concrete and create radial stresses. These stresses create cracks and split the surrounding concrete. This less ductile response commonly happens in the flanges with negative moment bending, or where there are not sufficient stirrups crossing the splitting plane (Triska, 2010).

2.2 Literature Review

A literature review was conducted to form an understanding of anchorage failures of bars embedded in concrete and epoxy. Research on reinforced concrete bond and anchorage is available dating from the early 1950s to the present. However, the majority of near-surface mounted (NSM) fiber reinforced polymer (FRP) literature was written in the last 14 years.

2.2.1 Steel Reinforcing Bar Bond Stress

Mylrea (1948) summarized the body of knowledge on bond stress and bar anchorage up to 1948. Generally, the pull-out test was accepted as the most common way to establish bond properties. Throughout the research, it was concluded that pull-out tests provide higher bond stresses than were apparent in a full-scale beam. It was established that bond stress is not uniformly distributed over the bar and increases non-linearly with movement of the bar. Furthermore, the largest bond stress achieved in beam tests is always prior to the first slip. After initial concrete crushing or slipping, it is easier to propagate cracks and create

more bar slip. Bond stress from plain bars in pull-out tests ranged from 200-400 psi (1.38-2.76MPa).

Clark (1949) investigated the bond stresses in several proprietary bars in reinforced concrete. The study proposed a new larger deformation pattern on reinforcing steel that was used in the experimental tests. The experiment used scaled beam tests with varying embedment length, bar type, and depth. The beam end specimens were 8 x 8 x 78 in. (0.2 x 0.2 x 1.98 m) concrete prisms with various reinforcement lengths and depths. The beam specimens had a loading point directly over the termination of the bar cutoff. The specimens failed by bond slippage if the bar had a short embedment length, or by diagonal tension and bond failure with a longer embedment length. In general, the loaded end bars experienced larger slips at lower bond stresses; while the free ends experience a high bond stress before any significant slipping. Clark reported a mean average bond stress of 300-400 psi (2.07-2.76 MPa) for a #7 (22M) bar in the beam end test after slipping. The results confirmed that higher deformations on the reinforcing bar created a stronger bond. Furthermore, the specimens with the newly proposed deformation pattern achieved the greatest bond stress, thus contributing to the adoption of ASTM A305-47T into ACI 318.

Mains (1951) measured the distribution of bond stresses along reinforcing bars using a method that would not affect bond of the bar to concrete. The reinforcing bars of interest were cut in two sections and had strain gages placed inside a groove cut into the bar near the neutral axis. Several beam and pull-out specimens were tested with plain and deformed bars. Previous code requirements assumed even distribution of bond stress over the bar. Main's new technique had proved otherwise, and proved that calculated bond stress is

frequently less than measured bond stress. A straight embedment of deformed bars in pull-out specimens attained 770 psi (5.31 MPa) at the highest test load. Beam specimens with deformed bar straight terminations achieved bond stresses from 540-815 psi (3.72-5.62 MPa) at the highest test loads. All bars in the beam tests failed by fracture, not bond. Experimental tensile forces increased when subjected to combined shear and moment, thereby exceeding the calculated tensile demand. Evidence was presented that cracking in the beam increased the local stresses along the reinforcing bars. The presence of a crack will create a local maximum and minimum stress peak around the crack.

Ferguson and Breen (1965) considered lap splice length in a constant moment region. Tests were conducted on rectangular full scale beams with four bars of flexural reinforcement and no transverse reinforcement. A lap splice was embedded at length, *L*, at midspan under a constant moment region. Ferguson and Breen found that lap splices could be 5-6 in. (127-152 mm) apart and still be effective. Bond stress decreased as the splice length increased. The larger #11 (36M) bars had a greater bond stress than the #8 (25M) bars. The #11 (36M) bars had an average bond stress ranging from 350-475 psi (2.41-3.27 MPa) with increasing splice lengths. Specimens with stirrups increased the average bond stress to 560 psi (3.86 MPa). Other conclusions were that concrete strength did not significantly affect splitting failures, steel strains have little influence in reducing bond strength in a splice, and the presence of transverse steel increased the lap splice strengths.

Orangun *et al.* (1977) reevaluated previous data on development length and splices. An equation for determining development length was proposed based on a nonlinear regression of previous beam tests. A bond stress formula was calculated using tangential

forces from the longitudinal bond stress and radial forces from deformations on the bar. However, since the angle of the radial stress is difficult to quantify, an empirical method to determine development length was used. Based on previous data, the proposed development length equation reflects the length, cover, spacing, bar diameter, and transverse reinforcement.

$$l_d = \frac{10200 d_b}{\sqrt{f'_c}\left(1 + \frac{2.5C}{d_b} + K_{tr}\right)} \quad [2.4]$$

where d_b is the bar diameter, f'_c is the compressive strength of concrete in psi, C is the lesser of the clear cover or half the clear spacing, and K_{tr} is as follows:

$$K_{tr} = \frac{A_{tr} f_{yt}}{600 s d_b} \leq 2.5 \quad [2.5]$$

where A_{tr} is the area of transverse reinforcement, f_{yt} is the yield strength of stirrups, and s is the stirrup spacing. All units are in English and f'_c is in psi. This equation accounted for stress transfer between reinforcing bars in concrete. Furthermore, Orangun *et al.* concluded that for the same bar diameter, clear spacing, cover and concrete strength the values for development length and lap splice length were interchangeable. Furthermore, the new equation required an increase of anchorage length from 10-25% from current ACI 318-71 provisions (Orangun, 1977). However, the presence of transverse reinforcement may reduce the anchorage lengths.

Darwin (1996) tested a large array of splice and development length specimens investigating the influence of transverse reinforcement, concrete strength, and rib area. Similar to previous studies, Darwin found that the development length and bond forces are linear, but not proportional. To accurately calculate bond, the number and size of

transverse reinforcing bars present over the developing length should be used. Larger relative rib areas on steel may decrease development and splice lengths. It was also found that reducing the contribution from concrete strength would more accurately represent bond stress. Furthermore, variability in splice and development length design calculations implies that the code safety factors may need to be altered. The expression formulated for the steel reinforcing bar development length incorporated a reliability-based strength reduction factor:

$$\frac{l_d}{d_b} = \frac{\frac{f_y}{f'^{1/4}_c} - 1900}{72\left(\frac{c + K_{tr}}{d_b}\right)} \quad [2.6]$$

where the variables are defined previously. This equation is a simplification of the proposed detailed design equation. A ϕ factor of 0.9 is incorporated as well as simplifying a cover ratio to 1.

McLean and Smith (1997) investigated non-contact lap splices in panels and column shaft connections. Two dimensional and three dimensional models were used to predict behavior of the specimens respectively. McLean and Smith performed experimental tests on near full-scale panel specimens and on 1/4-scale column-shaft specimens under monotonic and cyclic loading. The offset splice spacing in the panels ranged from 6-15 in. (152-381 mm). Three preliminary specimens did not have transverse reinforcement. A discrepancy in the relation of bond stresses and non-contact lap splices arose from using either an effective lap length or an overall lap length. The proposed overall splice length is composed of the effective length plus the length added from the bar spacing and crack angle. All the preliminary specimens without transverse reinforcement failed as a result of tension

cracking of the concrete perpendicular to the spliced bars. The failure loads were only 40-60% of the bar yielding force. The greater the offset spacing, the greater the amount and extent of cracking occurred in the tests. A strut and tie methodology could be used for design: the transverse reinforcement acts as a tie and the concrete compression strut acts between diagonal cracks between bars. After testing, McLean and Smith recommended the use of the longer embedment length and to use the less conservative splice length if splicing two different bars.

Darwin (2005) surveyed current design provisions and compared experimental data to calculated results. Because of high variability in bond stress, Darwin recommended that an adequate splice length be recommended instead of a maximum bond stress. Furthermore, yielding of the steel reinforcing bar did not significantly affect bond strength. Darwin confirmed bond strength is a function of several factors: the development length, the side and bottom cover, spacing of the reinforcing bar, transverse reinforcement, the top bar factor, the bar surface condition, and the concrete strength. Development and splice length were compared in the following codes: AASHTO, ACI 318, ACI Committee 408, CEB-FIB Model Code 1990, and Eurocode 2. Of those codes, Darwin found that ACI 408 provided the best match with test results for both developed and spliced bars. The ACI 408 equation for development length was derived from work by Zuo & Darwin (1998) as:

$$l_d = \frac{\left(\frac{f_y}{{f'_c}^{1/4}} - 48\omega\right)\alpha\beta\lambda}{1.5\left(\frac{c\omega + K_{tr}}{d_b}\right)} d_b \qquad [2.7]$$

where $c=c_{min}+0.5d_b$, $\omega=0.1(c_{max}/c_{min})+0.9\leq 1.25$, c_{max} and c_{min} are the maximum and minimum of c_b (the bottom cover) and c_s (the side cover). α, β, and λ are terms for excess reinforcement.

Triska (2010) constructed and tested four full scale vintage T beam specimens. The specimens reflected previous work simulating vintage RCDG details performed by Higgins (2004). The typical specimen was 26 ft (7.92 m) long, with a 14 x 42 in. (356 x 1067 mm) web, and a 6 x 36 in. (152 x 914 mm) thick deck. Vintage concrete mixtures with strengths around 3300 psi (22.75 MPa) were used. Lower-strength shear reinforcing bars were used to simulate in-situ bridge strength. The specimens had three or four #11 (36M) bars with a built in anchorage deficiency. Two flexural steel reinforcing bars were terminated one-third of the specified development length past a preformed diagonal crack to simulate an anchorage deficiency. The angle of the preformed diagonal crack varied from 0, 45, and 60 degrees. Reinforcing bar strain and cutoff bar slip was monitored to verify the design and analysis. All specimens failed in shear-tension due to anchorage slip of the cutoff bar. Stirrups confined the cutoff bar and creating a ductile slipping anchorage failure. The average cutoff bar bond stress was 851 psi (5.87 MPa). Average bond stress for the anchored bars was 284 psi (1.96 MPa). All bond stress values were measured from the intersection of the preformed crack to the end of the cutoff bar. Triska determined that the AASHTO LRFD specifications for tensile demand are adequate at failure. The preformed diagonal crack did not dictate the failure crack and may not significantly weaken the structure at service loads. Lastly, chevron crack were found to propagate along the cutoff bar close to failure.

2.2.1.1 Summary of Bond Stresses in Concrete

To measure bond stress, early research often relied on beam mechanics to find the forces in the tension bars described in Eq. [1.2]. In addition, reinforcing steel bar ends were left exposed to measure slip, which occasionally influenced bond at the termination of the reinforcing steel. Prior to 1948, bond stress was assumed to be uniformly distributed along the length of the bar. Mylrea established that bond stresses are non-uniform and increase non-linearly with slip. Furthermore, bond strengths from pull-out tests are not representative of actual strengths in larger scale beam tests. To improve upon bond measurement techniques, Main instrumented the inside of the steel reinforcing bar and monitored the strains while testing. Ferguson, Breen, and Orangun defined the influence of stirrups more thoroughly and confirmed that development length and lap splice length can be interchangeable. Darwin determined that several code specified development length values are non-conservative and proposed a new equation for l_d. In 2005, Darwin recommended a prescriptive splice length instead of limiting the stresses in the bars. After surveying current codes, Darwin also determined that ACI 408 provided the most accurate development lengths. Tests conducted by Triska (2010) will be in direct comparison to the current testing regime. Specimen geometry and instrumentation will reflect Triska's T-specimens. Table 2.1 below summarizes the relevant bond stresses from the literature.

Table 2.1 -Summary of bond stress in steel reinforcing bars from literature

Author	Bar Type	Bar Diameter (in) [mm]	Bar Embedment (in) [mm]	Test Type	Average Bond Stress (psi) [MPa]
Mylrea	Plain Bar	1.00 [25.4]	10 [254]	Pull-out	400 [2.76]
Clark	Deformed Proprietary	0.875 [22.2]	8 – 16 [203-406]	Beam End	300 – 400 [2.07-2.76]
Mains	Deformed	0.875 [22.2]	21 [533]	Pull-out	770 [5.31]
	Deformed	0.875 [22.2]	78 [1981]	Beam	540 – 815 [3.72-5.62]
Ferguson	Deformed	1.41 [35.8]	Fully Anchored	Beam	560 [3.86]
	Deformed	1.41 [35.8]	30 – 80 [762-2032]	Beam	350 - 475 [2.41-3.27]
Triska	Deformed	1.41 [35.8]	Fully Anchored	T Beam	284 [1.96]
	Deformed	1.41 [35.8]	Cutoff 1/3 ld	T Beam	851 [5.87]

2.2.2 Near-surface mounting technique review

The near-surface mounting technique of retrofitting has emerged as a potential solution for strengthening infrastructure in the past three decades. A literature review was conducted to briefly identify trends in testing, analysis, and design. The purpose, testing methodology, and conclusions are summarized. Specific data are listed if the literature included relevant bond stress or load deformation responses. The development of code specifications can be seen in the gradual presentation of analytical methods. Articles commonly focused on carbon fiber reinforced polymer (CFRP) reinforcement and short bond lengths.

Rizkalla et al. (2003) wrote an overview of the history, properties, and use of FRP in strengthening concrete structures. FRP emerged in the mid-1950s but did not become a commercially recognized material until the late 1970s. Mechanical properties are dependent on the resin modulus, failure strain in the fiber, and the bond between the resin and fiber. Currently, ASTM D3039-08 is used for tensile testing of polymer matrix composite materials. In many cases, serviceability criteria, fatigue, and creep rupture endurance limits may control the design because of its linear elastic behavior and tendency for sudden failures. Specifically, near-surface mounted FRP systems can strengthen regions where external reinforcement would be subject to damage. In addition, the NSM rods have shown a greater anchoring capacity compared to the surface bonded FRP. Failure modes of NSM strips include epoxy split failure (can be avoided with increasing epoxy thickness), or concrete split failure where the tensile strength of the epoxy exceeds the concrete (widening the groove can minimize the induced tensile stresses).

De Lorenzis *et al.* (2000) discussed the advantages and bond strength of NSM FRP strengthening in concrete. Direct pull-out and a beam pull-out tests were used to measure bond stress in the FRP material. The experimental variables included the bonded length, diameter of rod, type of material (glass fiber reinforced polymer (GRFP) or CFRP), surface configuration, and size of groove. In general, deformed CFRP bars appeared to be more efficient and achieved higher bond strengths. Furthermore, increasing the groove size led to higher bond strength and decreased the failure by splitting of the epoxy cover. Ultimate load increased with an increased embedded length; however, the average bond strength was decreased as the bonded length increased, similar to reinforcing bar concrete bond stress behavior. A #4 (13M) CFRP bar embedded 6 in. (152.4 mm) had an average bond

strength of 1078 psi (7.43 MPa). With a 12 in. (304.8 mm) embedment, the #4 (13M) CFRP bar had an average bond strength of 620 psi (4.27 MPa). Several large scale T-specimens were cast and retrofit with FRP. The specimens had two # 7 (22M) bars as flexural reinforcement and were tested with four point bending. The NSM retrofit consisted of two #4 (13M) CFRP bars and increased the capacity of the baseline specimen by 44.3%. The baseline specimen had a capacity of 35.2 kips (157 kN) with a deflection of approximately 1.6 in. (40.6 mm). The strengthened specimen had a capacity of 50.79 kips (226 kN) with a deflection of approximately 1.1 in. (27.9 mm). The retrofitted beam had a much stiffer load displacement response and decreased the ductility from the control specimen.

After prior studies, De Lorenzis and Nanni (2001) discussed a design procedure for flexural and shear strengthening of reinforced concrete beams with NSM FRP reinforcement. The proposed design procedure for flexure consisted of obtaining the local bond strength of NSM bars from literature or bond tests, u_f, computing the minimum stabilized crack spacing, l_{min}, computing the delamination stress, $\sigma_{fdelmax}$, computing the nominal ultimate moment using conventional reinforced concrete theory, and finally computing the design ultimate moment by applying reduction factors. A critical component in this design is the delamination stress where σ_{fdel} is equal to:

$$\sigma_{fdel} = \frac{2bL_p l}{3n\pi d_b^2 h'} f_{ct} \qquad [2.8]$$

where b is the width of the beam, L_p is the effective length of the NSM bars in the shear span, l is the crack spacing, n is the number of NSM bars, d_b is the bar diameter, h' is the distance from the top of the section to the centroid of NSM, and f_{ct} is the concrete tensile

strength. This equation would govern the available tensile stress for strengthening. However, this equation was not incorporated into the code, and a different empirical equation for delamination strain was used. De Lorenzis also proposed a development length equation calculated based on minimum crack distances in the concrete, l_{min}. The minimum crack distance is based on the area of concrete in tension, the concrete tensile strength, and bond strength between the concrete-reinforcing bar interface and the NSM bar-epoxy interface. This method is similar to techniques described by McLean for bars in concrete but was not adopted into the ACI 440 code.

De Lorenzis (2002) investigated modified pull-out or bond tests for NSM FRP rods. Failure modes of the pull-out tests are often governed by the distance from the concrete edge and the short bonded length. Since these behaviors may not occur in full-scale specimens, a modified approach was necessary. The test specimens were "C" shaped concrete blocks with a pre-formed groove for the FRP. The variables tested were the groove filling material, groove size, and rod surface (sandblasted, spirally wound, and ribbed). The epoxy-concrete was the critical interface. A #4 (13M) spirally wound CFRP bar embedded in epoxy a length of four times the bar diameter had an average bond strength of 1637 psi (11.29 MPa). The average bond strength at the epoxy-concrete interface τ_{av1u} was expressed as:

$$\tau_{av1u} = \frac{P_{max}}{3 d_g l_b} \quad [2.9]$$

where P_{max} is the ultimate load, d_g is the groove size, and l_b is the bonded length. De Lorenzis used Eq. [2.9], obtained peak stresses, and used a Bertero-Popov-Eligehausen (BPE) relationship to fit the experimental data. From this, De Lorenzis determined a

generalized bond stress relationship between concrete-epoxy and epoxy-bar interfaces. However, this method must be calibrated using experimental results before being used to develop the required embedment length. Other conclusions recommend saw cutting of grooves, and observing that the average bond stress decreases as the groove size and embedment length increases.

Hassan (2003) conducted an experimental study of the bond of NSM FRP strips. Small scale T-specimens were constructed and designed to fail in flexure. Each beam was strengthened with one 0.05 x 1.97 in. (1.2 x 50 mm) strip of CFRP that extended varying lengths from 5.9 in. to 47.2 in. (150 mm to 1,200 mm) on each side of midspan. The specimens were tested with 3 point loading and a significant strength increase was associated with embedment lengths over 5.9 in. (150 mm). However, debonding was prevalent until the embedment lengths reached 33.5 in. (850mm). This indicates the full composite action was not developed due to anchorage concerns. The control specimen had a capacity of 11.7 kip (52 kN) and a deflection of approximately 2.56 in. (65 mm). The shortest fully composite beam used a 33.5 in. (850 mm) development length and reached a load of 17.6 kip (79 kN) with approximately 1.1 in. (28 mm) of deflection. The NSM retrofit response was much stiffer and increased the baseline capacity by 52% but decreased the deformation capacity by 57%. Furthermore, Hassan found that the load required to debond the NSM FRM material generally increased with embedment length, concrete strength, and groove width. Lastly, greater internal reinforcing steel ratios increased the required development length by shifting the neutral axis and increasing load required to debond the NSM FRP.

De Lorenzis (2004) continued research on developing an anchorage length for NSM FRP based on analytical modeling. An analytical model was calibrated to experimental results and used to compute the bond failure load as a function of the anchorage length. Primarily, short bond lengths were used. The service level anchorage length at is determined by l_m, the embedment length at which the bar does not slip. This equation was described in previous work by De Lorenzis (2002) and calculated as:

$$l_m = \sqrt{\frac{2 * s_m}{\chi * \tau_m} * \frac{(1+\alpha)}{(1-\alpha)^2}} \quad [2.10]$$

where α is the parameter influencing the shape of the ascending branch of the bond slip curve and is calculated by the area under curve until the peak bond stress, τ_m. s_m is the slip at peak bond stress. The cross section parameter, χ, is calculated for the rod–epoxy interface and epoxy-concrete respectively as:

$$\chi = \frac{4}{E_b * d_b} \quad or \quad \chi = \frac{3d_g}{E_e * A_{om}} \quad [2.11]$$

where E_b and E_e are the elastic moduli of bar and groove filler respectively. A_{om} is the cross-sectional area of the groove-filling constituents, and d_b and d_g are the diameter of the bar and depth of the square groove. Using this analytical approach, the experimental results agreed with the predicted development length and maximum load.

Novidis (2008) summarized the results of 45 short-anchorage eccentric pull-out concrete specimens with NSM FRP. The study investigated the size and surface roughness of the groove, the embedment length, the surface finish of the bars, and isolated the pull-out section with vertical foam sheets. The foam sheet pull-out specimen, called the novel specimen, avoided axial compression in the concrete surrounding the bar. The anchorage

lengths ranged from 3, 4, and 10 bar diameters from the top of the block. A 0.47 in. (12 mm) diameter CFRP bar was embedded 10 bar diameters and failed at the concrete epoxy interface achieving a bond strength of 654 psi (4.51 MPa). In general, the capacity increased with the length of embedment, but the bond stress decreases after a critical value. The bar stiffness and deformation pattern played a significant role in determining the amount of bond that may be mobilized in the NSM setup.

Bournas and Triantafillou (2009) presented results of a large scale program focusing on the flexural strengthening of columns with several NSM techniques and materials. While this study focused on columns, a majority of the experimental results could be applicable to beams. The specimens were strengthened with CFRP strips, GFRP bars, and stainless steel bars. Specimens with less internal (or existing) steel reinforcement experienced larger strength increases with the application of the NSM CFRP material. The addition of CFRP strips to a constant internal reinforcing steel ratio also almost linearly increased the strength of the column. The NSM reinforcement selection was based on equal tensile strength. The stainless steel NSM strengthened column was significantly stiffer than the other NSM strengthened columns. All specimens failed in flexure, as per design calculations. Buckling of the longitudinal reinforcing steel bars always occurred immediately after the failure of the NSM reinforcement. Load cycling may indicate a detrimental effect on the tensile strength of CFRP. Partial debonding reduced the lateral restraint of the NSM materials and made the NSM materials more vulnerable to compressive stresses. Overall, strengthening with the stainless steel NSM bars resulted in a substantial increase in stiffness and dissipated energy. In this application, stainless steel and GFRP outperformed CFRP by 25%. An average bond stress along the bonded length

was found for most specimens. The specimen with CFRP strips had an average bond stress of 590 psi (4.07 MPa), while the stainless steel NSM had an average bond stress of 873 psi (6.02 MPa) along the instrumented length.

Al-Mahmoud *et al.* (2009) considered the global behavior of several reinforced concrete beam specimens with CFRP NSM retrofitting techniques. The experimental variables include the concrete strength, embedment length, bond materials, and CFRP diameter. The specimens were 118 in. (3 m) long beam with a 59 x 110 in. (150 x 280 cm) cross section. They were retrofit with one or two CFRP rods. The specimen was tested with a monotonic increasing four point load. The control specimen had two 0.47 in. (12 mm) diameter steel reinforcing bars as flexural reinforcement. The moment capacity of the control specimen was approximately 19.9 kip-ft (27 kN-m), with 2.36 in. (60 mm) of deflection. The specimen retrofitted with one 0.47 in. (12 mm) diameter CFRP bar with 4.4 ksi (30 MPa) concrete strength demonstrated a 126% increase in capacity. The strengthened specimen achieved an ultimate capacity of 48.2 kip-ft (65.4 kN-m) with 1.73 in. (44 mm) of deflection. The CFRP diameter greatly influenced the strength and stiffness of the beam. The specimens with one 0.47 in. (12 mm) diameter bar (instead of two bars) increased the stiffness of the beam which encouraged the displacement of the reinforcing steel yielding threshold. The ultimate loads of the specimens with the 0.47 in. (12 mm) diameter NSM CFRP bar were higher than those with the 0.24 in. (6 mm) specimen with a similar failure mechanism. Furthermore, Al-Mahmoud concluded that concrete strength does not influence the load-carrying capacity of the strengthened beam when failure occurs by the NSM system failure. Fig. 2.3 shows the capacity and ductility of the specimens in tested by Al-Mahmoud strengthened with CFRP rods.

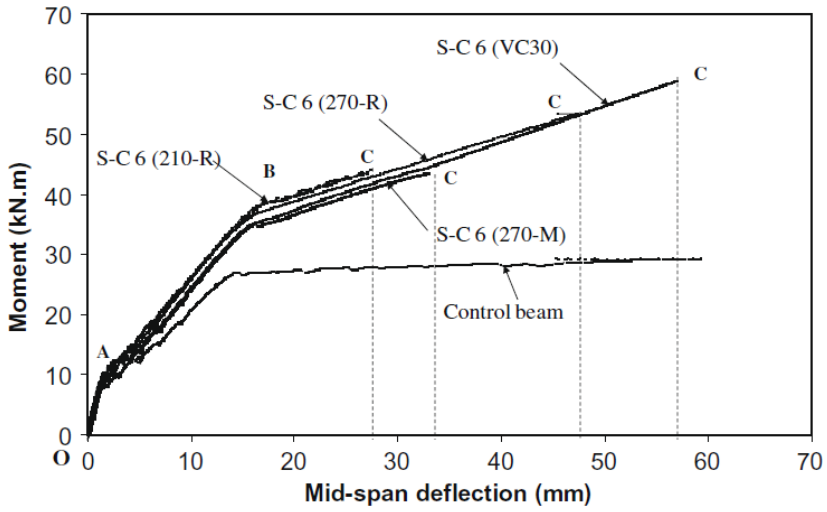

Fig. 2.3 - Midspan moment and deflection for CFRP strengthened specimen (Al-Mahmoud et al., 2009

Al-Mahmoud *et al.* (2010) investigated the anchorage and tension-stiffening effect between NSM CFRP and concrete. A pull-out test and direct tension member test was performed with varying concrete strengths, groove dimensions, and bond materials. The pull-out and tension member specimens were concrete blocks with dimensions of 19.7 in. (500 mm) in length with a 3.93 x 3.93 in. (100 x 100 mm) cross section. Both used a 0.47 in. (12 mm) diameter sand coated CFRP rod embedded 2.36 in. (60 mm). The pull-out specimen was contained in a steel box to minimize loading eccentricity. These tests determined an optimal groove width to rod diameter ratio between 1.7- 2.5. The maximum load for the pull-out test with resin was 7.78 kip (34.6 kN). The direct tension test embedded the NSM CFRP fully along the length and applied a load at each end. This test found that the active bond length was less than 3.93 in. (100 mm) (before the first gage) because the strains at each location were equal until cracking.

2.2.2.1 Near-surface mounted technique summary

Strengthening with near-surface mounted materials has undergone much critique. The CFRP reinforcing material was the subject of several studies to investigate retrofitting techniques with the high strength corrosion resistant material. The NSM CFRP strengthening typically fails by debonding of the epoxy-concrete or the epoxy-bar interface. Often, NSM CFRP strengthening is limited by service level loads, anchorage, fatigue, and creep parameters. De Lorenzis used a modified approach to pull-out tests to decrease the impact of axial and compression forces. Saw-cutting grooves were also recommended by De Lorenzis to most accurately model the concrete-epoxy interface. And, similar to bond of steel reinforcing bars in concrete, the average bond stress decreased as the groove size and embedment length increased. Hassan found that small scale T-specimens with NSM CFRP had a stiffer response than the control specimens. The beams experienced an increase in capacity but a decrease in ductility. In addition, Hassan found that higher steel reinforcement ratios produced a longer NSM development length due to shifting of the neutral axis. Bond tests primarily use short bond lengths to capture the active portion of bond strength. De Lorenzis continued work on an analytical method of finding bond stress from pull-out tests. Bournas used stainless steel and CFRP NSM bars to retrofit columns, and found that stainless steel NSM bars may outperform CFRP NSM bars in cyclic tests. Al-Mahmoud found that when retrofitting RC beams it may be more efficient to use larger diameter bars rather two smaller bars. In 2010, Al Mahmoud determined that a 0.47 in. (12 mm) diameter CFRP rod had an active bond length less than 3.93 in. (100 mm).

Table 2.2 - Bond Stress in NSM reinforcing bars from literature

Author	Bar Type	Bar Diameter (in.) [mm]	Bar Embedment (in.) [mm]	Test Type	Average Bond Stress (psi) [MPa]
De Lorenzis (2000)	CFRP	0.5 [12.7]	6 [152]	Pull-out	1078 [7.43]
	CFRP	0.5 [12.7]	12 [305]	Pull-out	620 [4.27]
De Lorenzis (2002)	CFRP (Spiral wound)	0.5 [12.7]	2 [50.8]	Modified Pull-out	1637 [11.29]
Novidis	CFRP	0.5 [12.7]	4.7 [120]	Modified Pull-out	654 [4.51]
Bournas	CFRP (Strip)	0.63 x 0.08 [16 x 2]	2.75 [70.0]*	Column	590 [4.07]
	Stainless Steel	0.47 [12]	2.75 [70.0]*	Column	873 [6.02]

*Length between strain gages, fully embedded along the column

2.3 Design Specification Review

Over time, design codes and specifications have formed to influence bridge design. Research on reinforced concrete has improved the understanding of the of bond and stress behavior of reinforcing steel bars in concrete. This section reviews changes in AASHTO and ACI specifications regarding bond stress and development length for steel reinforcing bars and NSM bars. All equations listed use English units. Design equations for shear, flexure, and flexural tension using current ACI and AASHTO are detailed in the appendix.

2.3.1 AASHO Allowable Stress Design

A compilation of standards and specifications for bridge design began in 1921 with the formation of the American Association of State Highway Officials. The first edition of the AASHO standards was published in 1931. In the 1953 edition, several assumptions were

used in reinforced concrete design. These assumptions included the assumption that concrete has negligible tensile strength and the bond between concrete and reinforcing steel bars remain intact within the working or service stress range. From 1953 through 1973, AASHO codes recommended using allowable stress design. That is, structures were designed to a specified stress limit chosen at service level loads. The 1953 edition provided typical reinforced concrete design equations assuming plane sections remain plane. The tensile unit stress in longitudinal reinforcement, f_s, is seen below:

$$f_s = \frac{M}{A_s jd}$$

AASHO Sec. 3.7.3.b [2.12]

where M is the applied moment, A_s is the area of steel, and jd is the distance between the compression and tension zones. From the equation 2.12 above, bond stress per unit area u is calculated below:

$$u = \frac{V}{Zojd}$$

AASHTO Sec. 3.7.3.c [2.13]

Eq. [2.13] represents the stress on the surface between the steel reinforcing bar and concrete. Zo is the sum of perimeters of bars in the area considered, V is the total shear applied, and d is depth from the top of the section to the tension steel. The steel reinforcing bars should be detailed and extended in a manner to develop the tension in the straight steel reinforcing bar without exceeding the maximum working bond stress u_{max}:

$$u_{max} = 0.10 * f'_c \leq 350$$

AASHTO Sec. 3.4.12 [2.14]

where f'_c is the compressive strength of concrete. Other anchorage requirements include extending a bar at least 15 diameters, but not less than 1/20 of the span length past where calculations indicate the bar is no longer needed in a simply supported beam.

The 1957 AASHO Specifications for Highway Bridges have similar bond requirements. It was assumed that there is no slip in service level conditions and had the same bar termination requirements. This version of the code also required new reinforcing bar standards such as ASTM A 305-53T.

The 1973 AASHO specifications observed a shift in analysis and design of reinforced concrete bridges. The code was split in to allowable stress design and load factor design. The calculated bond stress was equivalent to Eq. [2.13] but had different stress limits. The allowable stress design specified a limit for working bond stress for a bottom size #3-#11 steel reinforcing bar as shown:

$$u_{max} = \frac{4.8\sqrt{f'_c}}{D} \leq 350 \qquad \text{AASHO Sec. 1.5.1.D.2} \quad [2.15]$$

where D is the diameter of the steel reinforcing bar and f'_c is defined in the equation above. Anchorage requirements from the 1953 code were still applicable with some additions for beam end requirements. For example, in restrained or continuous beams, at least 1/4 of the positive moment reinforcement shall extend beyond the face of supports. Additionally, steel reinforcing bars were more likely to be Gr. 60 (Gr. 420) or Gr. 40 (Gr. 280) and conform to ASTM A 615-73. No formal development length equations were listed but the development bond stress was computed. The bond stress for a developing steel reinforcing

bar was calculated as the bar forces divided by the perimeters of bars multiplied by the embedment length.

2.3.2 AASHTO-LRFD Bridge Design Specifications

Load factor design required consideration for several limit states: strength, service, and fatigue. To design for strength, the concrete strain is limited at a maximum value of 0.003 (concrete crushing strain), and the stress in the reinforcing steel bars is set at yield. The 1973 AASHO included an expanded section pertaining to the development of reinforcement. The AASHO load factor design code had more stringent requirements and states that reinforcement shall extend a distance equal to the effective depth *d* of the member or 12 bar diameters, whichever is greater. Also, flexural reinforcement shall not be terminated in a tension zone and a development length equation was accepted. For #11 (36M) bars or smaller the development length can be taken as:

$$L_d = \frac{0.04 a_s f_y}{\sqrt{f'c}} > 0.0004 D f_y$$

AASHO Sec. 1.5.29.E.1 [2.16]

where a_s is the individual area of the bar, f_y is the yield strength, and all other variables are defined previously. After equating L_d, the value was multiplied by applicable modification factors to obtain the required development length.

After years of development, AASHO became the American Association of State Highway Transportation Officials (AASHTO) and fully incorporated Load Factored Resistance Deisgn (LRFD) into specifications. The 4th edition, published in 2007, is the edition used in this paper for design calculations. Some updates to current specifications include

considering additional demands on tension steel from shear and cracks, calculated as the tensile demand in the steel reinforcing bars as:

$$A_s f_y \geq \frac{|M_u|}{d_v \varphi_f} + 0.5\frac{N_u}{\varphi_c} + \left(\left|\frac{V_u}{\varphi_v}\right| - 0.5V_s\right) cos\theta$$

AASHTO Eq. 5.8.3.5-1 [2.17]

where d_v is the distance from compression to tension centroids (formerly jd), N_u is the applied axial force, V_u is the applied factored shear, V_s is the shear capacity of stirrups, Θ is the angle of the crack, and φ_f, φ_c, φ_v, are modification factors from the concrete and geometry. A simplified version of this equation is described in section *2.1 Anchorage Concerns* above.

AASHTO LRFD 2007 development length, l_d, can be taken for #11 (36M) steel reinforcing bars and smaller as:

$$l_d = \frac{1.25 A_b f_y}{\sqrt{f'_c}}$$

AASHTO Sec. 5.11.2.1.1 [2.18]

where A_b is area of bar or wire, and all other variables are defined previously. Additionally, this equation is multiplied by applicable modification factors. Similar flexural bar termination requirements are maintained as the 1973 code.

2.3.3 ACI 318 Building Code for Structural Concrete

In 1956, the American Concrete Institute published the Building Code Requirements for Reinforced Concrete (ACI 318-56). During this time, allowable stress design was permitted for reinforced concrete structures. The bond stress calculation similar to Eq. [2.13] and maintained allowable stress requirements as described in Eq. [2.14]. Similar to

current AASHTO standards, bar termination requirements required the steel reinforcing bar must extend at least 12 bar diameters past the theoretical cutoff point.

Like AASHTO specifications, ACI adopted LRFD. The calculations in this paper are based off the current code ACI code (ACI 318-11). Since allowable stress is not used to design for bond stresses, ACI created a general and detailed equation to determine development length given a bar size. ACI 318-11 equates straight development length, l_d, of #7 bars and larger as:

$$l_d = \left(\frac{f_y \psi_t \psi_e}{20\lambda\sqrt{f'_c}}\right) d_b \qquad \text{ACI 318 Sec. 12.2.2 [2.19]}$$

where ψ_t and ψ_e are modification factors for the location of bar and coating of the bar respectively. λ is the lightweight concrete factor and all other variables are defined in equations above. The more detailed equation recognizes the contribution of the transverse reinforcement and cover of the bar, thus providing a more accurate development length shown as:

$$l_d = \left(\frac{3}{40\lambda}\frac{f_y}{\sqrt{f'_c}}\frac{\psi_t \psi_e \psi_s}{\frac{c_b + K_{tr}}{d_b}}\right) d_b \qquad \text{ACI 318 Eq. 12-1 [2.20]}$$

where ψ_t is the size factor for the bar, c_b is either the smallest of the side or top cover, or half the center to center spacing between the bars. K_{tr} is the contribution of confining reinforcement and is calculated by:

$$K_{tr} = \frac{40A_{tr}}{sn} \qquad \text{ACI 318 Eq. 12-2 [2.21]}$$

where A_{tr} is the area of transverse reinforcement across the splitting plane, s is the spacing of stirrups, and n is the number of bars being developed. K_{tr} may be taken as zero for a conservative design. General requirements for the development of flexural reinforcement include extending a distance d or $12d_b$ past the point where reinforcement is no longer required.

2.3.4 ACI 440 Guide for Design of Externally Bonded FRP systems

ACI created a committee focused on the design and construction for strengthening reinforced concrete using external fiber reinforced polymer (FRP) systems. The two systems described include FRP laminate sheets and FRP rods and strips used for a near-surface mounted (NSM) application. The majority of the code is based on behavior of reinforced concrete sections strengthened with FRP laminate. NSM strengthening guidelines include groove spacing, depth, effective strain and required development length.

To determine the strength of the cross section retrofitted with NSM materials the effective strain in NSM material was calculated. The effective strain in the NSM material was taken as the lesser of the concrete crushing or debonding strain in the NSM material shown as:

$$\varepsilon_{fe} = 0.003\left(\frac{d_f - c}{c}\right) - \varepsilon_{bi} < \varepsilon_{fd} \qquad \text{ACI 440 Eq. (10-3) [2.23]}$$

where d_f is the distance from the extreme compression fiber to the centroid of the NSM reinforcement, c, is the distance from the extreme compression fiber to the neutral axis, and ε_{bi} is the existing strain in the reinforcement calculated from the dead load. The advantage of a mechanical anchorage decreases the probability of a bond failure so the bond depended coefficient may be less stringent for the NSM titanium and stainless steel near

hooked bar terminations. ε_{fd} is the debonding strain for the NSM material and is calculated as:

$$\varepsilon_{fd} = \kappa_m \varepsilon_{fu} \qquad \text{ACI 440 Eq. (10-2) [2.24]}$$

where κ_m is the bond depended coefficient for the NSM material provided by the manufacturer taken as 0.7. The 70% reduction in ultimate strain is due to concrete dilation and tendency to debond after cracking. ε_{fu} is the ultimate strain of the NSM material.

The development length, l_{db}, for straight circular FRP bars is calculated as:

$$l_{db} = \frac{d_b}{4\tau_b} f_{fd} \qquad \text{ACI 440 Eq. (13-3) [2.22]}$$

where τ_b is the average bond stress, taken as 1000 psi, and f_{fd} is the debonding stress of FRP, based on the debonding strain of the section. Essentially, Eq. [2.22] is equivalent to Eq. [2.1] but uses FRP debonding stress instead of yield stress.

Minimal guidance is given on termination of NSM bars. However, ACI 440 recommends extending the FRP a distance from the maximum moment to at least 6 in. past the location of the first cracking moment or the development length, whichever is greater to minimize debonding failures.

2.4 Conclusions

Based on a review of the literature and design specifications, several conclusions on bond and behavior of steel reinforcing bars in concrete and NSM FRP bars have been made.

- Bond strengths from pull-out tests are not representative of actual strengths in beam tests. Furthermore, there is limited research of large-scale specimens.
- The development length of steel reinforcing bars in concrete is based on bar strength, diameter, placement, covering, spacing, transverse reinforcement, and concrete strength.
- The average bond stress in steel reinforced concrete beam tests can range from 540-815 psi (3.72-5.62 MPa).
- Strengthening with NSM FRP bars significantly increases the strength and stiffness of the beam.
- Shorter bond lengths produce higher average bond stresses and the concrete epoxy bond is the most critical interface.
- Anchorage of NSM bars limits the effective design stress in FRP systems.
- Average bond stress in NSM FRP pull-out tests can range from 620-1637 psi (4.27-11.3 MPa).

2.5 Research Objective

This project had several research objectives stemming from the investigation of retrofitting anchorage deficiencies in positive moment regions of RCDG bridges. This program supplements previous research on behavior of full-scale vintage concrete girders from Oregon State University. Two metallic materials not commonly used in civil infrastructure are investigated. Their tensile and bond strengths are investigated using ASTM E8 and an adapted method of ASTM A944. A goal of this research is to observe how the stresses in the internal reinforcing bars transfer to the NSM materials as an external lap splice. This behavior is investigated with the presence of a 45° preformed diagonal crack. Test results can be compared to design calculations and programs utilizing Modified Compression Field Theory (MFCT). A methodology of bending and instrumenting titanium and stainless steel bars was investigated. A case study was used to verify the effectiveness of the NSM titanium strengthening technique.

3 EXPERIMENTAL SETUP

An experimental program was developed to investigate full-scale RCDG with anchorage deficiencies in positive moment bending strengthened with NSM titanium and stainless steel bars. This chapter describes the design, details, construction, instrumentation, and testing protocols used to characterize the retrofit of poorly detailed flexural steel reinforcement with the presence of diagonal cracks.

3.1 Specimen Design

In a typical RCDG, three failure modes are likely to control: shear-tension failure due to lack for shear reinforcement, shear-tension failure due to inadequate anchorage, and flexural failure. The intent of this study was to strengthen T-specimens in positive moment bending that would otherwise fail due to anchorage deficiencies. A survey was conducted prior to this experimental work to characterize typical vintage concrete deck girders. The survey provided the geometry and reinforcing steel details of vintage girders (Higgins *et al*., 2004). All specimens in this program were 26 ft (7.92 m) long, with a 14 in. (356 mm) thick web, 42 in. (1067 mm) tall stem, 36 in. (914 mm) wide flange, and a 6 in. (152 mm) thick deck. Two #11 (36M) steel reinforcing bars were in the flange to serve as compression steel. The flexural reinforcement consisted of five #11 (36M) steel reinforcing bars in two layers: three #11 (36M) bars extended past the support location (two hooked one straight), and two “cutoff” bars that extended only 1/3 of the specified development length past a preformed diagonal crack. The intersection of the preformed diagonal crack with reinforcing bars created an additional demand of the flexural reinforcing steel. The additional demand of the cutoff bars created an anchorage deficiency.

In this study, three strengthened specimens containing preformed diagonal cracks intersecting flexural steel bars near the cutoff location were tested. A baseline T-specimen was used from previous research (Triska, 2010) to compare to the three strengthened T-specimens tested in this study. The specimens from the current program had variations in stirrup spacing, and were strengthened NSM titanium or stainless steel. The naming convention used in this study is shown in Fig. 3.1. Table 3.1 lists the specimens considered in Chapter 3 and 4 of this study.

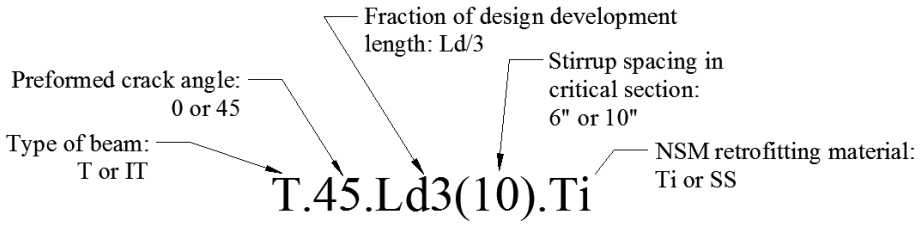

Fig. 3.1-Specimen naming convention

Table 3.1-Specimen summary and year tested

Specimen ID	Retrofitting Material	Year Tested
T.45.Ld3(10)	-	2010
T.45.Ld3(10).Ti	Titanium	2014
T.45.Ld3(6).Ti	Titanium	2014
T.45.Ld3(6).SS	Stainless Steel	2014

To create an anchorage deficiency, the development length of a #11 (36M) reinforcing steel bar must be calculated. The minimum development length of the mild reinforcing steel bars was determined using the AASHTO LRFD and ACI 318-11 specifications. The smallest and least conservative value was chosen for the development length. Calculations were performed with an expected yield stress of 68.5 ksi (472 MPa) for the flexural steel,

and expected yield stress of 50.7 ksi (350 MPa) for transverse steel. The nominal concrete strength used was 3500 psi (24.1 MPa), typical of bridges in the 1950s.

Development length based off of ACI and AASHTO specifications are shown in Table 3.2. A stirrup spacing of 10 in. (254 mm) and value of c_b of 2.02 in. (51 mm) was used in the detailed ACI 318 equation. As seen in Table 3.2, the smallest permissible length to develop the #11 (36M) Gr. 60 (Gr. 420) bar is 61.2 in. (1554 mm).

Table 3.2- Summary of expected development lengths of #11 (36M) steel reinforcing bars

Method	**AASHTO LFRD (in.) [mm]**	**ACI 318-11 (in.) [mm]**
Straight Bar	71.4 [1813]	61.2 [1554]
Straight Bar Simplified	-	81.6 [2072]
Hooked Bar	28.6 [726]	32.6 [828]

The baseline tests by Triska confirm an anchorage failure is prevalent using 1/3 of the specified 61.2 in. (1554 mm) embedment length. Therefore, the strengthened T-specimens will extend the cutoff bar 20.4 in. (518 mm) past the preformed diagonal crack.

3.2 Specimen Details

This section describes the internal reinforcing steel details, specimen construction, and NSM details and installation.

3.2.1 Reinforcing Steel and NSM Details

The transverse reinforcing steel consisted of open leg #4 (13M) stirrups. Two straight #11 (36M) bars make up the compression steel. The flexural reinforcement consisted of five #11 bars (36M) in two layers. Three #11 (36M) bars were fully anchored on the bottom layer of flexural reinforcement. The top layer of reinforcement consisted of two cutoff steel reinforcing bars. The cutoff steel reinforcing bars were embedded 20.4 in. (118 mm) past the preformed diagonal crack. The cross section and elevation of the specimens can be seen in Fig. 3.2 through Fig. 3.8. Stirrup spacing was either 6 in. (152 mm) or 10 in. (254 mm) throughout the entire beam in the fully anchored specimens.

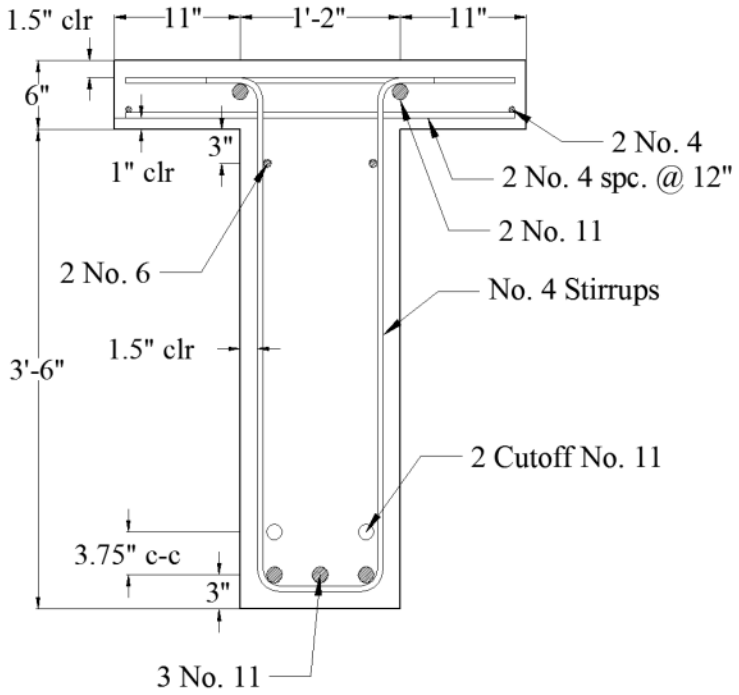

Fig. 3.2 - Cross section of T.45.Ld3(10)

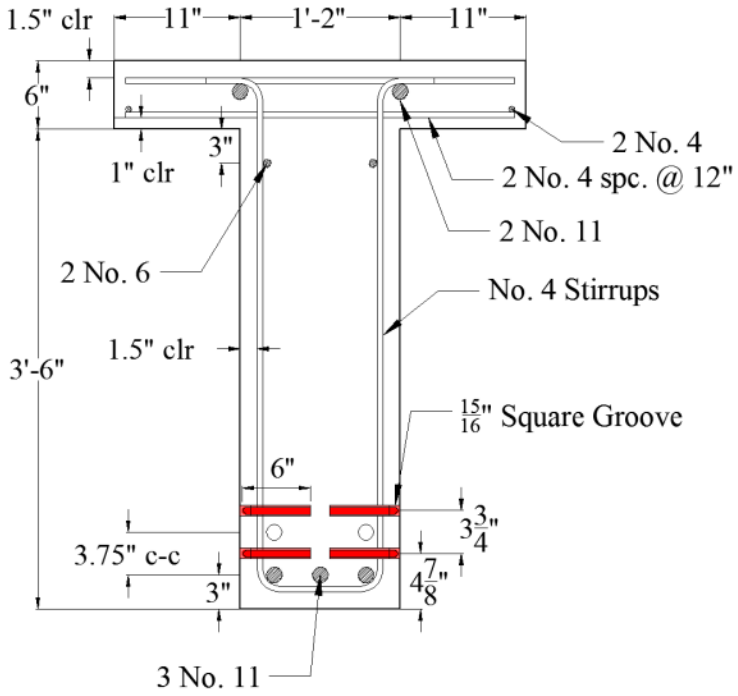

Fig. 3.3 - Cross section of T.45.Ld3(10).Ti and T.45.Ld3(6).Ti

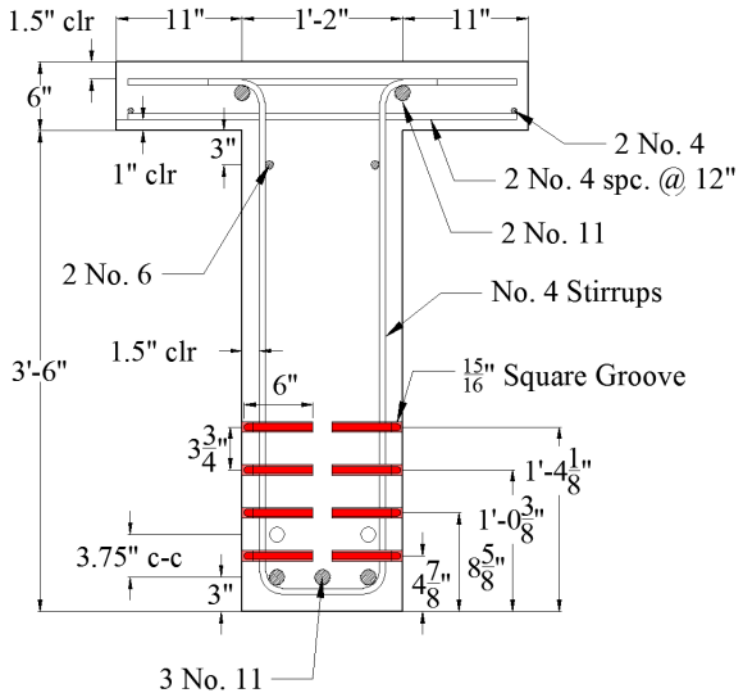

Fig. 3.4 - Cross section for specimen T.45.Ld3(6).SS

Fig. 3.3 and Fig. 3.4, show the hooked termination detail of the NSM material in red. Between the terminations, a small square groove is cut into the section's concrete cover. The NSM retrofit location and extent is also shown as the red lines on the Fig. 3.6 through Fig. 3.8. The metallic NSM retrofit bars are 12.5 ft (3.81 m) long (out-to-out) with a 90° hook at the ends with a length of 6 in. (152 mm) (out-to-out). The titanium strengthened specimens had four 5/8 in. (16 mm) (nominal) diameter bars bonded into the square saw-cut grooves, two on each side of the web. Stainless steel specimens had eight 5/8 in. (16 mm) diameter bars bonded into the square saw-cut grooves, four on each side of the web. The baseline specimen elevation is shown in Fig. 3.5.

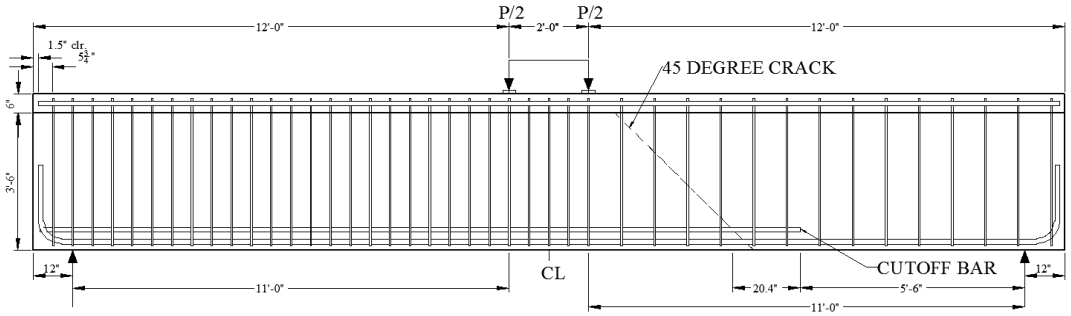

Fig. 3.5 - Elevation of baseline specimen T.45.Ld3(10)

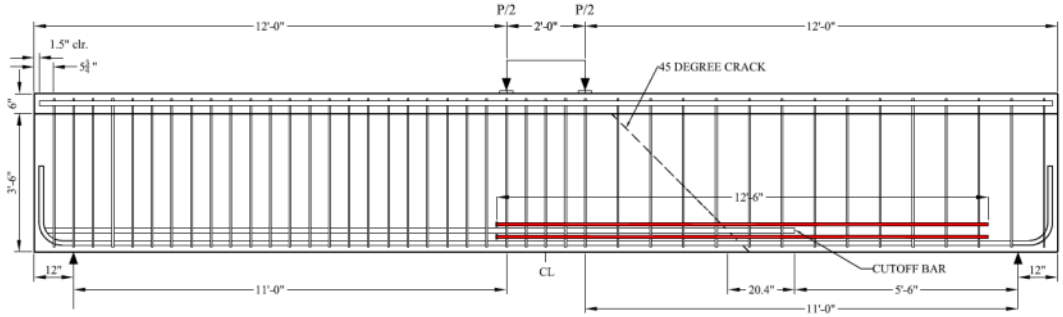

Fig. 3.6 - Elevation of specimen T.45.Ld3(10).Ti

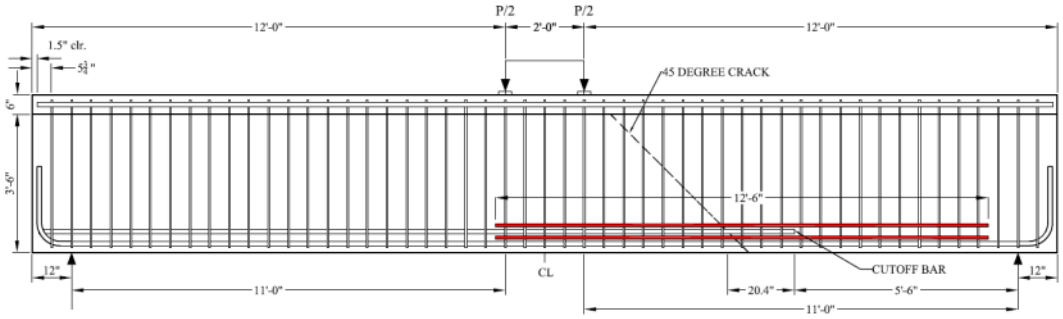

Fig. 3.7 - Elevation of specimen T.45.Ld3(6).Ti

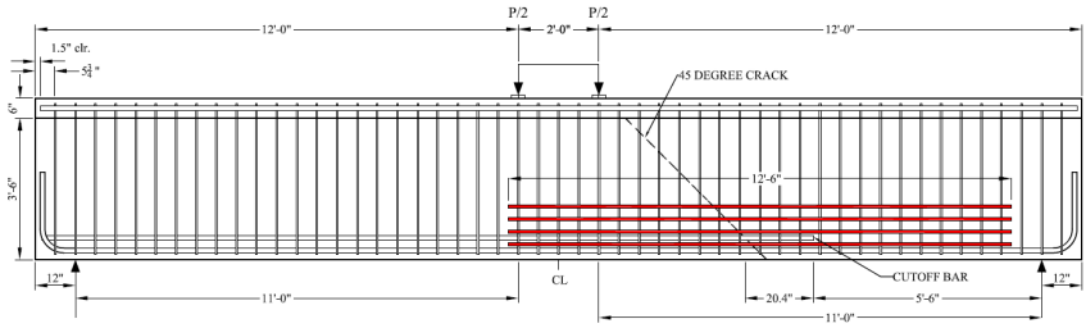

Fig. 3.8 - Elevation of specimen T.45.Ld3(6).SS

All specimens utilized a tight stirrup spacing of 6 in. (152 mm) on the half of the specimen with fully anchored reinforcing steel. The control specimen and the T.45.Ld3(10).Ti specimen had a 10 in. (254 mm) stirrup spacing on the half with a predicted anchorage deficiency. T.45.Ld3(6).Ti and T.45.Ld3(6).SS both had 6 in. (154 mm) stirrup spacing throughout the full length to preclude the possibility of a shear-tension failure on the strengthened half.

3.2.2 Construction

The construction of the T-specimens initiated after strain gage sensors were applied to the internal reinforcing steel as described in Section *3.4.1 Internal Sensor Array*. This section describes the cage construction, the preformed crack details, and the concrete casting process.

3.2.2.1 Steel Reinforcing Cage Construction

To create the steel reinforcing cage, stirrups spaced 6 in. (152 mm) or 10 in. (254 mm) apart were hung from the compression steel. Three #11 (36M) were tied to the stirrups as the lower layer of flexural reinforcement. The top cutoff layer was spaced 3.75 in. (95.3 mm) from the center of the lower layer. 1.5 in. (38 mm) wide spacers were attached to the stirrup legs to provide sufficient cover. Fig. 3.9 is a typical reinforcing cage for T-specimens.

Fig. 3.9 - Typical reinforcing cage for T-specimen

In specimens T.45.Ld3(10) and T.45.Ld3(10).Ti, a block-out was placed around the ends of the cutoff bar. The block-out provided a location for wires to exit the web and a place to measure the end slip of the cutoff bar. While testing T.45.Ld3(10).Ti, the NSM titanium reinforcement was not bonded over the block-out length. This reduced dowel action and produced bending stresses in the titanium and lower layer of reinforcing steel. To maintain the dowel action in the titanium bars and reinforcing steel, a small diameter side port was used to measure end slip of the cutoff bar. A nut was welded to the side of the cutoff steel reinforcing bar and was enclosed by a piece of polyvinyl chloride (PVC) pipe tapered to the bar. Once cast, the circular end of the PVC pipe was exposed and a threaded rod was inserted into the nut. The displacement sensor was attached to the nearby concrete with an epoxied steel dowel and reacted against the threaded rod anchored to the cutoff reinforcing steel bar. These techniques are shown in Fig. 3.10.

Fig. 3.10 - Cutoff bar slip sensor ports (left), and block-out box (right)

3.2.2.2 Preformed Diagonal Crack

The preformed diagonal crack angle was chosen as 45° based on a common cracks observed in a reinforced concrete girders with relatively high shear and flexure. The preformed crack eliminates aggregate interlock along the section and provides a known point of geometry where the bond and flexural tension stresses can be assessed. The

preformed diagonal crack was made with a 1/16 in. (1.6 mm) thick polycarbonate sheet. This thickness is representative of wide diagonal cracks observed in the field. The crack angle is projected from the edge of the loading plate to the soffit of the web. However, the polycarbonate sheet does not extend into the theoretical compression zone, to reduce the chance of an early compression failure. Laterally, the preformed crack extends between the stirrups with notches at each leg to provide support. Several ties were used to secure unsupported regions of the polycarbonate sheet.

3.2.2.3 Concrete Casting

Concrete was provided by a local ready-mix supplier. Concrete was placed in a concrete bucket and then placed in the forms. Care was taken to balance the concrete around the preformed diagonal crack. Fifteen 4 x 8 in. (102 x 203 mm) concrete cylinders were cast per specimen to characterize concrete strength. The concrete was consolidated with a mechanical vibrator then finished to create a smooth loading surface shown in Fig. 3.11.

Fig. 3.11 - Typical construction of T-specimen

Once cast, the specimen was covered and cured for seven days in the formwork. After initial curing, the specimens were removed from the form and placed in a stable configuration for cutting the grooves into the stem for the NSM retrofit. Testing of the specimens occurred after the concrete had a compressive strength of at least 3,000 psi (20.7 MPa).

3.2.3 NSM Material Details and Installation

The design intent of the metallic NSM strengthening was to retrofit anchorage deficiencies in RCDGs. To accomplish this, the flexural reinforcing steel needed to be effectively extended via the NSM material until a permissible termination location. To determine where anchorage deficiencies lie, the demand on flexural reinforcing steel from shear and moment contribution was compared to the flexural tension capacity provided in the section determined from AASHTO equations. If the demand exceeded the capacity, an anchorage failure was likely to occur. Two metallic materials, titanium and stainless steel, were used instead of CFRP due to their high strength, ductility, and ability to fabricate hooks.

The NSM titanium bar selected had a 0.61 in. (15.5 mm) diameter with a nominal yield stress of 145 ksi (1000 MPa). The NSM stainless steel bar selected had a 0.625 in. (16 mm) diameter with a nominal yield stress of 75 ksi (517 MPa). Using these material properties, the predicted flexural tension capacity could be found. A short 6 in. (152.4 mm) hooked development length was assumed for the titanium and stainless steel NSM bars. However, the NSM bars were conservatively extended at least 1 ft (305 mm) past the theoretical cutoff point (where the capacity exceeded the calculated demand). To validate the development length assumption of this unique material and anchorage, a bond strength

study was conducted in section *3.6 Bond Strength Study*. Based on the theoretical cutoff points, it was determined that a NSM bar length of 12.5 ft (3.66 m) out-to-out was required. Fig. 3.12 shows the flexural tension capacity and demand of the control specimen and the strengthened specimens. A description of determining an anchorage failure from flexural tension forces can be found in Appendix G.

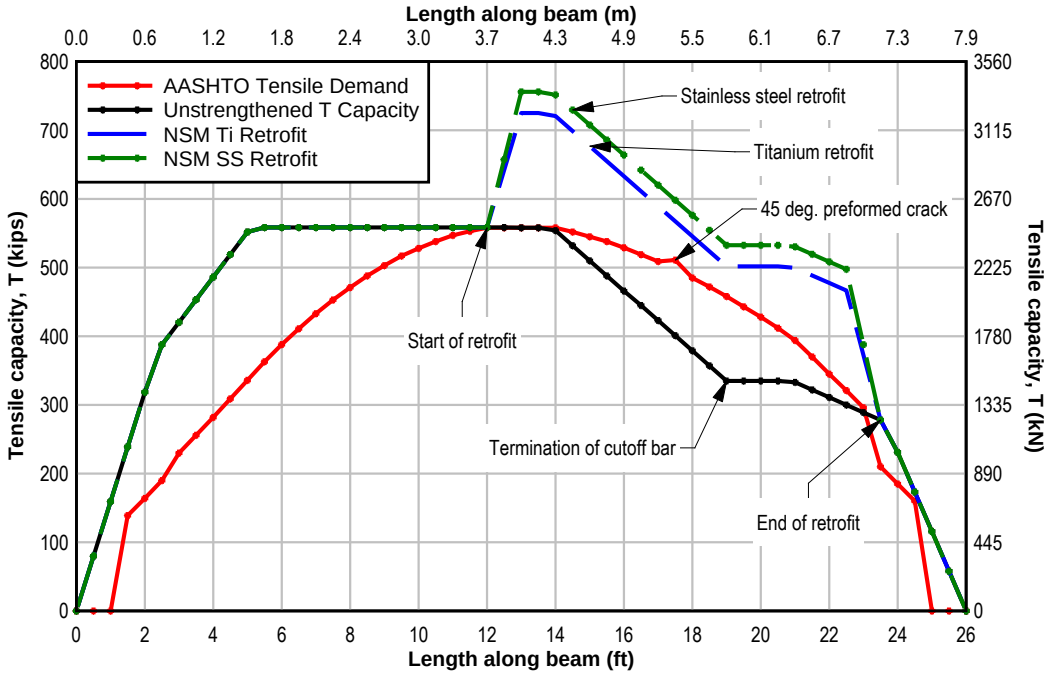

Fig. 3.12 – Flexural tension capacity and demand for typical specimen at failure load

Important NSM strengthening design specifications are described in section *2.3.4 ACI 440 Guide for Design of Externally Bonded FRP Systems*. The code is calibrated for strengthening with carbon fiber reinforced polymer (CFRP), but factors such as groove depth, epoxy cover, and NSM material spacing are applicable to any NSM material. Therefore, ACI 440 groove dimensions and spacing requirements were followed in this study. The groove depth requirements state that the groove must be 1.5 times the diameter

of the bar, $d_{b,}$ in width and height. The groove spacing requirements limit overlapping tensile stresses and risk of debonding. ACI 440 recommends a clear spacing of at least greater than twice the groove depth, and a clear distance between the groove and the edge of the concrete of at least four times the groove depth. A comparison of effective stresses achieved in the NSM materials and discussion is described in section *5.6 ACI 440 Design Recommendations for Metallic NSM Materials*.

Concrete cover depth is often a retrofitting design constraint with vintage RCDG's. Following ACI 440 groove depth requirements, the maximum permissible NSM bar size with a cover depth of 1.5 in. (38 mm) is a #5 (16M) bar. Once the diameter of the bar was determined, the number of bars must be found. Often, the number of NSM bars to create an equivalent tensile force as the #11 (36M) steel reinforcing bar required a partial or an uneven number of bars. When this occurred, the NSM bars were conservatively increased to the nearest even bar to ensure symmetry in the section. This methodology caused over-strength as seen in Fig. 3.12. The use of nominal yield strength instead of real yield strength lead to the slight over-strength of the NSM stainless steel specimen.

The NSM titanium retrofitted specimens required four 0.61 in. (15.5 mm) diameter bars to exceed the required flexural tensile force of the two cutoff steel reinforcing bars. The NSM titanium retrofit dispersed two titanium bars on each side of the web for an extent of 12.5 ft (3.66 m). At the critical section (the diagonal crack location), two titanium bars should theoretically provide 56.4 kips (251 kN) of predicted strength above the tensile demand illustrated in Fig. 3.12. Eight #5 (16M) stainless steel bars are required for the equivalent retrofit. The stainless steel specimen had four stainless steel bars on each side of the web

with an extent of 12.5 ft (3.66 m). At the preformed crack section, the stainless steel bars could theoretically provide 87.3 kips (388 kN) of strength above the flexural tension demand.

After the number and length of NSM bars were determined for each retrofit, a standard 6 in. (152.4 mm) hook length was used for the mechanical end anchorage. The hooks were fabricated in a reinforcing bar bending machine around a 2 in (51 mm) diameter pin. All stainless steel bars were cold worked and exhibited minimal spring back while bending the 90° hooks. Due the surface deformations, titanium required warm working. The titanium hooks were heated with an acetylene torch to approximately 900 °F (482 °C) before bending for specimen T.45.Ld3(10).Ti. Titanium hooks for specimen T.45.Ld3(6).Ti were heated in a two burner propane forge to 900 °F (482 °C). The temperature was measured using a color indication system provided by the titanium manufacturer. Bending tolerances for the stainless steel and titanium bars were within 0.125 in (3.175 mm) due to the 0.75 in. (19.1 mm) diameter holes. Fig. 3.13 shows a typical 90° hook detail for the titanium and stainless steel materials.

Fig. 3.13 - Bending titanium (left) and stainless steel (right) hooks

After initial curing, the concrete T-specimens were placed in a stable configuration to cut the grooves required for NSM retrofit. Three longitudinal passes were cut into the concrete cover with a concrete saw as seen in Fig. 3.14. A roto-hammer was used to chip out the concrete and to expose a 15/16 in. (23.8 mm) square groove. At the end of the longitudinal grooves, a 3/4 in. (19 mm) diameter and 6 5/8 in. (161 mm) deep hole was drilled. The corners were chipped to accommodate the 2 in. (5 mm) diameter bend of the hooks. After bending the bar to length, the holes were drilled to fit each bar. The grooves and holes were cleaned with a wire brush and compressed air before epoxy was extruded. A pass of epoxy was placed into the groove before inserting the bar. If necessary, a second pass of epoxy was placed and then finished with a trowel. The epoxy was cured for at least 7 days with a regulated temperature according to the manufacturer's specifications.

Fig. 3.14 – Saw-cutting (left) and inserting NSM bars into the concrete grooves (right)

3.3 Material Properties

A unique concrete mixture was created for Oregon State University for research on vintage RCDG. The concrete mixture has a design compressive strength of 3000 psi (20.68 MPa) and minimal admixtures, representative of design specifications in the 1950s. The full

mixture design can be found in Appendix C. Cores taken from bridges of that era have in-situ strengths typically higher than the specified strengths. The present day strengths lie around 3300 psi (22.8 MPa) to 4000 psi (27.6 MPa). Therefore, a lower target strength would account for the in-situ and common design over-strengths in concrete. Experimentally measured test-day concrete strengths and the standard deviation of the samples is listed in the Table 3.3.

Table 3.3 - Concrete properties

Specimen ID	**f'_c (psi) [MPa]**	**Standard Deviation (psi) [MPa]**	**f_{ct} (psi) [MPa]**	**Standard Deviation (psi) [MPa]**	**Concrete Age (days)**
T.45.Ld3(10)	3302 [22.8]	373 [2.57]	272 [1.9]	28.0 [0.19]	30
T.45.Ld3(10).Ti	3712 [25.6]	169 [1.17]	418 [2.9]	17.8 [0.12]	36
T.45.Ld3(6).Ti	3823 [26.4]	65.0 [0.45]	363 [2.5]	7.3 [0.05]	30
T.45.Ld3(6).SS	3206 [22.1]	190 [1.31]	416 [2.9]	38.9 [0.27]	40

Compression and tensile strengths of concrete are useful in characterizing concrete cracking and crushing behavior. Test day compressive strengths, f'_c, were determined using standard test method ASTM C39-12a. Cylinders for split tensile strengths were crushed on the test date according to ASTM C496-11.

Lower grade, larger diameter steel reinforcing bars was typically used in mid-century bridge construction. These larger, weaker bars are no longer commercially available. Therefore, a smaller, stronger replacement was used. Longitudinal reinforcement consisted of ASTM A706-09 Gr. 60 (Gr. 420) bars, and ASTM A615-09 Gr. 40 (Gr. 280) was

selected for transverse reinforcement. All steel reinforcing bars were provided by a local reinforcing bar fabricator. Table 3.4 lists the material properties for the specimens tested in 2014. The material properties of the baseline specimen from Triska (2010) are included in Table 3.5.

Table 3.4 - Reinforcing bars material properties for strengthened specimens

Material	**Bar Size**	**Bar Area (in.^{2}) [mm^2]**	**Bar Diam. (in.) [mm]**	**Nominal f_y (ksi) [MPa]**	**MOE (ksi) [MPa]**
Transverse	#4 [13M]	0.2 [129]	0.5 [12.7]	40 [276]	29000 [200000]
Const. Steel	#6 [19M]	0.44 [284]	0.75 [19.1]	60 [414]	29000 [200000]
Flexural	#11 [36M]	1.56 [1006]	1.41 [35.8]	60 [414]	29000 [200000]
Titanium	#5 [16M]	0.29 [188]	0.61 [15.5]	140 [965]	15500 [106800]
Stainless Steel	#5 [16M]	0.31 [200]	0.63 [16.0]	75 [517]	29000 [200000]

Table 3.5 - Reinforcing bar measured material proerties for strengthened specimens

Material	Bar Size	f_y (ksi) [MPa]	Standard Deviation (ksi) [Mpa]	f_u (ksi) [MPa]	Standard Deviation (ksi) [Mpa]
Transverse	#4 [13M]	50.2 [346]	0.12 [0.83]	79.6 [549]	0.17 [1.17]
Const. Steel	#6 [19M]	72.2 [498]	0.14 [0.96]	107 [735]	0.06 [0.41]
Flexural	#11 [36M]	71.6 [494]	1.26 [8.68]	107 [738]	0.93 [6.41]
Titanium	#5 [16M]	145.4 [1002]	1.56 [10.75]	158 [1090]	0.35 [2.41]
Stainless Steel	#5 [16M]	83 [572]	0.68 [4.69]	127 [878]	1.39 [9.58]
T.45.Ld3(10) Transverse	#4 [13M]	50.5 [369]	-	84.6 [583]	-
T.45.Ld3(10) Flexural	#11 [36M]	71.7 [494]	-	105 [722]	-

Procedures from ASTM E8-13a were used to find yield, ultimate, and elongation values for all samples. To measure strain in the coupon, an extensometer with a 2 in. (50.8 mm) gage length was used. The universal testing machine held an initial loading rate of 0.001 in/sec (0.025 mm/sec) until yield, and then increased subsequently.

The NSM reinforcing materials, stainless steel and titanium, have several unique properties. Pictured in Fig. 3.15, both materials were chosen because of their high strength, ductility, environmental durability and ability to bend around a tight radius.

Fig. 3.15 - Deformation patterns on stainless steel (top) and titanium (bottom)

Titanium is not a common material in civil infrastructure, the majority of titanium's use is in based the medical and aerospace industries. The titanium manufacturer abides to the tight material tolerances required for the aerospace industry, thus, the titanium used in this study had remarkably small coefficients of variation (COV). The titanium alloy consists of 6% aluminum and 4% vanadium (Ti-6Al-4V), and meets ASTM B348 specifications. Titanium has a low coefficient of thermal expansion of around 4.78 μin/in °F (8.6 μm/m °C), and is impervious common environmental deteriorations. The unit weight of titanium is around half that of steel. Titanium has a unit weight of 276 lb/ft^3 ($4419kg/m^3$), much less than the unit weight steel of 490 lb/ft^3 ($7846 kg/m^3$). Titanium is a fairly elasto-plastic material without a well-defined yield plateau seen in Fig. 3.16 below. A 0.2% offset method was used to determine yield. The titanium bars had a yield stress of 145.2 ksi (1000 MPa) with 1.01% COV, an ultimate stress of 158.1 ksi (10,090 MPa) with 0.88% COV, and elongation of 11.3% with a2.66% COV. Measuring the MOE from a uniaxial strain test is not necessarily accurate so the MOE of titanium was taken from the manufacturer's tests. The softer MOE of titanium dictates that the strain in the titanium bar would be higher than the strains in a steel reinforcing bar at similar loads. A custom

deformation pattern was created for the NSM titanium bar to increase bond with the epoxy interface. Typical reinforcing bar deformations aid in aggregate interlock, but the large lugs were not necessary in the NSM application since the bar would be fully embedded in an epoxy filled groove. The surface pattern on the NSM titanium bar resembled threads on a threaded rod. The peaks and valleys on the "threaded" pattern were slightly rounded to minimize stress concentrations.

Instead of creating a custom deformation pattern, the stainless steel NSM bar deformations resembled typical reinforcing bar deformations. It has become increasingly common to require stainless steel reinforcing bar for projects in marine splash zones or in-water columns. Stainless steel reinforcing bars have also been used as an external retrofitting material. The stainless alloy used was Enduramet 32. The alloy was chosen for its high strength, ductility, and its work hardening characteristics. More specifically, Enduramet 32 is a "low-nickel, nitrogen strengthened austenitic stainless steel" (Carpenter Technology Corporation, 2006). The alloy is recommended for use in bridge deck repair, retaining walls, and costal infrastructure. Enduramet 32 meets or exceeds the requirements for ASTM A955 and has a nominal yield strength of 75 ksi (517 MPa). The unit weight of the stainless steel alloy is 483 lb/ft^3 (7747 kg/m^3), slightly lower than mild steel. Generally, stainless steel does not have a well-defined yield plateau. The average measured yield stress was 83 ksi (572 MPa) with 0.82% COV, the average ultimate stress was 127 ksi with 0.28% COV, and the average elongation was 49% with a 9.05% COV. The stress strain curves for both materials were created by testing three coupons of each material shown in Fig. 3.17. The coupon length was similar to the tensile tests conducted on the reinforcing steel and used a 2 in. (50.8 mm) gage length.

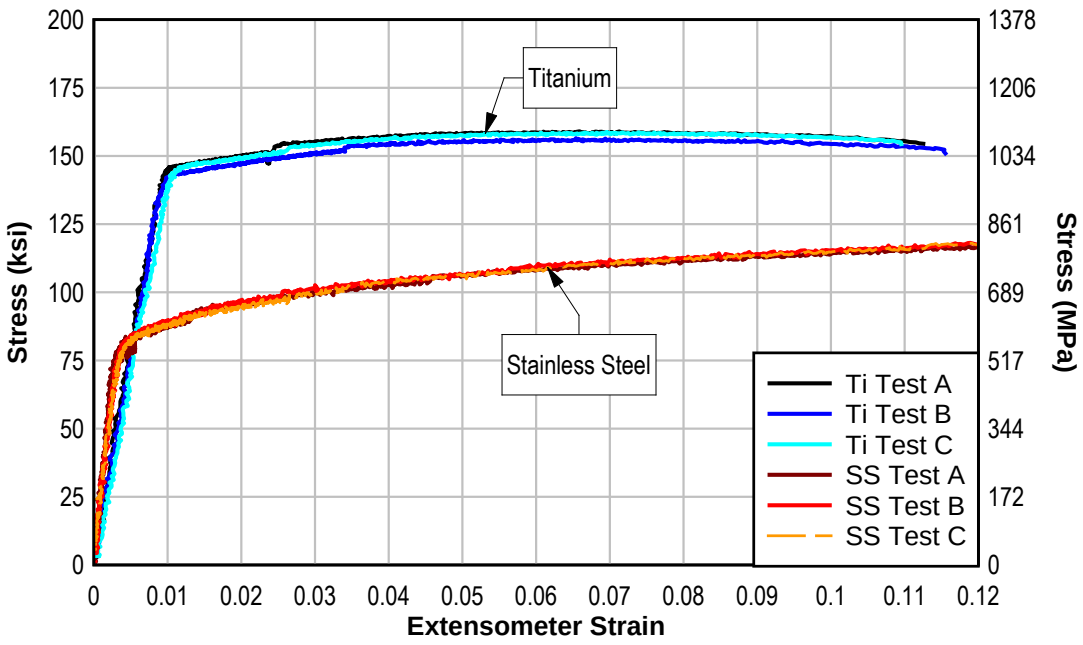

Fig. 3.16 - Stress-strain relationship for the titanium and stainless steel bars used in NSM strengthening

Both stainless steel and titanium alloys are high strength and ductile materials. Stainless steel exhibits more strain hardening before rupture than titanium. For the titanium alloy, the yield and maximum stresses were within 13 ksi (89.6 MPa) of the each other. Neither material exhibited a well-defined yield plateau.

A commercially available non-sag gel epoxy was used to bond the retrofitting materials into the grooves. It had a pot time of 15 minutes and was fully cured after seven days at a temperature of 77 °F. The material properties of the epoxy are in Table 3.6 below.

Table 3.6 - Epoxy strength data (7 day cure)

Tensile Strength (ksi) [MPa]	Elongation at Break (%)	Compressive Yield Strength (ksi) [MPa]	Bond Strength (2 day cure) (ksi) [MPa]
4 [27.6]	1	12.5 [86.2]	>2 [13.8]

3.4 Instrumentation

To collect data necessary for analysis, internal and external sensors were applied prior to testing. Data from all sensors was sampled at 5 Hz or 0.20 second intervals. Details and labeling conventions for the internal and external sensor array is described in Appendix A.

3.4.1 Internal Sensor Array

Bondable foil strain gages were used for the internal sensor array. The strain gages are general purpose linear strain gages and had 0.062 in. (1.6 mm) gage length with a 120 Ω resistance. Because of the sensitivity of the strain gages, the output of the collected data was in units of microstrain, an amplified in/in (mm/mm) value.

The steel reinforcing bars were instrumented with strain gages prior to tying the reinforcing bar cage. The process of applying a strain gage is summarized in Fig. 3.17. The bar deformations and mill scale were removed by grinding. Once smooth, the area was sanded with a fine grit sand paper. The area was cleaned using an acid and base combination as per recommendations by the strain gage manufacturer. The strain gage was adhered to the surface with cyanoacrylate glue. The strain gage was soldered to wire leads, tested for resistance, and covered with several protective layers. A water-proof electrical insulation

coating was applied first, then, a rubber mastic, and finally, aluminum tape to protect the strain gages during casting.

Fig. 3.17 – Application of strain gage on reinforcing bar

Instrumentation at each critical section included a strain gage on the hooked and cutoff reinforcing steel bars as well as the metallic NSM bars. The due to symmetry, only a quarter of the specimen required instrumentation. The locations of the longitudinal and transverse strain gages were similar to the baseline specimens to enable an accurate comparison.

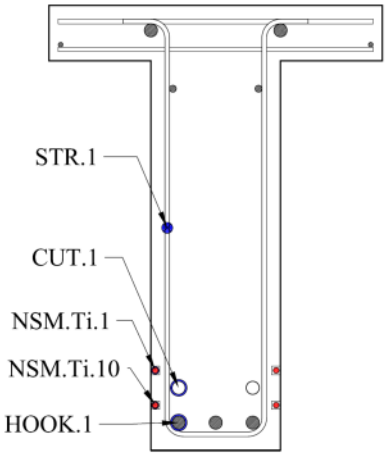

Fig. 3.18 - Typical titanium strengthened specimen cross section with labeled internal sensors

Longitudinal instrumentation was specifically focused around the termination of the cutoff bar and NSM reinforcement. At each section of interest, at least three strain gages were placed 6.5 in (165 mm) apart. A series of four strain gages along the termination of the cutoff bar was implemented to measure bond stress. In total, there were six strain gages on the cutoff bar, ten strain gages on the hook bar, ten strain gages on each titanium NSM bar, and 26 strain gages on the stainless steel NSM bars. Fig. 3.19 identifies the strain gages in their relative positions on a typical specimen.

To measure shear forces, strain gages were adhered to one leg of the transverse steel. Four stirrups intersecting the preformed diagonal crack were instrumented with strain gages for specimens T.45.Ld3(10) and T.45.Ld3(10).Ti. In specimens T.45.Ld3(6).Ti and SS, six instrumented stirrups crossed the preformed diagonal crack. After the preformed diagonal crack, the strain gages were placed mid-height on the stirrups. Specimen T.45.Ld3(10).Ti had nine stirrups instrumented and specimens T.45.Ld3(6).Ti and T.45.Ld3(6).SS had eleven stirrups instrumented.

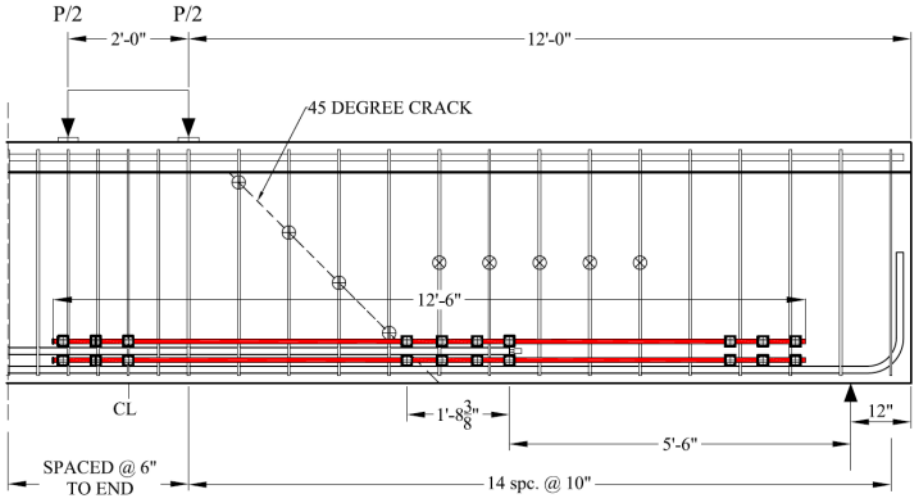

Fig. 3.19 - Typical internal sensor array

Titanium strain gages were placed at locations coincident of the cutoff and hooked bar strain gages. Both titanium bars were fully instrumented. The stainless steel bar instrumentation pattern differed due to the increased number of bars. The stainless steel reinforcing bars with the largest and smallest distance (top and bottom) from the compression zone had coincident strain gages as the hooked steel. The remaining two stainless steel bars had strain gages at the end of the bar and along the diagonal crack location. Appendix A provides supplementary information about strain gage labeling and location.

3.4.2 External Sensor Array

Three types of sensors were used to monitor the external response of the beam: string potentiometers, displacement sensors, and tilt sensors. All displacement sensors had units of inches and the tilt sensors measured in units of degrees.

The midspan displacement was monitored with two 10 in. (254 mm) stroke string potentiometers. Measuring the displacement on each side of the web enabled a calculation of average midspan displacement. Each string potentiometer was attached to a steel dowel that was epoxied into the web. Fig. 3.20 is an example of a string potentiometer measuring midspan displacement.

Support settlements were measured with two 1.5 in. (38.1 mm) displacement sensors. The sensor was clamped to a metal stand and reacted off of an aluminum angle glued to the web of the beam. Measured north and south settlements were averaged and subtracted from

the measured midspan displacement for the true midspan displacement. A picture of a typical support settlement sensor is seen on the right in Fig. 3.20 below.

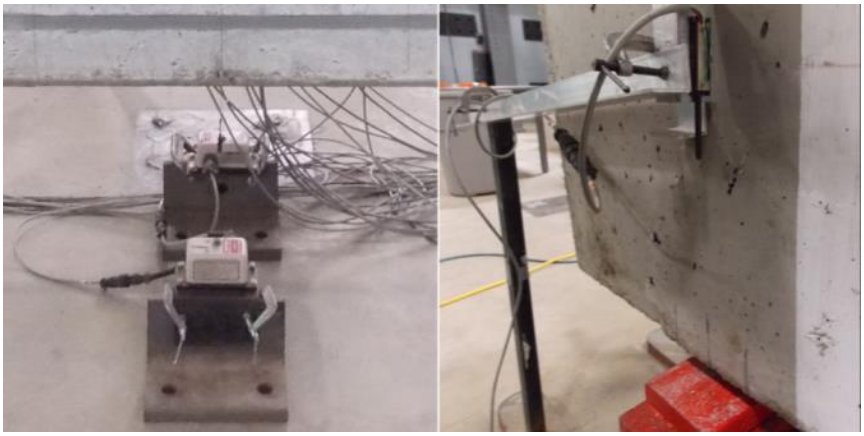

Fig. 3.20 - Midspan displacement (left), and support settlement (right)

Two 1 in. (25.4 mm) stroke displacement sensors measured the slip of the cutoff steel reinforcing bars through the concrete. In specimens T.45.Ld3(6)Ti and T.45.Ld3(6)SS a smaller, more effective way of measuring slip was devised. The left side of Fig. 3.21 illustrates measuring the reinforcing bar slip from the instrumentation box, and the right side illustrates the PVC port method. The larger block-out left the NSM bars unbonded in that region, producing localized bending of the NSM bars.

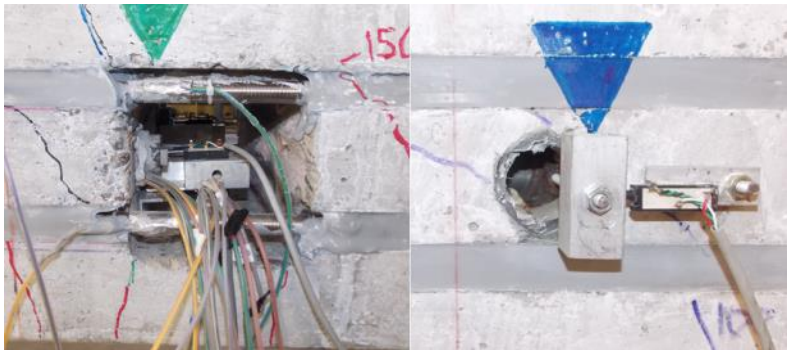

Fig. 3.21 - Slip displacement sensor configurations

Tilt sensors were attached to one side of the web over each support. The sensors measured the rotation of each side of the beam while loading. The amount of relative rotation could be used to create a moment rotation diagram.

Pairs of diagonal displacement sensors were used to measure crack growth and shear over regions of the beam. Each displacement sensor had a calibrated range of 1 in. (25.4 mm). The diagonal displacement sensors were attached to small threaded rods epoxied in the concrete web. The configuration of a typical diagonal displacement setup is illustrated in Fig. 3.22. Diagonal displacement configurations for each specimen can be found in Appendix A.

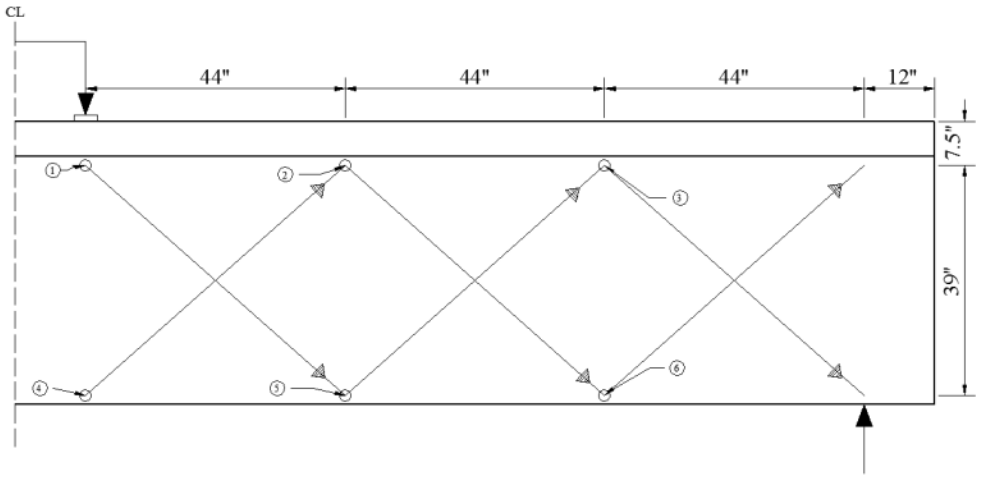

Fig. 3.22 - Typical location of diagonal displacement sensors

3.5 Test Protocols

All T-specimens were tested at the Oregon State University Structural Engineering Research Laboratory. A reaction frame was built to apply four-point loading on the specimen. The reaction frame was anchored into the strong floor and held the servo-

hydraulic load-controlled actuator. The actuator had a 500 kip (2224 kN) capacity and a 30 in. (762 mm) stroke. The simply supported T-specimens had a span length of 24 ft (7.32 m) from centerline of supports. The actuator force was distributed through a spreader beam creating a 2 ft (610 mm) constant moment region at midspan. All reaction points distributed the load from a 4 in. (101.6 mm) plate on a 2 in. (50.8 mm) diameter captive roller. Loading plates at midspan were leveled with a high strength grout. Prior to testing, the actuator was plumbed, and loading plates were shimmed if necessary. The loading setup is pictured in Fig. 3.23.

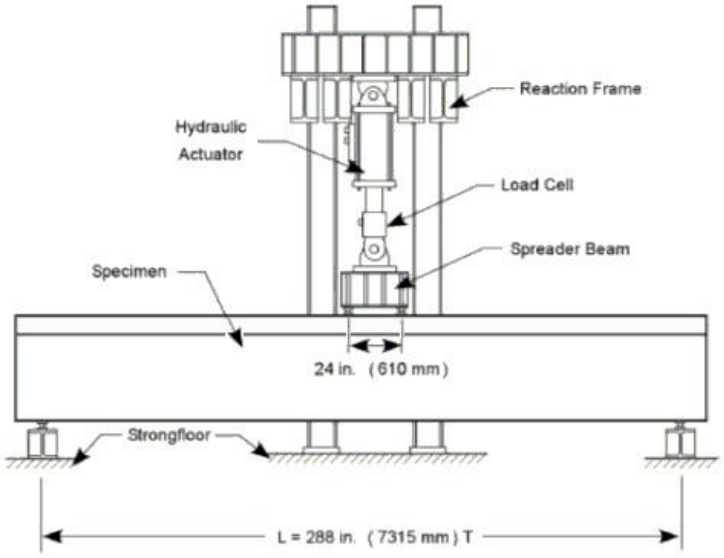

Fig. 3.23 - Test setup T-beam

The load was applied at 50 kip (222 kN) increasing increments and unloaded to 5 kips (22.2 kN) between each cycle until failure. The loading rate was pseudo static at 1 kip/sec (4.4 kN/sec) without load reversals. After reaching each target load step, the load was reduced by 25 kips (111 kN) then held to minimize creep effects while cracks were identified.

3.6 Bond Strength Study

A bond strength study was performed on the NSM reinforcing materials due to the unique characteristics of the proposed retrofitting technique. The goal of the study was to investigate the bond strength between the epoxy-bar and epoxy-concrete interfaces. Further, the study characterizes the bond along the length of the bar embedded in epoxy. Pull-out tests and hook toughness tests on the NSM titanium bars are described in a similar study by Barker (2014).

3.6.1 Bond Length Test

An adapted method of ASTM A944-10 was used to characterize the development length of titanium bars in a NSM retrofit. Six small 9x12x24 in. (229x305x610 mm) concrete blocks were built with two Gr. 60 (Gr. 420) #4 (13M) bars as the tension or flexural reinforcement. Each specimen had a saw-cut 15/16 in. (24 mm) square groove on the top of the block. Three specimens embedded the NSM material 4 in. (101.6 mm) and three specimens embedded the NSM material for 12 in. (305 mm). The concrete had a compressive strength over 4443 psi (30.6 MPa) and a tensile strength of around 389 psi (2.68 MPa).

Three displacement sensors were monitoring the elongation and slip of the NSM reinforcing bar. One was placed inside the groove to measure the free or embedded end slip of the material. Another sensor was placed at the end of the block to measure the loaded end elongation. A vertical sensor was placed at the free end of the embedded NSM bar to measure any vertical movement.

The specimens with a 12 in. (305 mm) embedment length were instrumented with three strain gages. The strain gages measured strain at 3 in. (76.2 mm), 6 in. (152.4 mm), and 9 in. (228.6 mm) from the embedded or free end of the bar. The design intent of the 12 in. embedded length was to measure the active bond length and find the real development length before the specimen failed at the concrete-epoxy interface. All instrumentation was sampled at 10 Hz.

The NSM material was epoxied into the groove and a 110 kip (489 kN) servo-hydraulic actuator pulled the NSM material (loaded end) out of the block. The loading rate was 0.002 in/sec (0.051 mm/sec) and the block reacted off of an angle bolted to the loading apparatus. Any upward eccentricity was counteracted with a tensioned plate reacting off the unloaded end of the specimen illustrated in Fig. 3.24.

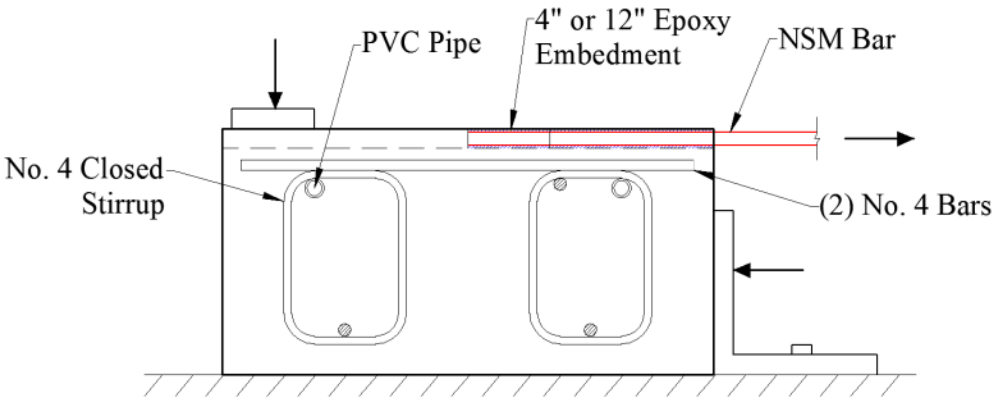

Fig. 3.24 - Typical bond strength specimen

The typical reinforcing cage is shown in Fig. 3.25, and the loading setup is pictured in Fig. 3.26.

Fig. 3.25 - Reinforcing cage for bond length specimens

Fig. 3.26 - Loading setup for bond length specimens

4 EXPERIMENTAL RESULTS

This chapter describes the experimental results of three T-specimens tested in this research program. The tested specimens were identified as T.45.Ld3(10).Ti, T.45.Ld3(6).Ti, and T.45.Ld3(6).SS and were compared to specimen T.45.Ld3(10) from Triska (2010). The reported data included the overall response, tension forces in the reinforcing steel and NSM bars, and bond stress of the full-scale specimens as well as the results of the sub-assemblage tests used to investigate bond. For common responses across the specimens, data from a typical specimen is presented. Comprehensive data sets for all specimens are contained in Appendix B for reference.

4.1 Overall Specimen Response

All NSM strengthened specimens were tested to failure and achieved greater loads than the comparable baseline specimen tested by Triska (2010). The NSM-strengthened specimens experienced ductile failures and displayed distributed cracking and signs of distress prior to failure. Specimen T.45.Ld3(10).Ti delayed the onset of an anchorage slip and specimens T.45.Ld3(6).Ti and SS eliminated anchorage driven shear-tension failure. The applied load, shear, V_{APP}, dead load shear, $V_{DL,}$ total shear, $V_{EXP,}$ midspan displacement, and observed failure crack angle are reported in Table 4.1. The reported midspan displacement corresponds to the peak load. The total shear is the applied shear from the actuator plus the dead load shear. Dead load shear was calculated from the weight of concrete acting across the failure plane.

Table 4.1- Summary of specimen capacity and midspan displacement

Specimen ID	Applied Load (kip) [MN]	Applied Shear (V_{APP}) (kip) [kN]	DL Shear (V_{DL}) (kip) [kN]	Total Shear (V_{EXP}) (kip) [kN]	Midspan Disp. (in). [cm]	Failure Crack Angle (deg.)
T.45.Ld3(10)	299.5 [1.33]	149.8 [665]	3.1 [14]	152.9 [679]	1.14 [2.9]	33
T.45.Ld3(10).Ti	392.9 [1.75]	196.5 [874]	3.5 [16]	200.0 [890]	2.11 [5.4]	33
T.45.Ld3(6).Ti	430.7 [1.92]	215.4 [958]	1.0 [4.0]	216.4 [963]	3.12 [7.9]	90
T.45.Ld3(6).SS	429.3 [1.91]	214.7 [955]	1.0 [4.0]	215.7 [959]	2.59 [6.6]	90

The titanium strengthening of specimen T.45.Ld3(10).Ti increased the load capacity by 31% and midspan ductility by 85% from the baseline specimen T.45.Ld3(10). Specimens T.45.Ld3(6).Ti and T.45.Ld3(6).SS both failed in flexure with a failure crack close to 90 degrees near midspan. Specimen T.45.Ld3(6).Ti increased the capacity by 44% and ductility by 174%, while specimen T.45.Ld3(6).SS increased the capacity by 43% and ductility by 127% compared to the un-retrofitted specimen. However, the significant increases in capacity and ductility of specimens T.45.Ld3(6).Ti and T.45.Ld3(6).SS was partially due to the increased shear capacity.

4.1.1 Load-Deformation Response

The load and deformation response describes the overall behavior of the specimens. Load deformation responses for the NSM retrofitted and baseline specimens are shown in Fig. 4.1. Each specimen was loaded in 50 kip increments, unloaded, and then preceded to the next load step until eventual failure. If the specimen was close to failure the load cycle was extended until the maximum capacity was reached.

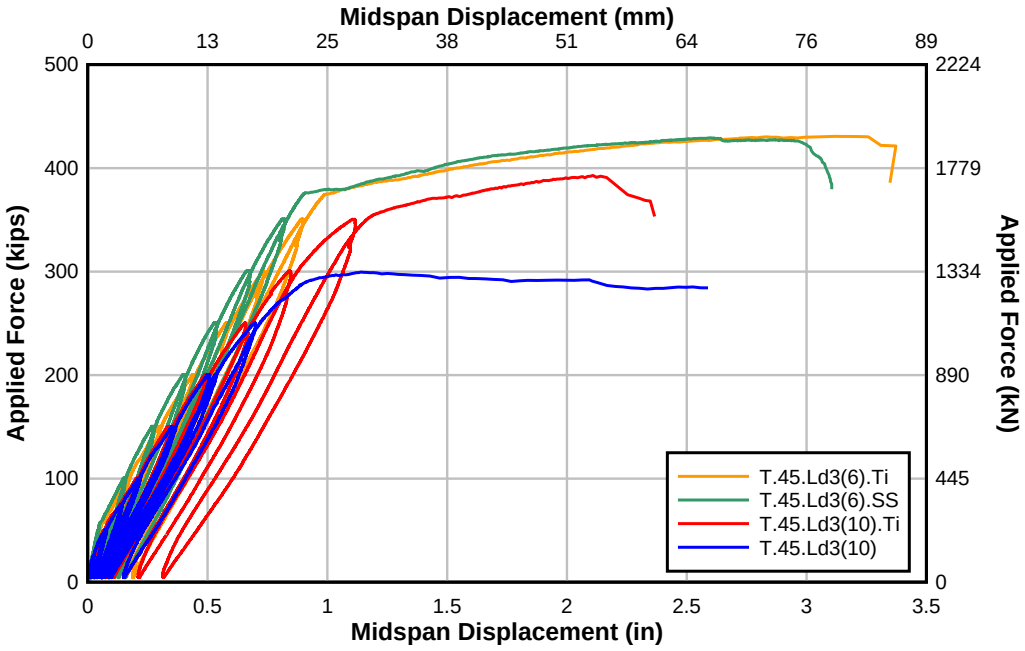

Fig. 4.1 – Overall load-displacement response at midspan for NSM retrofitted specimens and comparative baseline specimen

As illustrated in Fig. 4.1, the baseline specimen demonstrated significant ductility from a pull-out anchorage failure of the cutoff steel reinforcing bars. Specimens T.45.Ld3(10) and T.45.Ld3(10).Ti have a similar stiffness before the baseline specimen experienced an anchorage failure at a load of 299.5 kips (1330 kN). The NSM titanium retrofitted specimen, T.45.Ld3(10).Ti, experienced a shear-tension failure at a peak load of 392.9 kips (1750 kN), an increase of 93.4 kips (415 kN).

Specimens T.45.Ld3(6).Ti and T.45.Ld3(6).SS failed in flexure and had very similar load deformation plots. Both specimens used a 6 in. (152 mm) spacing for shear reinforcement and achieved larger loads and provided more ductility than the specimens with the 10 in. (254 mm) stirrup spacing. Specimen T.45.Ld3(6).SS had a stiffer ascending branch than

T.45.Ld3(6).Ti due to the higher modulus of elasticity of the stainless steel NSM bars and the amount of stainless steel reinforcing bars compared to the NSM titanium alloy specimens. After the specimen becomes inelastic, at a load of 374 kips (1664 kN), T.45.Ld3(6).Ti and T.45.Ld3(6).SS have a similar load deformation responses and fail in flexure just after the termination of the NSM reinforcement at midspan. Specimen T.45.Ld3(6).Ti provided the largest overall deformation capacity.

4.1.2 Crack Mapping

Concrete crack initiation and propagation was monitored throughout the test. After each load cycle, the load was decreased by 25 kips (111 kN) and then held to minimize creep effects. During this time, the specimens were inspected and cracks were measured and highlighted. Digital pictures were taken at each load step to record the cracked condition. The crack patterns at failure are shown in Fig. 4.2 for each specimen.

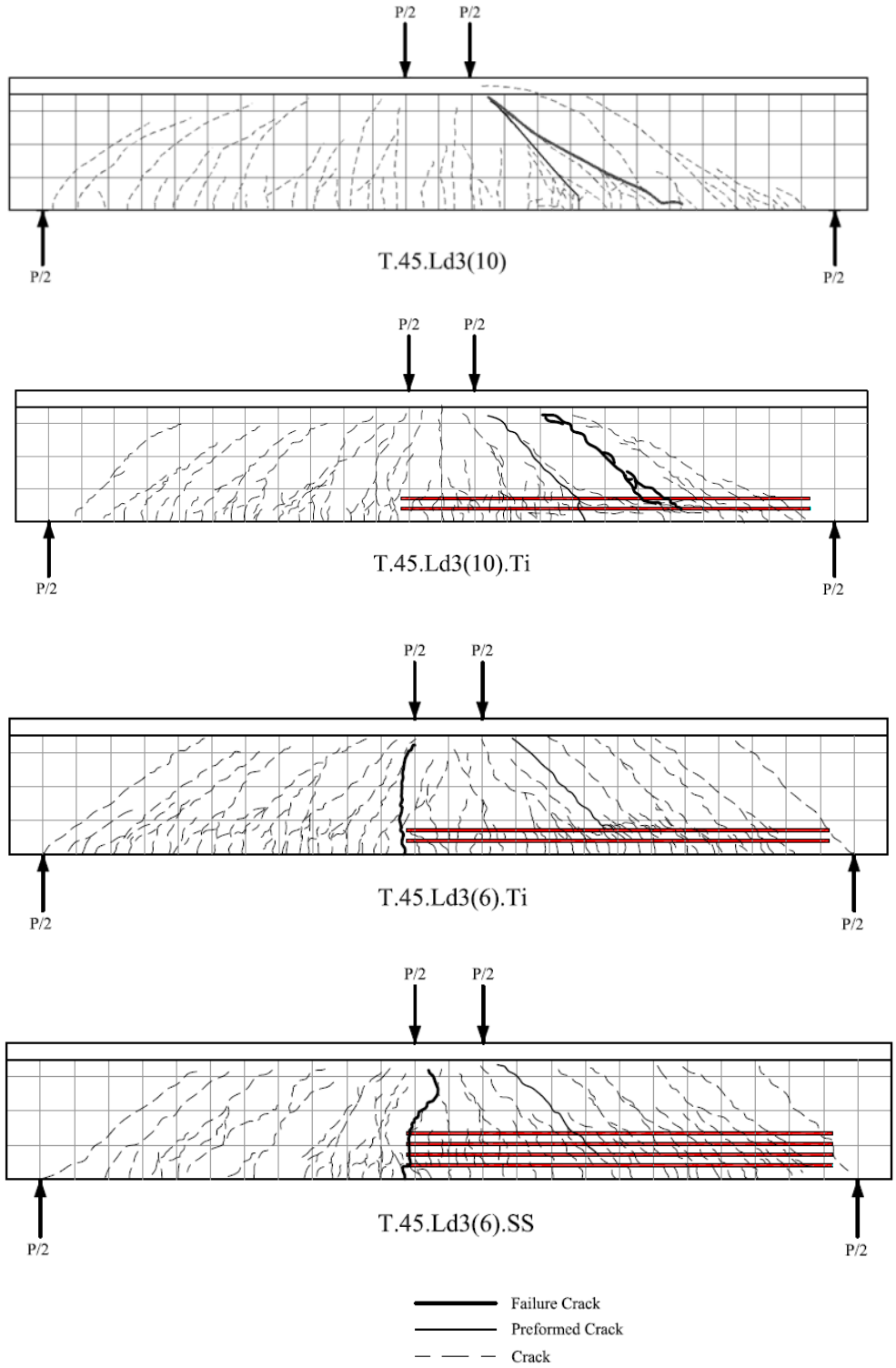

Fig. 4.2 - Crack patterns for T-specimens at failure (specimen T.45.Ld3(10) from Triska (2010))

Specimen T.45.Ld3(10) and the corresponding NSM-titanium retrofitted counterpart, T.45.Ld3(10).Ti, failed in a similar manner with the failure crack extending from the edge of the loading plate to the end of the cutoff reinforcing steel bars. Specimens T.45.Ld3(6).Ti and SS shifted the failure location to near midspan as discussed previously. The failure crack for T.45.Ld3(6).Ti and SS initiated just outside the constant moment region, traveled around the end of the hooks then curved towards the middle of the constant moment region. For simplification, the failure crack of the specimens with 6 in. (152.4 mm) stirrup spacing was estimated to be 90°. Chevron cracks, typical of anchorage failures, appeared near failure in specimens T.45.Ld3(10), T.45.Ld3(10).Ti, and T.45.Ld3(6).Ti. In all cases, the preformed diagonal crack did not dictate the failure location. The NSM retrofitted specimens displayed distributed cracking over the length of the specimens. Vertical cracks did not propagate through the epoxy until near failure loads and longitudinal splitting cracks in the epoxy were seen only at failure. The widespread extent of macro cracking in the concrete and around the epoxy provided visual indication of distress prior to failure. The flexural failures led directly to concrete crushing near the loading plates. Digital photos of each specimen after failure and details are shown in Fig. 4.3 through Fig. 4.5.

a)

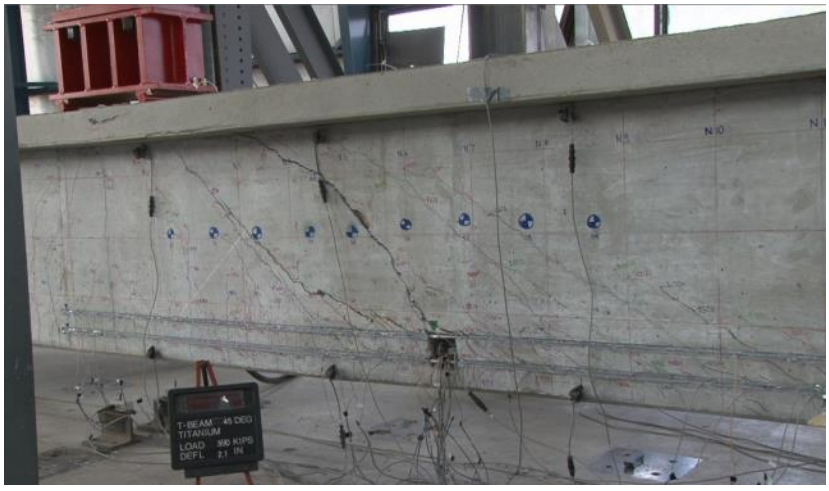

b)

c)

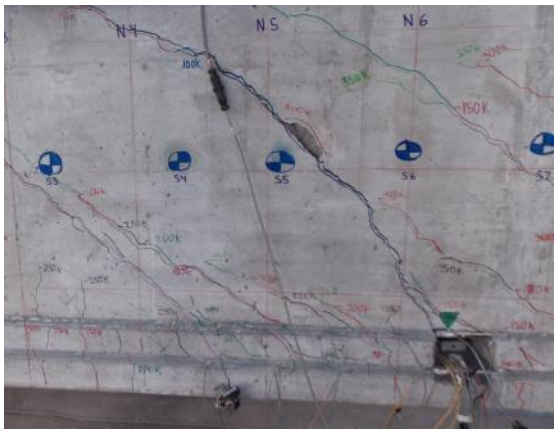

Fig. 4.3 - Specimen T.45.Ld3(10) at failure a) front, b) back, and d) detail of cutoff bar slip

a) 

b) 

c) 

Fig. 4.4 - Specimen T.45.Ld3(6).Ti at failure; a) front, b) back,
c) detail of cutoff bar slip

a) 

b) 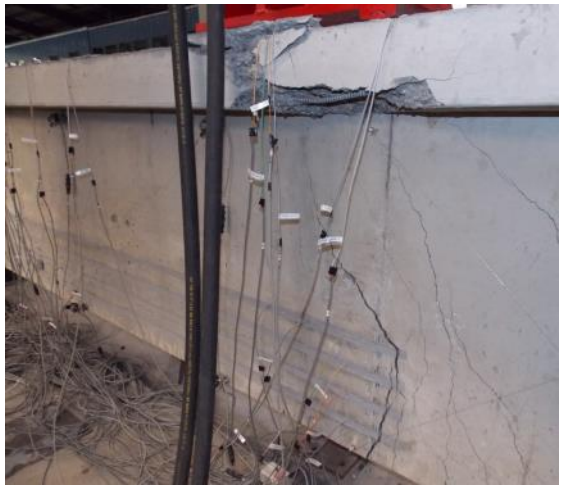

c) 

Fig. 4.5 - Specimen T.45.Ld3(6).SS at failure; a) front, b) back, and e) detail of flexural failure

4.1.3 Anchorage Slip Response

As the applied load increased, the cutoff steel reinforcing bars eventually exhibited some slip, regardless of the eventual failure mode or location. Cutoff steel reinforcing bar slip was measured by displacement sensors located near the end of the cutoff reinforcing bar and measured slip of the bar relative to the concrete surface. In specimens T.45.Ld3(6).Ti and SS the sensor was attached to the concrete adjacent to a slip port; because of this, cracking adjacent to the cutoff bar may have influenced the slip measurement (by incorporating crack opening into the slip measurement). To resolve this issue, the diagonal sensors in the zone of the slip gages were transformed into longitudinal deformation following the process described by Dawson (2008). A ratio of cracks intersecting the terminating bar over the total cracks was used to scale a more accurate crack width affecting the cutoff reinforcing bar slip. The resulting crack openings were approximately 1/3 of the measured end slip in specimen T.45.Ld3(6).Ti, as shown in Fig. 4.6.

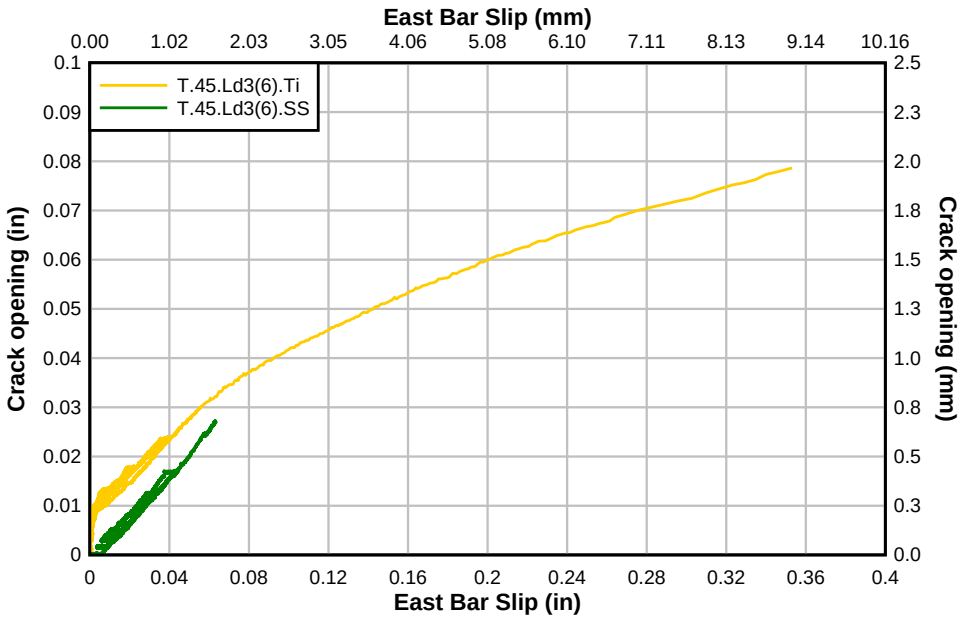

Fig. 4.6 - Crack width and propagation with slip

The slip sensor for specimen T.45.Ld3(10).Ti was mounted on the concrete surface upon which the cutoff steel reinforcing bar protrudes so cracking did not affect the measurement.

The slip of the west bar in each specimen is shown relative to the applied actuator force in Fig. 4.7. As the load increased, the slip increased. The responses are similar to the overall load-midspan displacement responses. The load-slip curves were generally elastic and had minor residual slip after unloading at each load step. As the applied load approached failure, slip increased larger residual slips were observed.

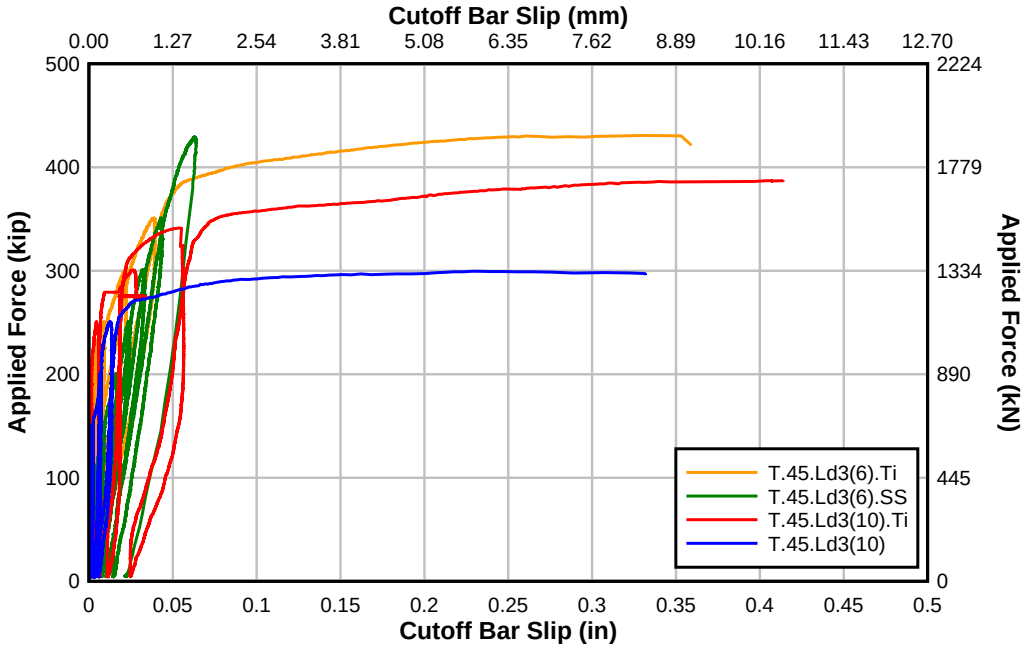

Fig. 4.7 - Anchorage slip response of specimens

Since the cutoff reinforcing steel bars were not anchored and detailed to modern engineering design practice, all specimens experienced some degree of anchorage slip. However, only specimens T.45.Ld3(10) and T.45.Ld3(10).Ti failed from a mode

dependent on the inadequate anchorage or the cutoff reinforcing steel. The titanium alloy and stainless steel NSM bars effectively increased the capacity and delayed loss of anchorage for the cutoff reinforcing steel bars. Specimen T.45.Ld3(6).SS had a similar overall load-displacement response as T.45.Ld3(6).Ti, but experienced smaller slip deformations at the cutoff reinforcing steel bar. The reduction in slip exhibited by specimen T.45.Ld3(6).SS was attributed to increased stiffness of the NSM stainless steel bars, which attracted additional force. During the elastic phase of testing, both titanium specimens had similar cutoff bar slip responses and delayed the slip of the cutoff reinforcing steel bars until higher loads were achieved. The slip response for specimen T.45.Ld3(10).Ti was observed to soften after the 340 kip (1512 kN) load cycle. Table 4.2 shows the slip magnitude of the cutoff reinforcing steel bars at the maximum recorded loads shown in Fig. 4.7.

Table 4.2 - West cutoff bar slip at maximum applied load

Specimen	Slip (in) [mm]	Load (kip) [kN]
T.45.Ld3(10)	0.229 [5.81]	299.5 [1330]
T.45.Ld3(10).Ti	0.412 [10.47]	387.6 [1720]
T.45.Ld3(6).Ti	0.329 [8.36]	430.7 [1920]
T.45.Ld3(6).SS	0.063 [1.60]	429.3 [1910]

4.1.4 Slip Strain Behavior

Slip strain responses were created for the cutoff steel reinforcing steel bars to characterize anchorage and development. Changes in strain along the cutoff bar, specifically from the end of the bar to the preformed diagonal crack, indicated how quickly the #11 (36M) bar

developed stress. The cutoff reinforcing steel bar slip reduced significantly between the 45^{o} performed diagonal crack and midspan of the specimens with NSM materials. Increases in bar strain indicate that the steel reinforcing bar is becoming fully anchored. Locations along the span designated as “Cut 4,” “Cut 5,” and “Cut 6” corresponded to the intersection of the preformed diagonal crack, and 7 (178 mm) and 14 in. (356 mm) from the crack towards the end of the cutoff reinforcing steel bar. The measured slip strain response of the NSM strengthened T-specimens are shown in Fig. 4.8 through Fig. 4.10

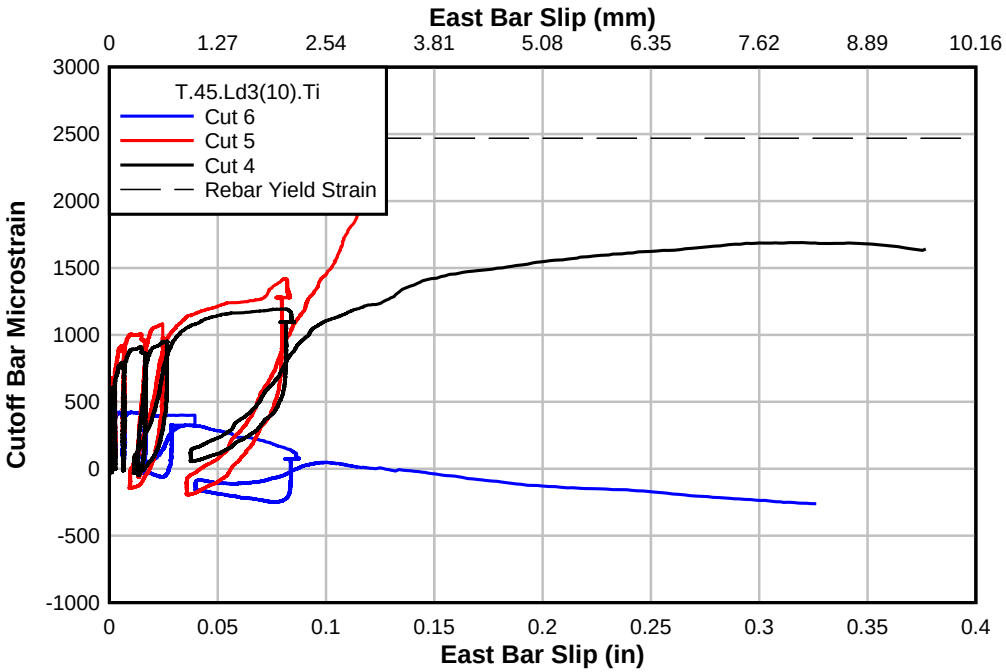

Fig. 4.8 - T.45.Ld3(10).Ti cutoff reinforcing steel bar strain vs slip

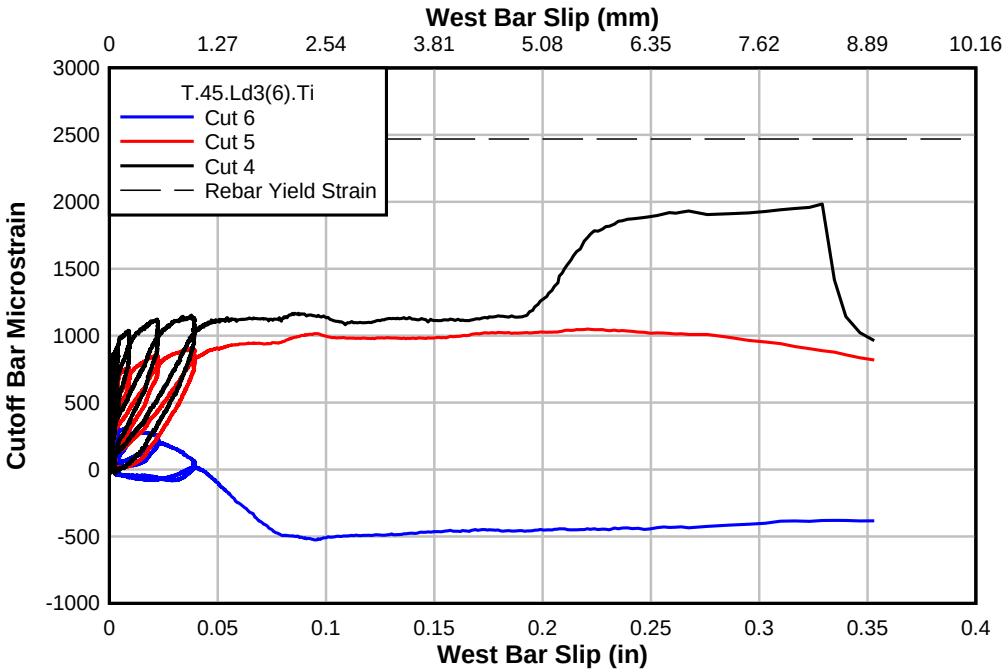

Fig. 4.9 - T.45.Ld3(6).Ti cutoff reinforcing steel bar strain vs slip

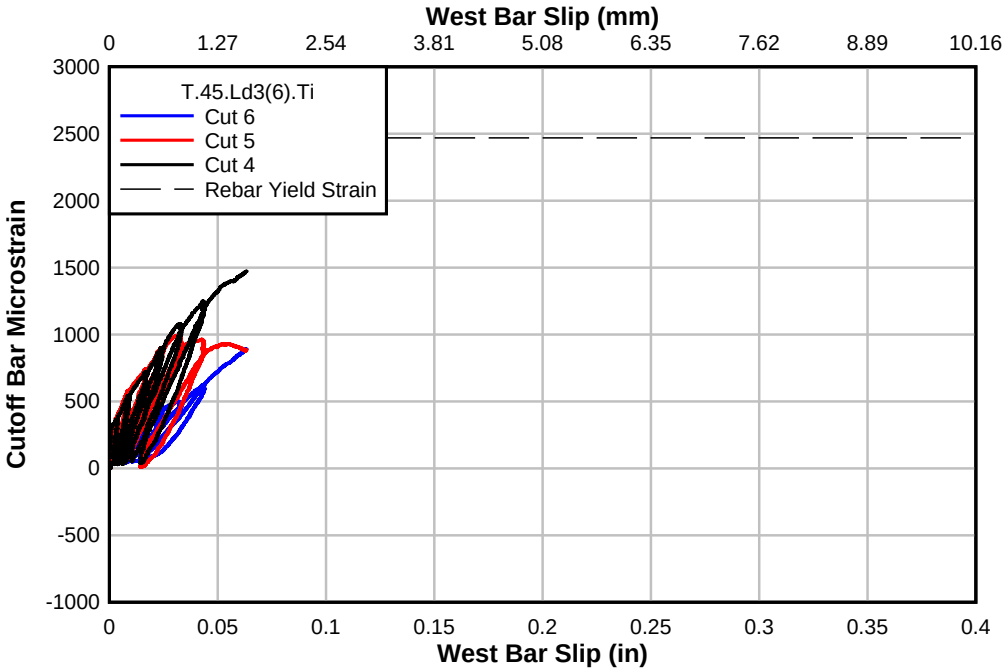

Fig. 4.10 - T.45.Ld3(6).SS cutoff reinforcing steel bar strain vs slip

In specimen T.45.Ld3(10).Ti and T.45.Ld3(6).Ti the strain decreased at “Cut 6” due to loss of bond in that location. This limited the strains at “Cut 4” and “Cut 5.” The specimens strengthened with NSM-titanium alloy bars had several cracks intersect the bar between strain gages at “Cut 5” and “Cut 4.” This cracking created an unbonded length producing similar strains between “Cut 4” and “Cut 5.”

The stainless steel NSM specimen, T.45.Ld3(6).SS exhibited less cutoff reinforcing steel bar slip than the other specimens. The strains were also seen to increase farther away from the termination of the cutoff reinforcing steel bar for this specimen.

For all specimens, “Cut 6” had small strains, and “Cuts 4” and “5” had an average value of 1000 microstrain. This means that the stress in the cutoff reinforcing steel bar was approximately 29 ksi (200 MPa), almost half of the nominal yield stress just 14 in. (356 mm) from the end of the bar. Consequently, the development length of a Gr. 60 (Gr. 420) #11 (M36) bar may be closer to approximately 30 in. (762 mm), much smaller than the 61.2 in. (1554 mm) expected value from ACI 318.

4.2 Material Strains

The instrumentation plan allowed monitoring of strains in different reinforcing bars on one quarter of the T-specimen. The instrumented bars included the cutoff and hooked reinforcing steel bars and NSM bars. This section reports the strain responses for each instrumented bar and cross section for specimen T.45.Ld3(6).Ti. All other specimen plots can be found in Appendix B.

In some cases, the instrumented bar displayed negative strain values. Negative strain values could be caused by several behaviors. As the steel reinforcing bar slips through the concrete, localized bending occurs, possibly creating negative strains. Strain reversals (decreasing magnitude of strains) were also observed due to the slip of the cutoff steel reinforcing bars. The placement of the strain gage on the flexural compression side of the reinforcing bars could have contributed to the negative strain readings especially in the case of NSM bars.

In design and analysis of a beam, strain compatibility is generally assumed. The experimental results showed that the internal steel reinforcing bars and NSM bar strains were compatible until concrete cracking and cutoff bar slip occurred. At higher loads strains in the different reinforcing bars were not fully compatible. Detailed data on strain compatibility is provided in Appendix D.

4.2.1 Comparative Material Strains

Fig. 4.13 through Fig. 4.16 show the individual material strains for specimen T.45.Ld3(6).Ti. The yield strain of each material is displayed on each plot for reference. Inconsistent initial strain values were due to noise in the instrumentation.

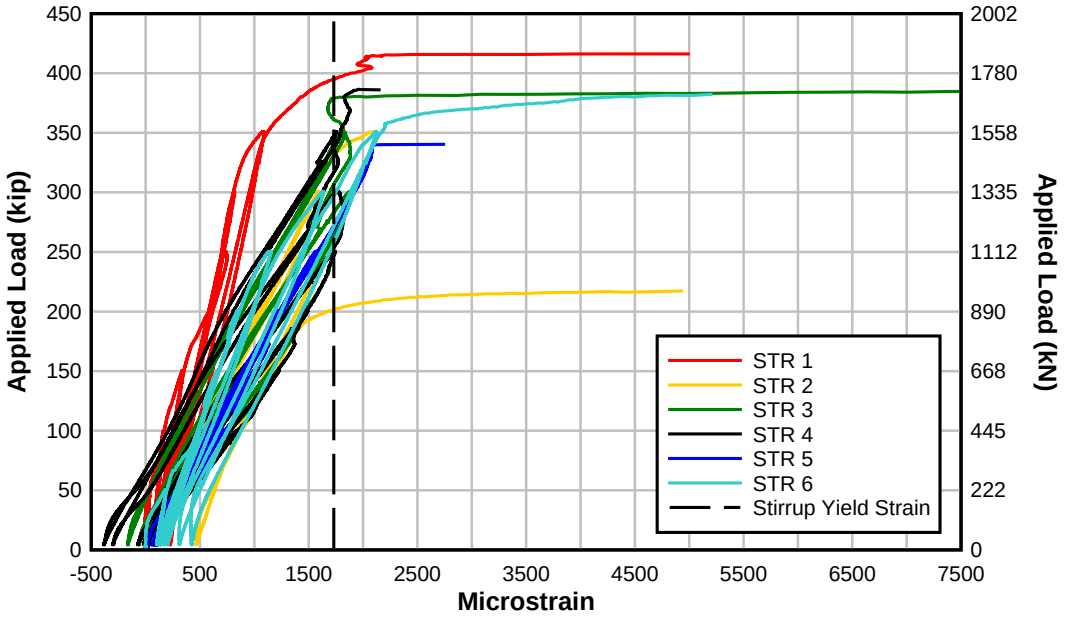

Fig. 4.11 - Stirrup strains along the preformed diagonal crack on specimen T.45.Ld3(6).Ti

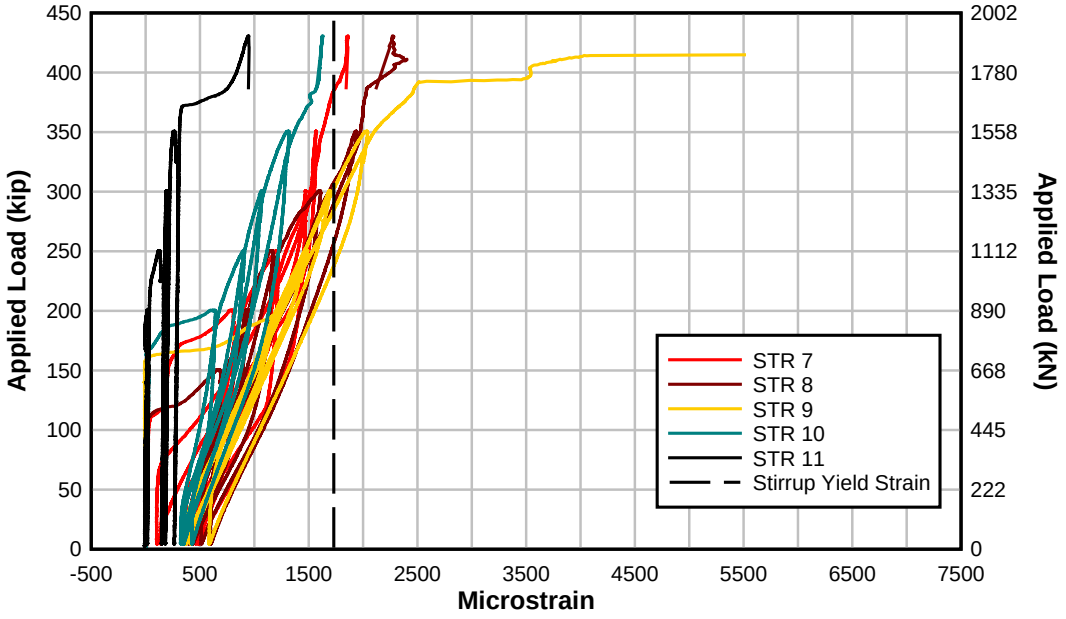

Fig. 4.12 - Strain in stirrups at mid-height in specimen T.45.Ld3(6).Ti

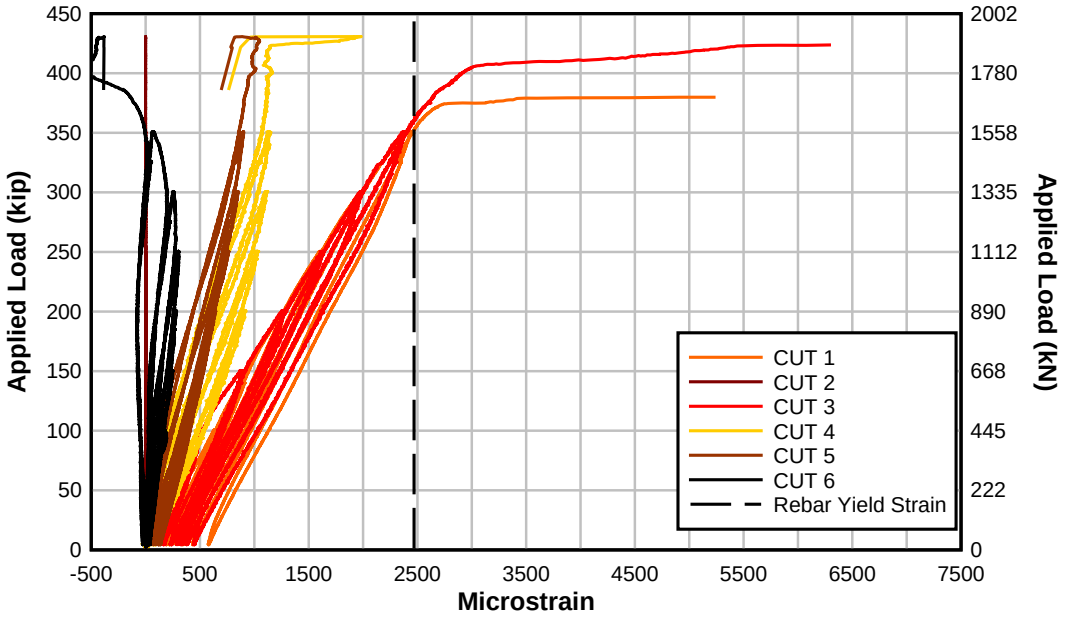

Fig. 4.13 - Strain in cutoff reinforcing steel bar in all locations on specimen T.45.Ld3(6).Ti

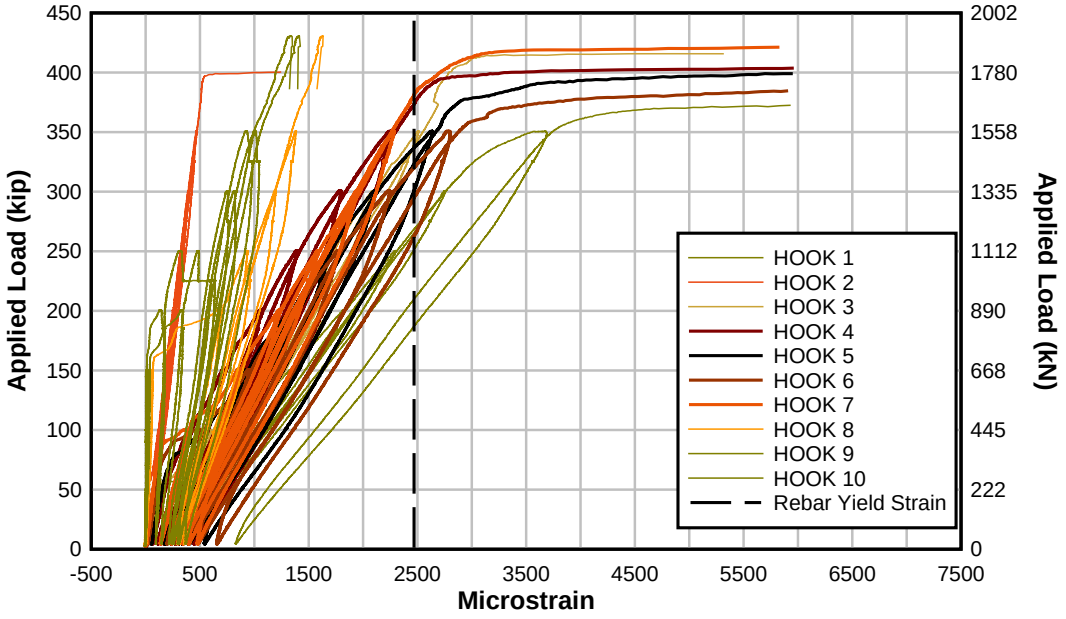

Fig. 4.14 - Strain in hooked reinforcing steel bar in all locations on specimen T.45.Ld3(6).Ti

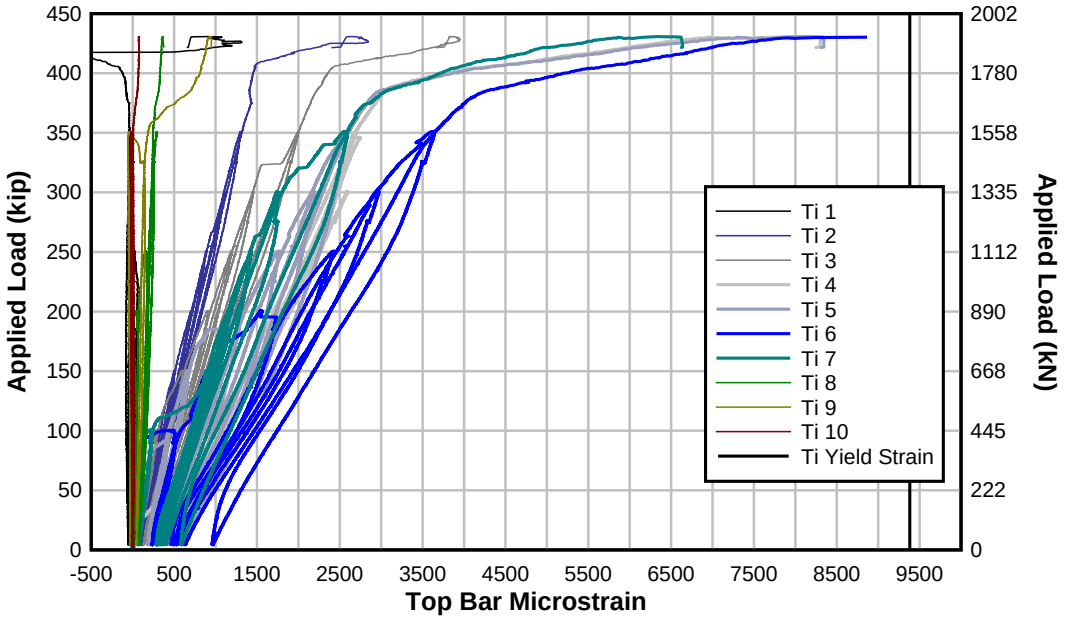

Fig. 4.15 - Strain in upper NSM titanium alloy bar in all locations of specimen T.45.Ld3(6).Ti

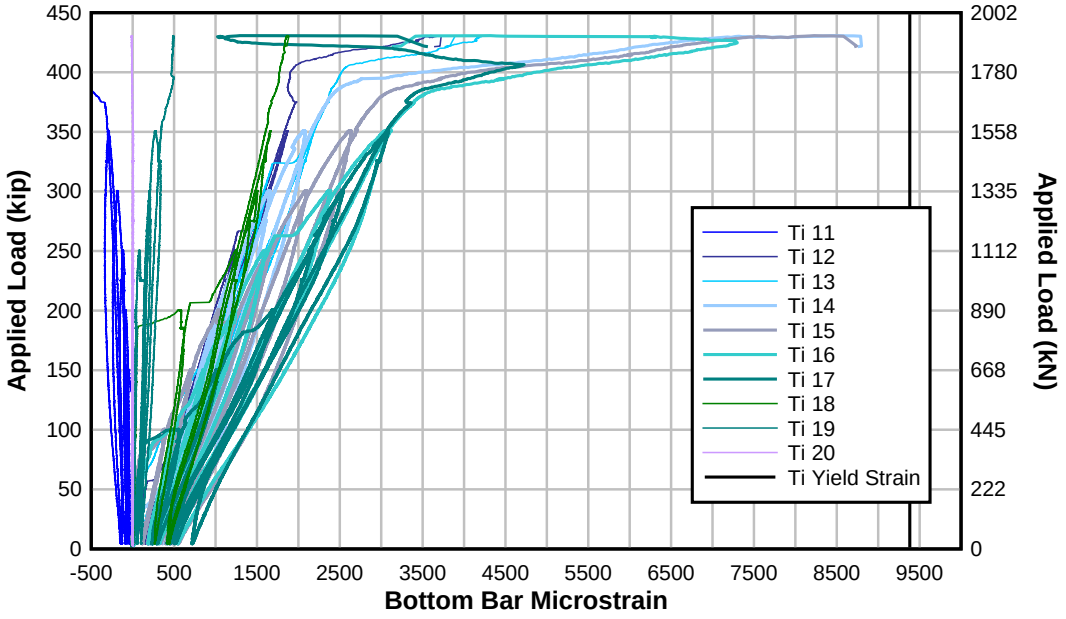

Fig. 4.16 - Strain in lower NSM titanium alloy bar in all locations of specimen T.45.Ld3(6).Ti

Stirrups crossing the diagonal crack reached yield and all but one of the mid-height stirrups yielded in specimen T.45.Ld3(6).Ti. Furthermore, two of the six locations along the cutoff reinforcing steel bar reached yield prior to failure and six of the ten locations on the hooked reinforcing steel bar reached yield prior to failure in specimen T.45.Ld3(6).Ti. The measured strains in the NSM titanium alloy bars were just below yield and may have achieved the yield strain if the strain gages were not damaged. In many cases, the strain gage was damaged prior to specimen failure and result in lower strain values.

4.2.2 Strains at Cross Sections Along the Length

Hook and cutoff steel reinforcing bars, and NSM bar strains were plotted at each instrumented cross section. This comparison illustrates the interaction between the NSM bar and developing cutoff steel reinforcing bar. The plots in this discussion focus on the critical section of T.45.Ld3(6).Ti with the general location identified in Fig. 4.17.

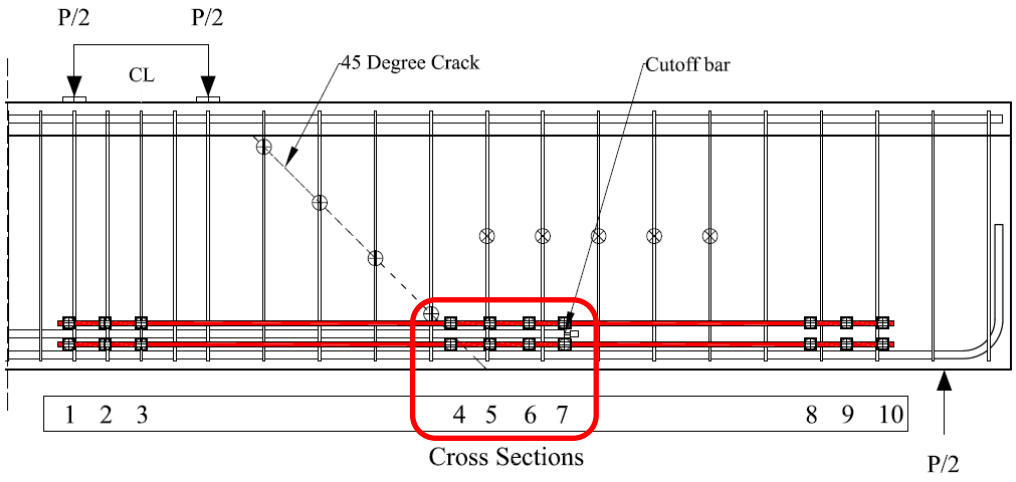

Fig. 4.17 - Labeling convention of cross sections in typical T-specimen

Fig. 4.18 through Fig. 4.21 show critical sections 4 through 7, respectively. Yield strain for the longitudinal reinforcing bars and the NSM titanium alloy bars are shown for reference in the black dashed and solid line.

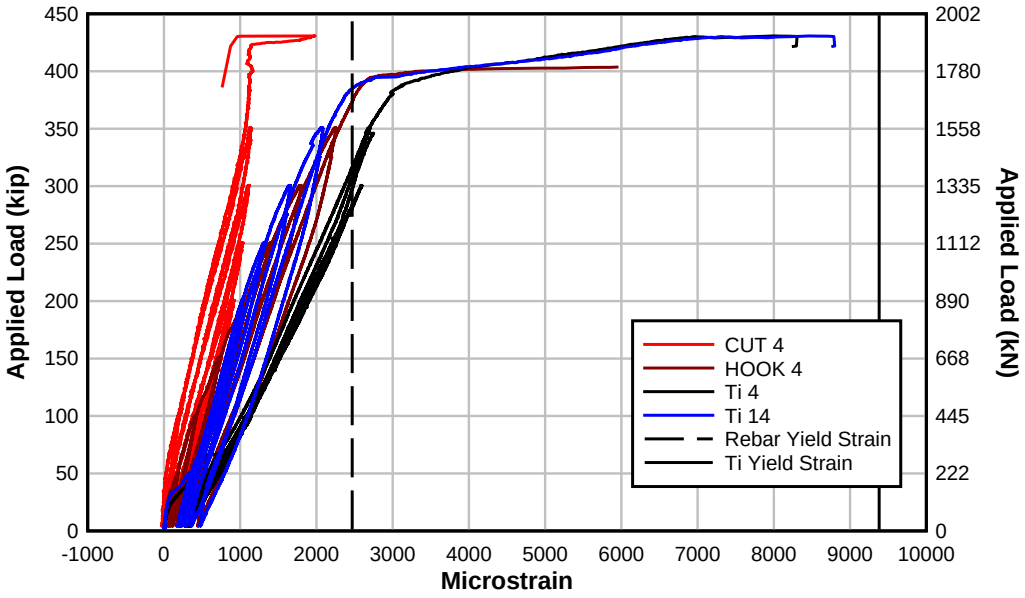

Fig. 4.18 – T.45.Ld3(6).Ti section 4 (at preformed diagonal crack) strain

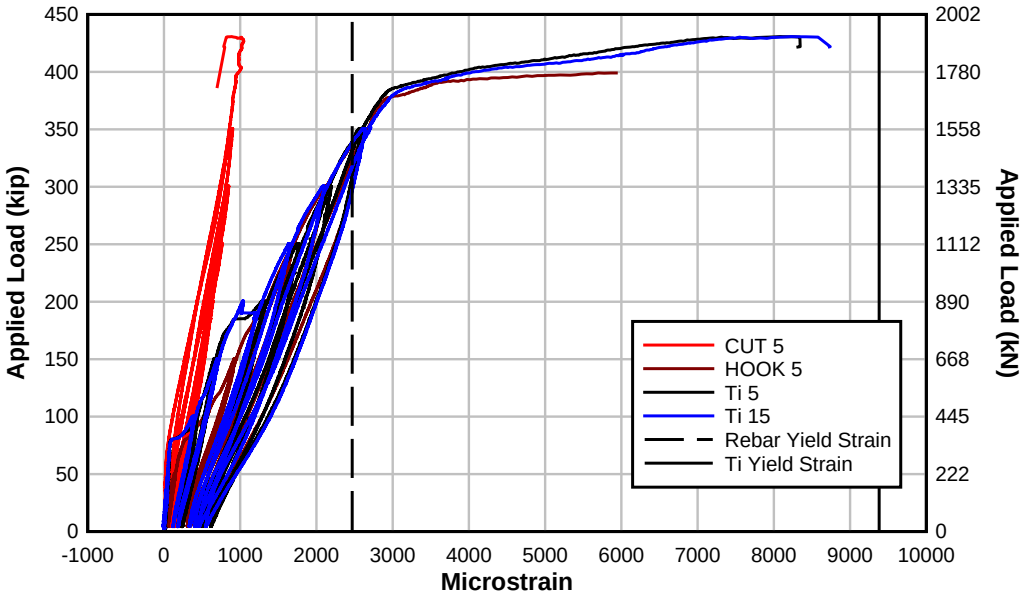

Fig. 4.19 - T.45.Ld3(6).Ti section 5 strain

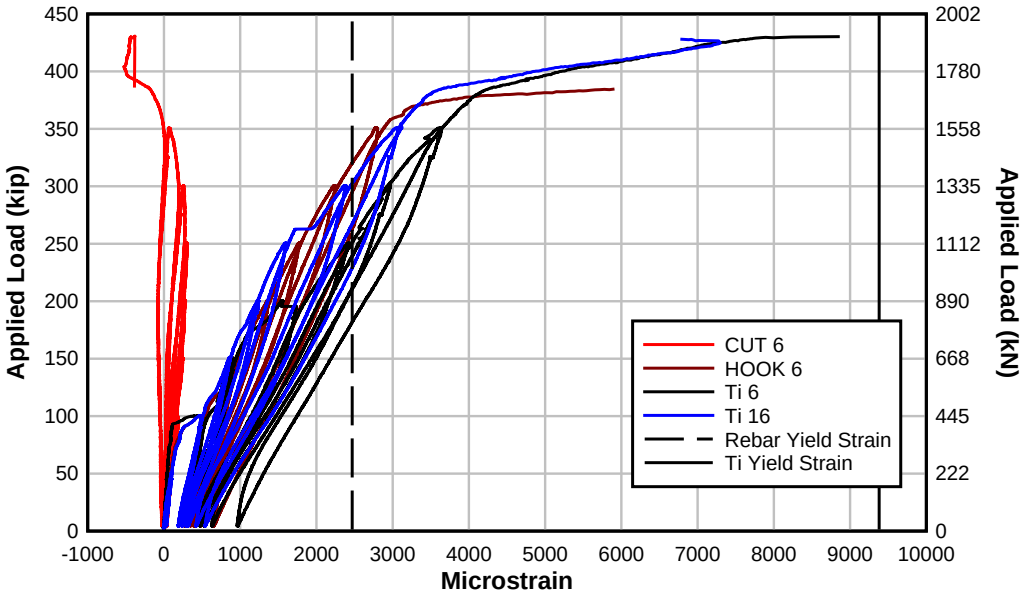

Fig. 4.20 - T.45.Ld3(6).Ti section 6 strain

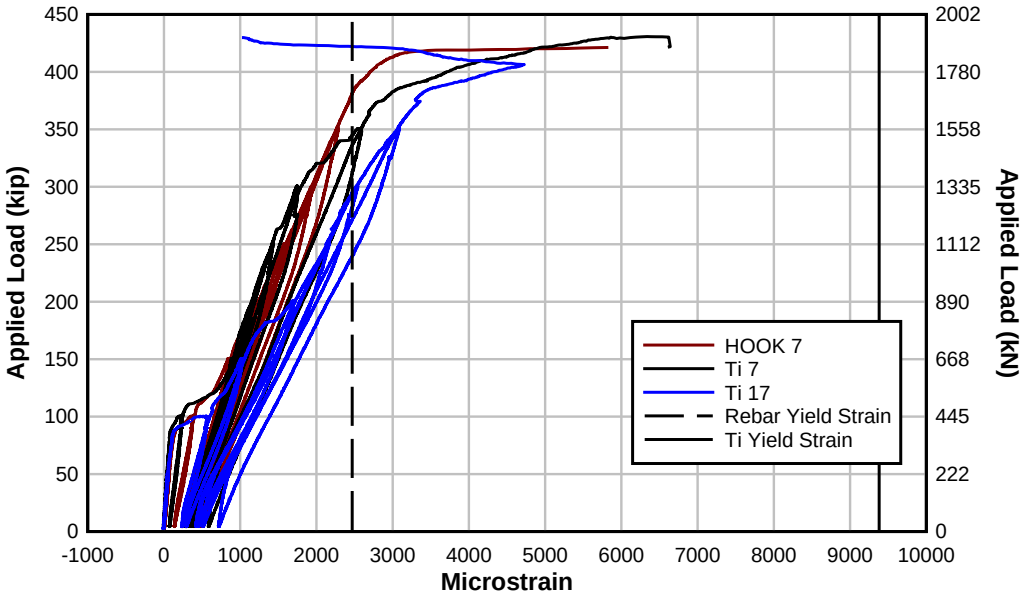

Fig. 4.21 - T.45.Ld3(6).Ti section 7 (end of cutoff) strain

All materials have similar strain magnitudes (strain compatibility) until the second load interval which produced concrete cracking. After several load cycles, strain reversal was observed in the cutoff steel reinforcing bar which indicated slip. As discussed in section *4.1.4 Slip-Strain Behavior*, the cutoff reinforcing steel bars experienced around 1000 microstrain at section 4 and 5. This shows that the bar is at approximately half of the yield strain. In sections 4, 5, 6, and 7 the hooked reinforcing steel bars were yielding and contributed the majority of the flexural tension capacity at that point. While the strains in the NSM titanium alloy bars track with the hooked reinforcing steel, the force carried by the NSM titanium alloy bars is about half that of the reinforcing steel due to the lower MOE of titanium. Specimen T.45.Ld3(6).Ti did not fail in diagonal tension. The NSM titanium alloy bars did not exhibit yielding at the strain gage locations but, may have reached yield locally, at crack locations, or just prior to failure. Slip of the cutoff

reinforcing steel bars created abrupt shifts in strain which was characterized by horizontal jumps in the measured response.

4.3 Tensile Capacity of Reinforcing Steel and NSM Bars

To determine if an anchorage failure is likely to occur, the tensile capacity in the reinforcing steel and NSM bars must be compared to the tensile demand at that section. The NSM retrofit design was based on increasing the available tensile capacity over the length of the specimen where demands exceeded the capacity. This section presents the measured flexural tension forces in the reinforcing steel and NSM bars at each instrumented section of the specimen.

Strains measured in the reinforcing steel and NSM materials were transformed into the experimental tensile force in each bar, T_{exp}, as:

$$T_{exp} = A_x E_x \varepsilon_x \quad [0.1]$$

where A_x is the bar cross sectional area, E_x is the material modulus of elasticity, and ε_x is the measured strain in the bar. The individual bar forces in the hook and cutoff reinforcing steel and the NSM bars were multiplied by the number of similar bars and summed into the total flexural tension force.

4.3.1 Experimental Tension forces along the specimen

Tensile forces were calculated at ten instrumented sections.

Fig. 4.22 will serve as a reference to section location. The intersection of the preformed diagonal crack and reinforcing steel is at section 4, and the end of the cutoff bar is at section 7.

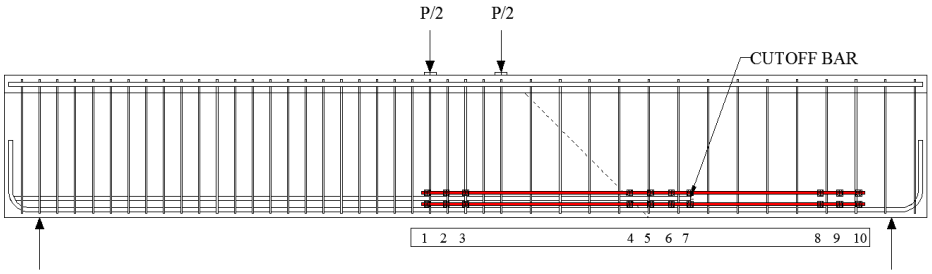

Fig. 4.22 - Instrumentation reference diagram sections 1-10

Tensile forces at 50 or 100 kip increments are presented in the figures. Strains were bounded by yield and zero. Fig. 4.23 presents the tensile forces in the reinforcing steel for the control specimen reported by Triska (2010). Only the critical section around the termination of the cutoff reinforcing bar was instrumented. The large spike in the tensile force at the peak load was omitted due to uncertainties in strain gage measurements.

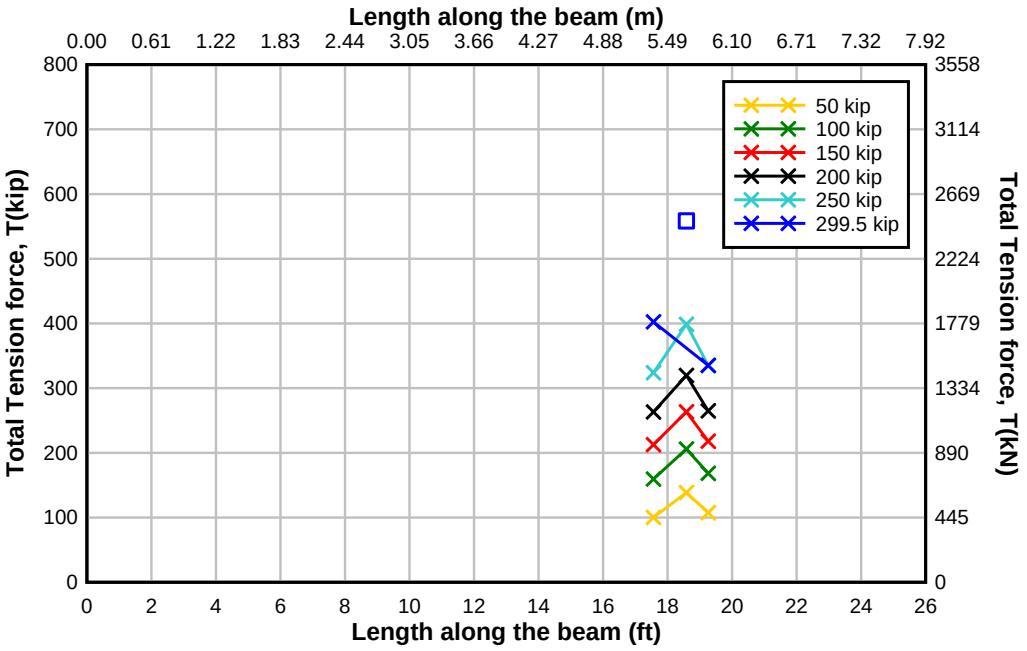

Fig. 4.23 - T.45.Ld3(10) Experimental tension force along length of specimen

Fig. 4.24 through Fig. 4.26 shows the total tension force in the reinforcing steel and NSM materials for the strengthened specimens. Some strain gages were damaged prior to achieving the peak load, creating abnormally low tensile forces that were not possible to maintain equilibrium in the section. The outlier data points were omitted from the curve but are shown in square boxes.

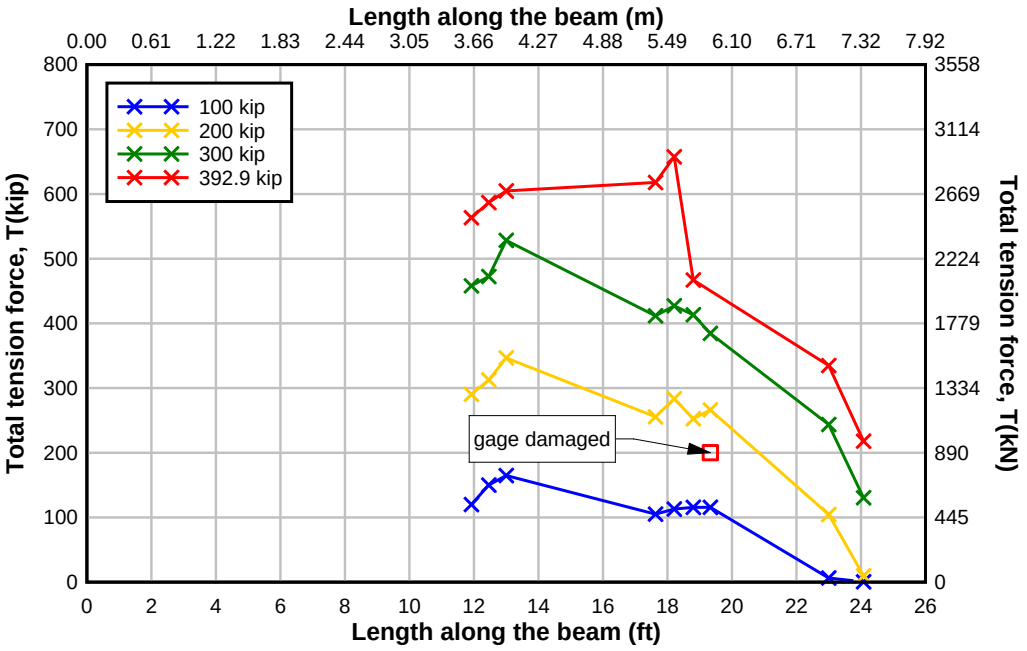

Fig. 4.24 - T.45.Ld3(10).Ti Experimental tension force along length of specimen

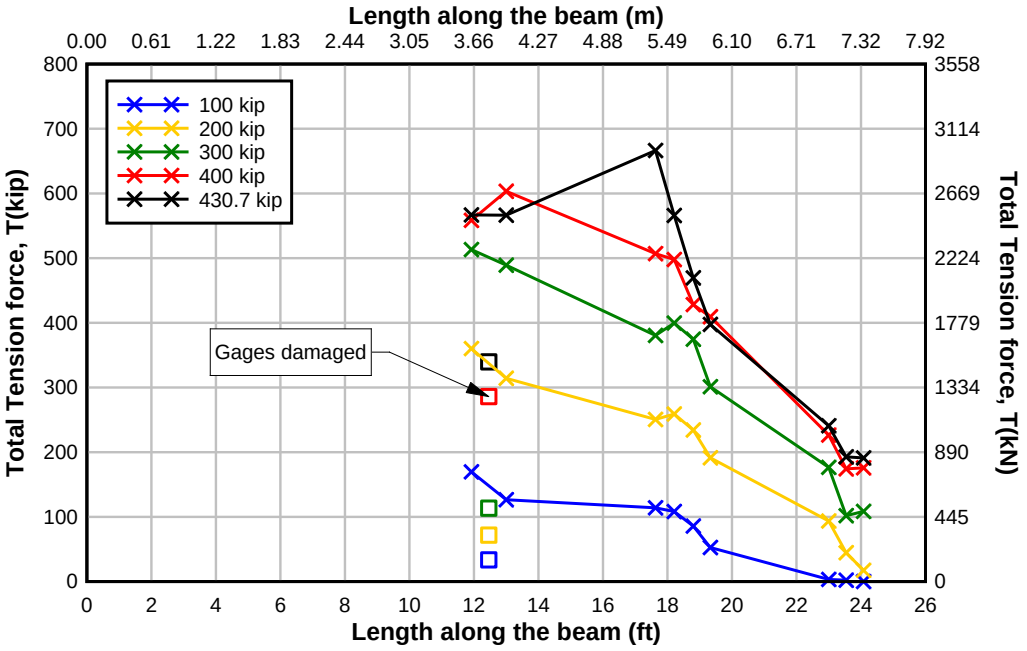

Fig. 4.25 - T.45.Ld3(6).Ti Experimental tension force along length of specimen

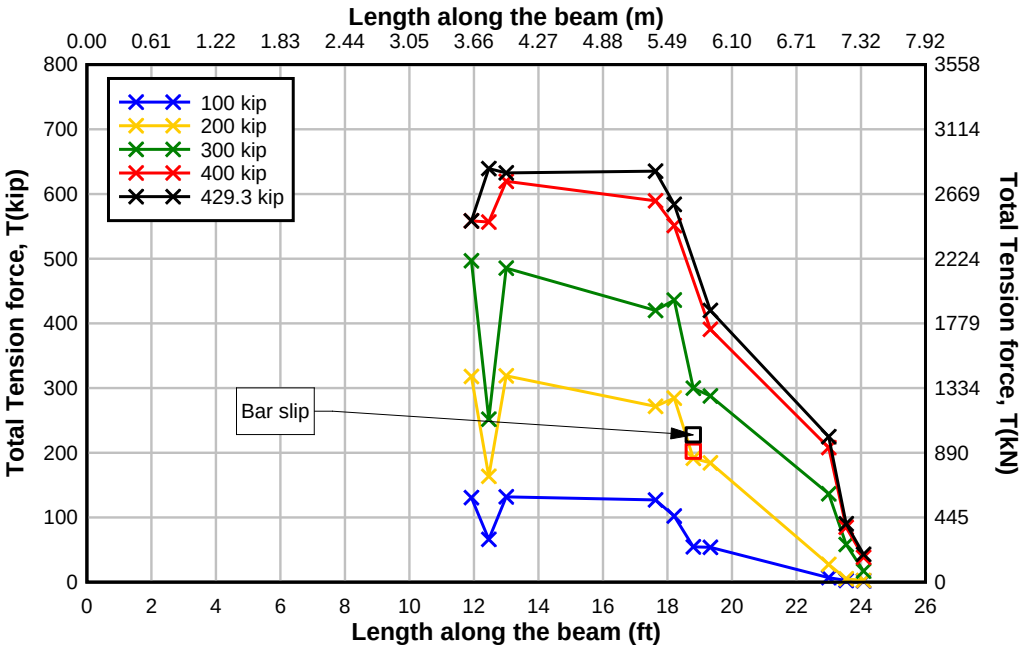

Fig. 4.26 - T.45.Ld3(6).SS Experimental tension force along length of specimen

The tension forces in the specimens increased as the load increased. During the last load cycle, tension forces peaked at the preformed diagonal crack location. Fig. 4.27 below compares the peak tensile force achieved in each specimen. The outlier data from previous plots were neglected for clarity.

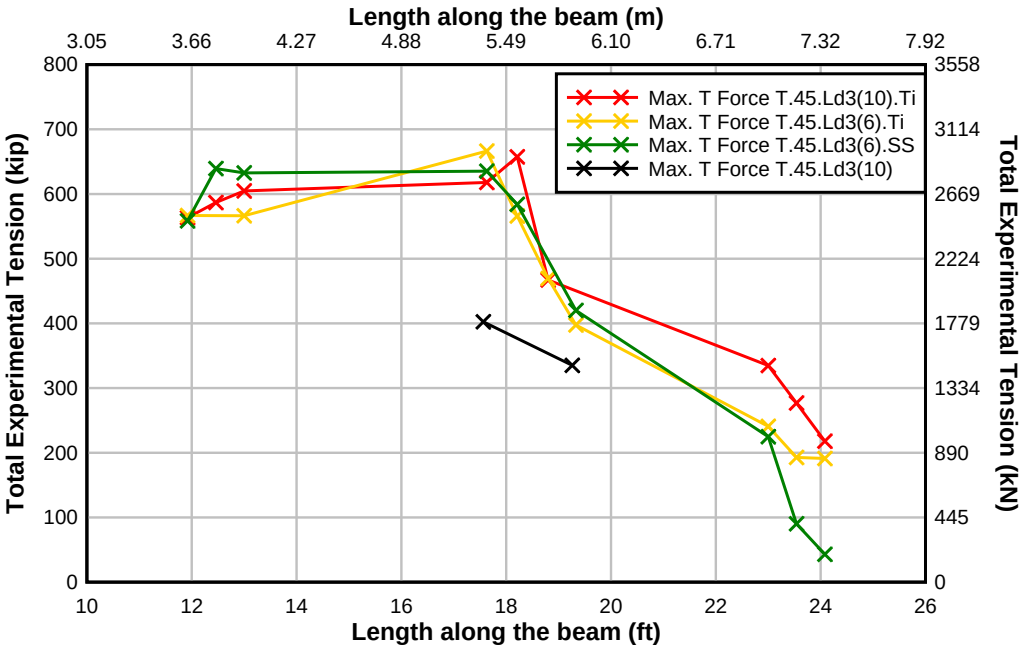

Fig. 4.27 - Summary of experimental tension forces in specimens

In all specimens, the tensile forces at the maximum load were relatively constant from midspan to the preformed diagonal crack. After the termination of the cutoff bar, the tensile force decreased. The average tensile force over the critical section in specimen T.45.Ld3(10) was 369 kips (1640 kN). The average tensile force in T.45.Ld3(10).Ti was 580 kips (2580 kN) over the same critical length. The NSM materials contributed tensile capacity of approximately 211 kips (939 kN) along the preformed diagonal crack to the end of the cutoff bar. This corresponds to the equivalent of more than two #11 (36M) Gr. 60 (Gr. 420) reinforcing steel bars.

4.3.2 Maximum Measured Steel Reinforcing Bar and NSM Bar Tension Forces

The following bar charts differentiate the tensile contribution of the internal reinforcing steel and the NSM material. Sections 1 through 3 are located at midspan of the specimen and sections 8 through 10 are located at the termination of the NSM material near the support. Damage of the strain gage and unreliability of the values was noted on each chart. Fig. 4.28 through Fig. 4.30 represents specimens T.45.Ld3(10).Ti, T.45.Ld3(6).Ti, and T.45.Ld3(6).SS.

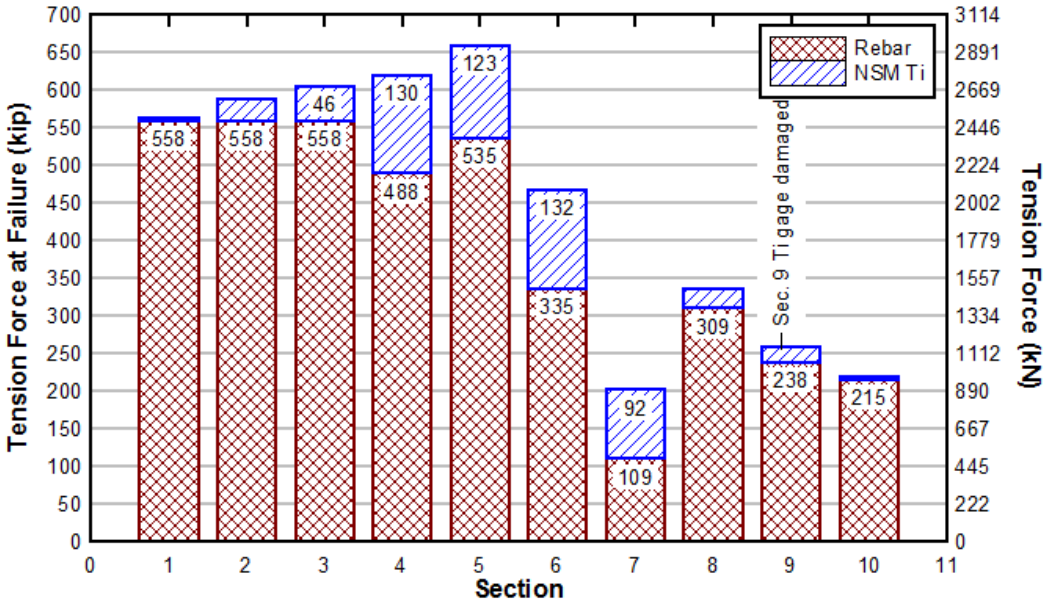

Fig. 4.28 - T.45.Ld3(10).Ti Maximum experimental steel reinforcing and NSM bar tensile forces

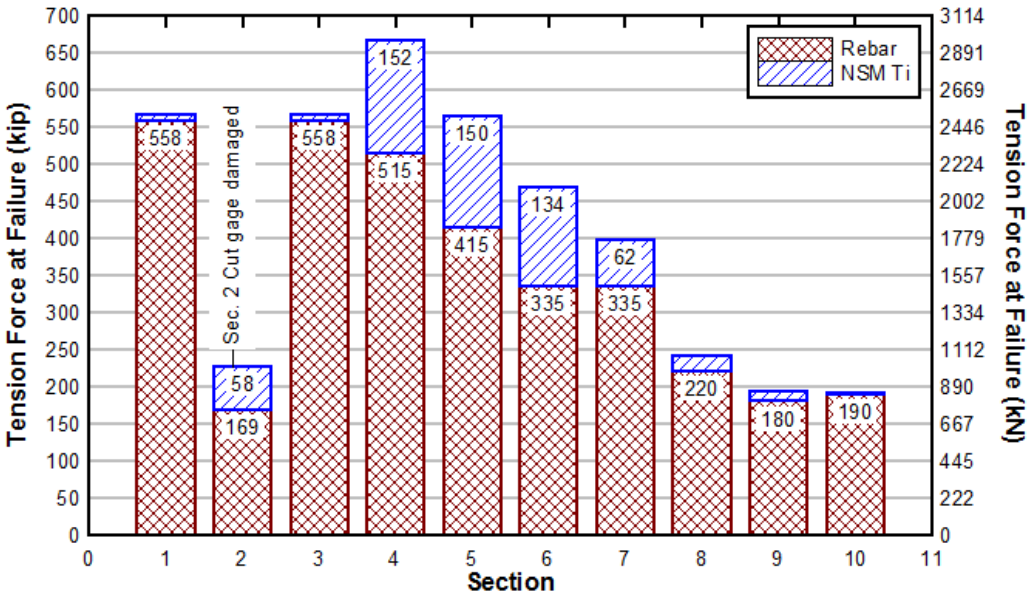

Fig. 4.29 - T.45.Ld3(6).Ti Maximum experimental reinforcing bar and NSM tensile force

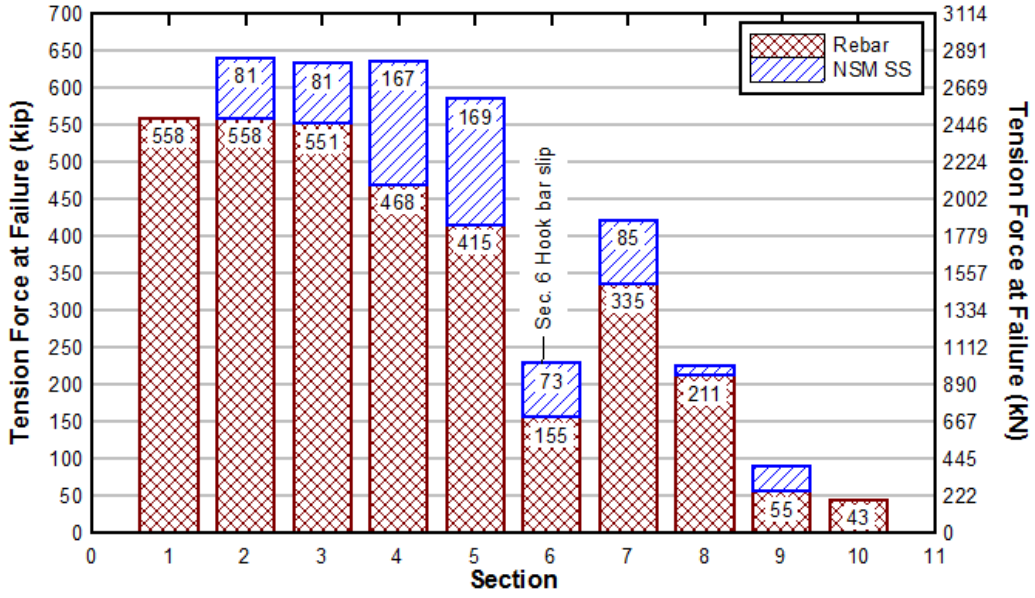

Fig. 4.30 - T.45.Ld3(6).SS Maximum experimental reinforcing bar and NSM tensile force

Despite using twice the number of NSM reinforcing bars, the NSM stainless steel strengthened specimen had similar contributions of the NSM materials as the NSM titanium strengthened specimen. In each retrofitted specimen, the relative contribution of the NSM materials increased in sections 4, 5, and 6 (length from preformed crack to end of cutoff reinforcing steel bar). There was minimal contribution from NSM materials at the termination of the NSM bars (at midspan and close to the support). The majority of the flexural tension load was carried by the internal reinforcing steel. In all cases, the NSM reinforcing bars could not provide equivalent tensile strengths as the internal reinforcing steel. This is due to the direction of the load path and the stiffness of the NSM materials. However, the presence of the NSM bars enabled the cutoff and hooked steel reinforcing bars to carry more load.

Experimental tensile forces were compared to the AASHTO tensile demands and are listed for different locations in Table 4.3 and Table 4.4. To compare the peak experimental tensile forces, the maximum actuator load and span geometry was used to determine the shear and moment demand in the cross section for use in the AASHTO equation. All stirrups crossing the preformed diagonal crack were at yield experimentally and were used to calculate the contribution of the stirrups, V_s. Two locations were compared for the strengthened specimens, the preformed diagonal crack and at the failure location. The percent difference between the experimental tensile capacity and demand was found for each specimen.

Table 4.3 - AASHTO predicted tensile demand and experimentally measured tensile capacity at the preformed diagonal crack

Specimen	Tensile demand maximum (kip) [kN]	Tensile capacity experimental (kip) [kN]	% Difference
T.45.Ld3(10).Ti	777 [3450]	618 [2750]	20%
T.45.Ld3(6).Ti	838 [3730]	666 [2960]	21%
T.45.Ld3(6).SS	866 [3850]	635 [2820]	27%

Table 4.4 - AASHTO predicted tensile demand and experimentally measured tensile capacity at the failure location

Specimen	Tensile demand maximum (kip) [kN]	Tensile capacity experimental (kip) [kN]	Failure location	% Difference
T.45.Ld3(10).Ti	507 [2255]	467 [2077]	End of Cutoff	8.2%
T.45.Ld3(6).Ti	687 [3055]	558 [2481]	Midspan	21%
T.45.Ld3(6).SS	716 [3184]	558 [2481]	Midspan	25%

In specimens T.45.Ld3(6).Ti and T.45.Ld3(6).SS the tensile demand exceeded the experimentally measured values. This excess demand could have contributed to cutoff steel reinforcing bar anchorage slip that occurred prior to failure. At the preformed diagonal crack, the AASHTO flexural tension demand was around 20% higher than the experimentally observed tensile capacity for all specimens. The demand at the failure location was representative of the capacity for specimen T.45.Ld3(10).Ti. However, due to the partial contribution of the NSM materials at midspan for specimens T.45.Ld3(6).Ti and SS, the tensile demand was over 20% higher than the calculated experimental capacity.

4.4 Experimental Bond Stress Analysis

Bond stresses develop by several means: chemical adhesion from the reinforcing bar to the concrete, the reinforcing bar bearing on lugs, and friction along the reinforcing bar after initial slip. The peak bond stress was measured after the onset of significant slip of the cutoff bar. Significant slip was defined either as a value of 0.005 in. (0.13 mm) or at the point when the strain in the cutoff reinforcing steel bar reversed. The maximum usable value of bond stress incorporates the initial chemical bond stress as well as residual friction after initial slip has occurred. Maximum bond stress is reported and compared to previous work performed by Triska (2010). The load at which slip was observed for each specimen is reported in Table 4.5 and Table 4.6 below. The difference between the reinforcing steel strains from location to location is a measure of bond stress between the sections. If the difference in strains is large between two strain gages, the bond stress is large. If the difference is small it implies the bar is un-bonded or the moment is constant along the length.

Bond stress was calculated using three or more consecutive strain gages along the bar of interest from the preformed diagonal crack to the end of the cutoff bar. The equation used for calculating average bond stress, $\mu_{avg,}$ is:

$$\mu_{avg} = \frac{\Delta f_s d_b}{4L} \qquad [0.2]$$

where Δf_s is the change in stress between two instrumented locations, $d_{b,}$ is the bar diameter, and the embedded length, L, is taken as the distance between the two instrumented locations. The average bond stress between each strain gage was summed and divided by the number of instrumented sections around the cutoff bar to obtain the mean

average bond stress along the cutoff length. The peak average bond stress was taken as the maximum bond stress value of the strain gaged sections. Bond stress data ceased after the first strain gage became damaged. The experimental strain values were limited to yield but incorporated negative strains found at the section.

Fig. 4.31 through Fig. 4.33 plots the mean average bond stress of the cutoff steel reinforcing bar versus the cutoff bar slip for each specimen. The bond stress at first significant slip (when the bar strain reversed) and the maximum bond stresses are reported on the figures. The maximum usable bond stress was selected before the strain gages exhibited widespread strains above yield.

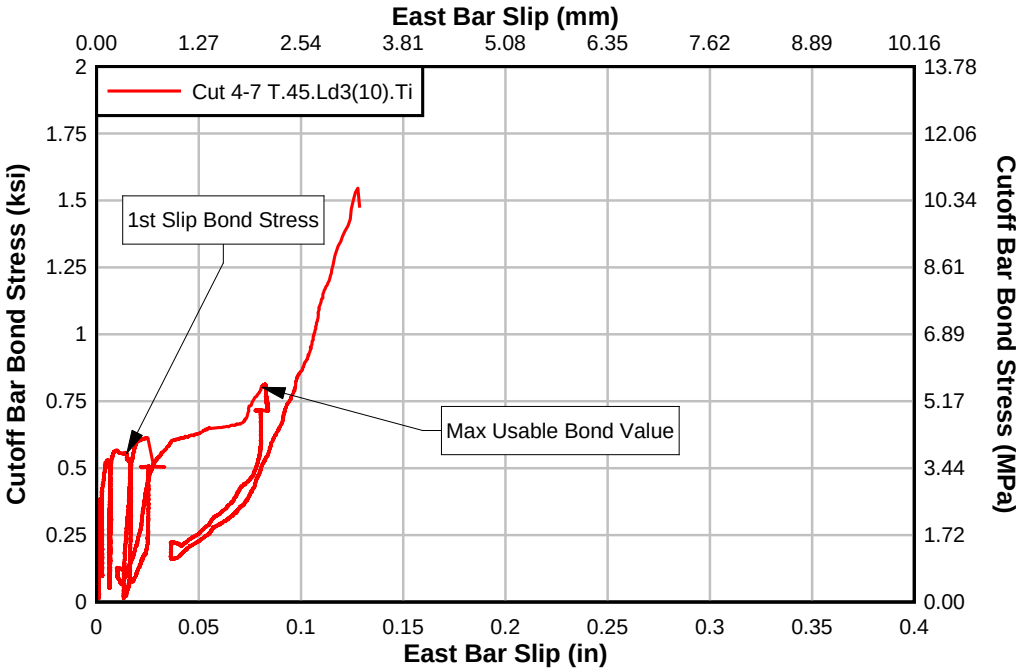

Fig. 4.31 – Average cutoff reinforcing steel bond stress and bar slip for specimen T.45.Ld3(10).Ti

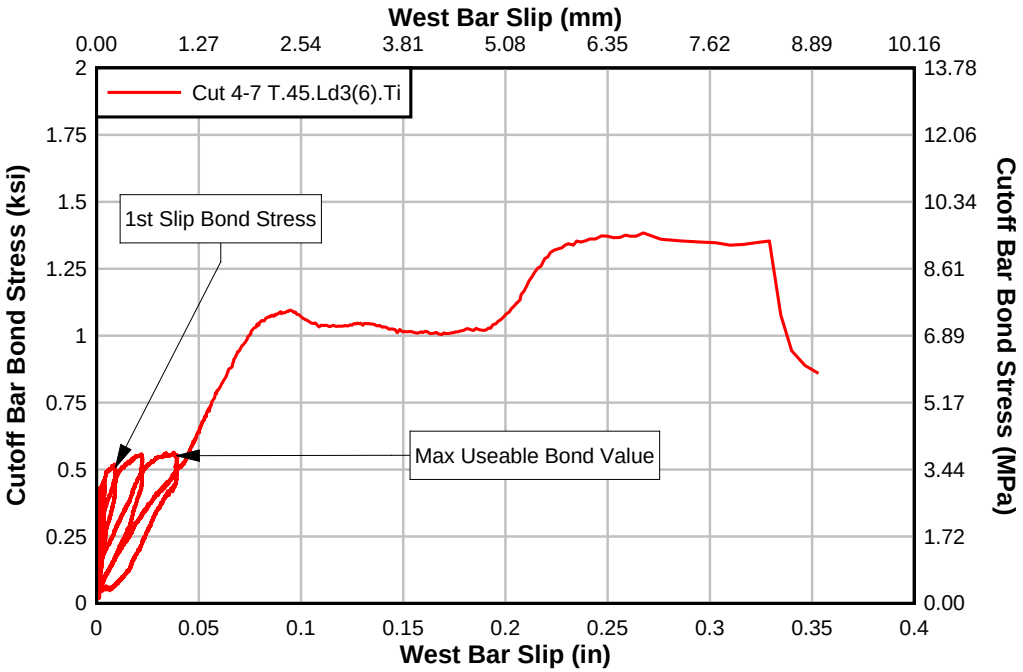

Fig. 4.32 – Average cutoff reinforcing steel bond stress and bar slip for specimen T.45.Ld3(6).Ti

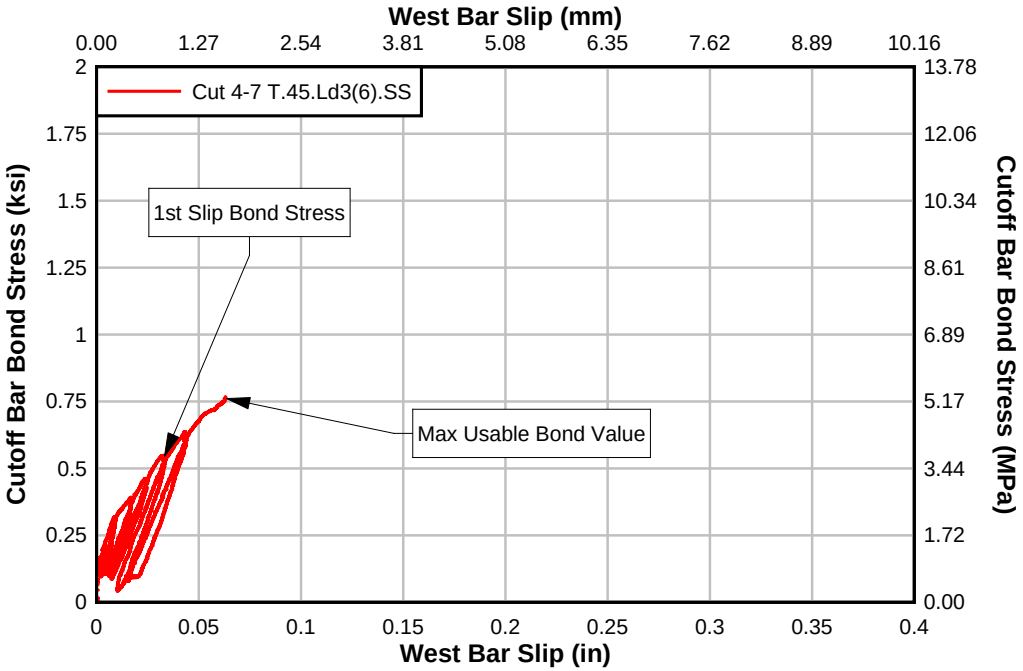

Fig. 4.33 – Average cutoff reinforcing steel bond stress and bar slip for specimen T.45.Ld3(6).SS

The cutoff reinforcing steel bar average bond stress at initial slip occurred at values of at least 500 psi (3.45 MPa). Specimen T.45.Ld3(10).Ti exhibited residual slip deformations that correlated with higher average bond stress values. The cutoff bar slip sensor of specimen T.45.Ld3(10).Ti detached during the middle of the test and had to be re-attached, creating some variability in the slip measurement. Specimen T.45.Ld3(6).Ti experienced increasing amounts of residual slip but at similar bond stress values. Specimen T.45.Ld3(6).SS experienced the smallest slip of the cutoff reinforcing steel bar and obtained a near-linear average bond stress increase.

The average bond stress at initial slip for each specimen is shown in Table 4.5. The average maximum bond stress values for each specimen are shown in Table 4.6. These bond stress values occur at larger slip deformations and at higher applied loads that occurred near failure. Table 4.7 summarizes the bond stress at initial slip and maximum bond stress for each material by averaging values from all three specimen tests.

Table 4.5 - Bond stress of materials taken at onset of slip in each specimen

Specimen	Cutoff bar slip (in) [mm]	Load (kip) [kN]	Mean Onset μ_{avg} (ksi) [Mpa]	Peak Onset μ_{avg} (ksi) [Mpa]
Cutoff bar (section 4-7)				
T.45.Ld3(10).Ti	0.0148 [0.376]	32.5 [145]	0.555 [3.826]	0.956 [6.587]
T.45.Ld3(6).Ti	0.0092 [0.234]	250.3 [1113]	0.513 [3.536]	0.668 [4.599]
T.45.Ld3(6).SS	0.0324 [0.823]	300.3 [1336]	0.547 [3.772]	0.788 [5.428]
Hooked bar (section 4-7)				
T.45.Ld3(10).Ti	0.0148 [0.376]	32.5 [145]	0.032 [0.223]	0.039 [0.266]
T.45.Ld3(6).Ti	0.0092 [0.234]	250.3 [1113]	0.453 [3.120]	0.954 [6.574]
T.45.Ld3(6).SS	0.0324 [0.823]	300.3 [1336]	0.241 [1.660]	0.576 [3.969]
NSM Upper bar (section 4-7)				
T.45.Ld3(10).Ti	0.0148 [0.376]	32.5 [145	0.022 [0.148]	0.038 [0.261]
T.45.Ld3(6).Ti	0.0092 [0.234]	250.3 [1113	0.253 [1.743]	0.366 [2.524]
T.45.Ld3(6).SS	0.0324 [0.823]	300.3 [1336	0.342 [2.356]	0.606 [4.175]
NSM Lower bar (section 4-7)				
T.45.Ld3(10).Ti	0.0148 [0.376]	32.5 [145	0.015 [0.104]	0.028 [0.193]
T.45.Ld3(6).Ti	0.0092 [0.234]	250.3 [1113	0.115 [0.794]	0.211 [1.456]
T.45.Ld3(6).SS	0.0324 [0.823]	300.3 [1336	0.371 [2.553]	0.855 [5.891]

Table 4.6 – Maximum bond stress of materials taken at maximum usable stress in each specimen

Specimen	Cutoff bar slip (in) [mm]	Load (kip) [kN]	Mean Maximum μ_{avg} (ksi) [Mpa]	Peak Maximum μ_{avg} (ksi) [Mpa]
Cutoff bar (section 4-7)				
T.45.Ld3(10).Ti	0.081 [2.05]	353.1 [1571]	0.802 [5.52]	0.858 [5.90]
T.45.Ld3(6).Ti	0.039 [0.99]	350.3 [1558]	0.552 [3.80]	1.212 [8.35]
T.45.Ld3(6).SS	0.064 [1.61]	428.8 [1907]	0.761 [5.24]	1.422 [9.78]
Hooked bar (section 4-7)				
T.45.Ld3(10).Ti	0.081 [2.05]	353.1 [1571]	0.000 [0.00]	0.000 [0.00]
T.45.Ld3(6).Ti	0.039 [0.99]	350.3 [1558]	0.335 [2.31]	0.697 [4.80]
T.45.Ld3(6).SS	0.064 [1.61]	428.8 [1907]	- [-]	- [-]
NSM Upper bar (section 4-7)				
T.45.Ld3(10).Ti	0.081 [2.05]	353.1 [1571]	0.450 [3.09]	1.057 [7.28]
T.45.Ld3(6).Ti	0.039 [0.99]	350.3 [1558]	0.262 [1.80]	0.392 [2.70]
T.45.Ld3(6).SS	0.064 [1.61]	428.8 [1907]	0.142 [0.97]	0.278 [1.91]
NSM Lower bar (section 4-7)				
T.45.Ld3(10).Ti	0.081 [2.05]	353.1 [1571]	0.359 [2.47]	0.889 [6.12]
T.45.Ld3(6).Ti	0.039 [0.99]	350.3 [1558]	0.116 [0.79]	0.187 [1.28]
T.45.Ld3(6).SS	0.064 [1.61]	428.8 [1907]	0.667 [4.59]	1.457 [10.03]

Table 4.7 - Average onset of slip and maximum bond stress of materials

Bar	Mean Onset μ_{avg} (ksi) [Mpa]	Peak Onset μ_{avg} (ksi) [Mpa]	Mean Maximum μ_{avg} (ksi) [Mpa]	Peak Maximum μ_{avg} (ksi) [Mpa]
Cutoff	0.539 [3.71]	0.804 [5.54]	0.705 [4.86]	1.164 [8.02]
Hook	0.242 [1.67]	0.523 [3.60]	0.168 [1.15]	0.349 [2.40]
NSM Ti	0.101 [0.70]	0.161 [1.11]	0.296 [2.04]	0.631 [4.35]
NSM SS	0.356 [2.45]	0.730 [5.03]	0.404 [2.79]	0.867 [5.98]

A reduction in bond stress indicates either that the bar was debonded (from concrete cracking and slipping), or that the bar was yielding along the instrumented length. The cutoff steel reinforcing bar experienced much higher bond stresses than the hooked and NSM reinforcement. This indicates a significant stress transfer between the concrete and cutoff steel reinforcing bars in the termination region. The bond stress in the hooked steel reinforcing bars was lower than the cutoff counterpart because they were adequately anchored to the concrete and yielding. Shown from the material strain plots, the hooked steel reinforcing bar experienced strains near or at yield and provided the largest portion of the overall tensile capacity. The titanium NSM reinforcement exhibited lower bond stresses than the stainless steel NSM reinforcement at similar load levels.

4.5 Bond Length Investigation Results

To investigate the transfer of stress between the NSM materials, epoxy, and concrete, the bond length specimens were created. A square groove was saw-cut into reinforced concrete

block specimens. The geometry, materials, and test setup was described in Chapter 4. The NSM titanium of a specified length was placed into the epoxy filled groove. Six bond length specimens were tested: three with a 4 in. (102 mm) embedment length and three 12 in. (305 mm) bonded length. During tests, the force applied from the actuator and bar slip was measured. This section describes the average bond stress and bar slip responses observed from the experiments.

4.5.1 Bond Length Test: 4 in.(102 mm) Specimens

The typical failure surface of the 4 in. (102 mm) long embedded specimens was the concrete-epoxy interface. The surrounding concrete showed diagonal cracks initiating from the pulled (or loaded) end of the bar. The cracks were typical of bursting stresses and eventually progressed to the free end of the bar (mid-block). Fig. 4.34 below illustrates the cracking at failure and a detail of the concrete epoxy failure. Note that threaded turn imprint in the epoxy exhibited no distress, ensuring a concrete-epoxy failure.

Fig. 4.34 – Bond length specimen at failure (left) and detail of failure (right)

The applied load-slip responses for each 4 in. (102 mm) bond length specimen is shown in Fig. 4.35. The slip of the NSM titanium bar is measured at the free or embedded end of the bar mid-block. Since the observed failure surface was at the epoxy-concrete interface, bond stress was calculated using a rectangular surface shown in Eq. [4.1]:

$$\mu_{avggroove} = \frac{\Delta T}{3 d_g L} \qquad [4.1]$$

where ΔT is the change of force along the bar, taken as the actuator load, d_g is the depth of the groove taken nominally as 1 in. (25.4 mm), L is the bonded length, taken as 4 in. (102 mm). Fig. 4.36 shows the average bond stress (in the concrete-epoxy interface) transferred along the bonded length versus the free end bar slip. For comparison, the bond stresses along the bar-epoxy interface were computed by Eq. [2.1] and the results are shown in Fig. 4.37.

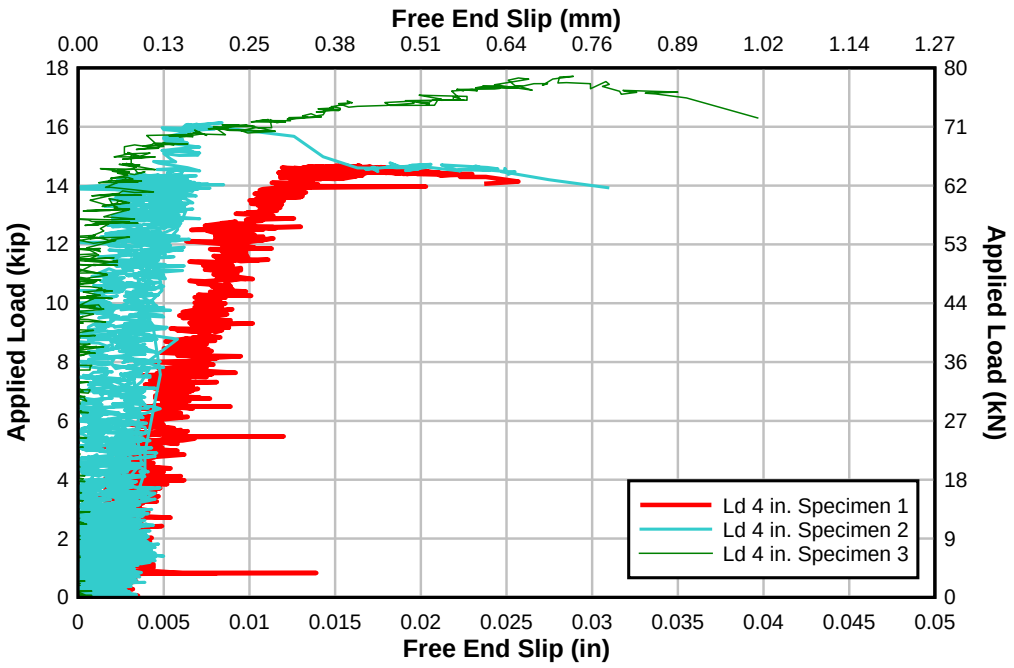

Fig. 4.35 - Load-slip response of 4 in. bond length specimen.

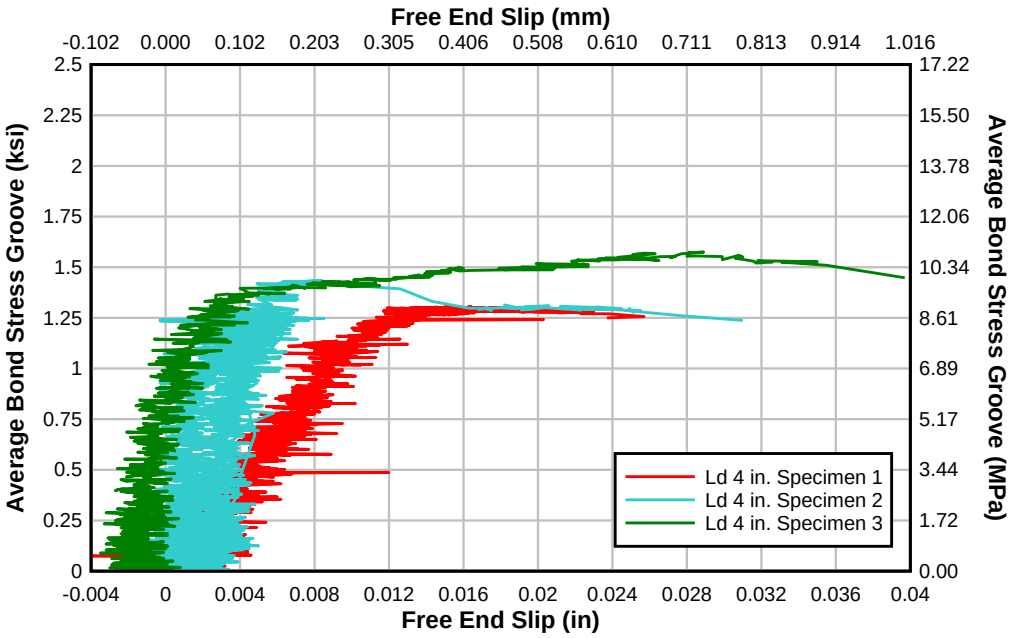

Fig. 4.36 - Average bond stress for 4 in. bond length specimen versus bar slip plot

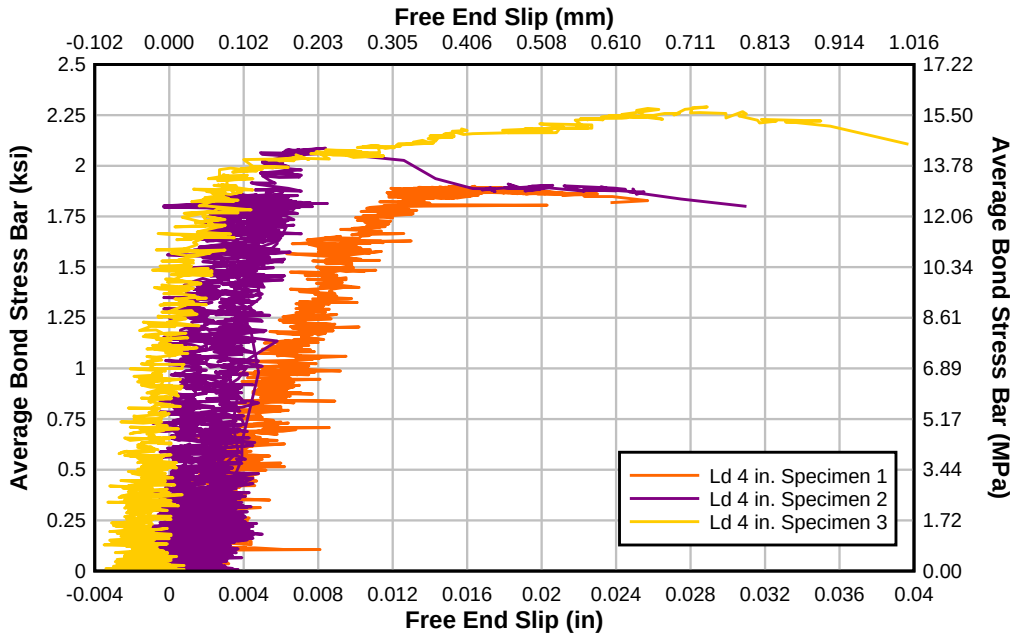

Fig. 4.37 - Average bond stress at bar-epoxy interface versus bar slip for 4 in. bond length specimens.

The bar slip versus load plot shows minimal bar slip until failure. Specimen 1 exhibited more bar end slip due to concrete cracking in the specimen. All failures were abrupt. Bond stresses computed using the failure surface (concrete-epoxy) Eq. [4.1], were less than those using Eq. [2.1] because the surface area of the bar-epoxy interface was smaller than that of the concrete-epoxy interface. The mean and maximum average bond stresses are reported in Table 4.8.

Table 4.8 - Bond stresses for the 4 in. bond length specimens of titanium alloy bars

Specimen	**Maximum μ_{avg} Groove (ksi) [Mpa]**	**Mean μ_{avg} Groove (ksi) [Mpa]**	**Maximum μ_{avg} Bar (ksi) [Mpa]**	**Mean μ_{avg} Bar (ksi) [Mpa]**	**Embedded End Slip (in) [mm]**
Ld 4 in. 1	1.305 [8.99]	1.437 [9.90]	1.899 [13.08]	2.091 [14.4]	0.016 [0.40]
Ld 4 in. 2	1.434 [9.88]		2.086 [14.37]		0.008 [0.21]
Ld 4 in. 3	1.574 [10.84]		2.290 [15.78]		0.029 [0.71]

Throughout the bond length tests the maximum NSM titanium bar stress achieved was around 60 ksi (414 MPa), which is less than half the yield stress of the NSM titanium bar. The 4 in. bond length specimen results indicate that the development length of a straight NSM titanium alloy bar is over 4 in (51 mm) and approximately 8 in. (102 mm).

4.5.2 Bond Length Tests: 12 in. (305 mm) Specimens

The intent of the 12 in. (305 mm) NSM titanium bar embedment length was to measure the active bond length and to further investigate the development length. Since the 4 in. (102

mm) specimens did not reach the yield stress of the NSM titanium bars, a longer embedment of 12 in. (305 mm) was chosen. The specimens were instrumented with three strain gages spaced at 3 in. (76.2 mm) intervals along the bonded length of the NSM titanium alloy bars. An average maximum actuator load of 16.3 kips (72.5 kN) was reached for the three 12 in. (305 mm) embedment tests. The average slip at peak load was 0.0035 in. (0.089 mm). When approaching the maximum load, the load-end slip displacement response softened. The titanium-epoxy and epoxy-concrete interfaces remained intact until near failure. The strength of the specimen became dependent on the concrete and internal reinforcing steel within the concrete block. This failure condition is shown in Fig. 4.38. As seen in this figure, the failure is controlled by the strength of the block rather than the epoxy bonded interfaces.

Fig. 4.38 - 12 in. bond length specimen at failure (left) and detail of remaining concrete (right)

The epoxy interfaces exceeded the tensile capacity of the concrete and the 12 in. (305 mm) titanium bond length specimens did not achieve the yielding load for the NSM titanium. The concrete had a compressive strength of 4000 psi (30.6 MPa) and a tensile strength of 389 psi (2.68 MPa). If the failure angle was approximated to 37° with a failure depth equal

to the depth of the groove (1 in. (25.4 mm)), the tensile force required to crack the concrete failure plane is approximately 5 kips (22.2 kN). Fig. 4.39 contains the free end bar slip of the titanium versus applied load for each test.

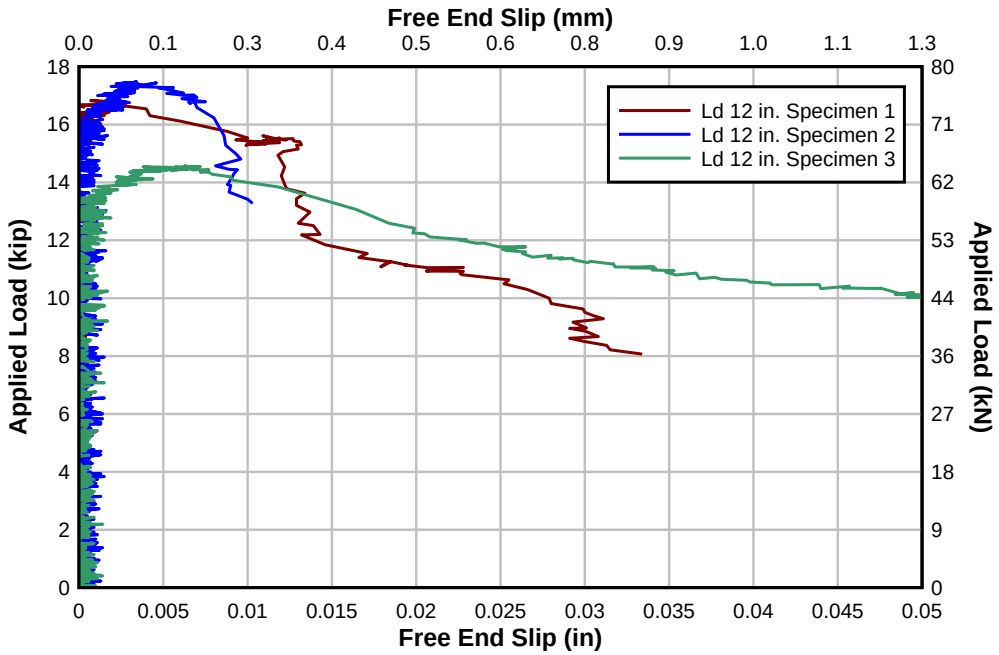

Fig. 4.39 - Bond length test applied load and embedded bar end slip

The embedded end did not slip until near failure loads. The load slip curves from the 12 in. (304 mm) embedment length are much stiffer than those from the 4 in. (102 mm) embedment length. The maximum average applied load in the 12 in. (304 mm) tests are almost identical to those of the 4 in. (102 mm) tests but with less bar slip. Similar maximum loads indicate that the material properties and geometry of the specimen were the limiting factors rather than the bonded length of the NSM titanium.

Strains at 3 in. (76.2 mm) intervals were monitored and can be seen at various loads in Fig. 4.40. The point at length 0 is representative of strain in the bar from the applied load. The point at 12 in. (305 mm) is the strain in the free end of the NSM titanium bar located at mid-block.

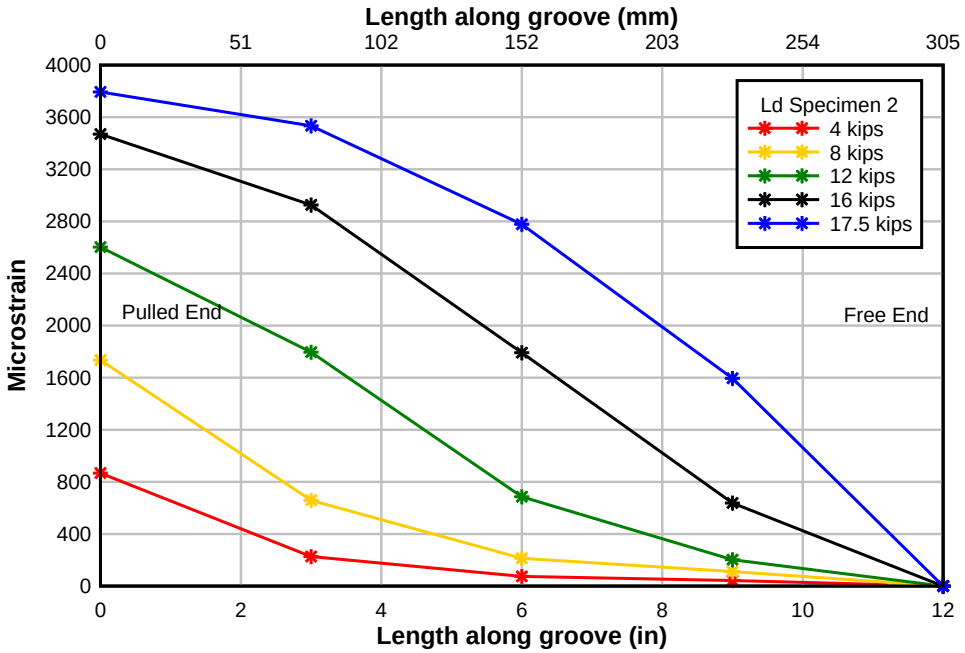

Fig. 4.40 - Variation in strains along 12 in. bond length specimen of NSM titanium

Similar strains at different locations along the bar imply that the bar is yielding or the debonded between the two strain gages.

Using methods described in Section *4.4 Experimental Bond Stress Analysis*, data were transformed into average bond stress. The free end of the bar had zero stress and the loaded end of the bar had the load applied from the actuator. The average bond stress in the bar versus free end slip is shown below in Fig. 4.41.

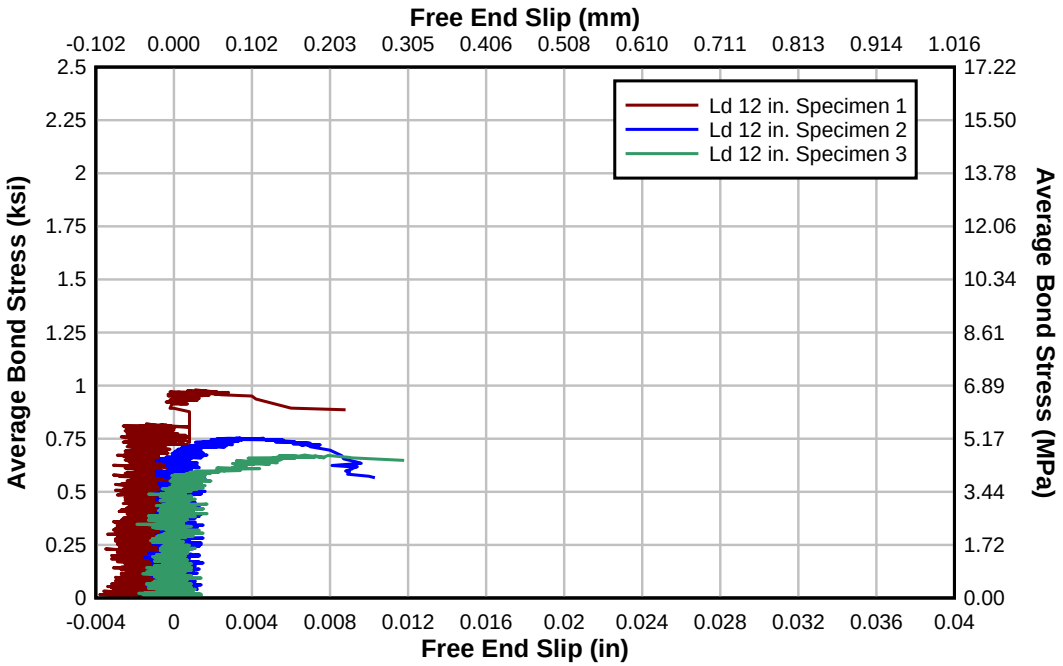

Fig. 4.41 - Average bond stress in bar-epoxy interface and free end slip for 12 in. bond length specimens

The maximum average bond stresses and the corresponding slip and load values are shown in Table 4.9.

Table 4.9 - 12 in. Bond length specimen maximum average bar bond stress

Specimen	Maximum μ_{avg} Bar (ksi) [Mpa]	Embedded End Slip (in) [mm]	Load (kip) [kN]	Average μ_{avg} Bar (ksi) [Mpa]
Ld 12 in. 1	0.980 [6.75]	0.0011 [0.03]	16.7 [74.4]	0.802 [5.528]
Ld 12 in. 2	0.754 [5.20]	0.0034 [0.08]	17.5 [77.8]	
Ld 12 in. 3	0.673 [4.64]	0.0067 [0.16]	14.4 [64.2]	

It is common in bond or development length tests to achieve higher bond stresses than in a full-scale specimen. Recall that the NSM titanium alloy bars in the full-scale T-specimens had a bond stress of 296 psi (2.04 MPa) over the cutoff bar termination. The average bond stress value from the bond length tests was 506 psi (3.49 MPa) higher than that measured in the T-specimens. While the bond length test bond stress values were higher, the test suggests that the deformation pattern on the titanium alloy bars is sufficient to preclude failure of the epoxy-titanium interface prior to failing the concrete interface.

5 ANALYTICAL METHODS

This chapter describes the analytical methods used to compare experimental findings, design specifications, and other past experiments found in the literature. The primary methods of analysis were Response 2000 (Bentz, 2000) and the AASHTO-LRFD and ACI 318-11 design specifications. Flexural strength predictions were determined using Response 2000 (R2K) and AASHTO-LRFD specifications. The development length of straight and hooked steel reinforcing bars were compared between the two design specifications. The experimentally measured flexural tension forces in the reinforcing materials were compared with the predicted forces using Response 2000, AASHTO, and ACI. The overall response and bond stress of the strengthened T-specimens were compared to historical tests from Higgins (2004). Lastly, design methodology was discussed using an equivalent area of steel method and ACI 440 specifications.

5.1 Predicted Load, Shear, and Moment Capacities

The following section discusses the AASHTO and ACI predictions of shear and moment capacities of the strengthened test specimens. The predicted capacities were compared to the predictions from R2K. R2K analyses were performed for each specimen along the critical sections producing shear and moment capacities which were turned into load predictions.

5.1.1 Load Capacity

To provide direct comparisons, the specimen strengths were translated into the applied actuator force at midspan to cause failure. The predicted actuator load at failure for each

specimen is shown in Table 5.1. Three critical sections were evaluated using R2K and the flexural capacity at midspan was evaluated using the AASHTO specifications.

The three critical sections evaluated using R2K included: the termination of the cutoff reinforcing bar (corresponding to a 33 degree crack extending from the load plate), the location where the cutoff bar is theoretically 1/3 developed (corresponding to the 45 degree preformed crack), and at midspan (flexural failure). To represent the locations of the critical sections in R2K, several moment-to-shear ratios were used. The M/V ratios ranged from 5.67:1 to 7.5:1. A diagonal tension failure less than d_v away from the load point is unlikely. Therefore, a larger ratio than 7.5:1 (the ratio of the 45 degree crack) was not used. Furthermore, to model the developing cutoff steel reinforcing bar in R2K, an equivalent area of reinforcing steel was used with the same yield stress as the #11 (36M) cutoff reinforcing steel bars. In the case of a flexural failure, the shear capacity was limited to $V_s/2$ in R2K, similar to the requirements in AASHTO specifications. Except for the #4 (13M) deck steel, all reinforcing bars were input into the R2K model. The material inputs corresponded to the real material properties in each specimen. The ACI development length of the straight #11 (36M) bar was calculated for each specimen based on the experimentally determined material properties and used in the R2K model. All predictions assumed the NSM materials were fully developed.

Like previously stated, the flexural capacity of the specimens was determined for midspan using AASHTO specifications. Flexural and compression reinforcing steel was incorporated into the AASHTO equation. The measured material properties were used in the calculations. To find the stress in the compression steel, the strain diagram was

controlled by concrete crushing and steel yielding at the tension centroid, d_s. The #6 bars were neglected due to their proximity to the neutral axis.

Table 5.1 - Failure load prediction using R2K at different critical sections and AASHTO hand calculations with and without NSM contribution at midspan

Specimen	R2K Critical Loc. 33^0 0 Ld (kip) [kN]	R2K Critical Loc. 45^0 1/3 Ld (kip) [kN]	R2K Vs/2 Flexure (kip) [kN]	AASHTO Flexure NSM (kip) [kN]	AASHTO Flexure No NSM (kip) [kN]	Applied Load (kip) [kN]	Failure Mode
T.45.Ld3(10)	288.2 [1280]	294.2 [1310]	-	-	-	299.5 [1330]	Diagonal Tension
T.45.Ld3(10).Ti	393.4 [1750]	389.6 [1730]	-	-	-	392.9 [1750]	Diagonal Tension
T.45.Ld3(6).Ti	-	-	453.4 [2020]	446.2 [1980]	345.8 [1540]	430.7 [1920]	Flexure
T.45.Ld3(6).SS	-	-	441.1 [1960]	450.1 [2000]	345.7 [1540]	429.3 [1910]	Flexure

R2K reasonably predicted the failure load for all specimens controlled by diagonal tension. At the observed failure location, the percent difference between R2K predicted and actual force was 3.85%, 0.13%, 5.13%, 2.71%, for specimens T.45.Ld3(10), T.45.Ld3(10).Ti, T.45.Ld3(6).Ti, and T.45.Ld3(6).SS respectively. R2K tended to overestimate the flexural capacity because it assumed the NSM materials fully participated, when the actual failure occurred at the end of the NSM bars.

The NSM reinforcing bars increased the baseline capacity by 131 kips (582 kN) for specimen T.45.Ld3(6).Ti and 130 kips (570 kN) for specimen T.45.Ld3(6).SS. The effectiveness of the NSM materials is also discussed through equivalent areas of steel in Section *5.4 Contribution of NSM reinforcing bars as equivalent area of reinforcing steel*.

5.1.2 Diagonal Tension Capacity

Diagonal tension capacities were calculated according to the AASHTO and ACI specifications. A description of these calculations can be found in Appendix G. The experimental shear demand, V_{exp}, was found by dividing the maximum actuator load by two and adding the DL shear contribution. For consistency, all calculations were performed d_v away from the loading point on the NSM strengthened side of the specimens. The diagonal tension capacities were compared with the experimental failure loads in Table 5.2.

Table 5.2 - Applied shear and predicted shear capacities

Specimen	**Applied Shear V_{exp} (kip) [kN]**	**AASHTO V_n d_v Away (kip) [kN]**	**ACI V_n d_v Away (kip) [kN]**
T.45.Ld3(10)	152.9 [679]	182.9 [814]	157.9 [979]
T.45.Ld3(10).Ti	200.0 [890]	173.5 [772]	159.6 [935]
T.45.Ld3(6).Ti	216.4 [963]	222.7 [991]	218.2 [1257]
T.45.Ld3(6).SS	215.7 [959]	205.9 [916]	206.3 [1172]

Specimens T.45.Ld3(10) and T.45.Ld3(10).Ti failed in diagonal tension. Both specimens experienced anchorage deficiencies and insufficient transverse reinforcing steel which led to the diagonal tension shear failure. In specimen T.45.Ld3(10).Ti the improved flexural anchorage provided by the NSM titanium alloy bars increased the member capacity, which resulted in higher applied loads and thus higher applied shear.

5.1.3 Moment Capacity

The methods used to compute moment capacity at midspan were described in Section *5.1.1 Load Capacity*. The applied load predictions in Table 5.1 were derived from the flexural moment capacities in Table 5.3. The R2K predictions reported used the fully developed NSM materials in the predictions.

Table 5.3 - Predicted and actual moment capacities using R2K and AASHTO

Specimen	**R2K $V_s/2$ M_n (kip-ft) [kN-m]**	**R2K AASHTO M_n (kip-ft) [kN-m]**	**AASHTO Flexure with NSM (kip-ft) [kN-m]**	**AASHTO Flexure w/o NSM (kip-ft) [kN-m]**	**Applied Moment (kip-ft) [kN-m]**
T.45.Ld3(10)	1964 [2663]	1833 [2485]	- -	1904 [2581]	1647 [2233]
T.45.Ld3(10).Ti	2521 [3418]	2369 [3211]	2453 [3325]	1902 [2578]	2161 [2930]
T.45.Ld3(6).Ti	2493 [3380]	2368 [3210]	2454 [3327]	1902 [2579]	2369 [3212]
T.45.Ld3(6).SS	2426 [3289]	2410 [3267]	2476 [3357]	1901 [2577]	2361 [3201]

If the NSM bars are not used, the flexural capacities at midspan for all the specimens were similar. The variance in baseline flexural capacities were due to small differences in concrete strength or the yield stress of the reinforcing steel bars (for specimen T.45.Ld3(10)).

5.2 Comparison of Flexural Tension Capacity

Flexural tension capacity was a key component of the experimental design. As discussed previously, the flexural tension capacities and demands were compared for the specimens

with NSM bars. Analyses were performed for the AASHTO, ACI, and R2K methods using the measured material properties.

To assess the flexural tension capacity, the minimum development lengths of the different internal reinforcing steel bars were predicted using the AASHTO and ACI design methodologies. The detailed development length equation (Eq. [2.20]) in ACI was used rather than the simplified approach. The predicted straight bar development lengths were computed for each specimen using the actual material properties for the steel and concrete and are reported in Table 5.4.

Table 5.4 - Comparison of minimum specified development length for straight and hooked #11 (36M) steel reinforcing bars

Specimen	**f_y (ksi) [Mpa]**	**f'_c (ksi) [Mpa]**	**ACI**		**AASHTO**	
			l_d (in) [mm]	**l_{dh} (in) [mm]**	**l_d (in) [mm]**	**l_{dh} (in) [mm]**
T.45.Ld3(10)	71.7 [494]	3.302 [22.8]	66.4 [1688]	35.2 [894]	76.9 [1954]	29.9 [758]
T.45.Ld3(10).Ti	71.6 [494]	3.712 [25.6]	62.6 [1590]	33.1 [842]	72.7 [1846]	27.8 [706]
T.45.Ld3(6).Ti	71.6 [494]	3.823 [26.4]	51.8 [1316]	27.4 [696]	71.4 [1814]	32.7 [829]
T.45.Ld3(6).SS	71.6 [494]	3.206 [22.1]	56.6 [1437]	35.7 [906]	78.0 [1980]	29.9 [760]

In all specimens the detailed ACI development length equation for straight bars was less than that of AASHTO. The AASHTO hooked bar development length was less than the ACI hooked bar development length for all specimens except T.45.Ld3(6).Ti.

The ACI and AASHTO development lengths were used to compute the flexural tensile force available along the length of the specimens. The flexural tension demand along the length of the specimens was determined by setting the flexural tension demand to the theoretically available resistance at midspan. ACI indirectly accounts for additional demand in the flexural tension forces from the influence of shear by requiring extensions of bars beyond theoretical locations a minimum dimension of the depth of the member. Therefore, the flexural tension demand was shifted horizontally at each location to a dimension equal to *d*.

The slope of the flexural tension capacity was related to the amount of reinforcing steel being developed based on the lengths shown in Table 5.4. The left side of each figure has a stirrup spacing of 6 in. (152.4 mm) and all steel reinforcing bars start developing from the end of the specimen. The location where the demand is closest to or exceeds the capacity is the expected location of anchorage failure. The NSM materials were installed to provide additional flexural reinforcing over the location of the specimens which was deficient in available tensile capacity due to the poorly detailed cutoff location. Fig. 5.1 through Fig. 5.4 shows the ACI flexural tension capacity and demand for the entire length of the specimen.

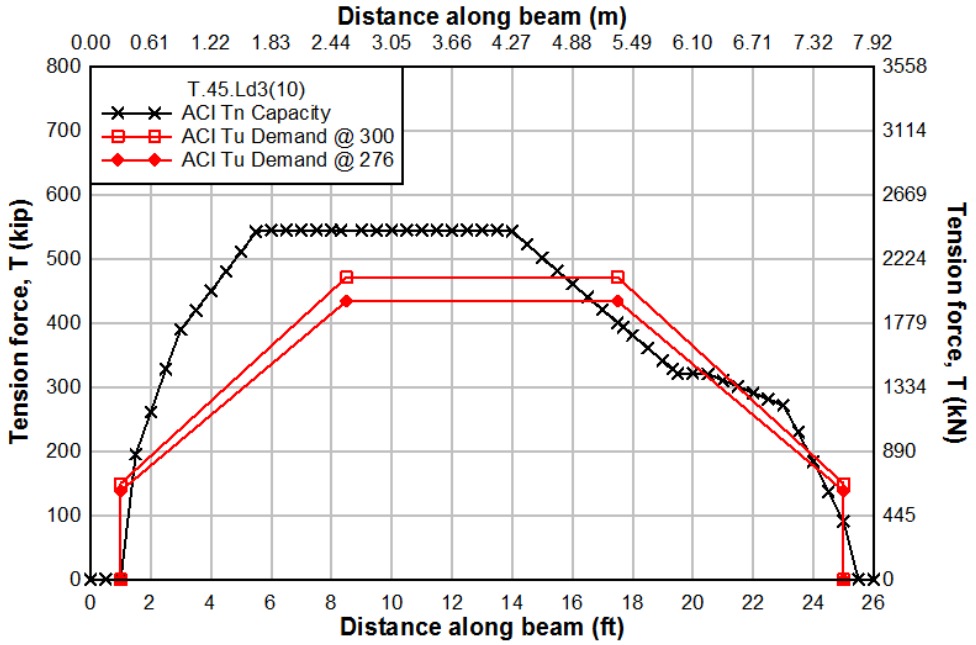

Fig. 5.1 – T.45.Ld3(10) ACI Flexural tension demand and capacity along the length of specimen

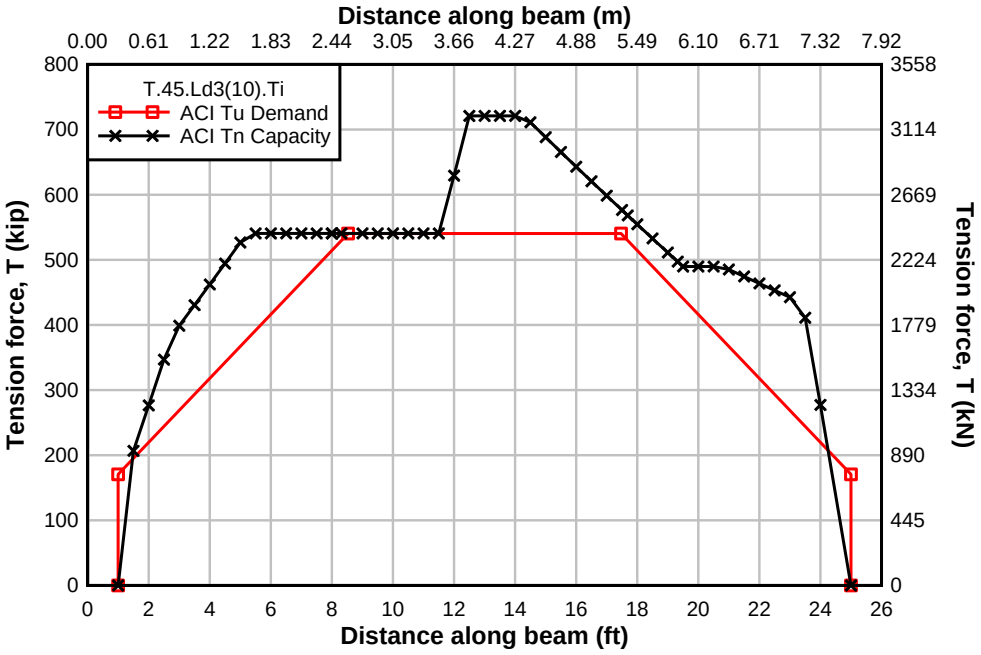

Fig. 5.2 - T.45.Ld3(10).Ti ACI Flexural tension demand and capacity along the length of specimen

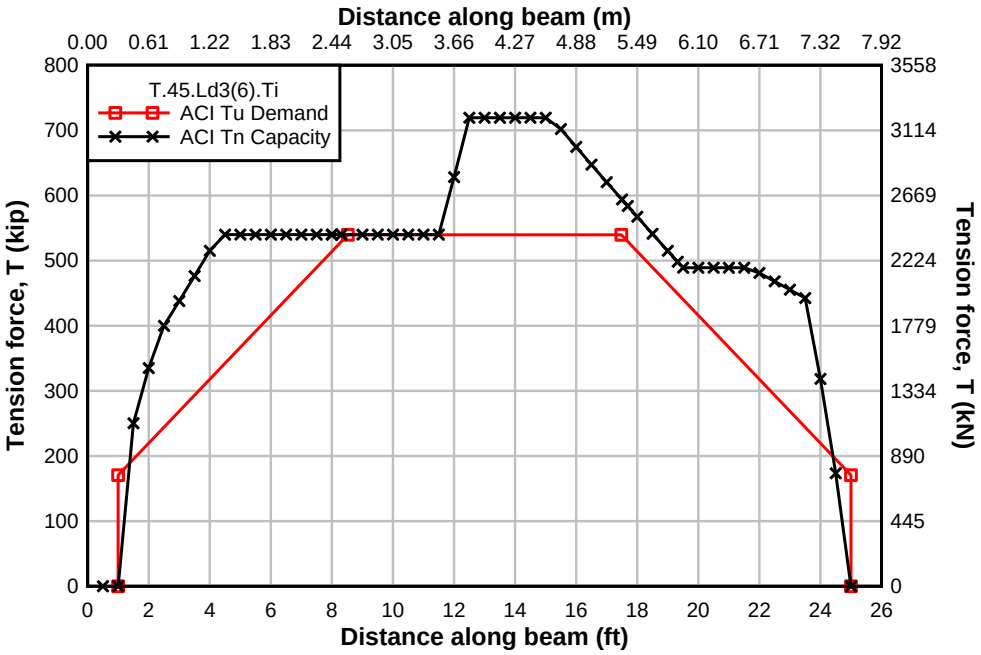

Fig. 5.3 - T.45.Ld3(6).Ti ACI Flexural tension demand and capacity along the length of specimen

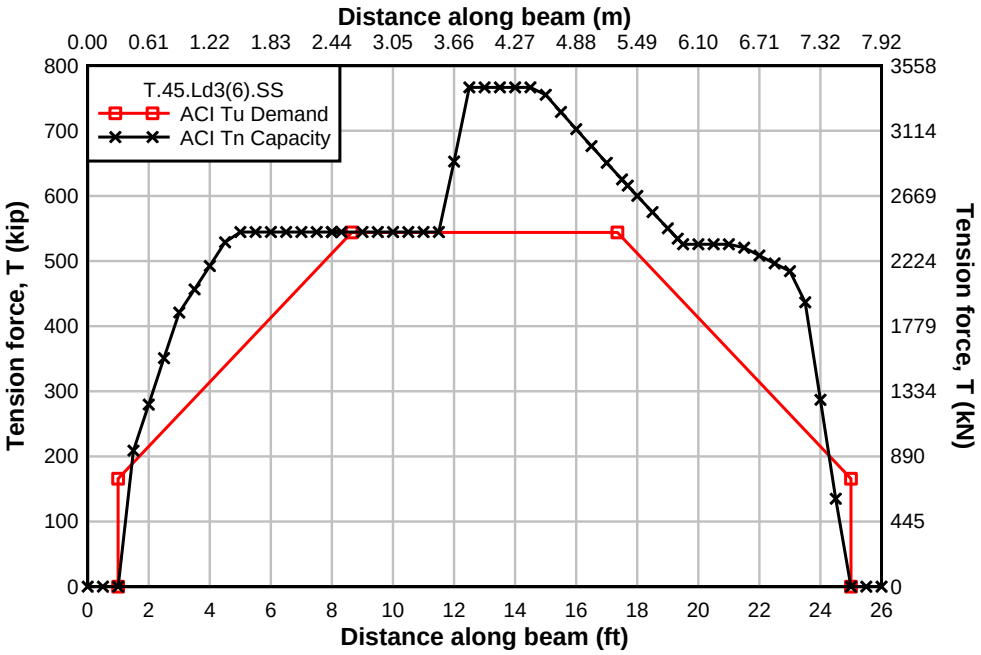

Fig. 5.4 - T.45.Ld3(6).SS ACI Flexural tension demand and capacity along the length of specimen

The ACI demand curve exceeded the capacity at the support location in the figures above. However, this is not a likely location of failure due to the clamping force provided by the bearing plates at the support locations which were not accounted for in the above calculations.

Similarly, the flexural tensile force that could be developed along the length of the specimens relative to the demands are shown in Fig. 5.5 through Fig. 5.8 for the AASHTO approach. In contrast to the ACI approach, AASHTO directly considers the additional tensile demand due to the influence of shear and the presence of a diagonal crack. A range of possible diagonal cracks were swept throughout the specimens creating a non-linear flexural tension demand curve. A spike in demand before 18 ft (5.48 m) was due to the presence of the preformed 45^{o} diagonal crack. The distance to the centroid reinforcing steel, d_s, changed after the addition of the NSM bars. The adjusted d_s value increased demand due to the geometry change in the NSM strengthened specimens.

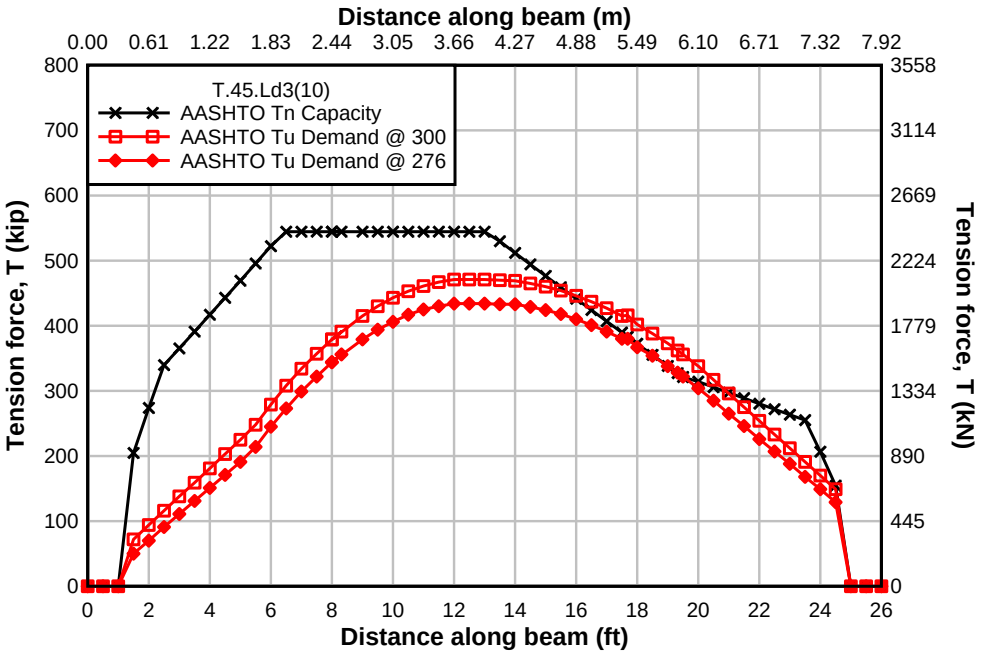

Fig. 5.5 - T.45.Ld3(10) AASHTO Flexural tension demand and capacity along length of specimen

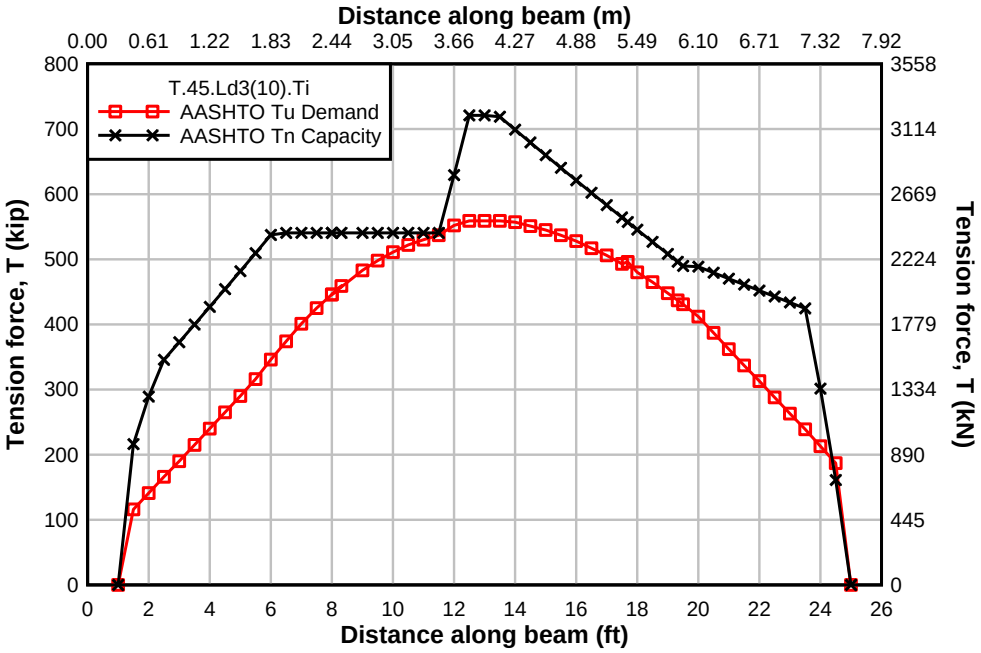

Fig. 5.6 - T.45.Ld3(10).Ti AASHTO Flexural tension demand and capacity along length of specimen

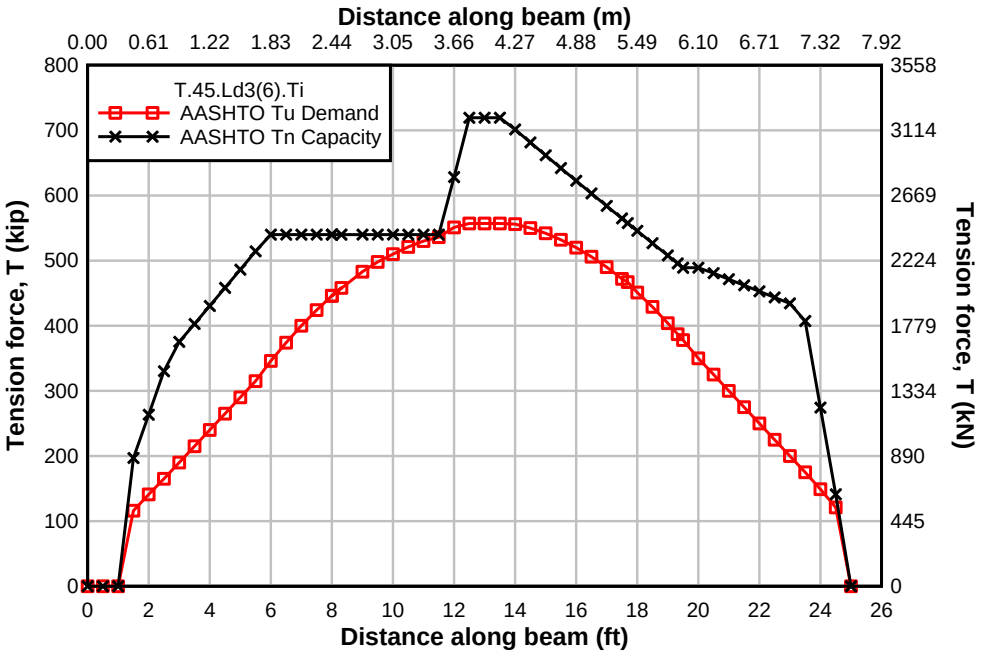

Fig. 5.7 - T.45.Ld3(6).Ti AASHTO Flexural tension demand and capacity along length of specimen

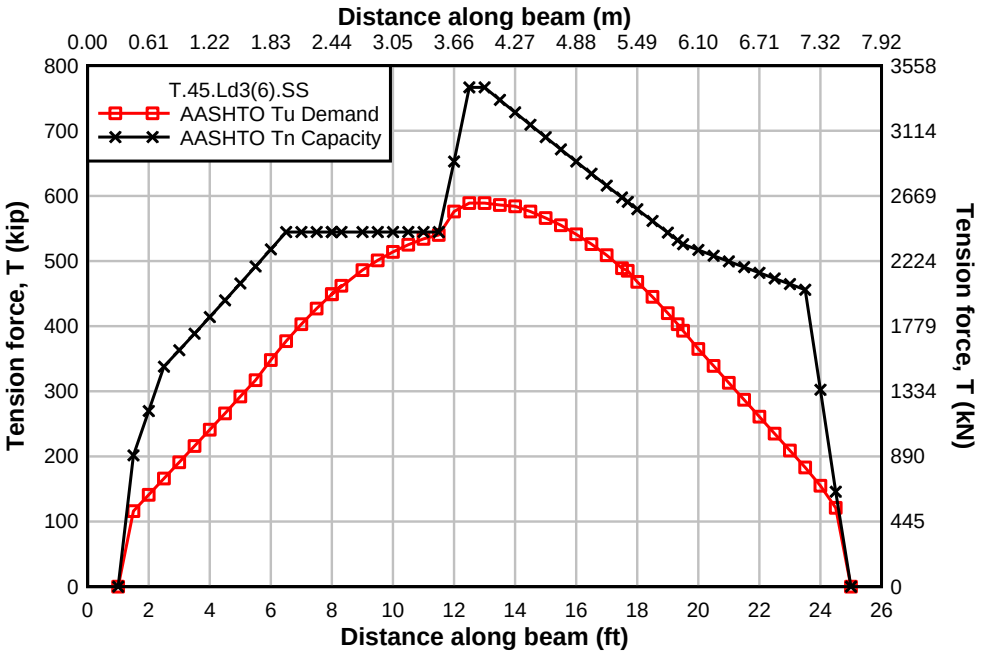

Fig. 5.8 - T.45.Ld3(6).SS AASHTO Flexural tension demand and capacity along length of specimen

Fig. 5.5 shows two demand curves; the lower curve, was based on an actuator load of 276 kips (1228 kN) which was the first load at which an anchorage failure expected to occur. The second demand curve in Fig. 5.5 was calculated from the experimental failure load of specimen T.45.Ld3(10).

The ACI and AASHTO demand curves indicate that the NSM retrofitted specimens should fail at the termination of the NSM bars near midspan of the specimens. However, specimen T.45.Ld3(10).Ti failed in diagonal tension at the end of the cutoff bar, not at midspan. This confirms that shear and moment capacities must be evaluated simultaneously with flexural tension capacities to establish critical sections of the member.

R2K was used to evaluate different cross-sections of the specimen around the termination of the cutoff reinforcing steel bar. The effective area of steel provided by the cutoff reinforcing bar was based on the percentage of the bar developed at the section assuming a uniform distribution bond stress along the development length. The R2K predicted flexural tension capacities at sections along the cutoff reinforcing steel bars with and without the NSM strengthening is shown in Fig. 5.9.

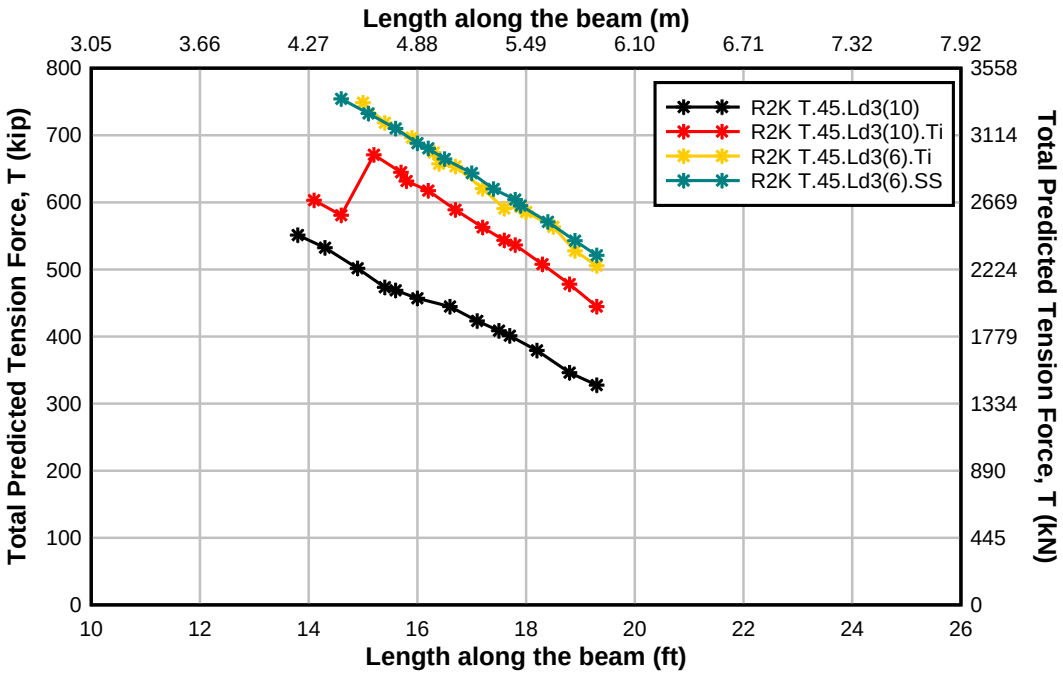

Fig. 5.9 - Summary of R2K predicted tensile forces along critical section

As seen in Fig. 5.9, Specimen T.45.Ld3(10) had the lowest flexural tension capacity along the developing bar. Specimen T.45.Ld3(10).Ti has a greater capacity due to the addition of the NSM titanium alloy bars. Specimens T.45.Ld3(6).Ti and SS have greater capacities from the increased shear capacity and the addition of the NSM materials. The R2K predictions are compared with the experimentally measured flexural tension data in Fig. 5.10 through Fig. 5.13. Strain gages were often damaged before the failure load which provided uncertain data at ultimate strength. Where sensor data was obviously compromised, it was omitted from the curve, but is reported as a data point in the figures.

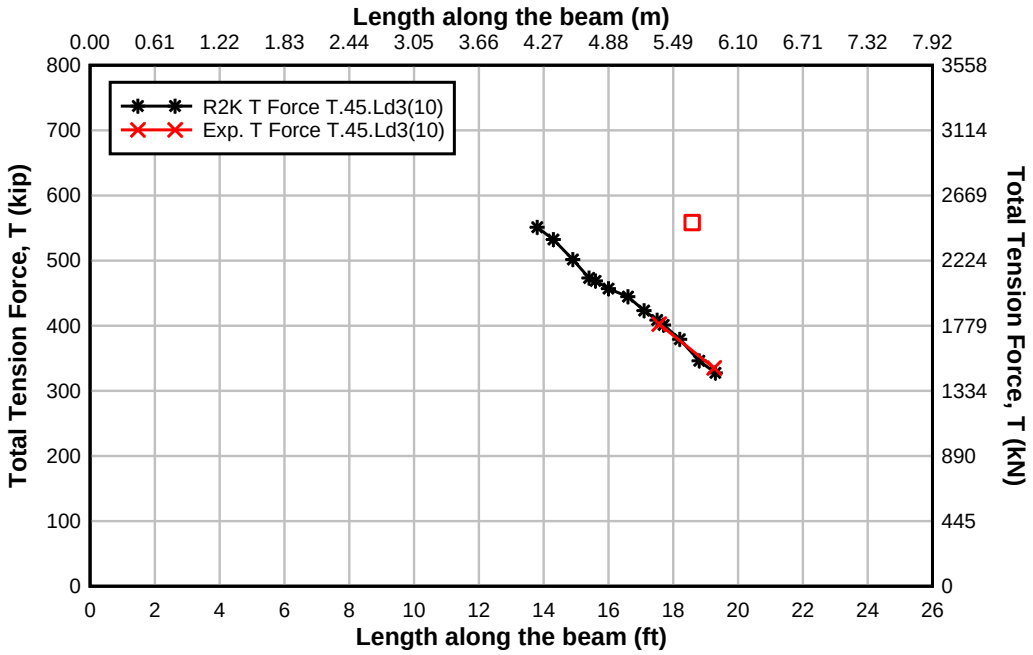

Fig. 5.10 - T.45.Ld3(10) Total experimental and R2K predicted tension force

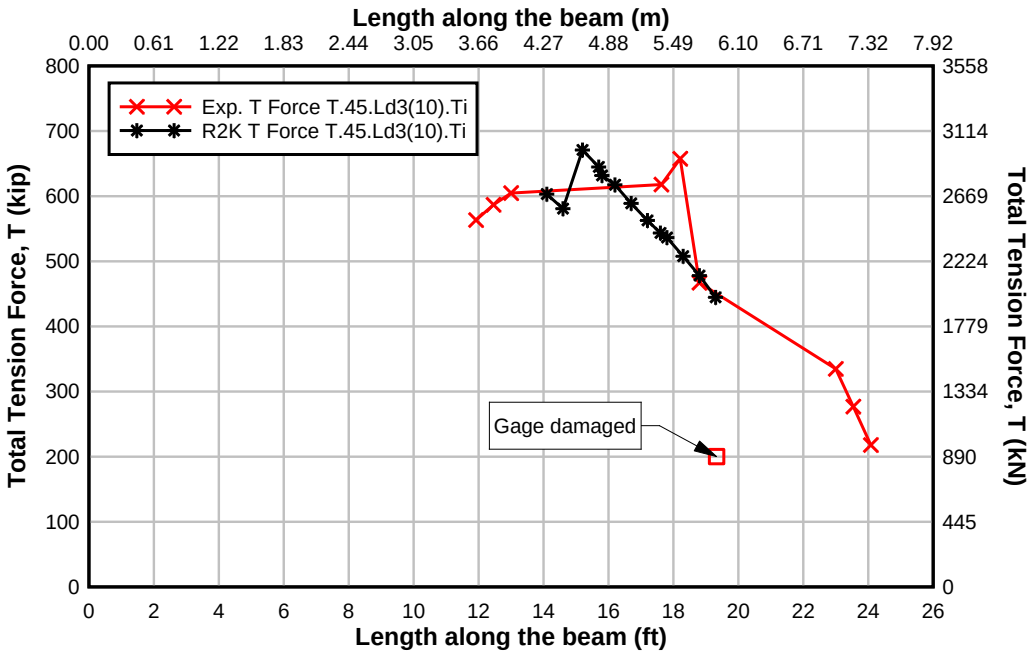

Fig. 5.11 - T.45.Ld3(10).Ti Total experimental and R2K predicted tension force

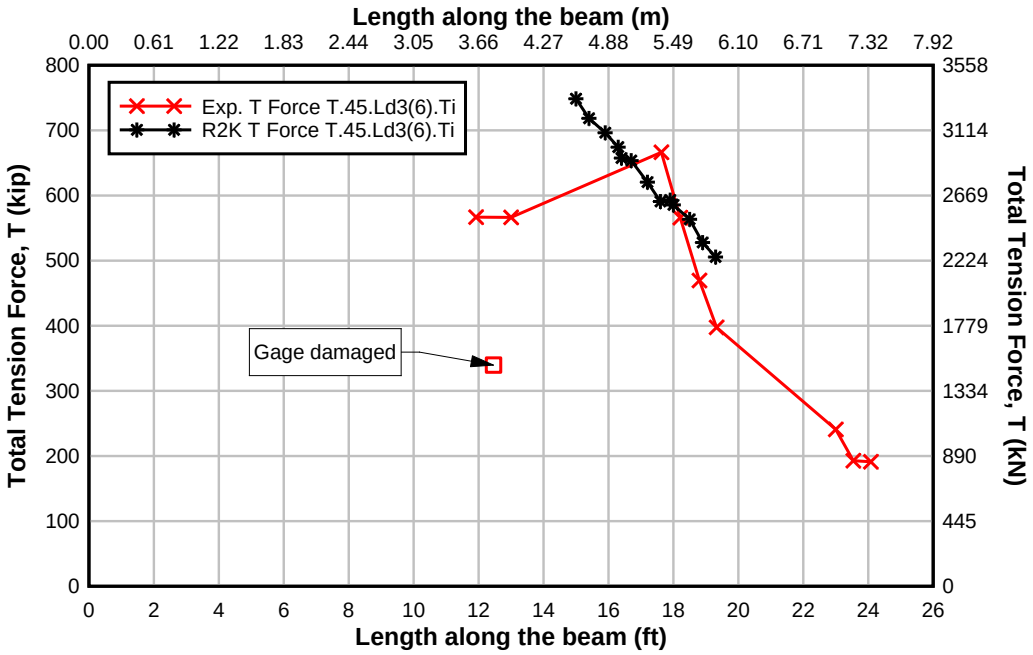

Fig. 5.12 - T.45.Ld3(6).Ti Total experimental and R2K predicted tension force

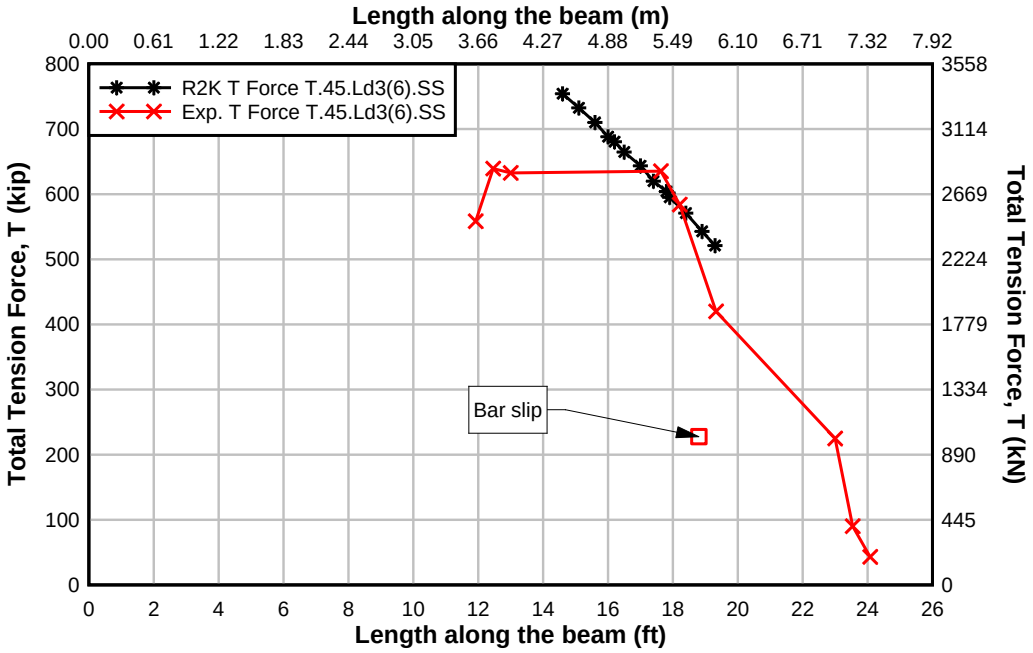

Fig. 5.13 - T.45.Ld3(6).SS Total experimental and R2K predicted tension force

In general, the experimental data for all the specimens followed the flexural tension trend predicted from R2K. The experimental data and R2K predictions were in good agreement around the preformed diagonal crack shown at 17.6 ft (5.36 m) for all specimens.

The AASHTO and ACI capacity curves were compared to R2K and experimental flexural tension results. Firstly, the AASHTO and ACI flexural tension capacities are shown relative to the R2K predicted tensile capacities in Fig. 5.14 and Fig. 5.17. In Fig. 5.18 and Fig. 5.21 the AASHTO and ACI flexural tension capacities are compared to the experimental data.

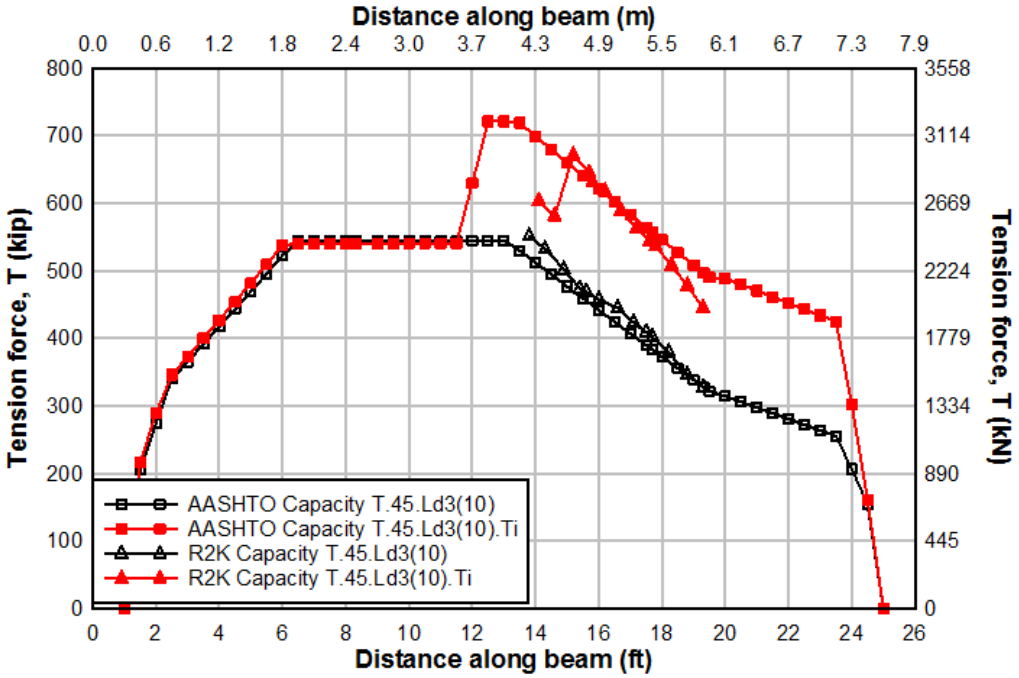

Fig. 5.14 - R2K and AASHTO predicted flexural tension capacities for specimens T.45.Ld3(10) and T.45.Ld3(10).Ti

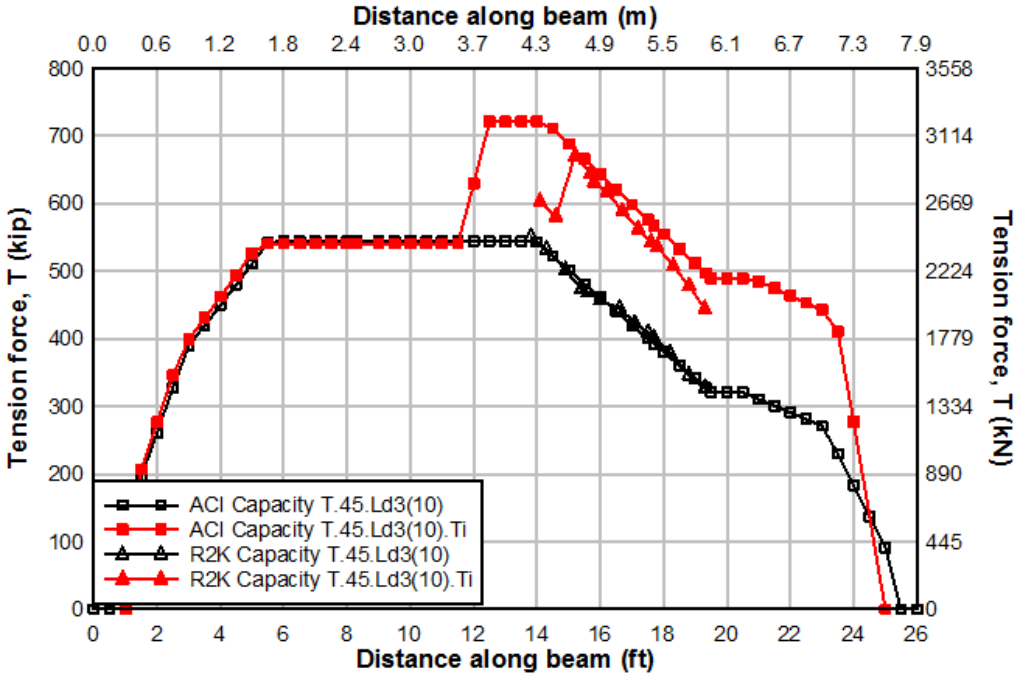

Fig. 5.15 - R2K and ACI predicted flexural tension capacities for specimens T.45.Ld3(10) and T.45.Ld3(10).Ti

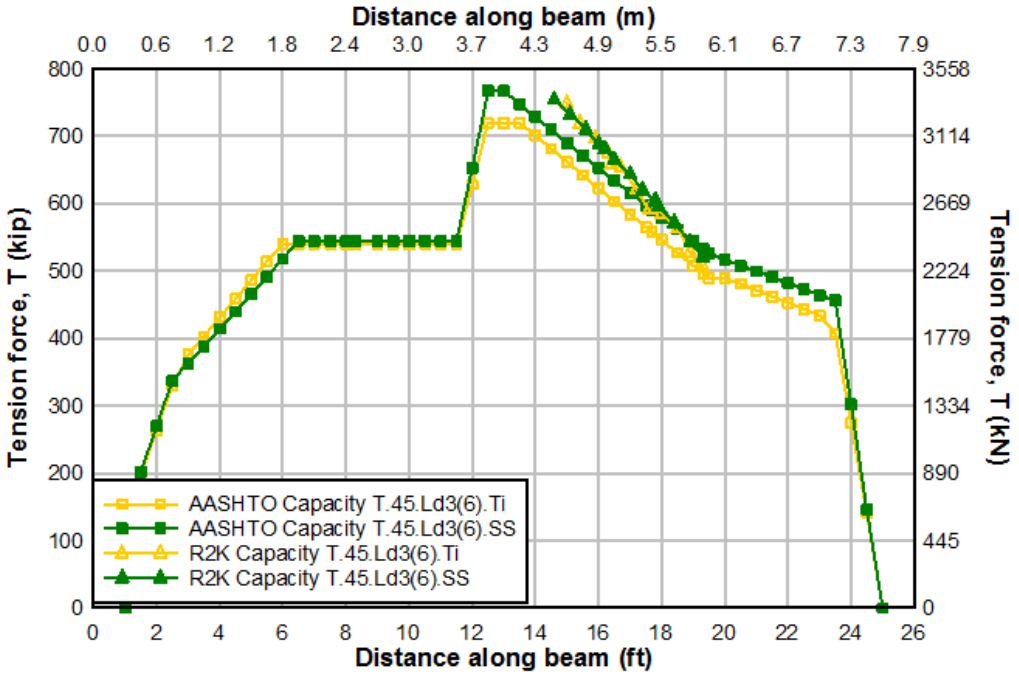

Fig. 5.16 - R2K and AASHTO predicted flexural tension capacities for specimens T.45.Ld3(6).Ti and T.45.Ld3(6).SS

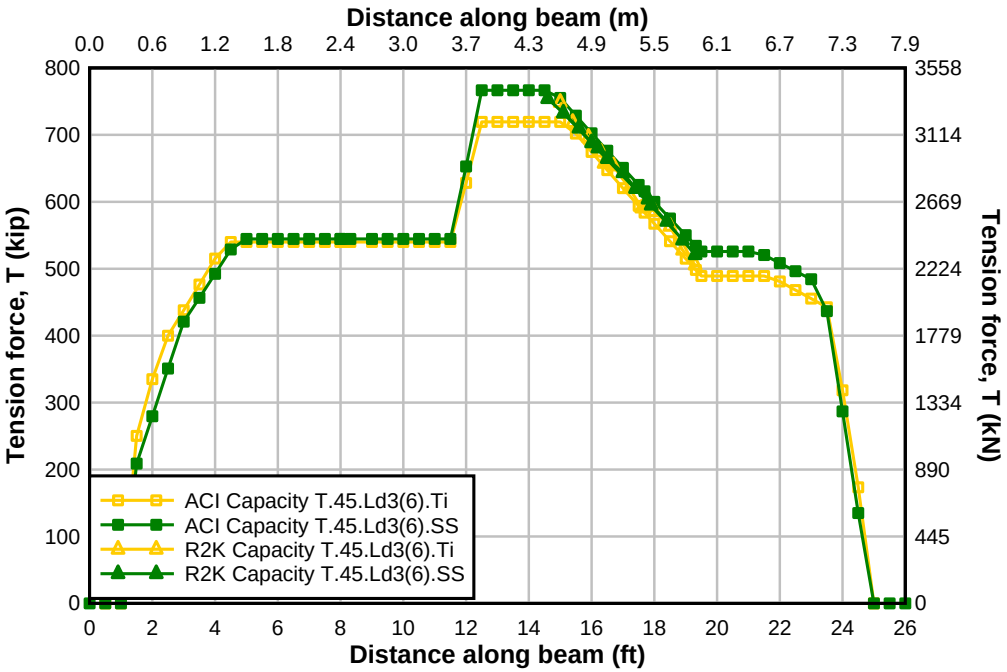

Fig. 5.17 - R2K and ACI predicted flexural tension capacities for specimens T.45.Ld3(6).Ti and T.45.Ld3(6).SS

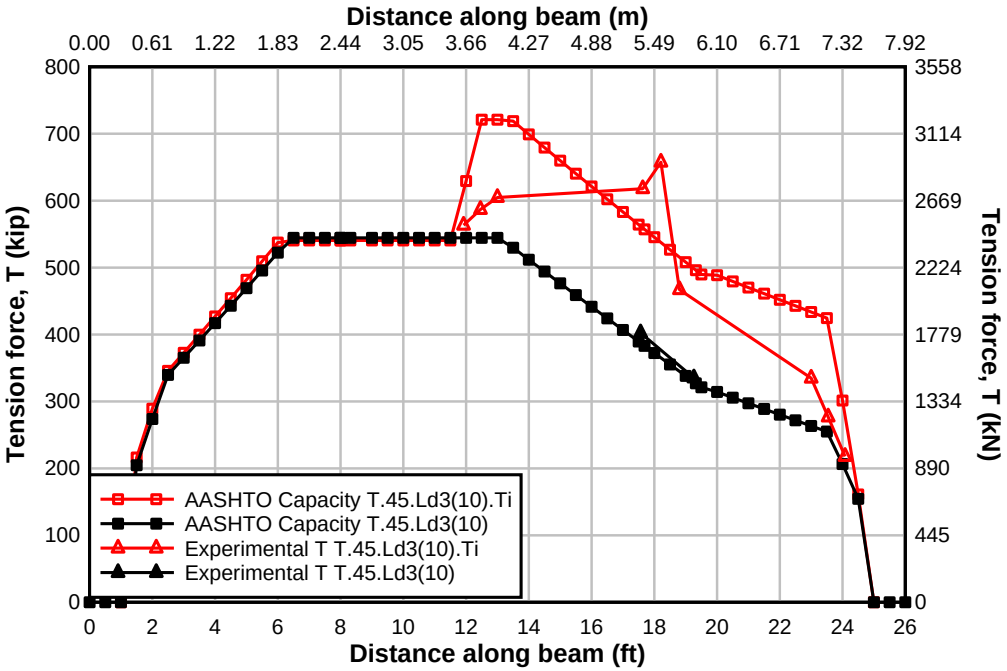

Fig. 5.18 - Experimentally measured and AASHTO predicted flexural tension forces for specimens T.45.Ld3(10) and T.45.Ld3(10).Ti

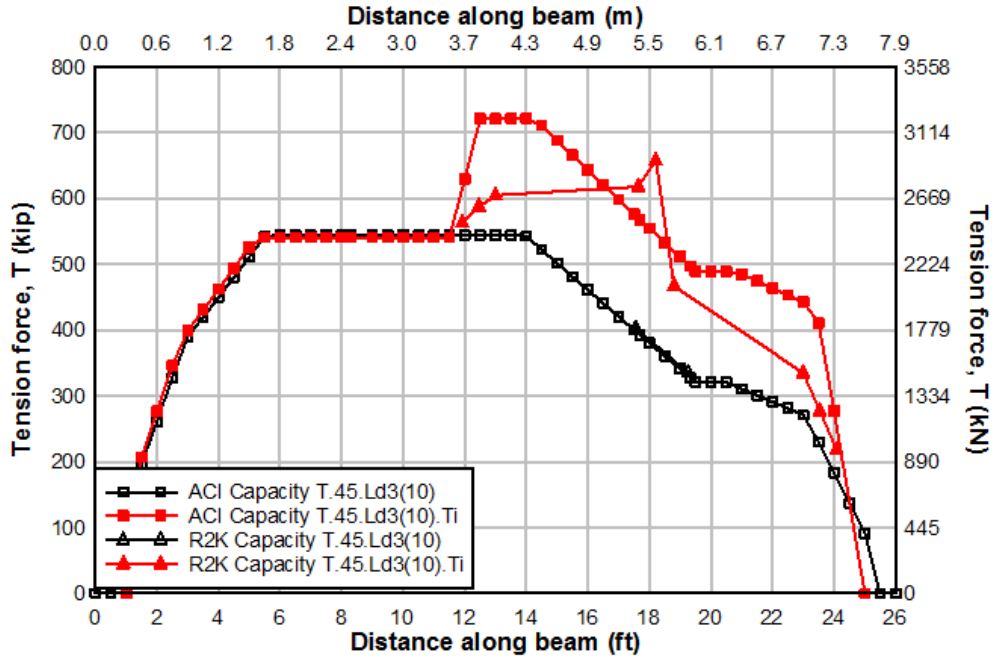

Fig. 5.19 - Experimentally measured and AASHTO predicted flexural tension forces for specimens T.45.Ld3(10) and T.45.Ld3(10).Ti

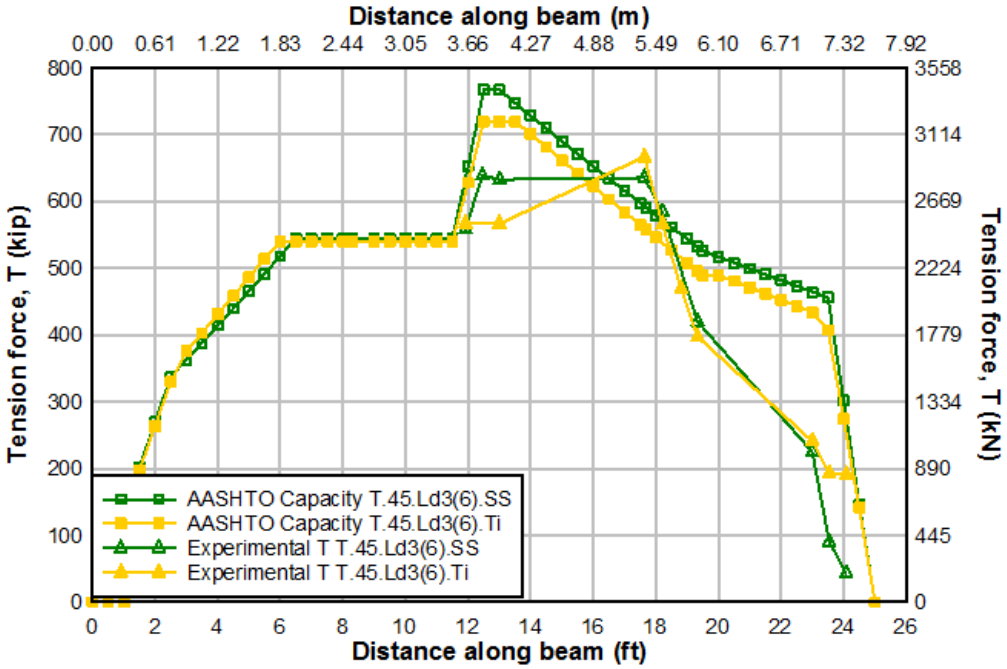

Fig. 5.20 - Experimentally measured and AASHTO predicted flexural tension forces for specimens T.45.Ld3(6).Ti and T.45.Ld3(6).SS

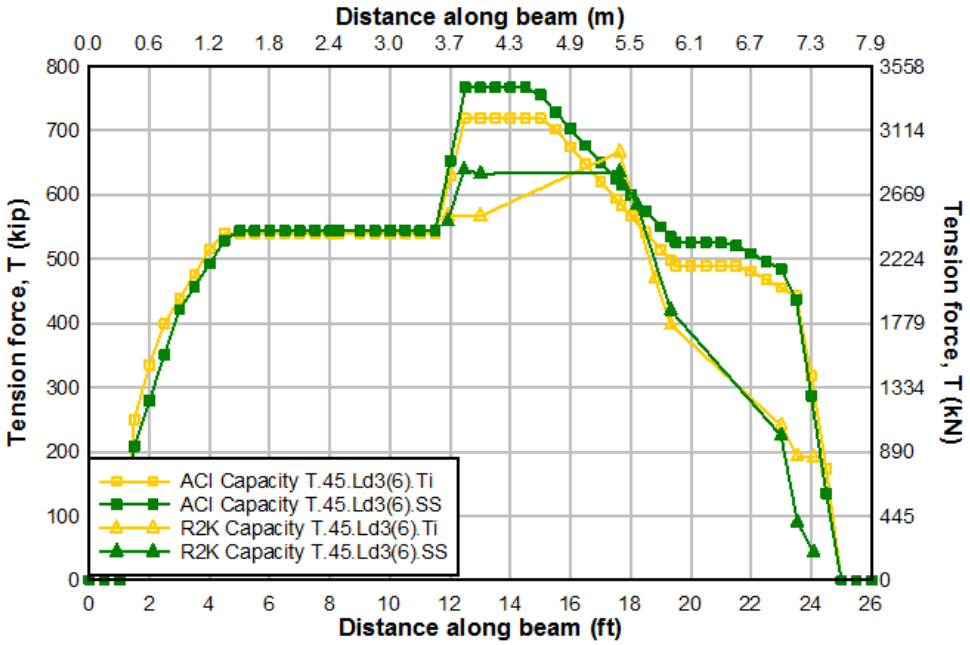

Fig. 5.21 - Experimentally measured and ACI predicted flexural tension forces for specimens T.45.Ld3(6).Ti and T.45.Ld3(6).SS

The AASHTO and ACI flexural tension capacities correlated very well with the R2K predictions for all specimens. The R2K predictions incorporate strain hardening into the reinforcing materials, producing somewhat higher flexural tension forces than the AASHTO specifications.

Variability in material properties, geometry, and strain measurements contributed to some additional uncertainty in the experimentally measured flexural tension forces for the specimens. However, the trend and magnitudes of the experimental data were similar to that of the predictions.

5.3 Experimental and Historical Capacity Results for T-specimens

A series of T and IT-specimens were tested to evaluate shear capacity in vintage RCDG bridges in the early 2000s (Higgins *et al.*, 2004). The suite of experimentally tested specimens was named SPR 350. The specimens failed in shear, flexure, and shear-tension. After analysis of the behavior of the SPR 350 specimens, the specimens created by Triska (2010) shortened the cutoff bar and installed a preformed diagonal crack to ensure an anchorage failure and to fail in shear-tension. This section utilizes historical data and compares the responses of full scale T-specimens with and without anchorage deficiencies.

The SPR 350 suite tested specimens with concrete strengths over 4000 psi (27.6 MPa). Stirrups were spaced at 10 in. (254 mm) and 12 in. (305 mm). The number of flexural steel reinforcing bars varied from specimen to specimen. Only two specimens had a built-in anchorage deficiency and the cutoff bar was terminated 60 in. (1.52 m) before the centerline of the support. The details and capacity of the SPR 350 specimens is shown in Table 5.5 through Table 5.7.

The T-specimens created by Triska (2010) had similar reinforcing bar details as the specimens in the current testing suite and can be found in Table 5.5 through Table 5.7. The baseline specimen T.45.Ld3(10), used for comparison to the strengthened specimens, is labeled as T 45 Ld/3 (5) for experiments performed by Triska (2010). The reinforcing steel cutoff location listed in the tables is the distance from the centerline of the support to the end of the cutoff bar.

Table 5.5 - Comparative Analysis Specimen Material Properties

Testing Program	Specimen	f'_c (psi) [MPa]	Stirrup Spacing S (in) [mm]	Transverse f_{yv} (ksi) [MPa]	Flexural f_y (ksi) [MPa]
SPR 350	1T6	4370 [30.1]	6 [152.4]	50.7 [349.6]	67.2 [463.3]
	2T10	3360 [23.2]	10 [254.0]	50.7 [349.6]	75.8 [540.5]
	6T10	4195 [28.9]	10 [254.0]	50.7 [349.6]	71.6 [493.6]]
	7T12	4310 [29.7]	12 [304.8]	50.7 [349.6]	74.8 [515.7]
	8T12-B3	4570 [31.5]	12 [304.8]	50.7 [349.6]	74.9 [516.4]
	8T12-B4	4725 [32.6]	12 [304.8]	50.7 [349.6]	74.9 [516.4]
	9T12-B4	4910 [33.8]	12 [304.8]	50.7 [349.6]	70.8 [488.1]
Triska (2010) T-specimen	T.45.Ld3.(4)	3165 [21.8]	10 [254.0]	50.5 [369]	71.7 [494.3]
	T.45.Ld3.(5)	3302 [22.8]	10 [254.0]	50.5 [369]	71.7 [494.3]
	T.60.Ld3.(5)	3417 [23.6]	10 [254.0]	50.5 [369]	71.7 [494.3]
	T.0.Ld3.(5)	3538 [24.4]	10 [254.0]	50.5 [369]	71.7 [494.3]
Strengthened T-specimen	T.45.Ld3(10).Ti	3712 [25.6]	10 [254.0]	50.2 [346]	71.6 [493.6]
	T.45.Ld3(6).Ti	3823 [26.4]	6 [152.4]	50.2 [346]	71.6 [493.6]
	T.45.Ld3(6).SS	3206 [22.1]	6 [152.4]	50.2 [346]	71.6 [493.6]

Table 5.6 - Comparative Analysis Specimen Details

Testing Program	Specimen	Span Length L (ft) [m]	Number of Bars			Cutoff Location (in) [m]
			Hooked	Straight	Cutoff	
SPR 350	1T6	24 [7.32]	3	3	0	-
	2T10	24 [7.32]	3	3	0	-
	6T10	21.6 [6.58]	3	3	0	-
	7T12	21.6 [6.58]	3	3	0	-
	8T12-B3	24 [7.32]	0	6	0	-
	8T12-B4	24 [7.32]	0	3	2	60 [1.52]
	9T12-B4	24 [7.32]	0	3	2	60 [1.52]
Triska (2010) T-specimen	T.45.Ld3.(4)	24 [7.32]	2	0	2	66.2 [1.68]
	T.45.Ld3.(5)	24 [7.32]	2	1	2	68.2 [1.73]
	T.60.Ld3.(5)	24 [7.32]	2	1	2	68.2 [1.73]
	T.0.Ld3.(5)	24 [7.32]	2	1	2	68.2 [1.73]
Strengthened T-specimen	T.45.Ld3(10).Ti	24 [7.32]	2	1	2	68.1 [1.72]
	T.45.Ld3(6).Ti	24 [7.32]	2	1	2	68.1 [1.72]
	T.45.Ld3(6).SS	24 [7.32]	2	1	2	68.1 [1.72]

Table 5.7 - Comparative Analysis Specimen Failure Loads

Testing Program	Specimen	Failure Mode	Applied Load (kip) [kN]	Failure Crack Angle (deg)
SPR 350	1T6	Flexural	413.0 [1837]	49
	2T10	Shear	410.6 [1826]	32
	6T10	Flexural	420.8 [1872]	37
	7T12	Shear	433.0 [1926]	33
	8T12-B3	Shear	367.8 [1636]	37
	8T12-B4	Shear	317.8 [1414]	36
	9T12-B4	Shear	307.0 [1366]	40
Triska (2010) T-specimen	T.45.Ld3.(4)	Shear-Tension	223.8 [995]	36
	T.45.Ld3.(5)	Shear-Tension	299.5 [1332]	33
	T.60.Ld3.(5)	Shear-Tension	308.0 [1370]	49
	T.0.Ld3.(5)	Shear-Tension	308.8 [1374]	35
Strengthened T-specimen	T.45.Ld3(10).Ti	Shear-Tension	392.9 [1748]	33
	T.45.Ld3(6).Ti	Flexural	430.7 [1916]	90
	T.45.Ld3(6).SS	Flexural	429.3 [1910]	90

All SPR specimens except for 1T6, had a larger, 10 or 12 in. (254 or 304.8 mm), stirrup spacing. The SPR 350 specimens 8T12-B4 and 9T12-B4 shared similar flexural reinforcement details as specimens tested by Triska (2010) and the NSM strengthened specimens. The SPR 350 specimens constructed with an anchorage deficiency had similar capacities as the specimens from Triska's (2010) analysis. The NSM strengthened T-

specimens that failed in flexure exhibited similar capacities, around 413-430.7 kips (1837-1915 kN), to those tested in the SPR 350 suite. From this comparison, it could be inferred that the NSM strengthening made the T-specimens behave like beams with fully anchored flexural reinforcement.

The load displacement curves from SPR 350, Triska (2010), and current specimens are shown in Fig. 5.22 through Fig. 5.25. The SPR 350 specimens were separated based on continuous and discontinuous cutoff reinforcing steel bars. The NSM strengthened specimens reached larger midspan displacements than the SPR specimens with fully anchored steel reinforcing bars.

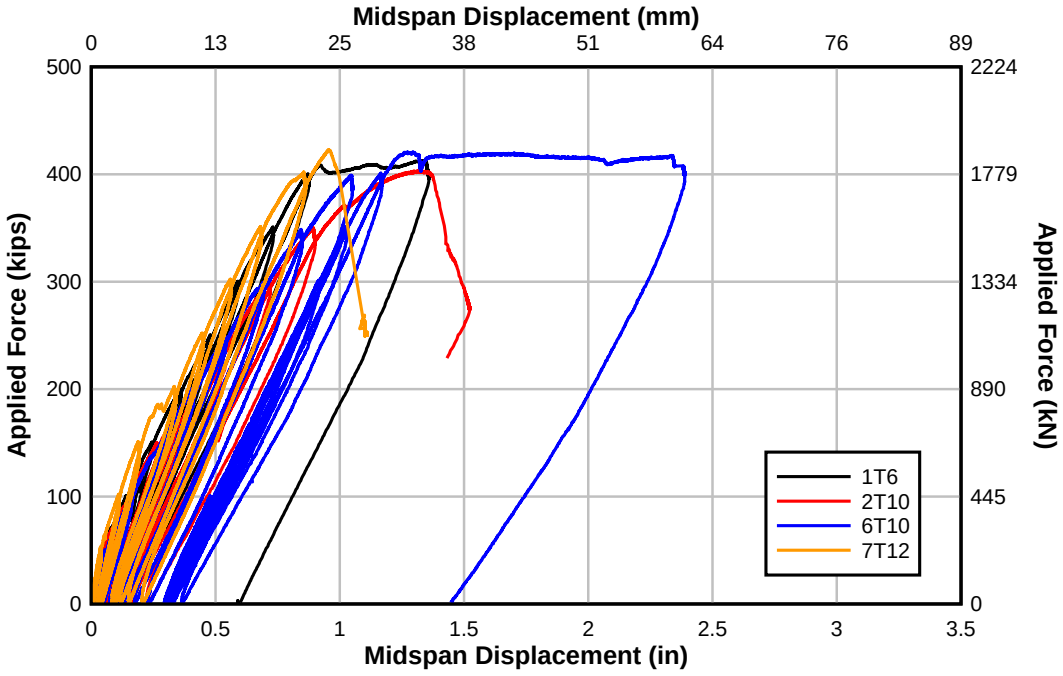

Fig. 5.22 - Load displacement of SPR 350 specimens with fully anchored bars

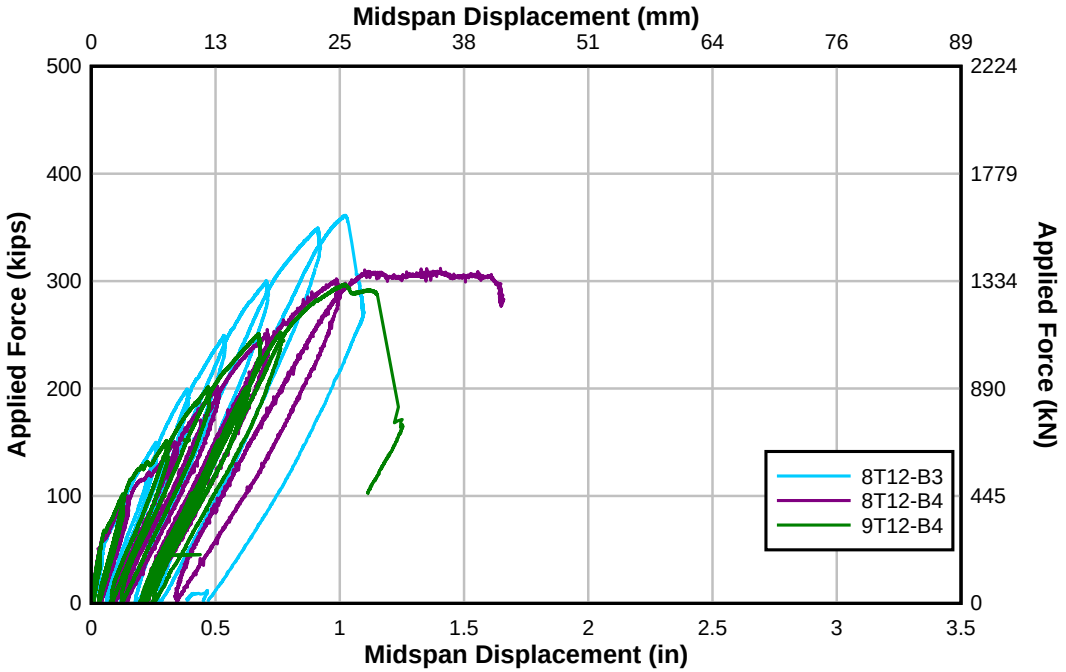

Fig. 5.23 - Load displacement of SPR 350 specimens with built-in anchorage deficiency

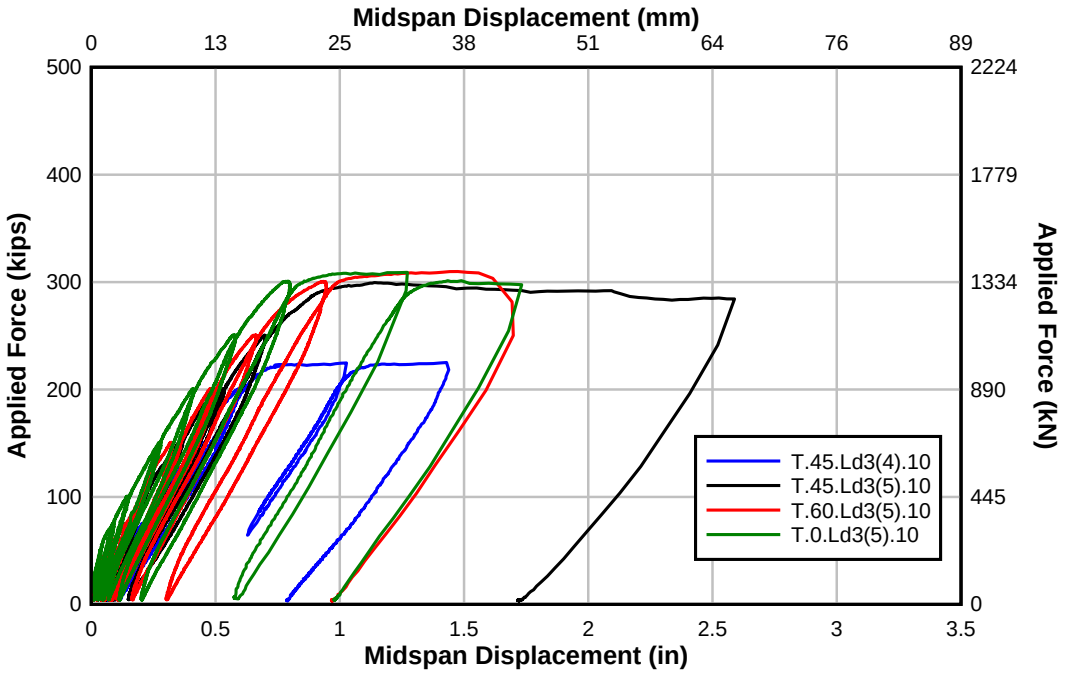

Fig. 5.24 - Load displacement of T-specimens by Triska

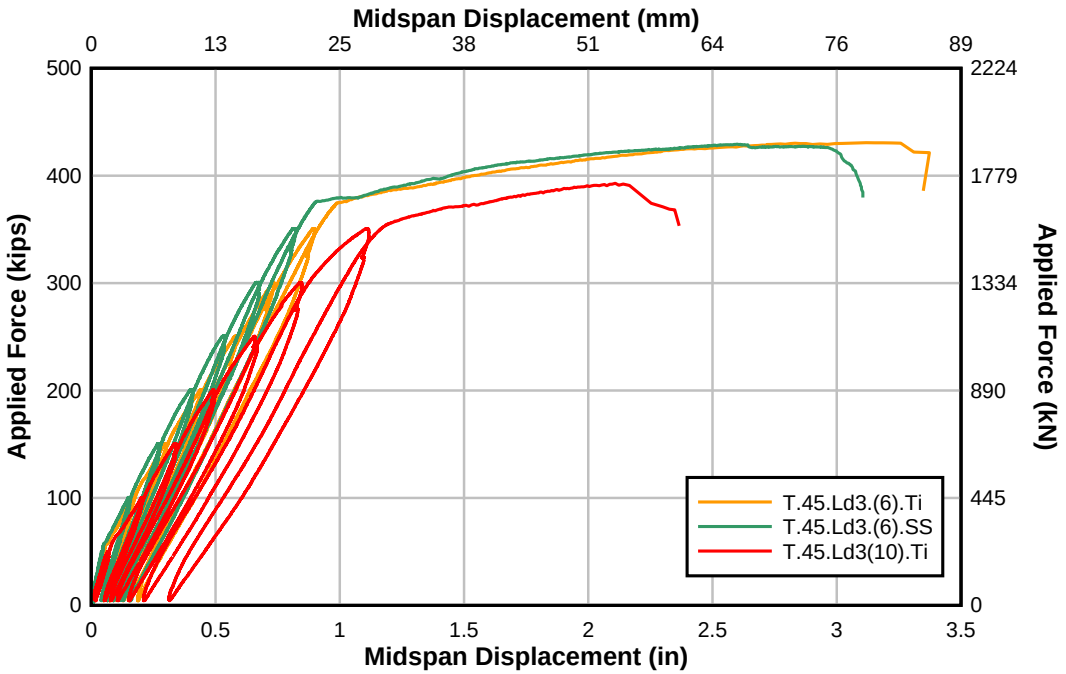

Fig. 5.25 - Load displacement of NSM strengthened T-specimens

5.4 Experimental Bond Stress and Literature Reported Bond Stress

Experimental average bond stresses were compared to the results reported in the literature in Table 5.8 for the internal steel reinforcing bars. Table 5.9 presents average bond stresses measured for NSM materials from the literature and the present experimental results. The bar diameter, embedded length, and test type significantly affect bond stress results and are included in the tables below. It is common to find higher bond stresses in small-scale tests than in full-scale beam specimens. The NSM materials included CFRP bars, CFRP strips, stainless steel bars, and titanium alloy bars.

Table 5.8 - Average bond stress reported in literature and experimental results for internal steel reinforcing bars

Steel Bar Type	Author	Test Type	Bar Diameter (in) [mm]	Bar Embedment (in) [mm]	Average Bond Stress (psi) [MPa]
Plain Bar	Mylrea	Pull-out	1 [25.4]	10 [254]	400 [2.76]
Deformed Proprietary	Clark	Beam End	0.875 [22.2]	8 – 16 [203-406]	300 – 400 [2.07-2.76]
Deformed	Mains	Pull-out	0.875 [22.2]	21 [533]	770 [5.31]
		Beam	0.875 [22.2]	78 [1981]	540 – 815 [3.72-5.62]
	Ferguson	Beam	1.41 [35.8]	-	560 [3.86]
		Beam	1.41 [35.8]	30 – 80 [762-2032]	350 - 475 [2.41-3.27]
	Triska	T Beam	1.41 [35.8]	Hook 20.75 [527]	284 [1.96]
		T Beam	1.41 [35.8]	Cutoff 20.75 [527]	851 [5.87]
	Barker	IT Beam	1.41 [35.8]	Hook 20.75 [527]	98 [0.65]
		IT Beam	1.41 [35.8]	Cutoff 20.75 [527]	156 [1.04]
	Amneus	T Beam	1.41 [35.8]	Hook 20.75 [527]	168 [1.15]
		T Beam	1.41 [35.8]	Cutoff 20.75 [527]	705 [4.86]

Table 5.9 - Average bond stress reported in literature and experimental results for NSM reinforcing materials

NSM Bar Type	Author	Test Type	Bar Diameter (in.) [mm]	Bar Embedment (in.) [mm]	Average Bond Stress (psi) [MPa]
CFRP	De Lorenzis	Pull-out	0.5 [12.7]	6 [152]	1078 [7.43]
		Pull-out	0.5 [12.7]	12 [302]	620 [4.27]
		Modified Pull-out	0.5 [12.7]	2 [50.8]	1637 [11.29]
	Novidis	Modified Pull-out	0.5 [12.7]	4.7 [120]	654 [4.51]
	Bournas	Column	0.63 x 0.08 [16 x 2]	2.75 [70.0]	590 [4.07]
Stainless Steel	Bournas	Column	0.47 [12]	2.75 [70.0]	873 [6.02]
	Amneus	T Beam	0.625 [15.8]	20.75 [527]	404 [2.79]
	Barker	IT Beam	0.625 [15.8]	20.75 [527]	404 [2.79]
Titanium	Barker	IT Beam	0.615 [15.6]	20.75 [527]	369 [2.46]
	Amneus	T Beam	0.615 [15.6]	20.75 [527]	296 [2.04]
		Devel. Test	0.615 [15.6]	12.0 [305]	802 [5.53]

The bond stresses measured in the hooked and cutoff reinforcing steel bars were slightly less than Triska's (2010) results. The hooked and cutoff reinforcing steel bar bond stresses in Barker's IT-specimens were lower than those found in the T-specimens and due to differences in the anchorage failure modes between T and IT-specimens. Transverse steel crossing the splitting plane of the T-specimens allows higher bond stresses to develop in the cutoff reinforcing steel bar even after initial slip occurs. The average bond stress for the

deformed steel reinforcing bars from this experimental data set was larger than the majority of reported bond stresses from the literature.

In Table 5.9, the bond stresses of the NSM bars in the T-specimen were significantly lower than those found in pull-out tests. Lower NSM bond stress values indicate the NSM bars were adequately anchored at that location. The average bond stresses measured in the NSM titanium alloy bar bond length tests were similar to those found for CFPR in similar type short bond tests.

Table 5.10 below lists the bond stresses required for specified development lengths of steel reinforcing bars using Eq. [2.1]. Since ACI and AASHTO development lengths do not apply to NSM materials, the straight development was assumed to be 6 in. (152.4 mm) in this analysis. Measured concrete and reinforcing material yield strengths were used in the average bond stress calculations.

Table 5.10 - Theoretical average bond stress based on straight development length

Material	**Real f_y (ksi) [Mpa]**	**Bar Diameter, d_b (in) [mm]**	**l_d (in) [mm]**		**Average Bond Strength (psi) [MPa]**	
			ACI 318	**AASHTO**	**ACI 318**	**AASHTO**
Steel	71.6 [493]	1.41 [36]	66.4 [1687]	76.9 [1953]	380 [2619]	328 [2261]
Titanium	145.5 [1002]	0.615 [16]	6 [152]		3728 [25689]	
Stainless Steel	83 [572]	0.625 [16]	6 [152]		2161 [14892]	

The mean average cutoff bar bond strength found in T-specimens was 705 psi (4.86 MPa), almost twice the bond strength assumed for development of the #11 (36M) bar using either specification. Therefore, the design development lengths were quite conservative compared to the experimental results.

5.5 Contribution of NSM Bars as Equivalent Area of Reinforcing Steel

Generally, when evaluating the flexural capacity of a reinforced concrete section, the strength increases as the area of flexural reinforcing steel increases. However, above a certain threshold of flexural steel, the member capacity plateaus because it becomes dependent on the shear strength of the section. This behavior is illustrated in Fig. 5.26 through Fig. 5.29. This section describes the NSM strengthening in terms of an equivalent area of reinforcing steel. Once the required area of reinforcing steel is found at the critical section, the area of steel can be transformed into an equivalent NSM strength.

The loads versus area of steel responses were computed using the specific specimen geometry and measured material properties. The cutoff reinforcing steel bar area was increased from 0 to 1.56 in^2 (1006 mm^2) for each bar. Then, the five flexural steel reinforcing bars were grouped into one area of steel at distance d_s from the top of the section. The combined area of steel was then increased incrementally to 20 in^2 (129 cm^2) of steel. The yield strength of the reinforcing steel was set as 71.7 ksi (494 MPa) for specimen T.45.Ld3(10) and 71.6 ksi (493 MPa) for the NSM strengthened specimens. Each point along each curve was evaluated for the same moment-to-shear ratio. The moment-to-shear ratios (M:V) chosen were at 5.67:1, corresponding to d_v away from the loading point, and 7.52:1, corresponding to the failure location. Choosing a moment-to-shear ratio d_v away

from the loading point provided a common location to compare between specimens. The predicted and experimentally measured failure loads for the specimens are shown in the figures for reference. Other relevant reference lines are also included for the NSM strengthened specimens.

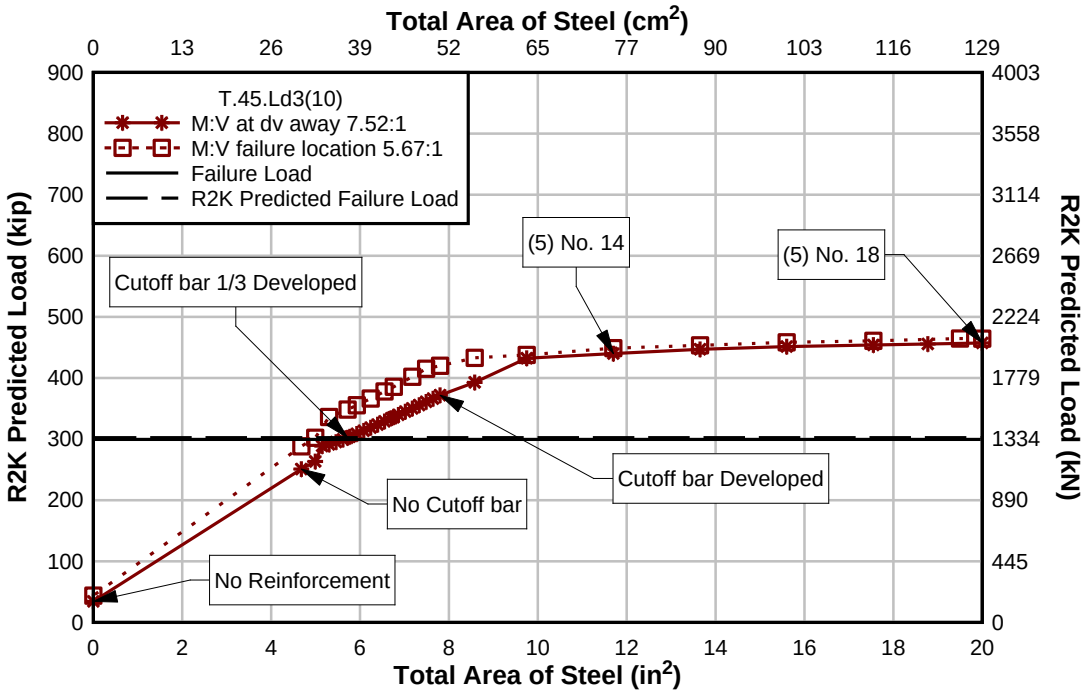

Fig. 5.26 - Specimen T.45.Ld3(10) predicted load for increasing area of equivalent flexural reinforcing steel area

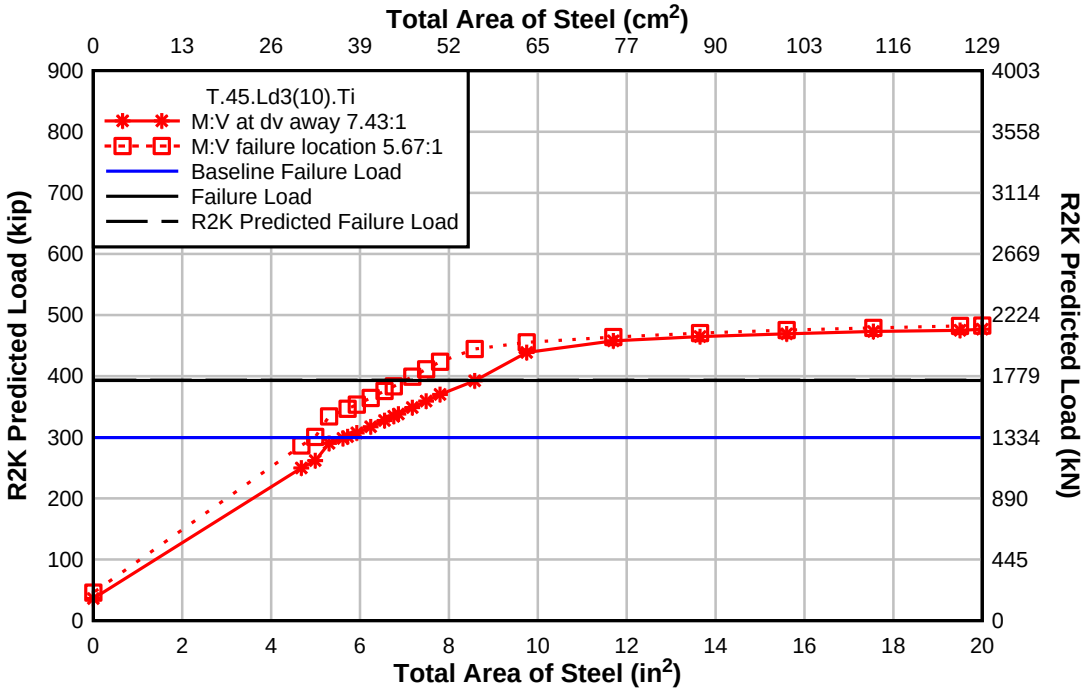

Fig. 5.27 - Specimen T.45.Ld3(10).Ti predicted load for increasing area of equivalent flexural reinforcing steel area

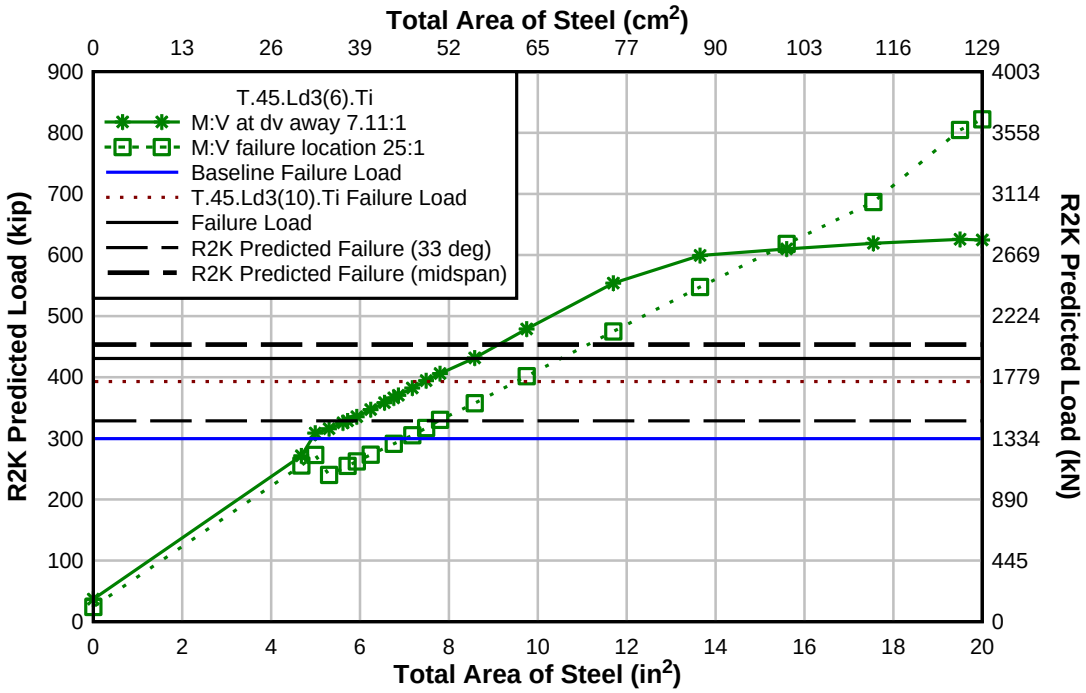

Fig. 5.28 - Specimen T.45.Ld3(6).Ti predicted load for increasing area of equivalent flexural reinforcing steel area

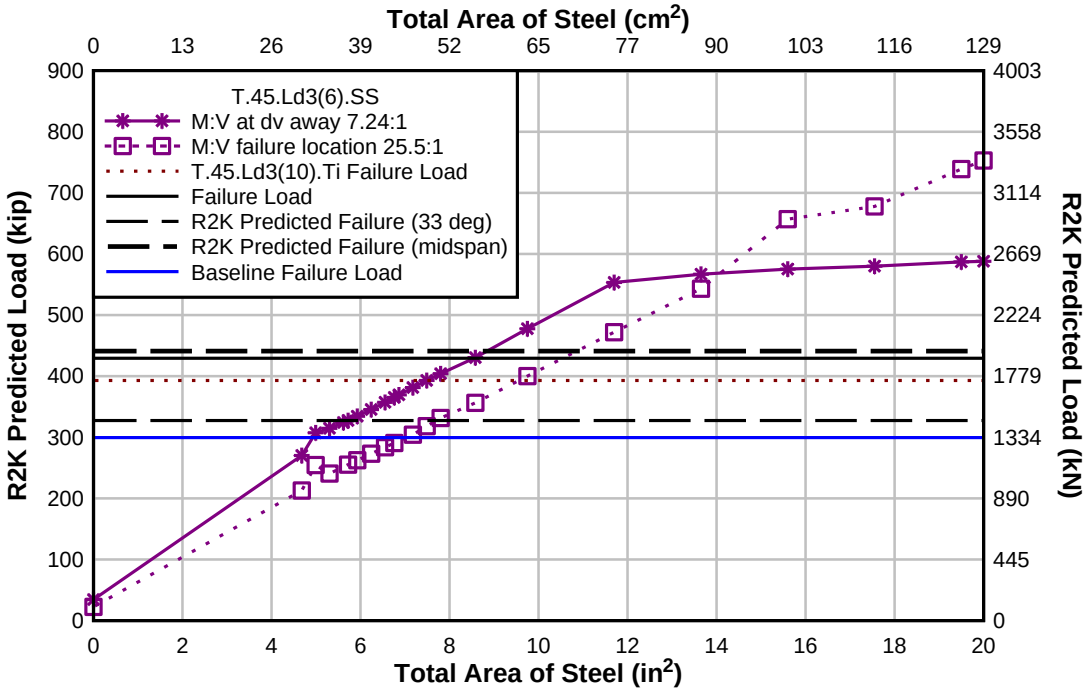

Fig. 5.29 - Specimen T.45.Ld3(6).SS predicted load for increasing area of equivalent flexural reinforcing steel area

Specimens T.45.Ld3(6).Ti and SS failed in flexure near midspan and thus used a larger M:V to predict the section capacity. The flexurally predicted load and area of steel curves were more linear than the curve at d_v away because shear does not control strength for the tightly spaced transverse reinforcing steel in these specimens.

The strengthened capacities of the NSM titanium alloy and stainless steel specimens were greater than the capacity of specimen T.45.Ld3(10). Using the reference lines, the area of internal reinforcing steel that would provide an equivalent strength as the NSM bars was determined. For example, specimen T.45.Ld3(10) had a maximum applied load of 299.5 kips (1332 kN), which corresponded to an equivalent area of internal reinforcing steel of approximately 5.7 in^2 (36.7 cm^2). The NSM titanium alloy bar strengthened specimen,

T.45.Ld3(10).Ti, failed at a load of 430.7 kips (1920 kN) and had an equivalent area of internal reinforcing steel of approximately 8.6 in^2 (55.5 cm^2). Therefore, installing four NSM titanium bars with a centroid over the cutoff bars was equivalent to increasing the area of steel reinforcing bars by 3.6 in^2 (23.2 cm^2). This is comparable to adding almost two #11 (36M) bars as internal reinforcement at d_v away from the loading point. The specimen retrofitted with 8 NSM stainless steel bars, T.45.Ld3(6).SS, provided approximately an additional 2.3 in^2 (14.8 cm^2) of equivalent area of internal reinforcing steel at d_v away to the baseline specimen.

5.6 ACI 440 Design Recommendations for Metallic NSM materials

This section provides design guidance for a metallic NSM strengthening. To confirm design methodology, calculations using titanium and stainless steel bars were compared to CFRP bars using ACI 440 guidelines. Applicable ACI 440 equations are described in section *2.3.4 ACI 440 Guide for Design for External FRP systems*.

The environmental factor was neglected in the following calculations since the intent of this section is to compare materials with identical exposure types. The yield strain of the metallic materials is listed in the tables for reference. In addition, the maximum strain in the NSM materials was calculated based on the strain diagram assuming strain compatibility. The maximum debonding strain, usually calculated by Eq. [2.23], was limited to the maximum debonding strain in the CFRP, 0.0117. Experimental research has determined the bond of NSM materials is typically limited by the concrete-epoxy interface; therefore, it is not feasible to achieve much greater bond strengths than those achieved by the CFRP NSM at non-termination locations. The effective strain in the NSM materials

was the lesser of the debonding strain or strain to achieve concrete crushing calculated in Eq. [2.23] and is listed in Table 5.11. Two CFRP bars of the same material but different diameters were chosen for comparison. The smaller 0.5 in. (12.7) diameter bar is more commercially available and would provide a tensile strength similar to the titanium NSM strengthening.

Table 5.11 - ACI 440 NSM stress and strain calculation

NSM Material	**# of NSM bars**	**Bar Diam (in) [mm]**	**Yield Strain ε_y**	**Max NSM strain in section ($f_s=f_y$)**	**Debonding Strain ε_{fd}**	**NSM Effective Strain ε_{fe}**	**NSM Effective Stress f_{fe} (ksi) [MPa]**
Titanium	4	0.625 [15.9]	0.0094	0.0286	0.0117*	0.0117	145 [999]
Stainless Steel	8	0.625 [15.9]	0.0026	0.0245	0.0117*	0.0117	75 [517]
CFRP	4	0.625 [15.9]	-	0.0159	0.0117	0.0117	210 [1450]
CFRP	4	0.5 [12.7]	-	0.0525	0.0117	0.0117	210 [1450]

*Debonding strain limited to CFRP debonding strain

In all materials, the effective strain was less than the theoretical maximum strain if the reinforcing steel was at yield. Limiting the debonding strain ε_{fd} shifted the failure mode of the metallic NSM materials from concrete crushing to debonding of the NSM. Since ACI 440 is predicated of the ultimate strain of a less ductile material, it is not appropriate to design with the ultimate strains of titanium and stainless steel. The titanium and stainless steel NSM materials still reach their yield strength, despite limiting ε_{fd} to the CFRP debonding strain. The ultimate stress for the CFRP material used was 300 ksi (2068 MPa).

Due to debonding issues, only 210 ksi (1447 MPa), or 70% of the material is utilized. The larger diameter CFRP bar has identical effective stress and strains than the smaller diameter CFRP bar.

Section properties including the distance to the neutral axis, curvature, average bond stress, and development length were calculated using ACI 440 requirements and are tabulated in the Table 5.12. The distance to the neutral axis, c, was calculated by iterating the AASHTO LRFD Eq. [F.7] equation and incorporated compression steel, the compression flange, and the NSM materials. The average bond stress was calculated using Eq. [2.1] and the ACI 440 development length (Eq. [2.22]).

Table 5.12 - ACI 440 NSM neutral axis, curvature, bond, and development length calculation

NSM Material	**ACI 440 c (in) [mm]**	**Curvature at midspan ψ (1/in) [1/mm]**	**Average Bond Stress, μ_{avg} (ksi) [MPa]**	**ACI 440 Development Length (in) [mm]**
Titanium	3.910 [99.3]	0.000767 [0.000030]	1.2 [8.6]	11.2 [285]
Stainless Steel	4.068 [103.3]	0.000738 [0.000029]	4.5 [31.1]	5.8 [148]
CFRP	6.546 [166.3]	0.000458 [0.000018]	1.0 [6.9]	16.3 [414]
CFRP	2.230 [56.6]	0.001345 [0.000053]	1.0 [6.9]	26.3 [668]

The curvature of the section, ψ, is related to the neutral axis location, c. The section strengthened with smaller diameter CFRP bars obtained the highest curvature. The curvature of the metallic NSM materials was similar. After the yielding moment is reached

in the metallic NSM strengthened section, the curvature and ductility will increase without a significant increase in moment capacity. The strains increase after the yield strain with minimal strain hardening in the metallic NSM materials.

ACI 440 uses an average bond strength of 1.0 ksi (6.89 MPa) that is calibrated to CFRP materials. Limiting the effective strain in the NSM titanium and stainless steel decreased the bond stress and development length. The modulus and yield strength of materials significantly affected the ACI 440 calculated development length. Throughout the current experimental program, the development length was assumed to be 6 in. (152.4 mm) for mechanically anchored NSM titanium and stainless steel. The ACI 318 hooked development length for reinforcing bar is approximately half that of the straight bar development length. Accordingly, the hooked NSM development length is assumed to be shorter than the straight bar development length calculated by ACI 440. Thus, the assumed hooked development length of 6 in. (152.4 mm) is reasonable for NSM titanium and stainless steel.

According to the ACI 440 design methodology, the maximum flexural tensile force provided by the NSM strengthening is equal to the effective stress multiplied by the number and area of the NSM bars. The number of NSM bars equivalent to a Gr. 60 (Gr. 420) #11 (36M) steel reinforcing bar tensile strength is listed in Table 5.13.

Table 5.13 - ACI 440 Calculation to determine number of NSM bars required to replace a #11 (36M) steel reinforcing bar

Material	Bar Area (in^2) [mm^2]	Effective Stress (ksi) [Mpa]	Effective Force (kip) [kN]	# of NSM Bars Required
Steel	1.56 [1006]	60 [413]	93.6 [416]	1.0
Titanium	0.31 [200]	145 [999]	44.95 [200]	2.1
Stainless Steel	0.31 [200]	75 [517]	23.25 [103]	4.0
CFRP	0.31 [200]	210 [1447]	65.1 [290]	1.4
CFRP	0.2 [129]	210 [1447]	42 [187]	2.2

To retrofit an inadequate anchorage detail of two Gr. 60 (Gr. 420) #11 (36M) cutoff reinforcing bars over four #5 (16M) titanium bars would be required. Eight #5 (16M) stainless steel bars, over two #5 (16M) CFRP bars, or over four #4 (13M) CFRP bars would be required for an equivalent retrofit. The design methodology used for strengthening the T-specimens is consistent with these values and proved to be successful at eliminating the anchorage deficiency. If extended past midspan, the flexural capacity of the specimen could have been increased. After limiting the metallic NSM material debonding strain, the metallic NSM materials were still able to achieve their yield strength prior predicted failure. Obtaining the design strength and similar strain values suggest that a metallic NSM material can be designed using the ACI 440 NSM CFRP strengthening methodology.

5.7 Summary

The NSM strengthened T-specimens exhibited increased strength and ductility compared to an otherwise similar specimen without NSM. Capacity predictions were conducted using Response 2000, ACI, and AASHTO specifications. Comparisons were made between applied load, diagonal tension strength, flexural strength, flexural tension forces, and bond stresses. In addition, a review of previous data and design methodologies was performed.

Diagonal tension failures were well predicted using R2K at the failure location. The NSM strengthened specimen with a wide stirrup spacing was able to prevent premature failure due to inadequate anchorage of the poorly detailed cutoff reinforcing steel bars. However, the specimen eventually failed diagonal tension due to inadequate transverse reinforcement. The two additional strengthened T-specimens with a tighter stirrup spacing precluded diagonal tension failure. The failure mode was shifted from a shear dominated failure to that of a ductile flexural failure. However, flexural strengths were difficult to predict because of the partial contribution of the NSM materials around the flexural hinge zone that occurred around the ends of the NSM bars. R2K and the design specifications underestimated or overestimated the flexural capacity depending if the NSM materials were included in the predicted strength. It was conservative to ignore the contribution of the NSM bars at their termination point. Based on load and flexural tension capacity, the NSM titanium and stainless steel provided similar strengths, although it required twice the amount of stainless steel.

When determining shear capacities AASHTO specifications predicted a larger capacity than ACI. According to the design specification predictions, specimen T.45.Ld3(10).Ti

was likely to exhibit a diagonal tension failure. The lower concrete compressive strengths in specimen T.45.Ld3(6).SS contributed to a reduced expected shear capacity. Differences in moment predictions between design specifications and R2K was most likely due to concrete strengths, the incorporation of #6 (19M) bars and strain hardening in R2K. Both failure modes need to be checked at each critical section.

The AASHTO and ACI predictions of available flexural tension strength were similar. Both methods indicated flexural failure should occur just after the termination of the NSM bars in a region of the specimen subject to ideal bending. However, if the NSM material terminates in a region subject to both bending and shear, the AASHTO approach may provide better insight at the critical sections than the ACI approach because it takes into account the geometry of the diagonal crack and the amount of transverse reinforcing steel. Experimentally measured tensile forces confirmed the predicted trends in tension demand along the development of the cutoff reinforcing steel bars. The R2K predictions and experimental results were in good agreement, particularly at the preformed diagonal crack location.

The NSM strengthened T-specimens exhibited similar behavior to the SPR 350 specimens with fully anchored flexural steel, inferring that the retrofit eliminated the anchorage failure. In addition, the NSM strengthened specimens achieved larger midspan displacements at similar ultimate loads as the SPR 350 specimens.

The cutoff reinforcing steel bars in the NSM strengthened specimens had reasonably similar bond strengths compared to those found in literature. This indicates that the

maximum average bond stresses is not changed by adding NSM materials. However, the bond strength is reached at larger applied load (and internal moment and shear) for the NSM strengthened specimens compared to those without NSM. In addition, the complex ACI development length equation provided a development length closest to the measured bond stresses.

After limiting the metallic NSM material effective strain, the metallic NSM materials were still able to reach their yield strength prior to predicted failure. Obtaining the design strength and similar strain values suggest that a metallic NSM material can be designed using the ACI 440 NSM CFRP strengthening methodology. The ACI 440 development length for metallic materials is comparable to those of CFRP. In addition, the assumed hooked bar development length in the current research is reasonable compared to the ACI 440 straight bar development lengths.

6 SUMMARY AND CONCLUSIONS

The objective of this research was to develop methods to extend the service life of diagonally cracked RCDGs with poorly detailed flexural cutoff reinforcing steel using metallic NSM materials. To meet this objective, three strengthened full-scale T-specimens were designed, constructed, and tested to failure. Specimens were designed to represent vintage RCDG construction practices. All specimens had flexural steel reinforcing bars that were cutoff in the flexural tension region and which extended only 1/3 of the design development length past a 45° preformed diagonal crack. The design intent of metallic NSM material was to create an external lap splice thereby providing reinforcing material that could extend the cutoff location. The NSM material would effectively eliminate the anchorage deficiency common in many vintage RCDGs built in the 1950s. Two specimens were strengthened with NSM titanium alloy bars and one specimen was strengthened with NSM stainless steel reinforcing bars. The NSM bars were terminated with 90° hooks with 6 in. (152 mm) long tails to provide a mechanical anchorage at the ends of the NSM bars. Data were collected to assess global and local structural responses at critical locations along the specimens. The experimental results were compared to ACI 318 and AASHTO-LRFD design specifications as well as a sectional analysis program, Response 2000 (R2K). Conclusions based on the experimental and analytical findings, recommendations, and additional research is discussed in the sections below.

6.1 Experimental Conclusions

This section summarizes the experimental conclusions made from strengthening the full-scale T-specimens. In all specimens, the preformed diagonal crack did not dictate the failure location. In specimens with a lower shear capacity, T.45.Ld3(10) and

T.45.Ld3(10).Ti, the failure location was at the termination of the cutoff steel reinforcing bar due to diagonal tension. Specimens T.45.Ld3(6).Ti and SS failed in flexure just past the termination of the NSM materials near midspan.

All NSM strengthened specimens exhibited increased capacity and ductility compared to an otherwise similar specimen tested by Triska (2010) without NSM. The retrofitted specimens displayed distributed cracking around the NSM bars. Longitudinal cracks along the epoxy-concrete interface appeared around the area of the cutoff reinforcing steel bar near failure. A controlled slip response was achieved in the titanium retrofitted specimens. In addition, the stainless steel strengthened specimen eliminated large cutoff bar slip due to the increased stiffness and distribution of the stainless steel bars over the depth of the stem. Based on slip strain response of the cutoff reinforcing steel bar, it was estimated that the cutoff reinforcing steel bar was halfway developed by the location of the preformed diagonal crack.

Strain compatibility between the internal reinforcing steel and NSM reinforcing bars remained only until first cracking occurred. Localized cracking and reinforcing steel slip produce some variation in strains at a section. Strain gages were commonly damaged prior to reaching the maximum load, so that the NSM material behavior at failure could not be fully characterized. From the available experimental data, it was noted that the NSM titanium and stainless steel bars did not reach yield around the termination of the cutoff bars. The specimens did not necessarily have to make use of the yield strength of the NSM materials to achieve the design objectives.

Measured flexural tension values peaked at the intersection of the preformed diagonal crack with the cutoff and hooked reinforcing steel. Experimental flexural tension forces between specimens were similar along the length of the specimen regardless of stirrup spacing and NSM material. The majority of the flexural tension force was carried by the hooked steel reinforcing bar, and less than 50% was contributed by the NSM materials in all instrumented locations. The AASHTO predicted flexural tension demands were larger than the measured flexural tensions.

Average bond stress was calculated immediately after initial slip, where strains in the cutoff reinforcing steel bar reversed. Furthermore, bond stress was also measured after significant slip, and was classified as maximum bond stress. Maximum bond stress was typically observed near failure. With increased stirrups and the addition of NSM reinforcement, the transition from initial to maximum bond stress was delayed until larger loads were achieved. Without the NSM reinforcement the specimens would have failed in diagonal tension due to poor detailing of the cutoff reinforcing steel bar and the high bond stresses in the region.

6.2 Analytical Conclusions

This section summarizes the analytical conclusions drawn from comparison of design codes and historical data to experimental results. Analytical predictions were conducted using R2K as well as the ACI and AASHTO design specifications. To predict the failure mode and location in the T-specimens, several locations along the span must be analyzed to identify the critical section. Key locations at which analyses were conducted included

midspan, d_v away from the loading point, and at the end of the cutoff bar. For each section shear, moment, and flexural tension forces must be checked.

Flexural tension or diagonal-tension failures were well predicted using R2K at the failure location. The NSM strengthened specimens prolonged or eliminated the flexural tension anchorage deficiency and shifted failure mode to a ductile flexure failure. Prediction of the flexural strength depended on the partial contribution of the NSM bars in the hinge region past midspan around the hook terminations of the NSM bars. The R2K predicted and experimentally measured flexural tensions were in good agreement, particularly at the preformed diagonal crack location. Based on load and flexural tension capacity, the NSM titanium alloy and stainless steel reinforcing bars can both be used to provide adequate strength and ductility. However, an NSM strengthening using stainless steel reinforcing bars requires twice the amount of material as that required for the titanium alloy strengthening.

The NSM strengthened specimen cutoff reinforcing steel bars exhibited reasonably similar bond stress values compared to those found in literature. In addition, the NSM strengthened T-specimens behaved similarly to previously tested beams with fully anchored flexural reinforcement.

ACI 440 design guidelines are applicable and practical for a metallic NSM strengthening. A limit to the debonding strain is proposed, but the yield strength of the metallic NSM materials can still be reached. The design methodology in ACI 440 was consistent with this experimental methodology for strengthening anchorage deficiencies.

6.3 Recommendations

In vintage RCDGs, cracking along the longitudinal steel reinforcement at known cutoff locations may indicate an anchorage deficiency and a need to strengthen. After installation of NSM reinforcing bars, small, distributed cracks along the epoxy-concrete interface along the grooves may indicate slip of the internal reinforcing steel. Longitudinal cracking of the epoxy along the NSM may indicate near failure conditions. While designing the NSM retrofit, avoid terminating all NSM bars in one location to prevent stress concentrations. Optimally, the NSM reinforcement should be vertically placed around the deficient longitudinal bar or below, possibly in the soffit of the web. As the NSM reinforcement is placed higher into the web it becomes less efficient. If terminated in a section with potential outward forces, a confining plate over the hooks would be a suitable precaution to prevent out-of-plane movement after loss of bond.

Titanium alloy bars and stainless steel reinforcing bars were chosen for use in NSM application because of their high strength, ductility, environmental durability, and ability to fabricate mechanical anchorages. Based on experimental results, both titanium alloy bars and stainless steel reinforcing bars were effective for NSM strengthening. The overall member performance was similar and the use of one material over the other may be dictated by project costs or other constraints. Use of titanium alloy bars required approximately half as many bars to achieve the same load and ductility as stainless steel strengthened specimen. While the material cost of titanium alloy bars may be greater than stainless steel reinforcing bars, lower construction costs related to cutting, epoxy, and fabrication contribute to the overall lower cost of a titanium NSM strengthening.

Ultimately, using NSM titanium alloy bars or stainless steel reinforcing bars could help maintain and improve the operational safety and mobility of the transportation system.

6.4 Additional Research

To supplement the research conducted and reported in this thesis, the following areas are suggested for future work:

- Fully characterize the straight and hooked development length of NSM titanium alloy and stainless steel reinforcing bars embedded in concrete grooves and bonded with epoxy.
- Investigate fatigue performance of NSM titanium alloy and stainless steel reinforcing bars under repeated loading.
- Investigate the potential to use unbonded titanium alloy bars which would eliminate the need for cutting concrete grooves and filling them with epoxy.
- Assess the environmental durability of NSM titanium alloy and stainless steel reinforcing bars bonded in epoxy filled concrete grooves on the surface of a concrete section.
- Investigate different bend radii of the hooked detail for NSM bars to optimize the hook performance and minimize concrete surface preparations.
- Investigate vintage RCDG with concrete and reinforcing steel deterioration.

7 BIBLIOGRAPHY

Al-Mahmoud, F., Castel, A., Francois, R., Tourneur, C. 2011. "Anchorage and tension-stiffening effect between near-surface-mounted CFRP." *Cement & Concrete Composites* 33: 346-352.

Al-Mahmoud, F., Castel, A., Francois, R., Tourneur, C. 2009. "Strengthening of RC members with near-surface mounted CFRP rods." *Composite Structures* 91: 138-147. *Elsevier.* Web. Aug. 1 2013.

American Association of State Highway Officials. 1953. "Standard Specifications for Highway Bridges," 6th Edition, *AASHO*, Washington, D.C.

American Association of State Highway Officials. 1973. "Standard Specifications for Highway Bridges," 11th Edition, *AASHO*, Washington, D.C.

American Association of State Highway and Transportation Officials. 2012. "AASHTO LRFD Bridge Design Specifications," 6th edition with 2013 interims, *AASHTO*, Washington, D.C.

American Concrete Institute. 1956. "Building Code Requirements for Reinforced Concrete (ACI 318-56)." *ACI Manual of Concrete Practice*, Detroit, Michigan.

American Concrete Institute. 2008. "Guide for the Design and Construction for Externally Bonded FRP Systems for Strengthening Concrete Structures (ACI 440.2R-08)," *ACI Manual of Concrete Practice*, Farmington Hills, Michigan.

American Concrete Institute. 2011. "Building Code Requirements for Structural Concrete (ACI 318-11) and Commentary," *ACI Manual of Concrete Practice*, Farmington Hills, Michigan.

ASTM A305-50T. 1950. "Tentative Specifications for Minimum Requirements for the Deformations of Deformed Steel Bars for Concrete Reinforcement," *ASTM International*.

ASTM A615/A615M-14. 2014. "Standard Specification for Deformed and Plain Carbon-Steel Bars for Concrete Reinforcement," *ASTM International*, West Conshohocken, Pennsylvania.

ASTM B348/B348M-13. 2013. "Standard Specification for Titanium and Titanium Alloy Bars and Billets," *ASTM International*, West Conshohocken, Pennsylvania.

ASTM C39/C39M-13a. 2013. "Standard Test Method for Compressive Strength of Cylindrical Concrete Specimens," *ASTM International*, West Conshohocken, Pennsylvania.

ASTM C496/C496M-11. 2011. “Standard Test Method for Splitting Tensile Strength of Cylindrical Concrete Specimens,” *ASTM International*, West Conshohocken, Pennsylvania.

ASTM E8/E8M-13a. 2013. “Standard Test Methods for Tension Testing of Metallic Materials,” *ASTM International*, West Conshohocken, Pennsylvania.

Barker, L. 2014. “Flexural Anchorage Performance and Strengthening on Negative Moment Regions Using Near-Surface Mounted Retrofitting in Reinforced Concrete Bridge Girders.” Unpublished master’s thesis, Oregon State University, Corvallis.

Bentz, E., 2000 “Response-2000 Reinforced Concrete Sectional Analysis using the Modified Compression Field Theory” [Computer software]. *University of Toronto*, Version 1.0.5, Toronto.

Bournas, D.A., & Triantafillou, T.C. 2009. “Flexural Strengthening of Reinforced Concrete Columns with Near-Surface-Mounted FRP or Stainless Steel.” *American Concrete Institute Structural Journal* 106.4: 495-505

Carpenter Technology Corporation. 2006. Enduramet 32 Stainless Steel [Material Data Sheet]. http://www.stainlessrebar.com/docs/CarpenterEnduramet32.PDF

Castro, H., Rodriguez, C., Belzunce, F.J., Canteli, A.F. 2003. “Mechanical properties and corrosion behavior of stainless steel reinforcing bars.” *Journal of Materials Processing Technology* 143.144: 134-137.

Clark, A. P. 1949. "Bond of Concrete Reinforcing Bars." *Journal of the American Concrete Institute Proceedings* 21.3: 161-84.

Darwin, D. 2005. “Tension Development Length and Lap Splice Design for Reinforced Concrete Members.” *Progress in Structural Engineering and Materials* 7.4: 210-225.

Dawson, M. 2008. “Scale Effects on Reinforced Concrete Beams Strengthened for Shear with Discrete Externally Bonded Carbon Fiber-Reinforced Polymer U-Wraps.” Masters Thesis, Oregon State University, Corvallis.

De Lorenzis, L., Nanni, A., La Tegola, A. 2000. “Strengthening of Reinforced Concrete Structures with Near Surface Mounted FRP Rods.” *International Meeting on Composite Materials Proceedings* PLAST: 1-8.

De Lorenzis, L., & Nanni, A. 2001. “Proposed Design Procedure of NSM FRP Reinforcement for Flexural and Shear Strengthening of RC Beams.” *Technical Report Bulletin 14*: Externally bonded FRP reinforcement for RC structures: 1-11.

De Lorenzis, L. 2004. “Anchorage Length of Near-Surface Mounted Fiber-Reinforced Polymer Rods for Concrete Strengthening- Analytical Modeling.” *American Concrete Institute Structural Journal* 101.3: 375-386.

De Lorenzis, Laura, Andrea Rizzo, and Antonio La Tegola. 2002. "A Modified Pull-out Test for Bond of Near-surface Mounted FRP Rods in Concrete." *Composites Part B: Engineering* 33.8: 589-603. *Elsevier*. Web. 7 Aug. 2013.

Erlin, B. 2006. “Embedded Metals and Materials Other than Reinforcing Steel.” *Significance of Tests and Properties of Concrete and Concrete-Making Materials* STP 169D: 174-183.

Ferguson, P. M. & Breen, J. E. 1965. “Lapped Splices for High Strength Reinforcing Bars.” *Journal of the American Concrete Institute* 62.9: 1063-1078.

Google Maps. 2014. [Mosier Bridge, Mosier, Oregon] [Street View]

Hassan, T. & Rizkalla, F. 2003. “Investigation of Bond in Concrete Structures Strengthened with Near Surface Mounted Carbon Fiber Reinforced Polymer Strips.” *ASCE Journal of Composites for Construction* 7.3: 248-257.

Higgins, C., *et al.* 2004. “Assessment Methodology for Diagonally Cracked Reinforced Concrete Deck Girders,” *Report No. FHWA-OR-RD-05-04*. Oregon Department of Transportation and Federal Highway Administration.

McLean, D. I. & Smith, C. L. 1997. “Noncontact Lap Splices in Bridge Column-Shaft Connections.” *Research Report* WA-RD 417.1, Washington State Department of Transportation: 1-44.

Novidis, D.G., Pantazopoulou, S.J. 2008. “Bond tests of Short NSM-FRP and Steel Bar Anchorages.” *ASCE Journal of Composites for Construction* 12.3:323-331.

Orangun, C. O., Breen, J. E., Jirsa, J. O. 1977. “A Reevaluation of Test Data on Development Length and Splices*.” Journal of the American Concrete Institute Proceedings* 74.3: 114-122.

Oregon Department of Transportation. 2013. Digital Photograph.

Oregon Department of Transportation. 2013. “Type, Size, & Location Narrative, I-84: Mosier WB Connection Bridge.” by Devin Connell. Oregon Department of Transportation, Salem, Oregon.

Rizkalla, S., Hassan, T., Hassan, N. 2003. "Design Recommendations for the Use of FRP for Reinforcement and Strengthening of Concrete Structures." *Progress in Structural Engineering and Materials* 5.1: 16-28.

Triska, M. A. 2010. “Flexural Steel Anchorage Performance at Diagonal Crack Locations.” Masters Thesis, Oregon State University, Corvallis.

APPENDICIES

APPENDIX A: INSTRUMENTATION DETAILS AND LABELING

Appendix A describes the internal and external configuration of sensors to monitor data for each specimen. Illustrations are included for the diagonal displacement sensors and strain gage configuration. Data for all sensors was sampled at a rate of 5 Hz.

Support Settlement: Support settlements were measured with two 2 in. (50.8 mm) displacement sensors placed on each side of the web. Each sensor was labeled with "North-East," "North-West," "South-East," or "South-West." The sensors measured the settlement of the specimen at the support with reference to the ground. The sensor pairs were averaged to equate the total support settlement.

Midspan Displacement: Midspan displacement was measured using two 10 in. (254 mm) long string potentiometers mechanically attached to each side of the web at midspan. The displacements on the East and West side of the web were averaged for account for any rotation while testing. The average midspan displacement subtracted the support settlement to obtain the true midspan displacement.

Cutoff Bar Slip: Cutoff bar slip was measured characterize anchorage response with two 1 in. (25.4 mm) displacement sensors. The displacement sensors were attached using methods discussed in *Chapter 3 Instrumentation*. Both east and west cutoff bar slip was measured.

Diagonal Displacement Sensors: Diagonal displacement sensors were used to measure the change in crack widths crossing the sensor. The diagonal displacement sensors were

mechanically attached to the stem of the specimens. Brass wire was strung from the diagonal displacement sensor to an opposing point. Two diagonal displacement sensors were placed over a specified length to measure compression and tension in the section. The sensors were numbered and installed according to Fig. A.1 and Fig. A.2 with the arrow indicating the direction of measurement.

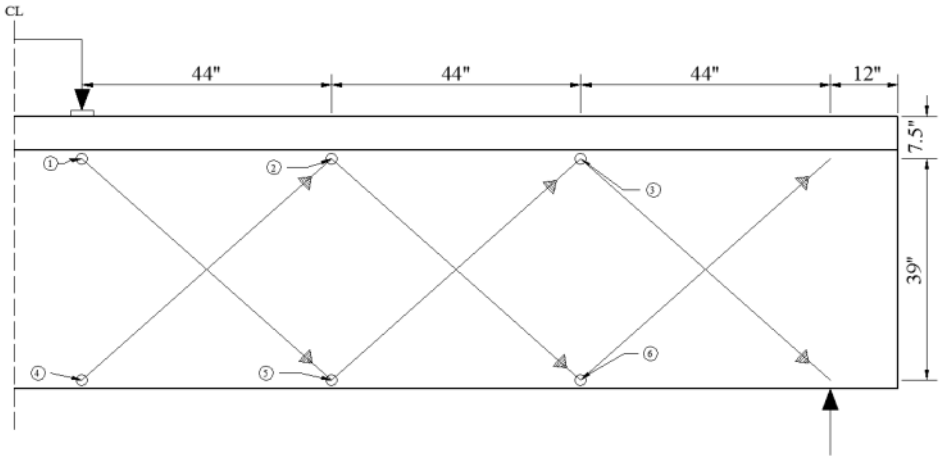

Fig. A.1 Diagonal displacement sensor numbering on North side of specimen T.45.Ld3(10).Ti, T.45.Ld3(6).Ti andT.45.Ld3(6).SS

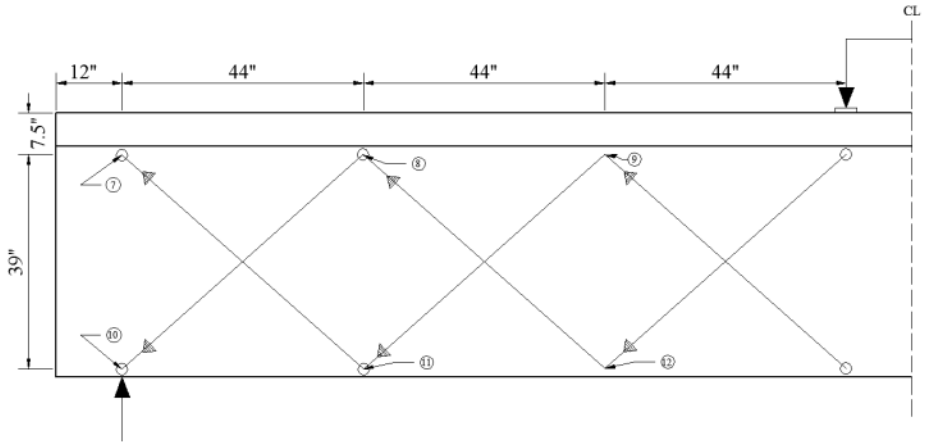

Fig. A.2 Diagonal displacement sensor numbering on South side of specimen T.45.Ld3(6).Ti andT.45.Ld3(6).SS

Strain Gages: Stain gages were adhered to longitudinal reinforcing steel, NSM materials, and stirrups legs. Along the longitudinal reinforcing steel and NSM materials strain gages were located at the termination of the NSM material and the termination of the cutoff steel reinforcing bar. Stirrup strain gages were implemented on one leg along the preformed diagonal crack and at mid-height. The labeling convention of the strain gages can be found in Fig. A.3 through Fig. A.5. The strain gage location on the stainless steel NSM is coincident with the titanium on the top and bottom bars (bars 1 and 4). However, the label number for the stainless steel NSM materials are opposite of the titanium NSM material. A cross section is provided in Fig. A.6 for the NSM titanium and stainless steel internal sensor configuration.

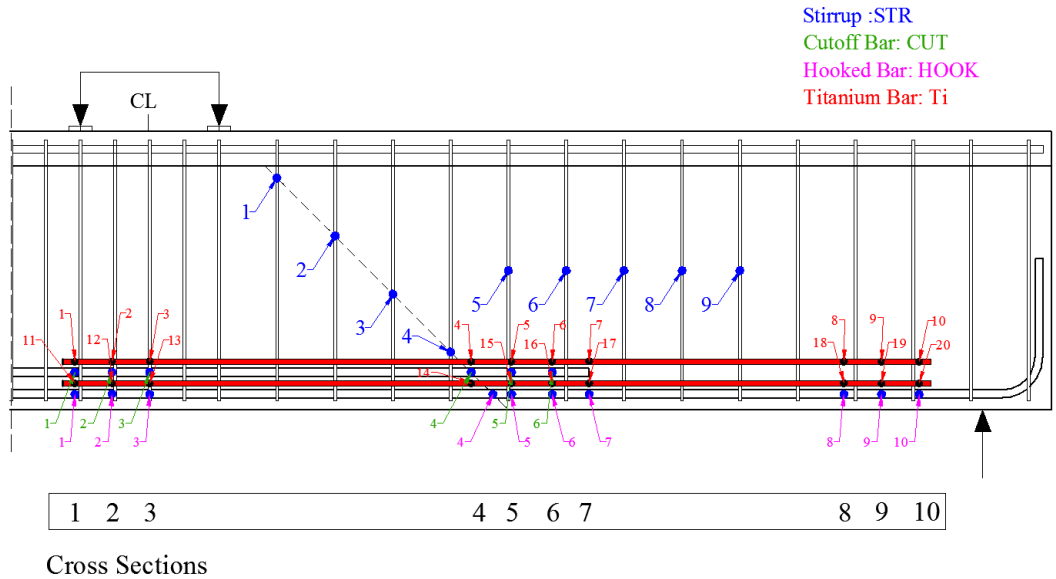

Fig. A.3 - Specimen T.45.Ld3(10).Ti Strain gage labeling convention

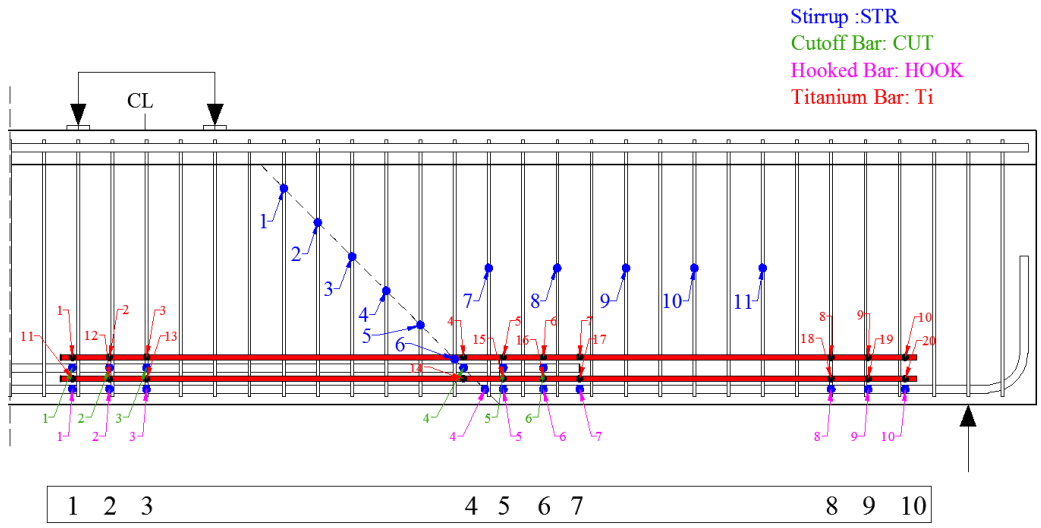

Fig. A.4 - Specimen T.45.Ld3(6).Ti Strain gage labeling convention

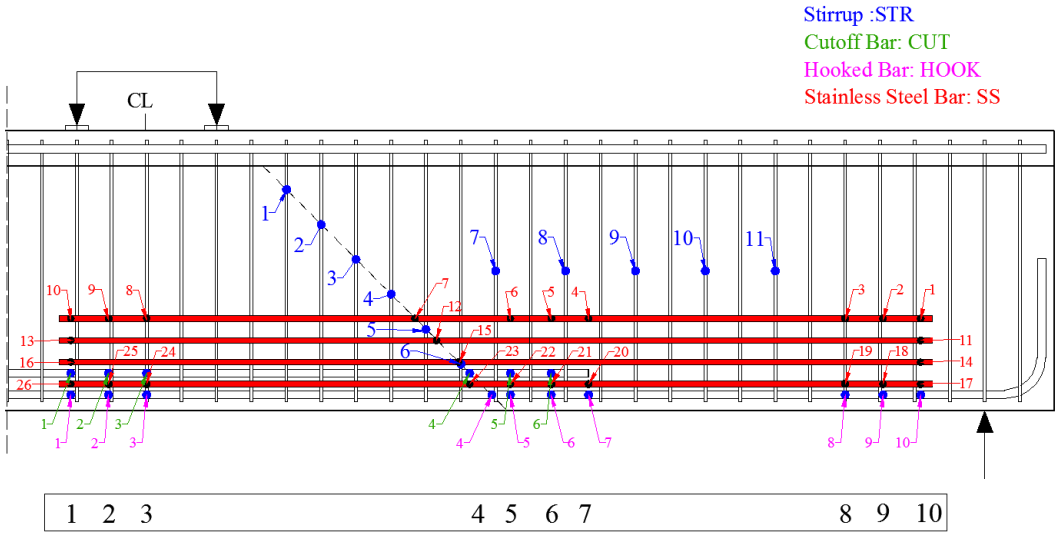

Fig. A.5 - Specimen T.45.Ld3(6).SS Strain gage labeling convention

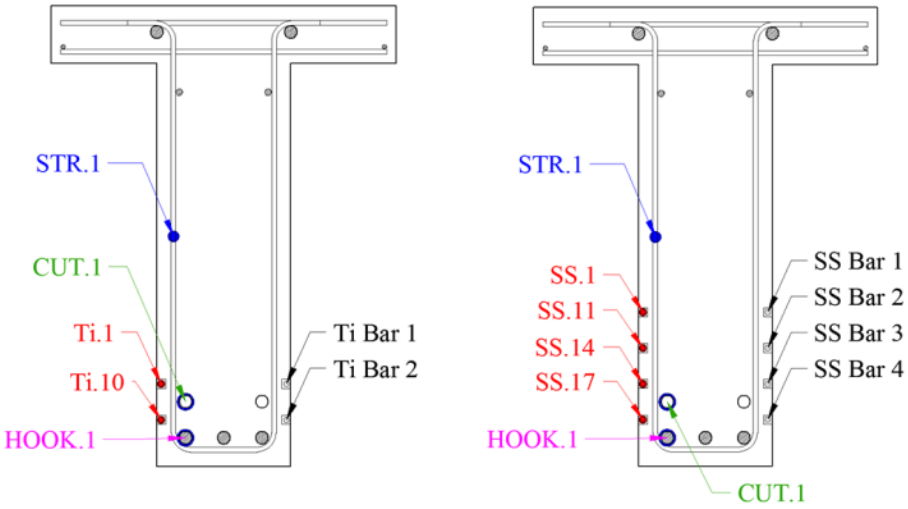

Fig. A.6 - Cross section for internal instrumentation for T.45.Ld3(10).Ti and T.45.Ld3(6).Ti (left) and T.45.Ld3(6).SS (right)

APPENDIX B: EXPERIMENTAL DATA

Appendix B contains the experimental data collected for specimens T.45.Ld3(10).Ti, T.45.Ld3(6).Ti and T.45.Ld3(6).SS. Plots from *Chapter 5, Analytical Methods*, are also included for each specimen.

B.1 T.45.Ld3(10).Ti

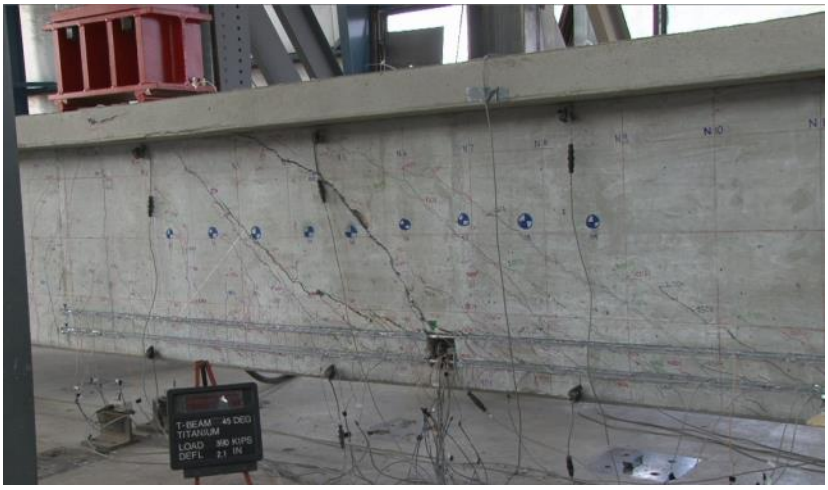

Fig. B.1 - Specimen T.45.Ld3(10).Ti at failure

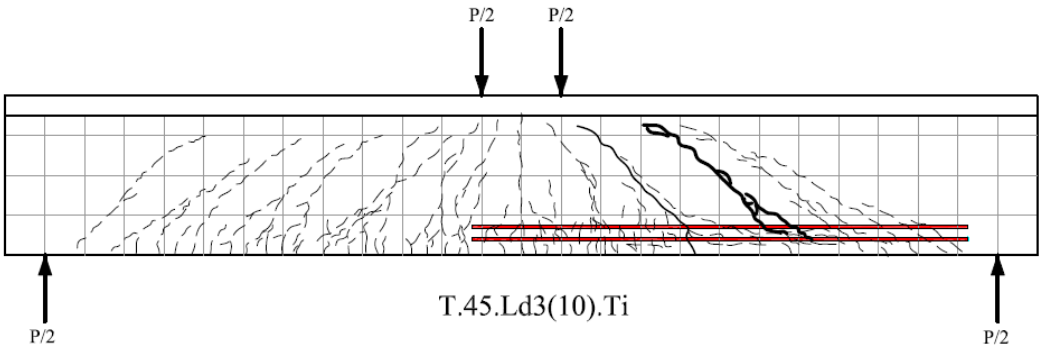

Fig. B.2 - Specimen T.45.Ld3(10).Ti crack map

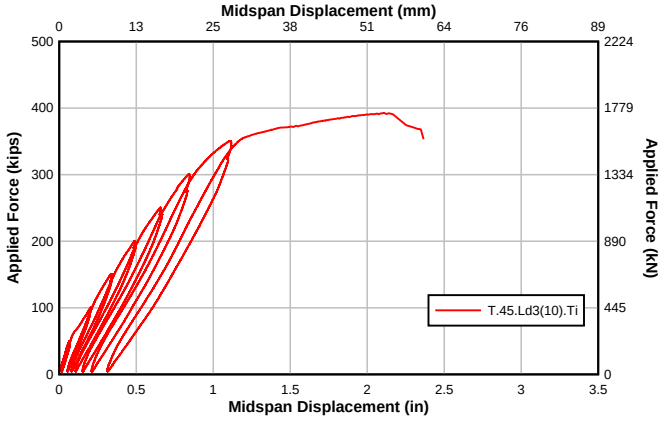

Fig. B.3 - Specimen T.45.Ld3(10).Ti Load displacement curve

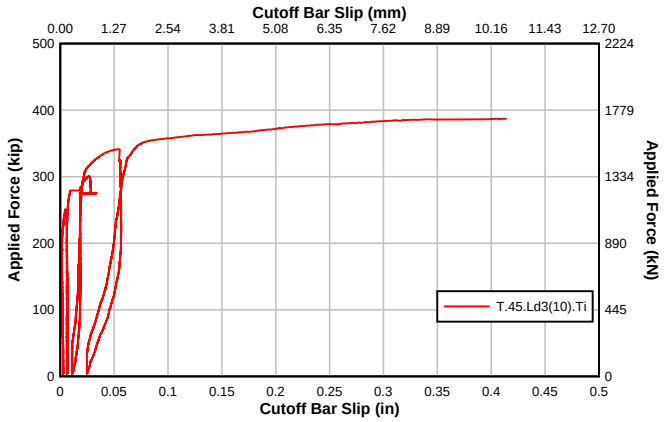

Fig. B.4 - T.45.Ld3(10).Ti Cutoff bar slip

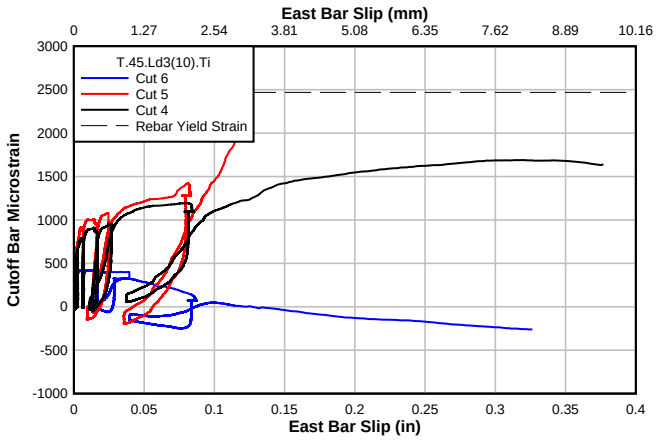

Fig. B.5 - T.45.Ld3(10).Ti Slip and cutoff bar strain

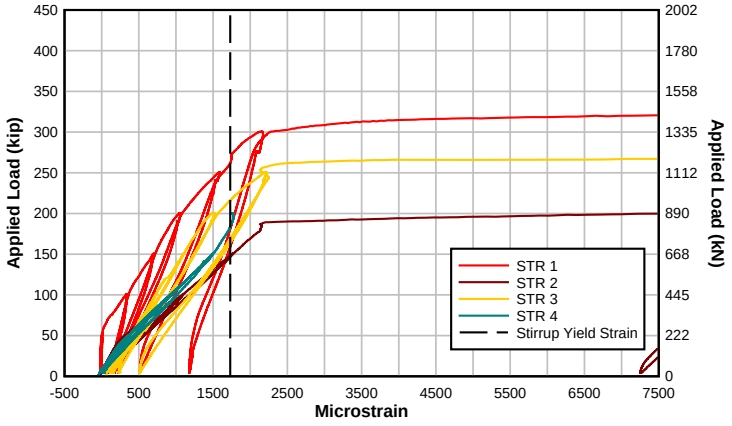

Fig. B.6 - T.45.Ld3(10).Ti Strain in stirrups along diagonal crack

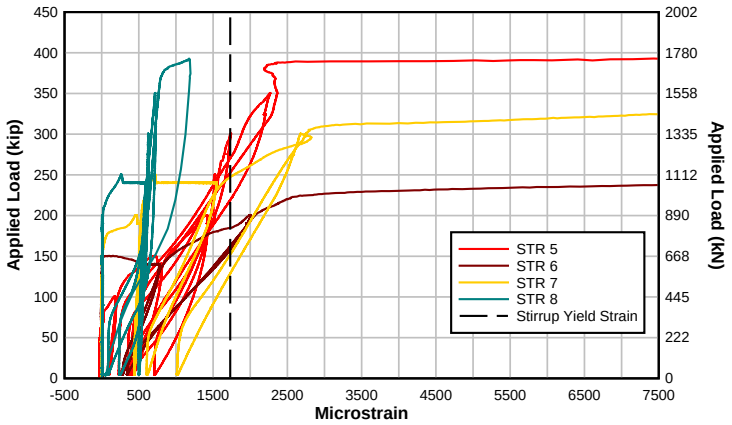

Fig. B.7 - T.45.Ld3(10).Ti Strain in stirrups mid height

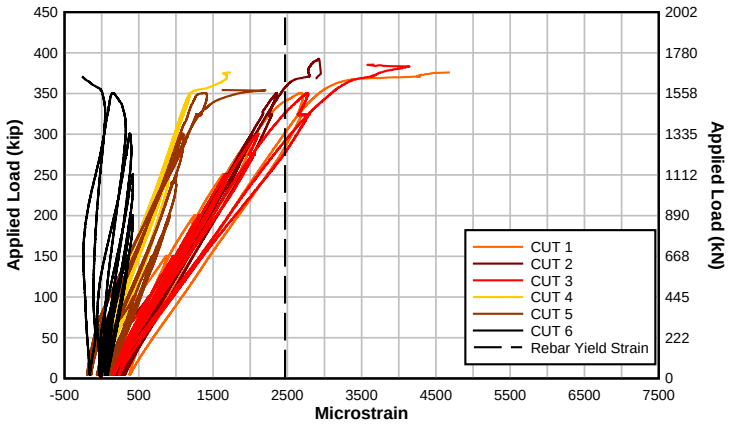

Fig. B.8 - T.45.Ld3(10).Ti Strain in cutoff bar

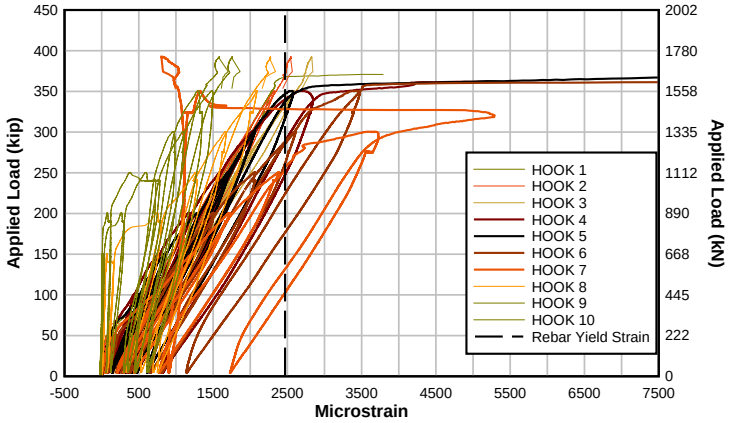

Fig. B.9 - T.45.Ld3(10).Ti Strain in hook bar

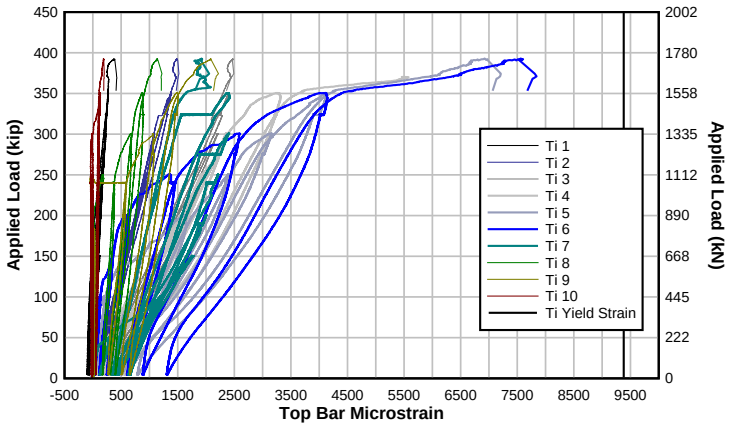

Fig. B.10 - T.45.Ld3(10).Ti Strain in upper titanium bar

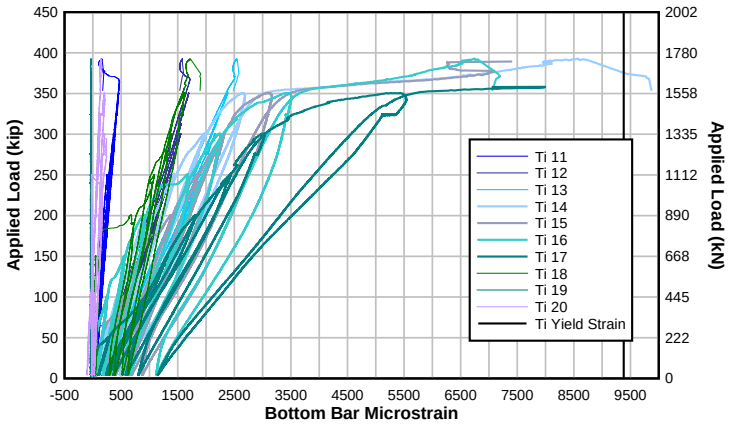

Fig. B.11 - T.45.Ld3(10).Ti Strain in lower titanium bar

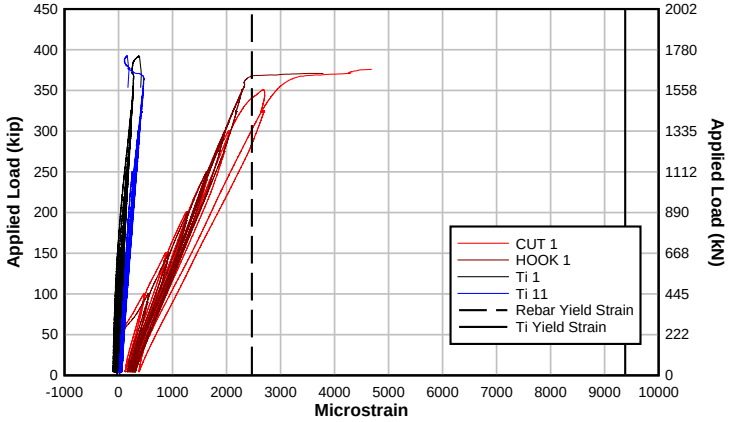

Fig. B.12 - T.45.Ld3(10).Ti Section 1 strain

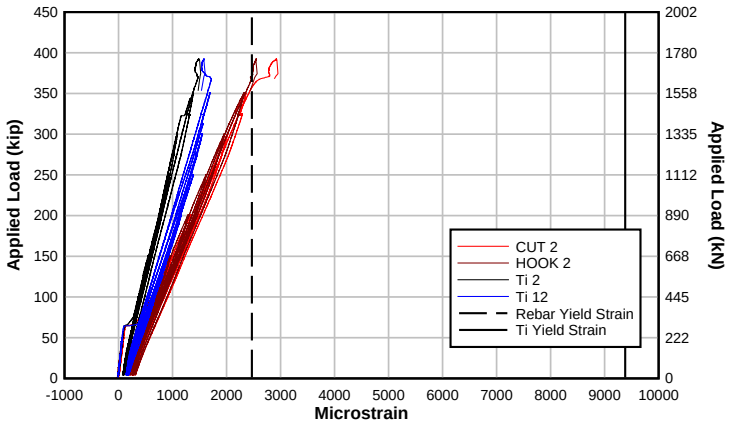

Fig. B.13 - T.45.Ld3(10).Ti Section 2 strain

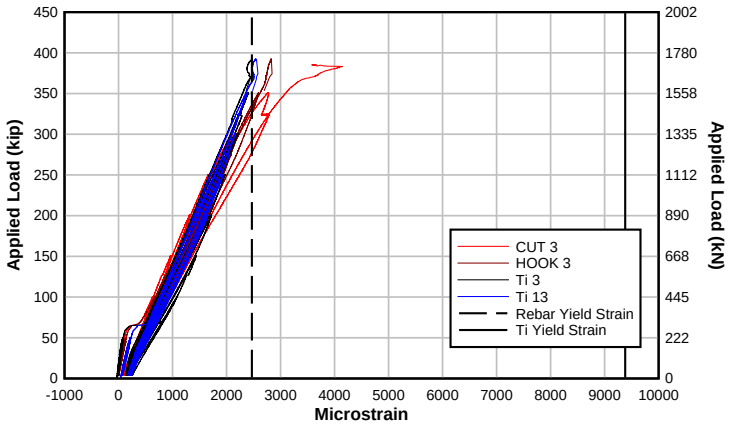

Fig. B.14 - T.45.Ld3(10).Ti Section 3 strain

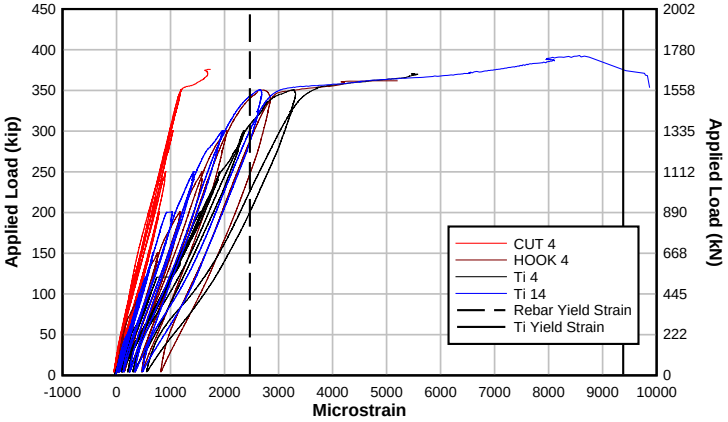

Fig.B.15 - T.45.Ld3(10).Ti Section 4 strain

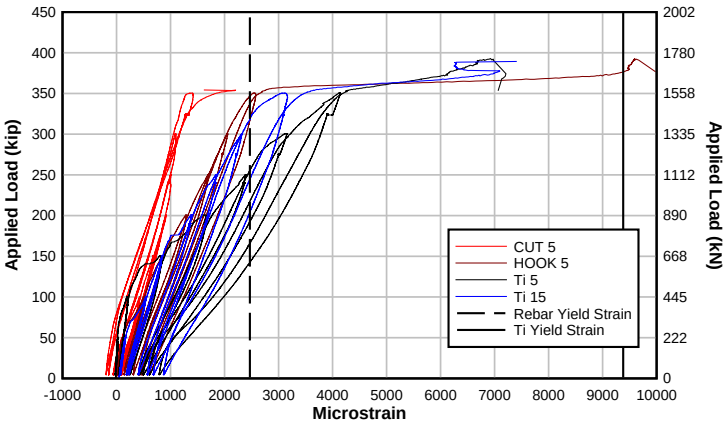

Fig. B.16 - T.45.Ld3(10).Ti Section 5 strain

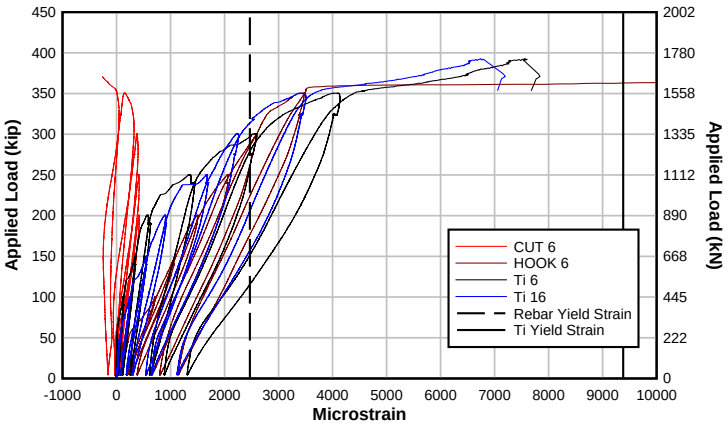

Fig. B.17 - T.45.Ld3(10).Ti Section 6 strain

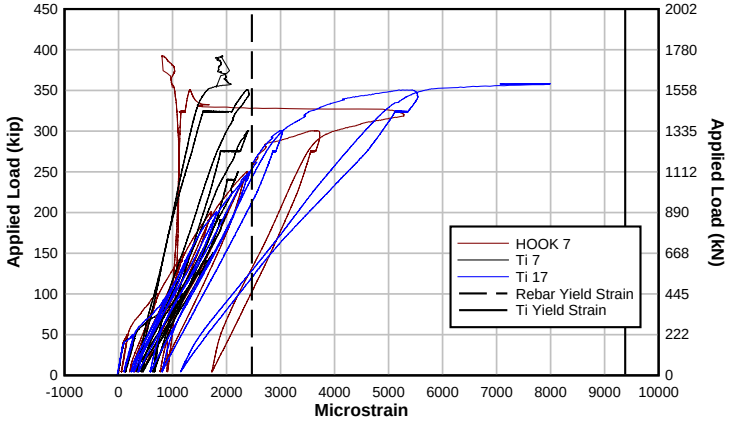

Fig. B.18 - T.45.Ld3(10).Ti Section 7 strain

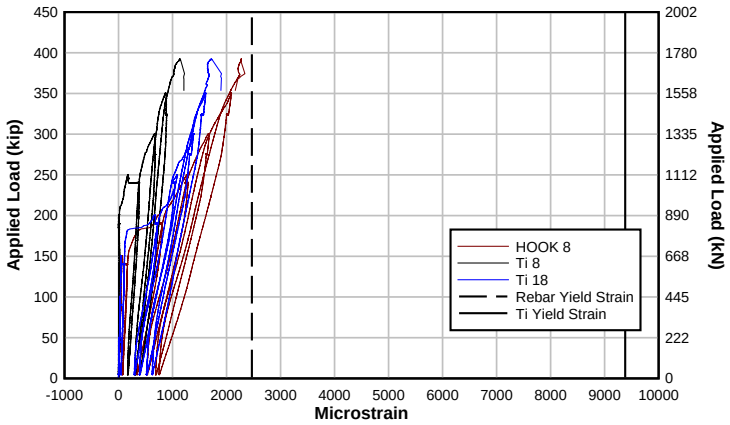

Fig. B.19 - T.45.Ld3(10).Ti Section 8 strain

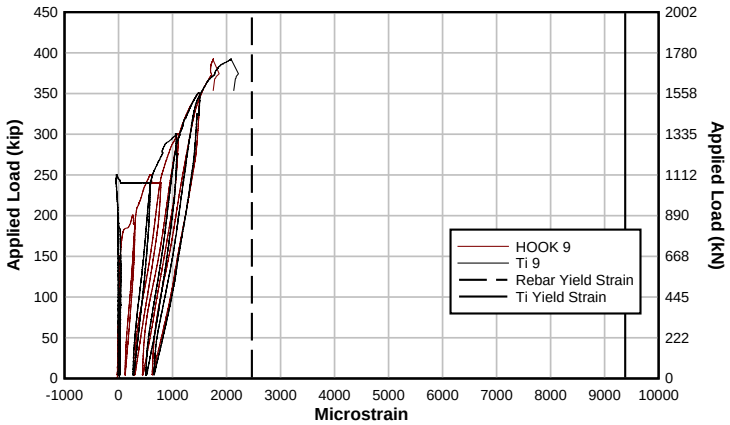

Fig. B.20 - T.45.Ld3(10).Ti Section 9 strain

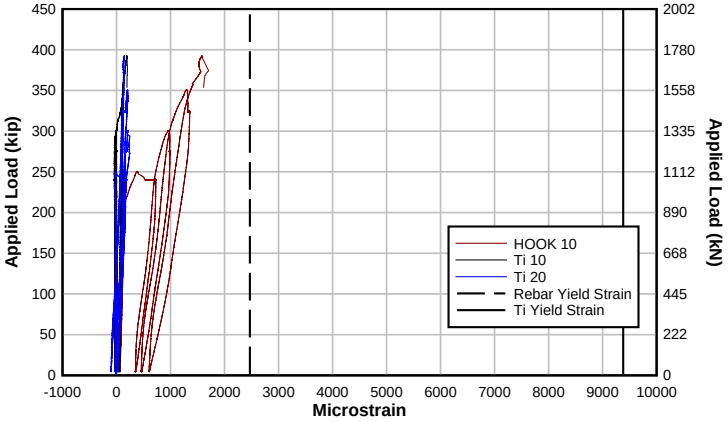

Fig. B.21 - T.45.Ld3(10).Ti Section 10 strain

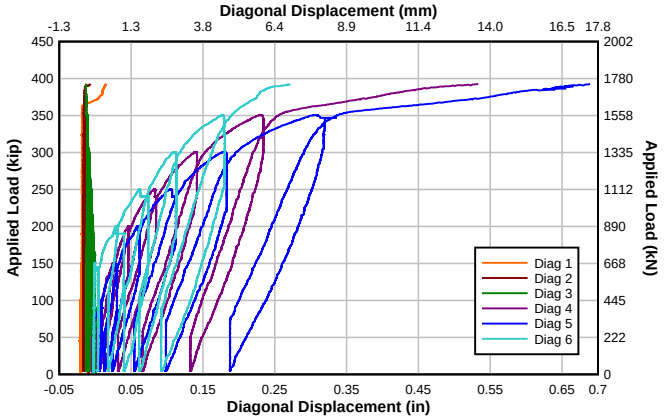

Fig. B.22 - T.45.Ld3(10).Ti Diagonal sensor displacement

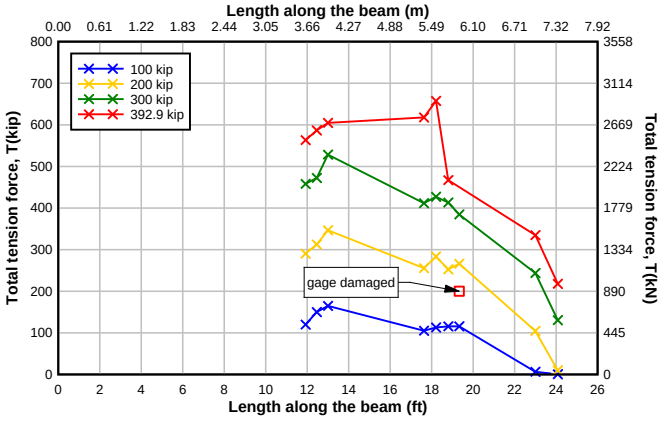

Fig. B.23 - T.45.Ld3(10).Ti Flexural tensile force along length at load intervals

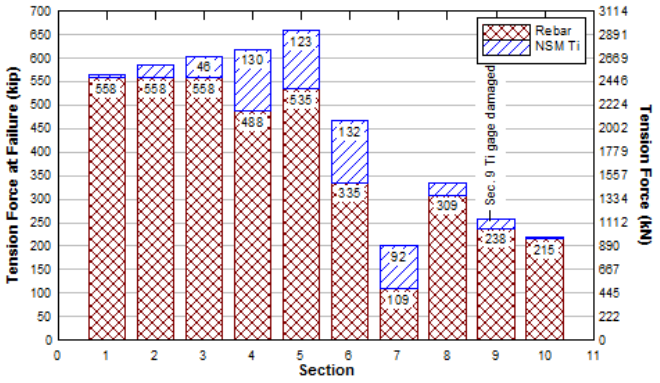

Fig. B.24 - T.45.Ld3(10).Ti Steel reinforcing bar vs NSM bar maximum tension force

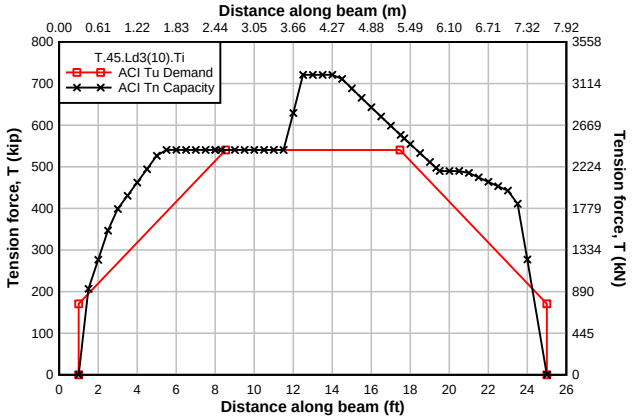

Fig. B.25 - T.45.Ld3(10).Ti ACI flexural tension demand and capacity

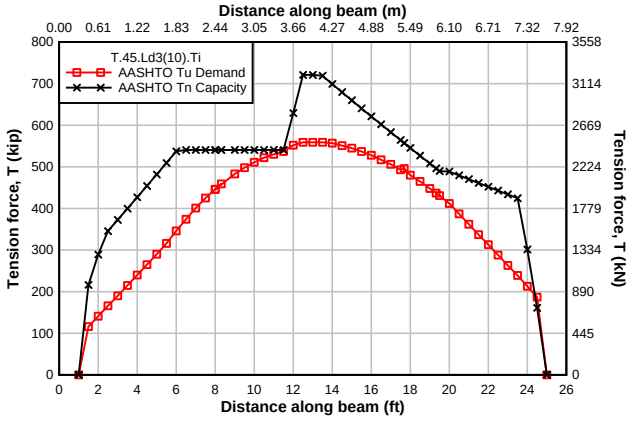

Fig. B.26 - T.45.Ld3(10).Ti AASHTO flexural tension demand and capacity

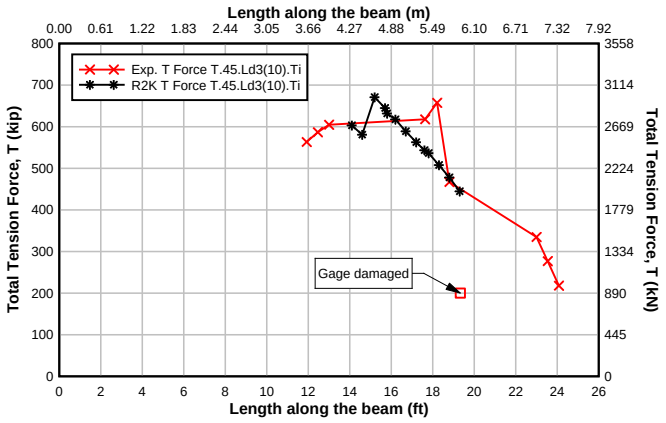

Fig. B.27 - T.45.Ld3(10).Ti Flexural tension force from experimental data and predicted R2K analysis

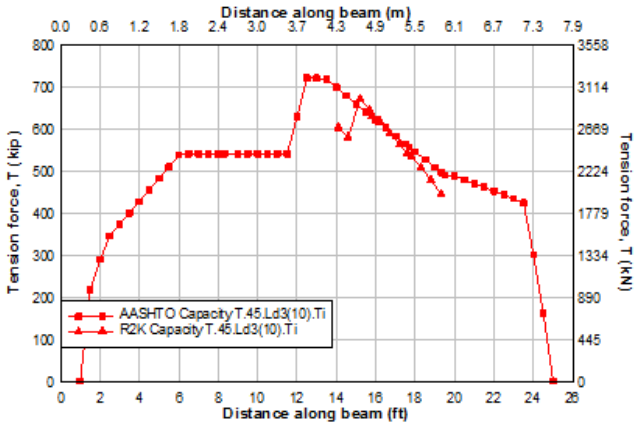

Fig. B.28 - T.45.Ld3(10).Ti Flexural tension predictions R2K and AASHTO

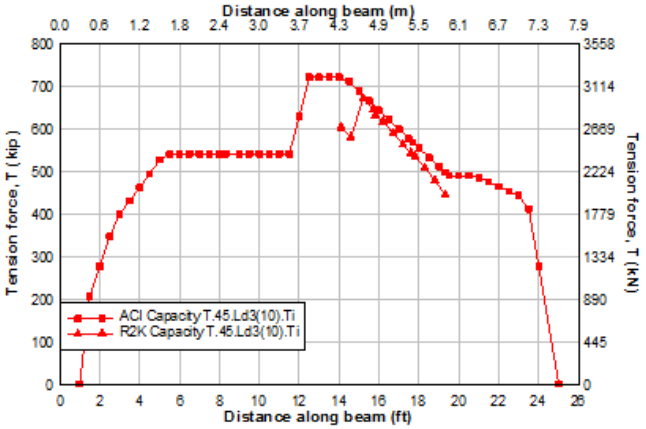

Fig. B.29 - T.45.Ld3(10).Ti Flexural tension predictions R2K and ACI

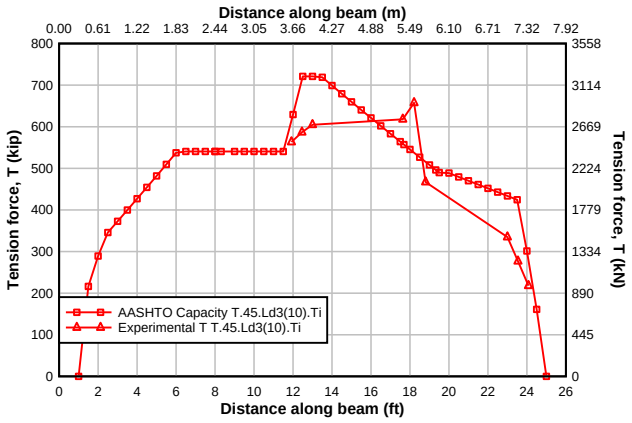

Fig. B.30 - T.45.Ld3(10).Ti Flexural tension prediction AASHTO and Experimental data

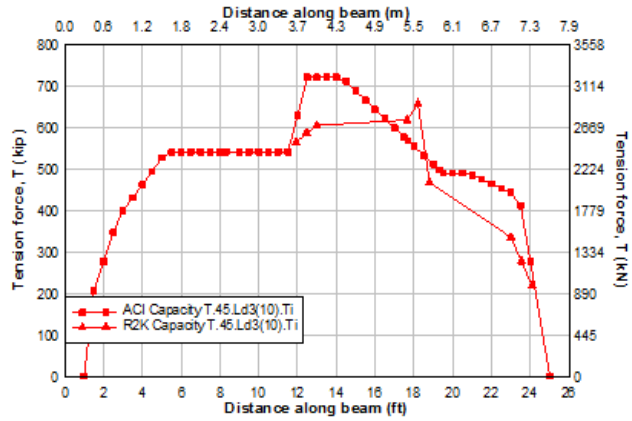

Fig. B.31 - T.45.Ld3(10).Ti Flexural tension prediction ACI and Experimental data

B.2 T.45.Ld3(6).Ti

Fig. B.31 - Specimen T.45.Ld3(6).Ti at failure

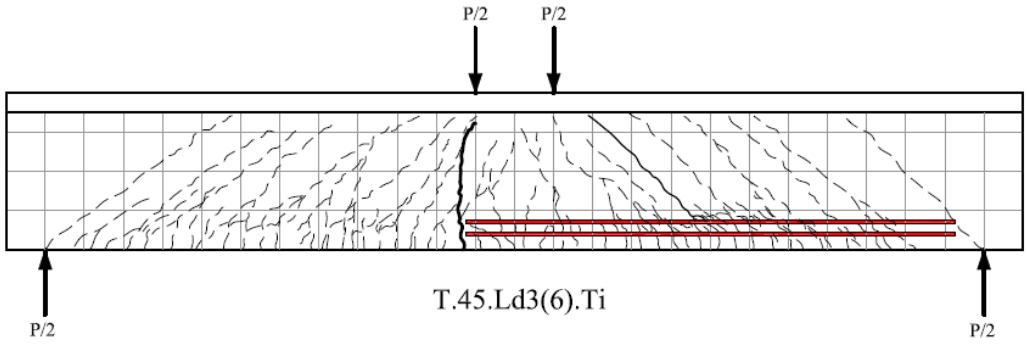

Fig. B.32 - Specimen T.45.Ld3(6).Ti crack map

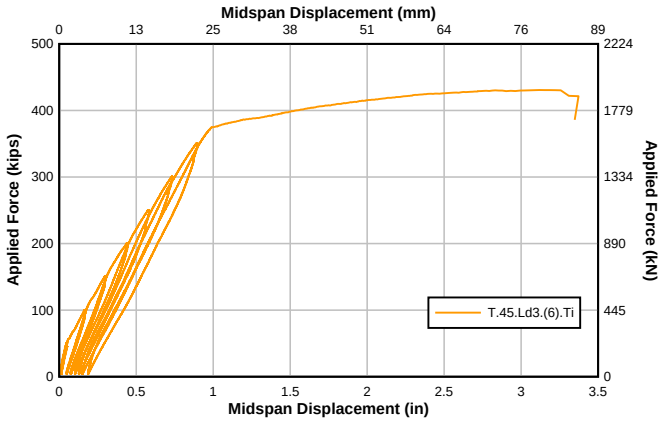

Fig. B.33 - Specimen T.45.Ld3(6).Ti Load displacement curve

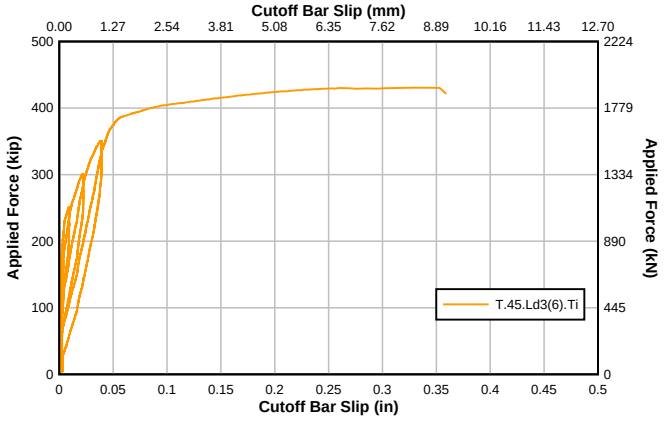

Fig. B.34 - T.45.Ld3(6).TI Cutoff bar slip

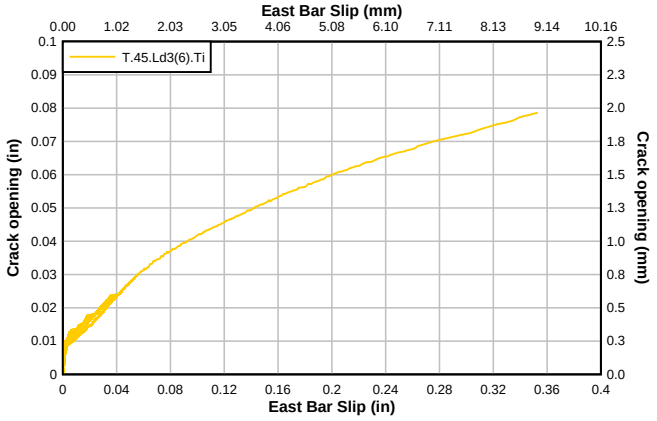

Fig. B.35 - T.45.Ld3(6).Ti Crack opening vs cutoff bar slip

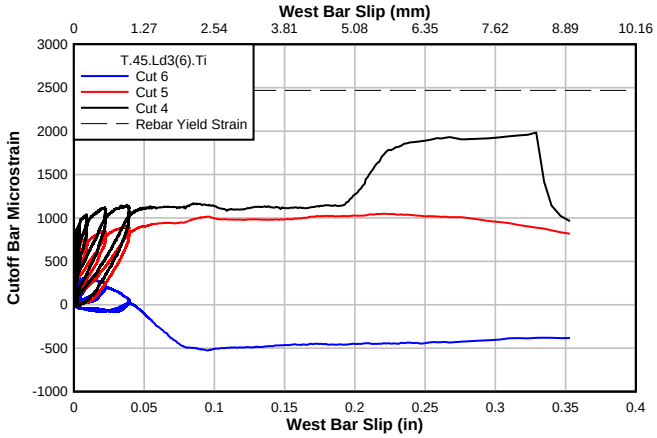

Fig. B.36 - T.45.Ld3(6).Ti Slip and cutoff bar strain

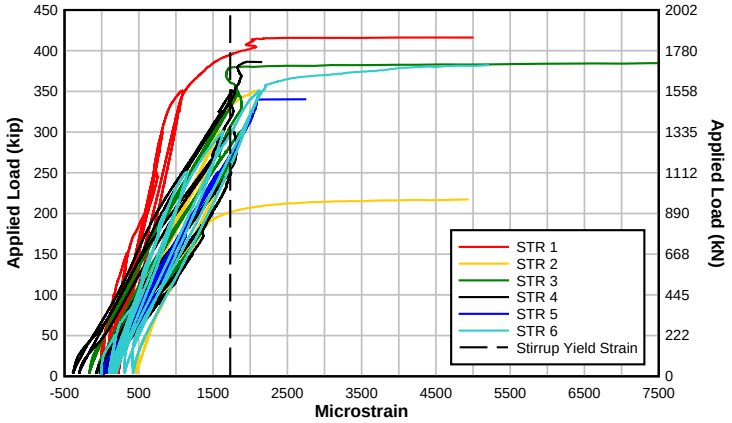

Fig. B.37 - T.45.Ld3(6).Ti Strain in stirrups along diagonal crack

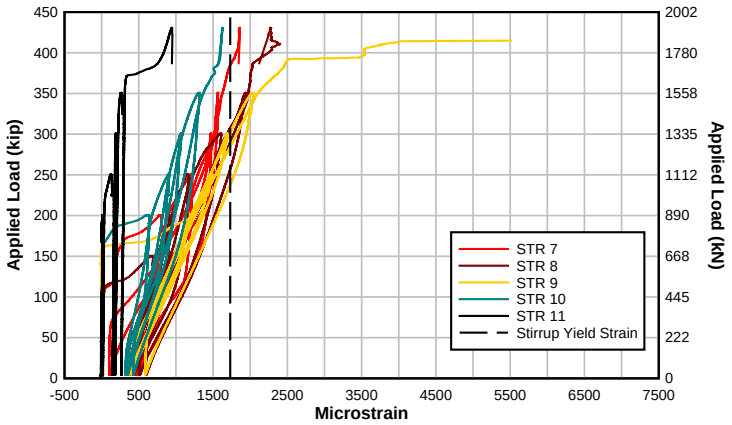

Fig. B.38 - T.45.Ld3(6).Ti Strain in stirrups mid height

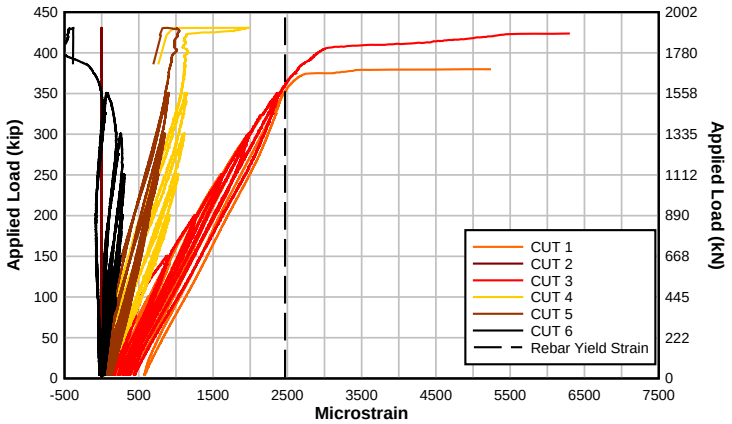

Fig. B.39 - T.45.Ld3(6).Ti Strain in cutoff bar

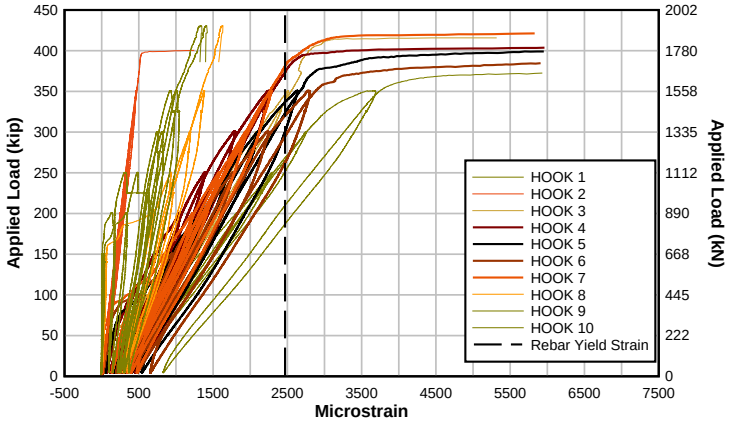

Fig. B.40 - T.45.Ld3(6).Ti Strain in hooked bar

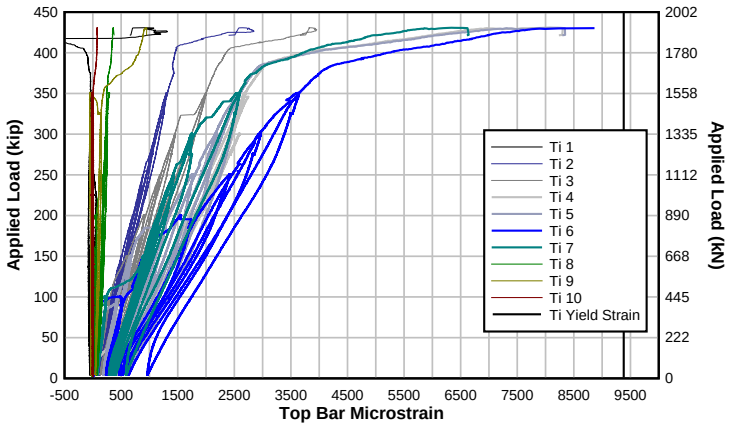

Fig. B.41 - T.45.Ld3(6).Ti Strain in upper titanium bar

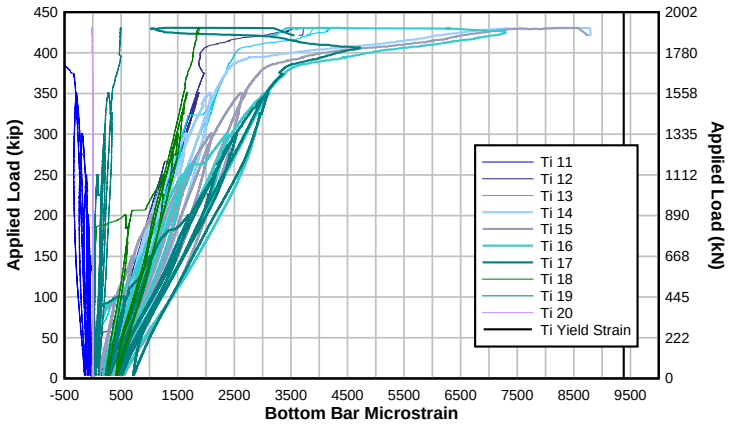

Fig. B.42 - T.45.Ld3(6).Ti Strain in lower titanium bar

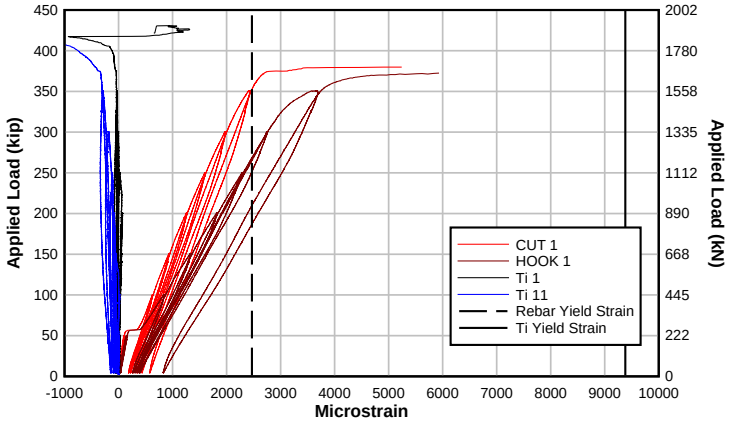

Fig. B.43 - T.45.Ld3(6).Ti Section 1 strain

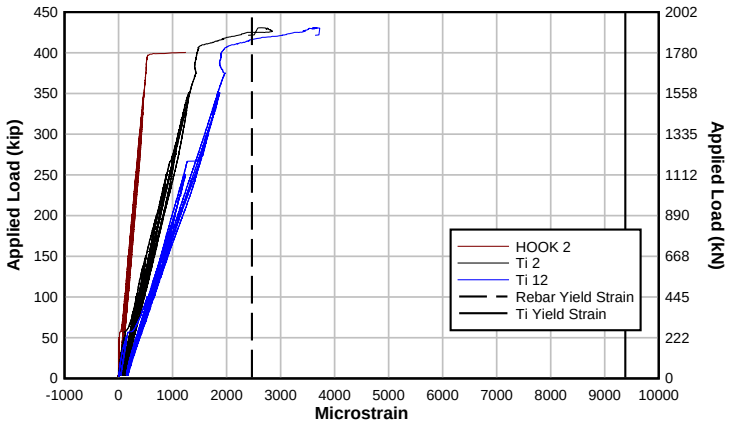

Fig. B.44 - T.45.Ld3(6).Ti Section 2 strain

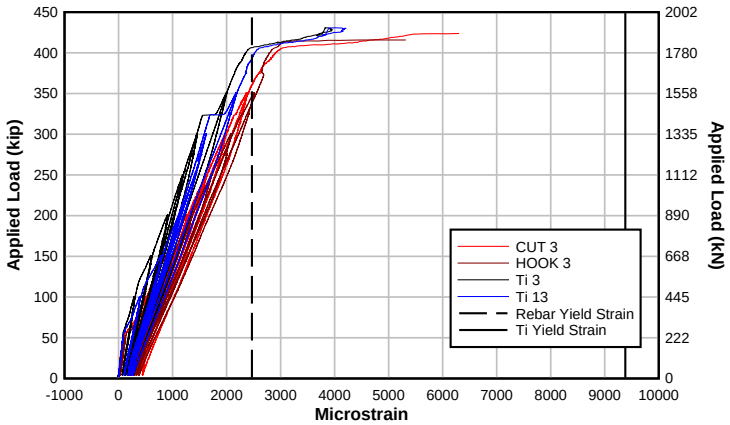

Fig. B.45 - T.45.Ld3(6).Ti Section 3 strain

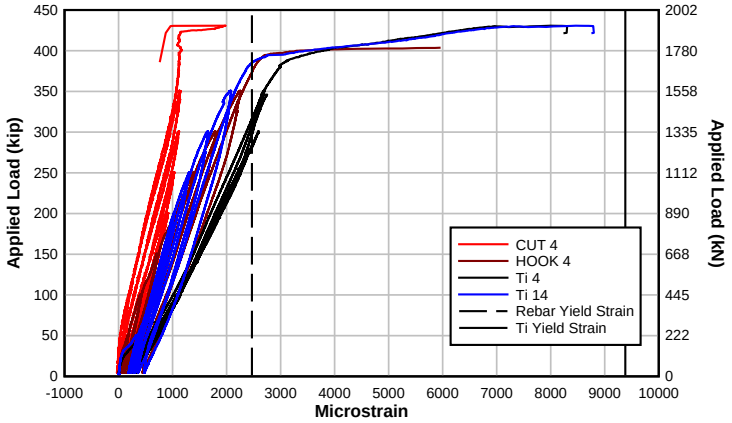

Fig. B.46 - T.45.Ld3(6).Ti Section 4 strain

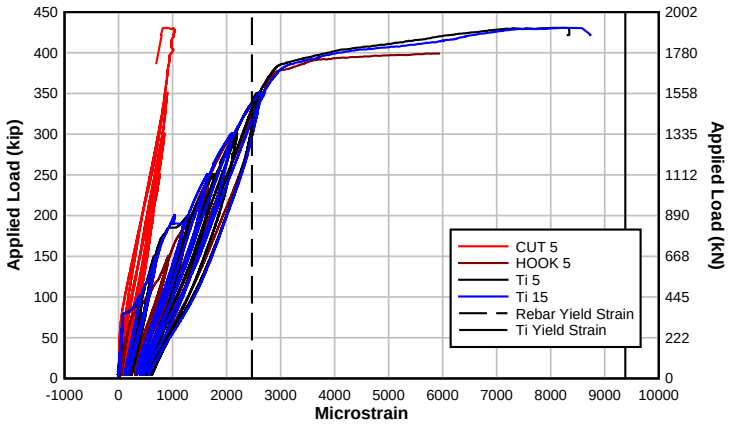

Fig. B.47 - T.45.Ld3(6).Ti Section 5 strain

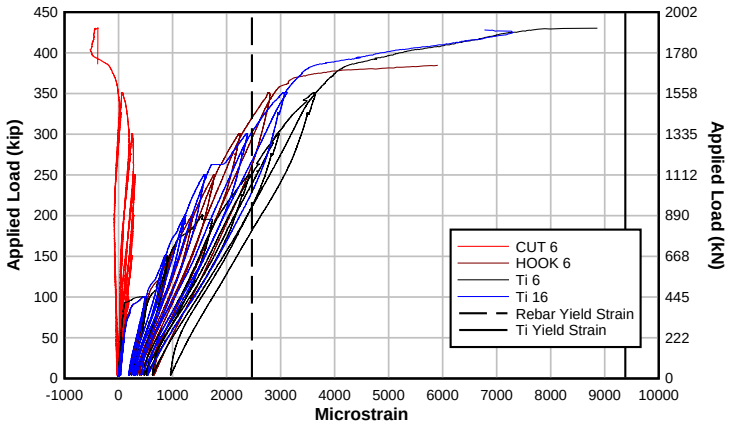

Fig. B.48 - T.45.Ld3(6).Ti Section 6 strain

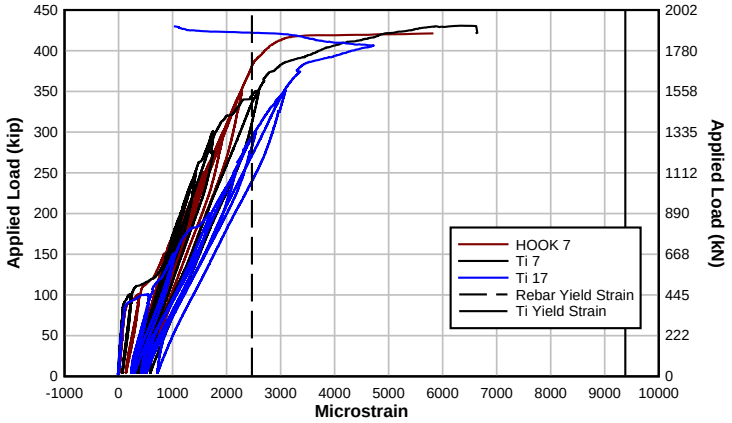

Fig. B.49 - T.45.Ld3(6).Ti Section 7 strain

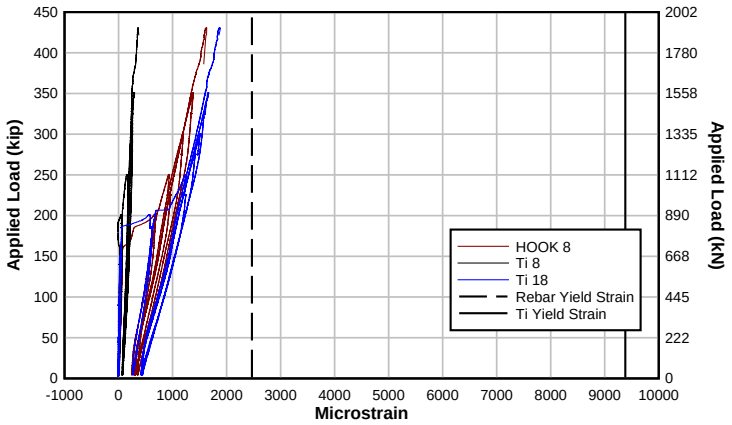

Fig. B.50 - T.45.Ld3(6).Ti Section 8 strain

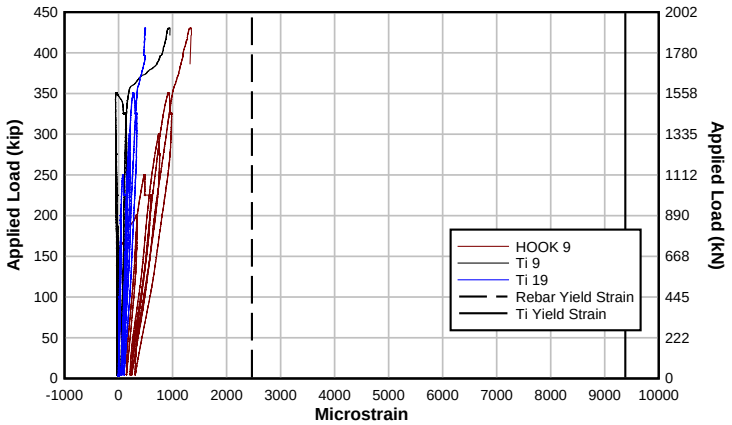

Fig. B.51 - T.45.Ld3(6).Ti Section 9 strain

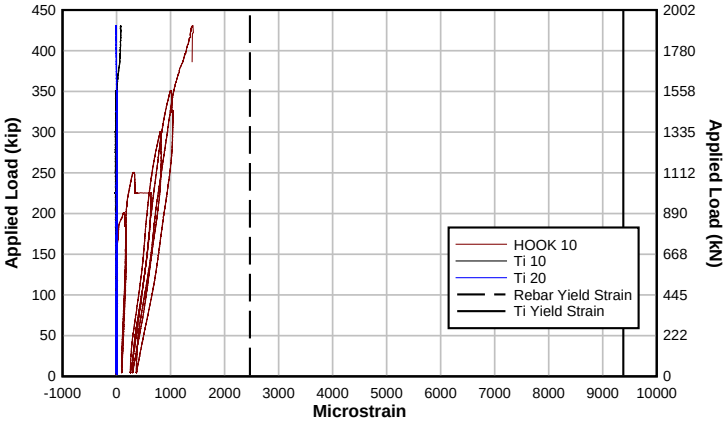

Fig. B.52 - T.45.Ld3(6).Ti Section 10 strain

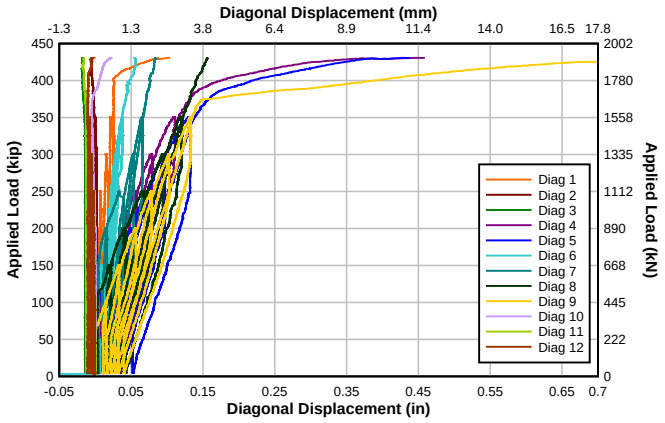

Fig. B.53 - T.45.Ld3(6).Ti Diagonal sensor displacement

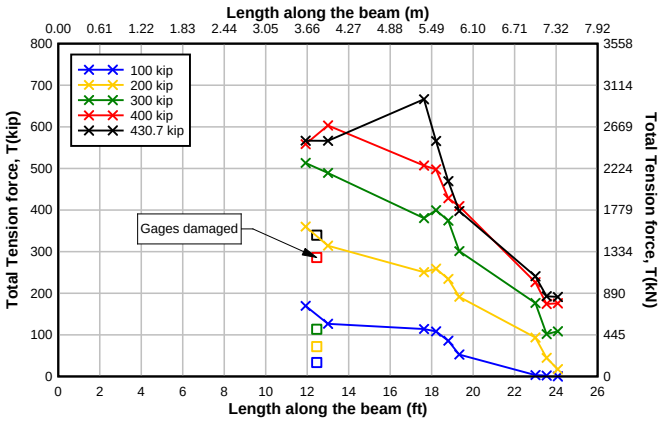

Fig. B.54 - T.45.Ld3(6).Ti Flexural tension force along the length at load intervals

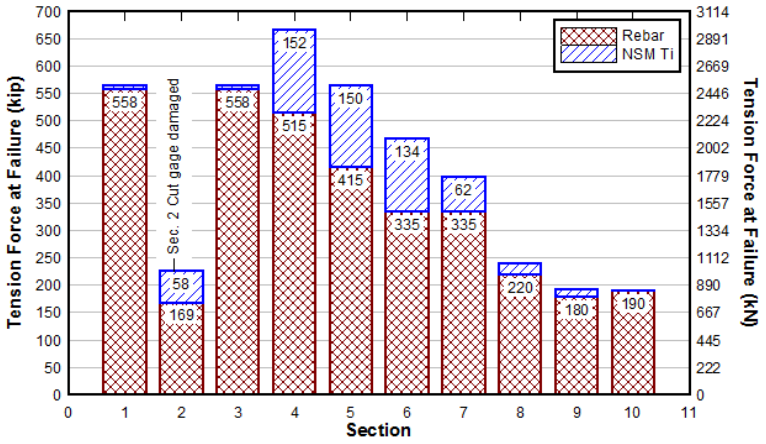

Fig. B.55 - T.45.Ld3(6).Ti Steel reinforcing bar vs NSM bar maximum tension force

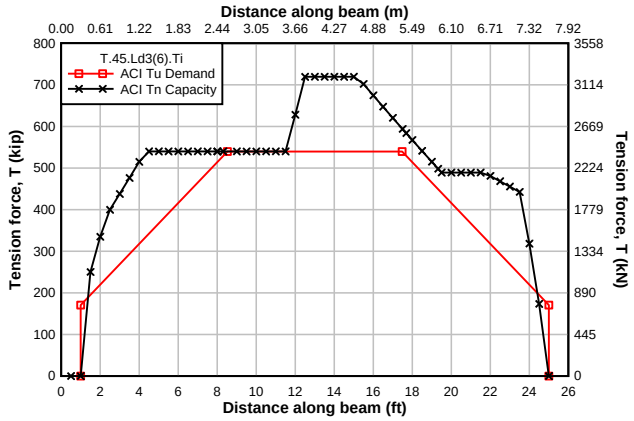

Fig. B.56 - T.45.Ld3(6).Ti ACI flexural tension demand and capacity

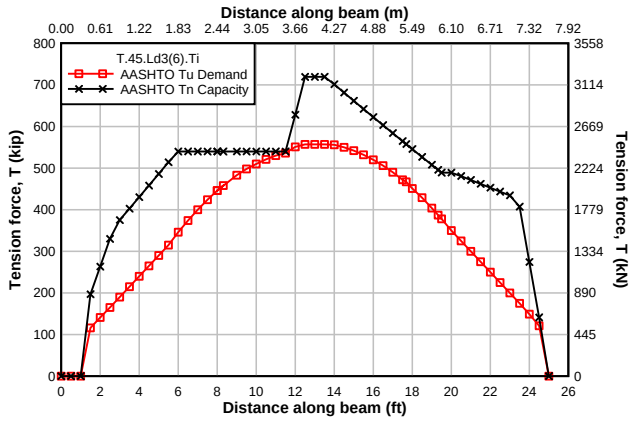

Fig. B.57 - T.45.Ld3(6).Ti AASHTO flexural tension demand and capacity

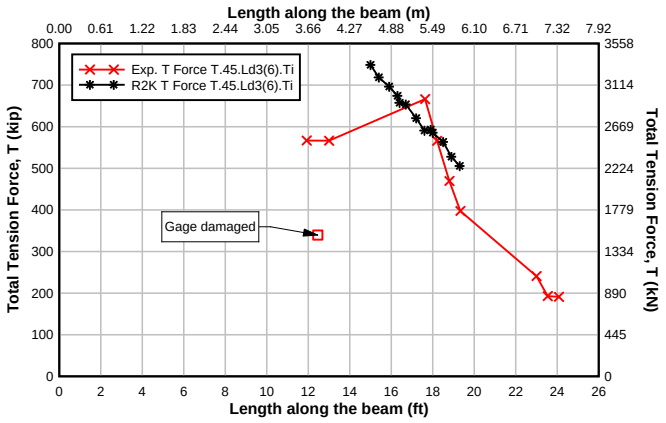

Fig. B.58- T.45.Ld3(6).Ti Flexural tension force from experimental data and predicted R2K analysis

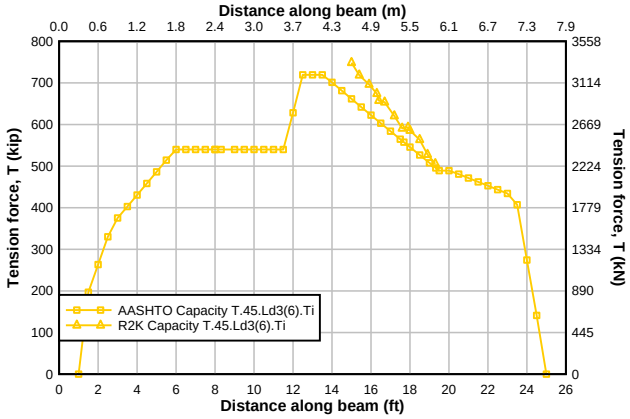

Fig. B.59 - T.45.Ld3(6).Ti Flexural tension predictions R2K and AASHTO

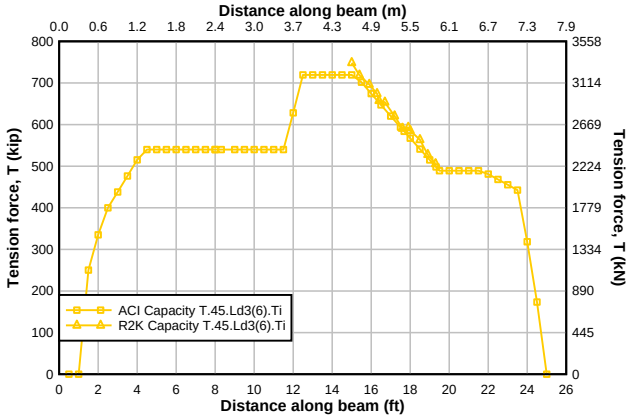

Fig. B.60 - T.45.Ld3(6).Ti Flexural tension predictions R2K and ACI

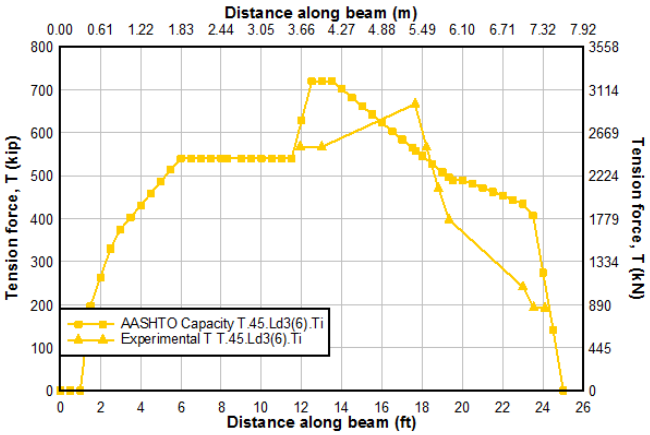

Fig. B.61 - T.45.Ld3(6).Ti Flexural tension prediction AASHTO and Experimental data

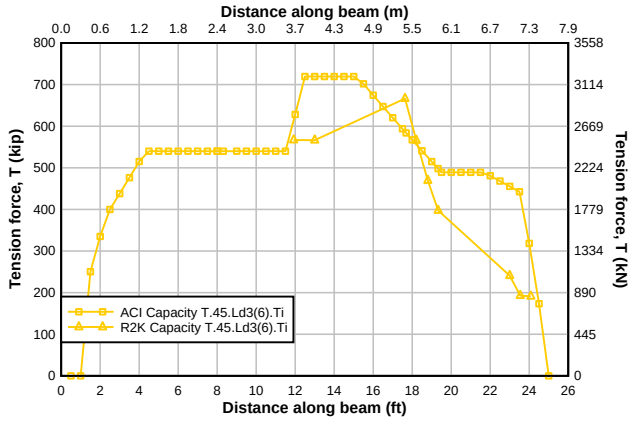

Fig. B.62 - T.45.Ld3(6).Ti Flexural tension prediction ACI and Experimental data

B.3 T.45.Ld3(6).SS

Fig. B.63 - Specimen T.45.Ld3(6).SS

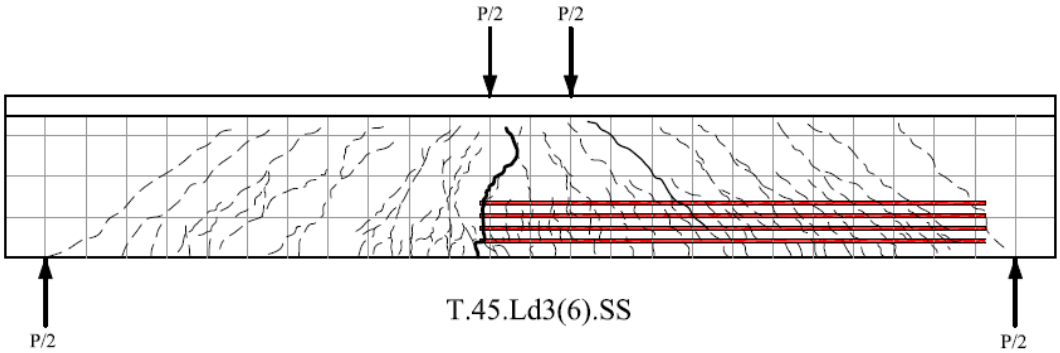

Fig. B.64 - Specimen T.45.Ld3(6).SS crack map

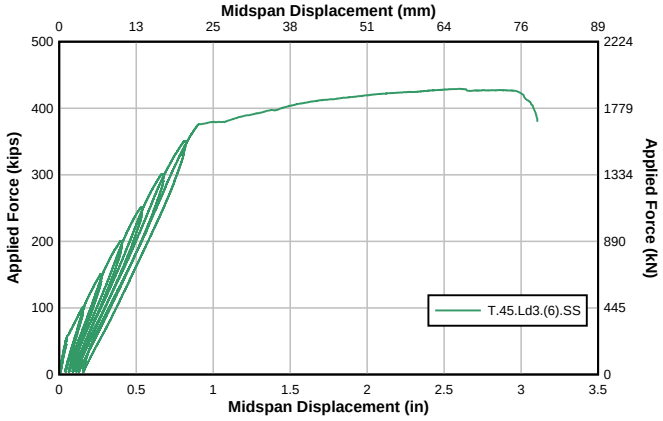

Fig. B.65 - Specimen T.45.Ld3(6).SS Load displacement curve

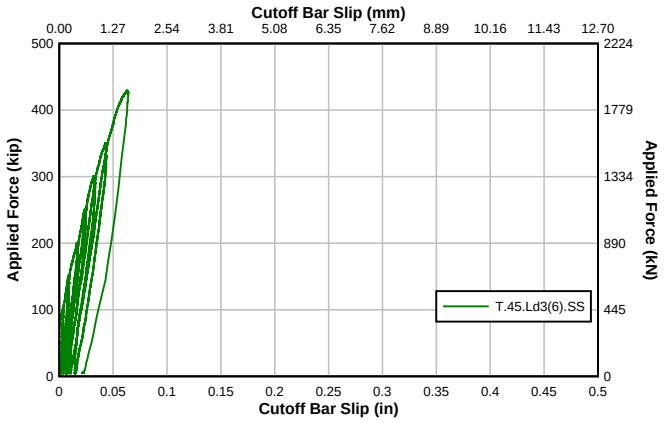

Fig. B.66 - T.45.Ld3(6).SS Cutoff bar slip

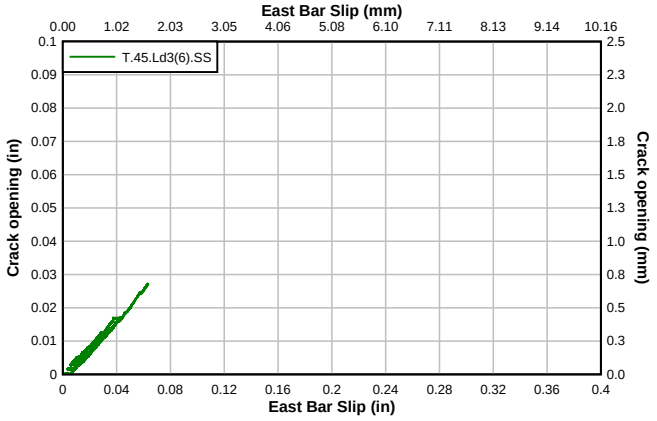

Fig. B.67 - T.45.Ld3(6).SS Crack opening and cutoff bar slip

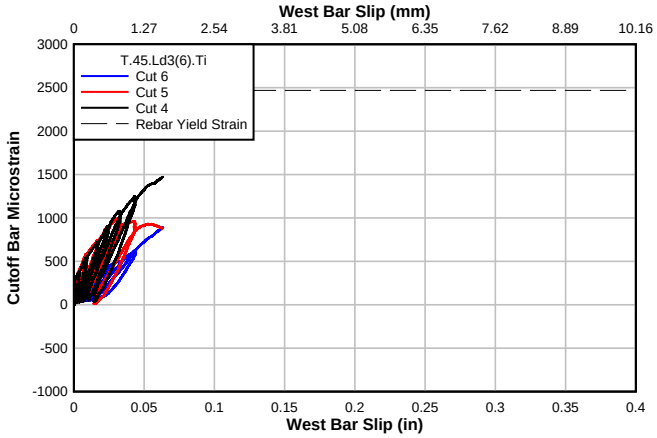

Fig. B.68 - T.45.Ld3(6).SS Slip and cutoff bar strain

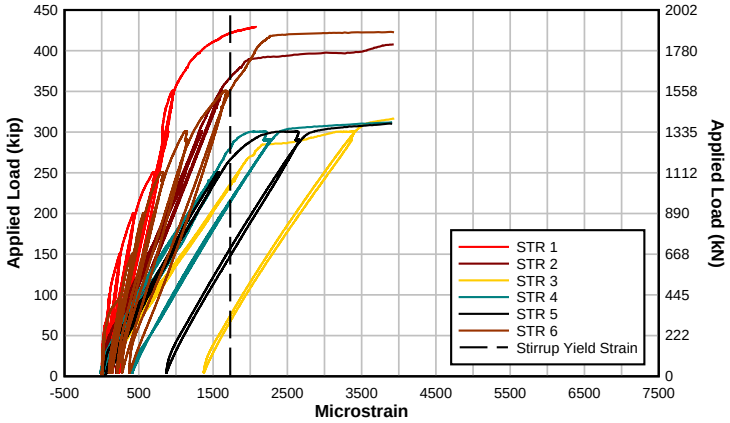

Fig. B.69 - T.45.Ld3(6).SS Strain in diagonal stirrups

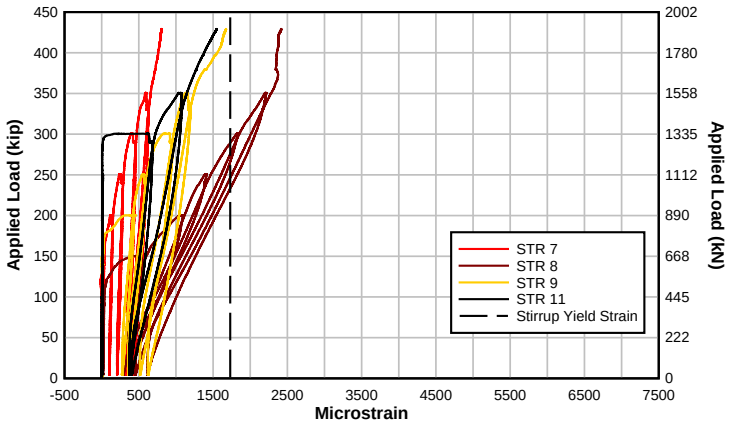

Fig. B.70 - T.45.Ld3(6).SS Strain in mid-height stirrups

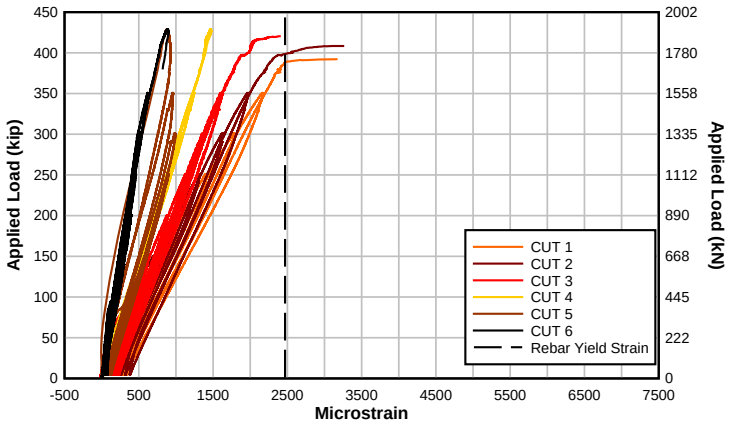

Fig. B.71 - T.45.Ld3(6).SS Strain in cutoff bar

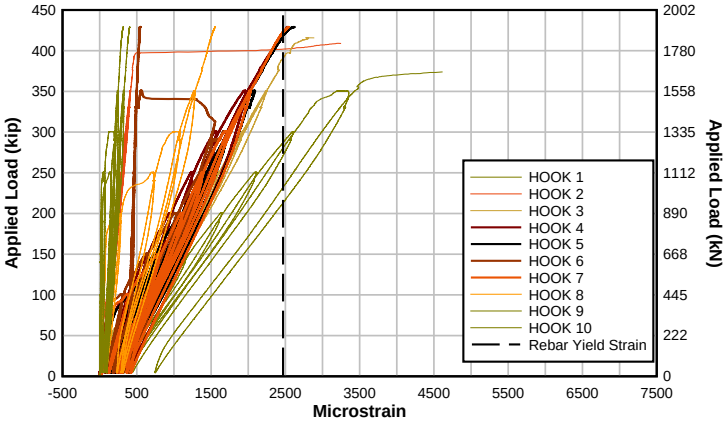

Fig. B.72 - T.45.Ld3(6).SS Strain in hooked bar

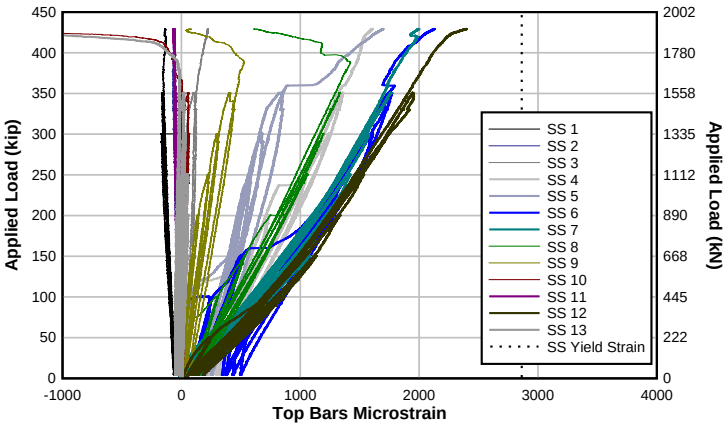

Fig. B.73 - T.45.Ld3(6).SS Strain in stainless steel bar 1 & 2

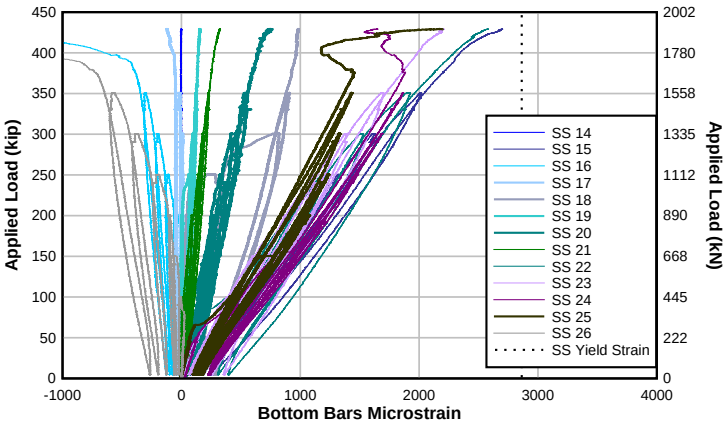

Fig. B.74 - T.45.Ld3(6).SS Strain in stainless steel bar 3 & 4

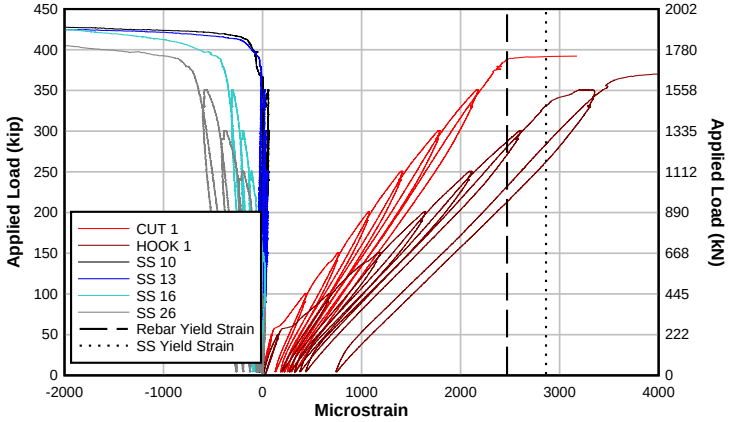

Fig. B.75 - T.45.Ld3(6).SS Section 1 strain

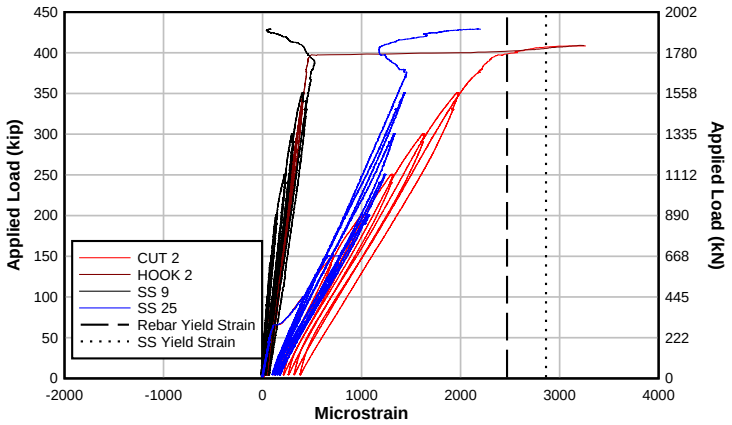

Fig. B.76 - T.45.Ld3(6).SS Section 2 strain

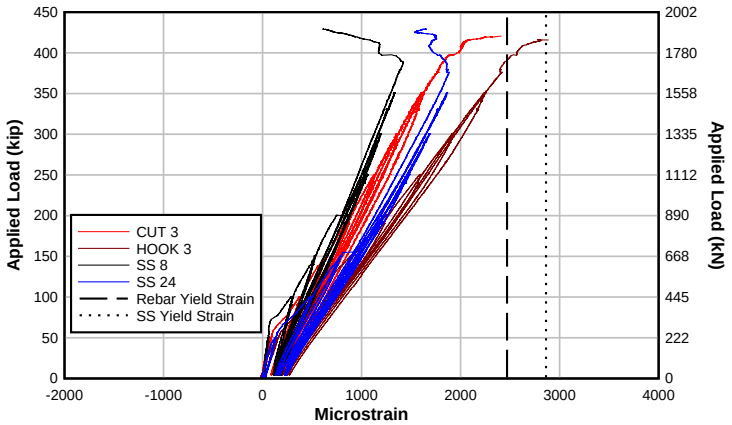

Fig. B.77 - T.45.Ld3(6).SS Section 3 strain

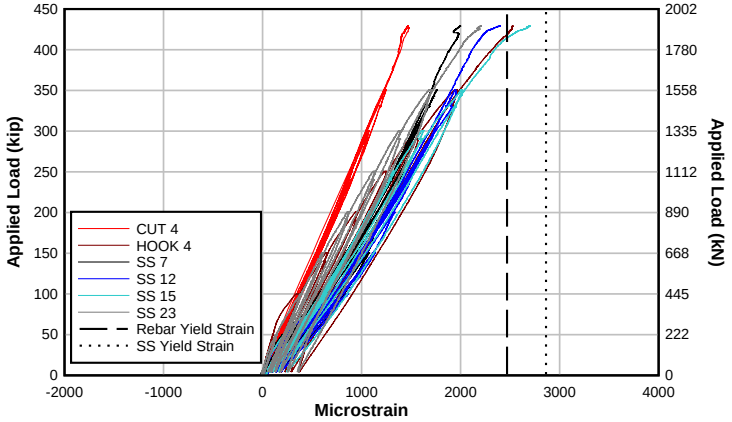

Fig. B.78 - T.45.Ld3(6).SS Section 4 strain

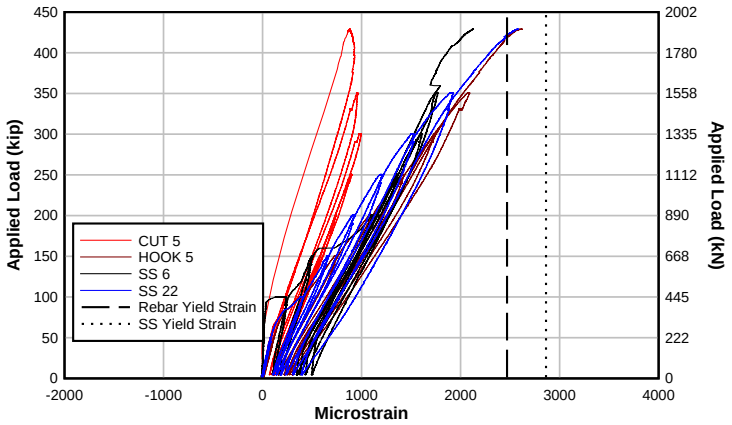

Fig. B.79 - T.45.Ld3(6).SS Section 5 strain

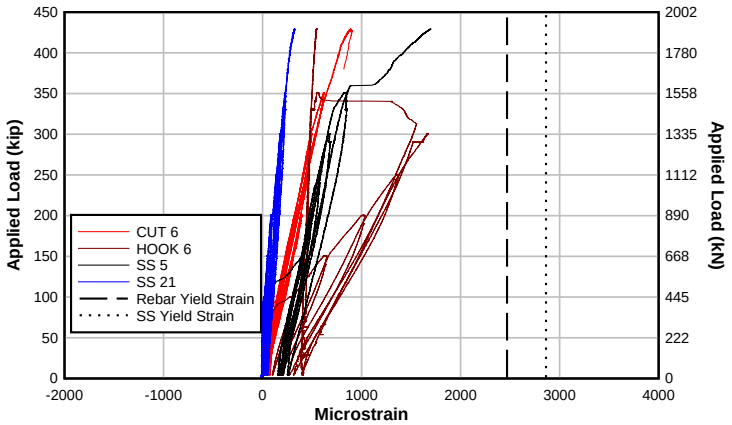

Fig. B.80 - T.45.Ld3(6).SS Section 6 strain

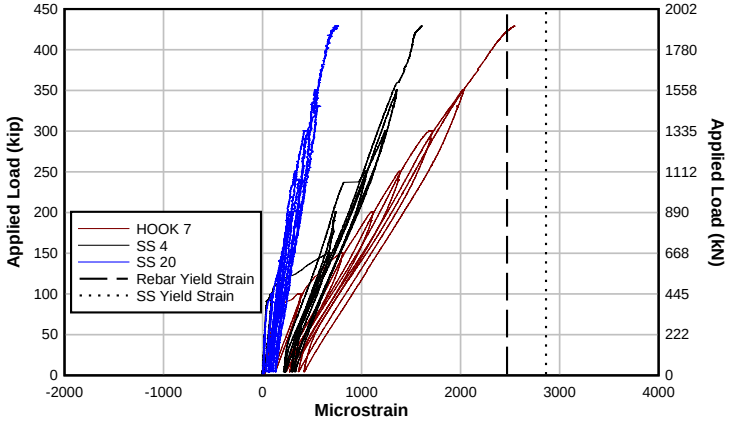

Fig. B.81 - T.45.Ld3(6).SS Section 7 strain

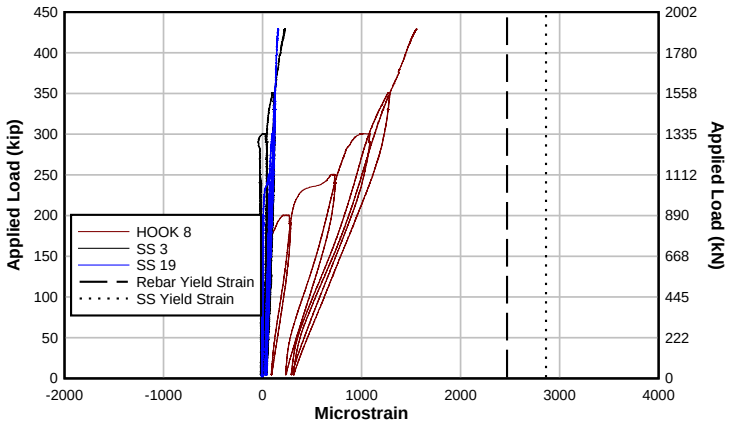

Fig. B.82 - T.45.Ld3(6).SS Section 8 strain

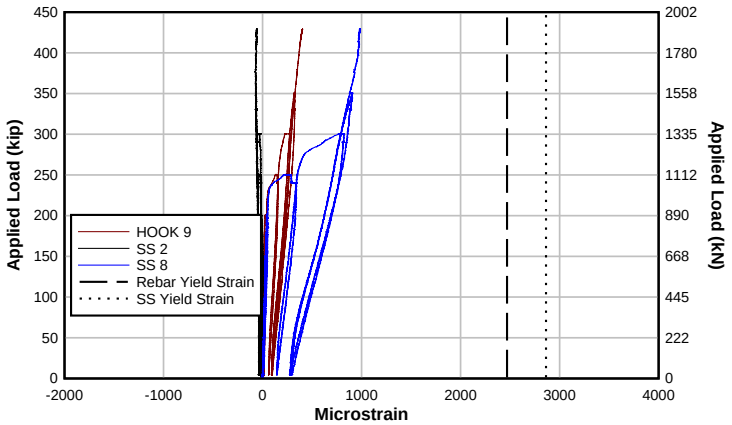

Fig. B.83 - T.45.Ld3(6).SS Section 9 strain

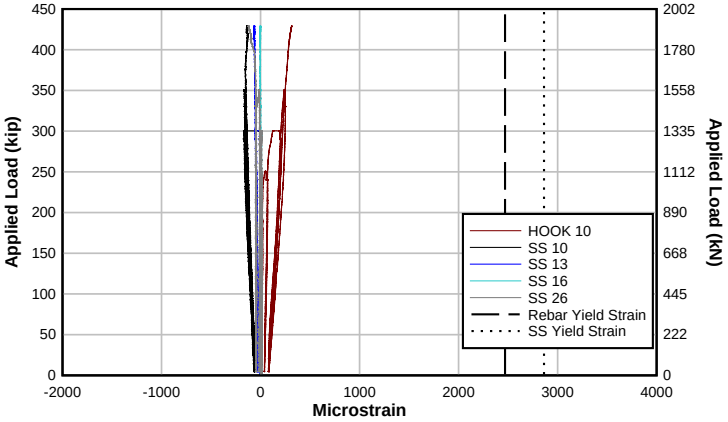

Fig. B.84 - T.45.Ld3(6).SS Section 10 strain

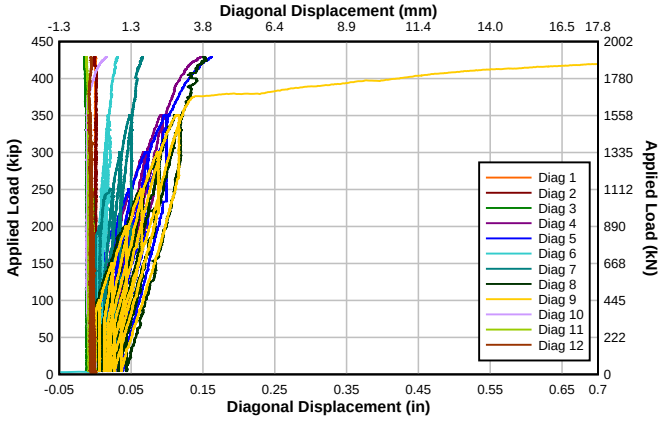

Fig. B.85 - T.45.Ld3(6).SS Diagonal sensor displacement

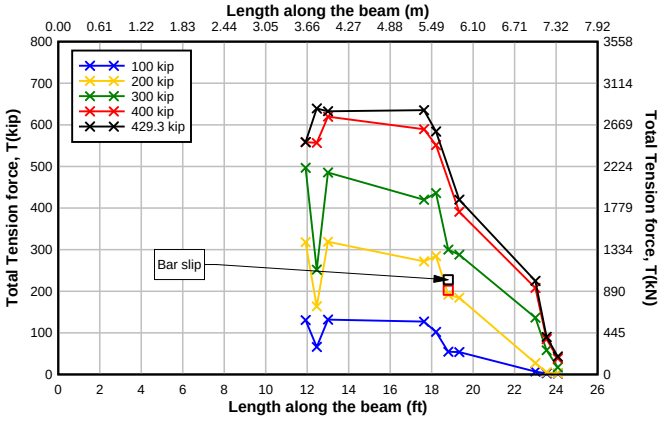

Fig. B.86 - T.45.Ld3(6).SS Flexural tensile force along length at load intervals

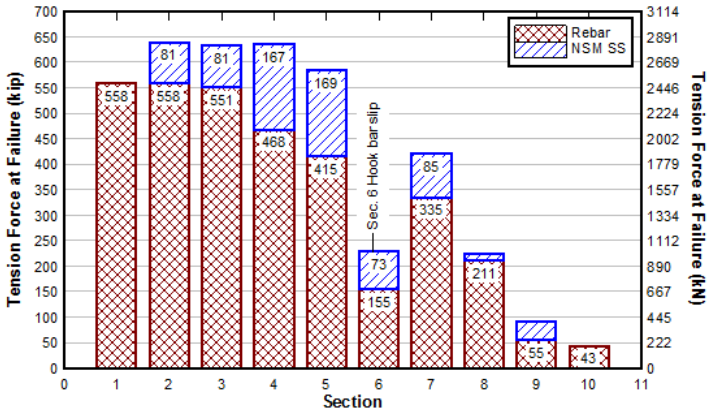

Fig. B.87 - T.45.Ld3(6).SS Steel reinforcing bar vs NSM bar maximum tension force

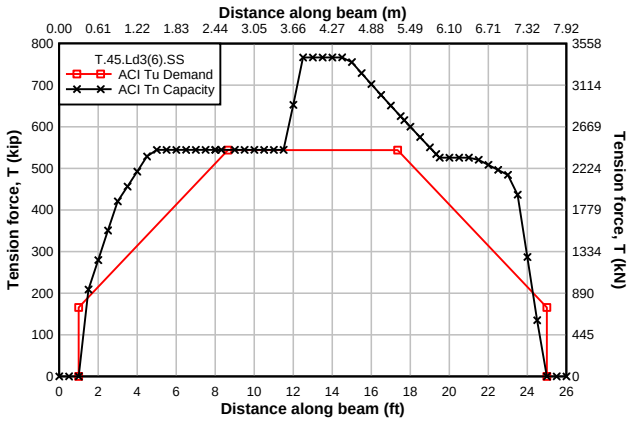

Fig. B.88 - T.45.Ld3(6).SS ACI flexural tension demand and capacity

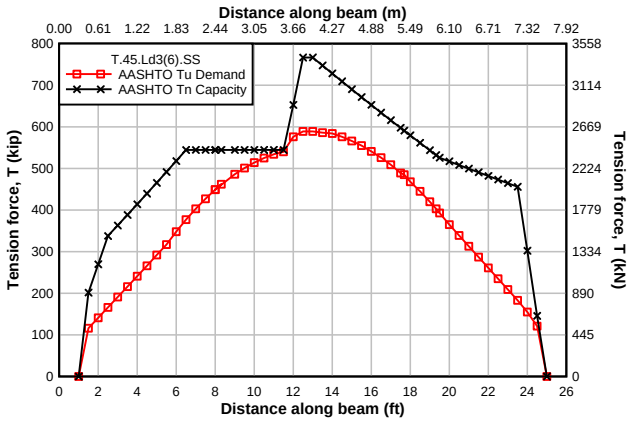

Fig. B.89 - T.45.Ld3(6).SS AASHTO flexural tension demand and capacity

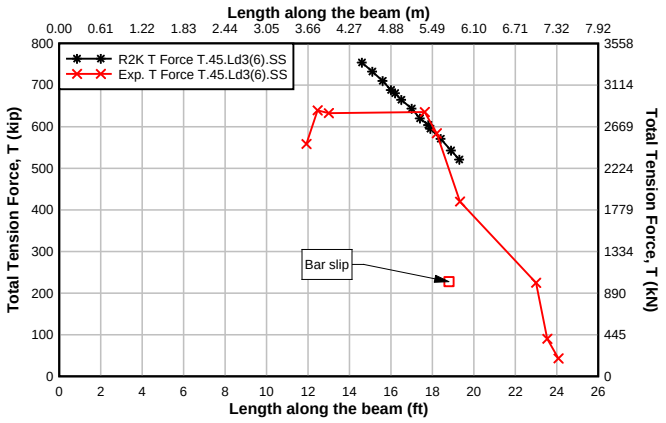

Fig. B.90- T.45.Ld3(6).SS Flexural tension force from experimental data and predicted R2K analysis

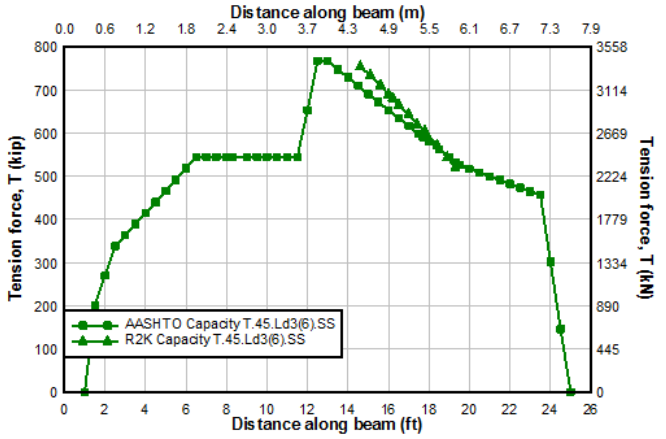

Fig. B.91 - T.45.Ld3(6).SS Flexural tension predictions R2K and AASHTO

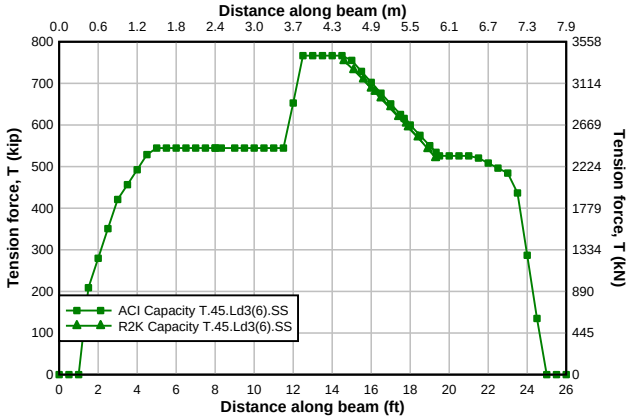

Fig. B.92 - T.45.Ld3(6).SS Flexural tension predictions R2K and ACI

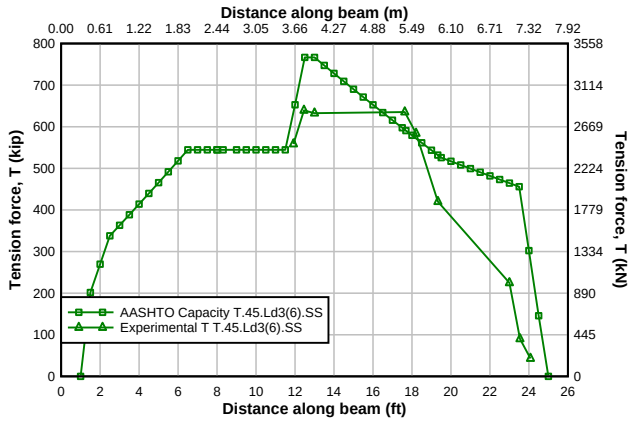

Fig. B.93 - T.45.Ld3(6).SS Flexural tension prediction AASHTO and Experimental data

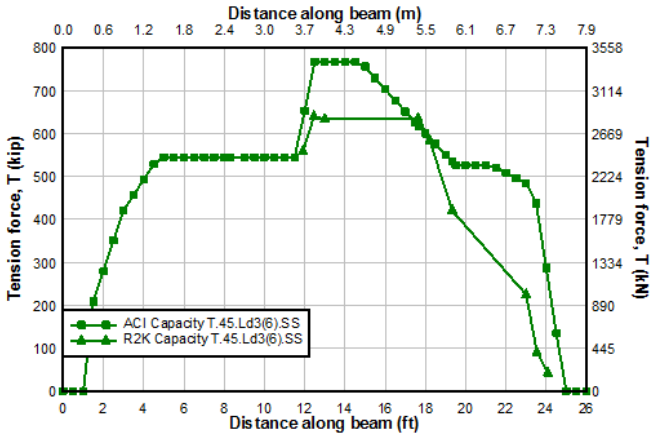

Fig. B.94 - T.45.Ld3(6).SS Flexural tension prediction ACI and Experimental data

APPENDIX C: CONCRETE MIXTURE DESIGN

Concrete was supplied by a local ready-mix company. The mixture had a target 28-day compressive strength of 3000 psi (20.7 MPa), similar to in-situ strengths of vintage RCDG. To simulate concrete mixtures typically made in the 1950s, the mixture had a water to cement ratio of 0.55 and rounded river rock for aggregate. The mixture had a design unit weight of 143 pcf (2291 kg/m^3). A water reducing admixture and an air entrainment admixture was added for workability. The air entrainment admixture, Daravair 1000, was dosed at a rate of 1.4 oz/yd^3 (54.5 mL/m^3). The water reducing admixture was dosed at a rate of 18.8 oz/yd^3 (727.3 mL/m^3).The target slump for the mixture in 5 in. (127 mm). If the measured slump was less than 5 in. (127 mm), one gallon of water per yard per inch of slump desired was added. Typically, each specimen required 6 yd^3 (4.6 m^3) of concrete. The concrete was sent in two trucks timed to arrive after the first specimen was poured. When casting during the winter months, the water was heated before being added to the mixture to accelerate curing. Table C.1 describes the design concrete mixture used for all specimens.

Table C.1 – Typical Concrete Mixture Design

Material	**Specific Gravity**	**Weight (lb) [kg]**	**Volume (ft^3) [m^3]**
Cement	3.15	470 [279]	2.39 [0.089]
Water (total)	1	259 [154]	4.15 [0.154]
3/4-#4 Round PCC	2.6	1741 [1032]	10.73 [0.397]
Manufactured Sand	2.56	209 [124]	1.31 [0.048]
PCC Sand	2.58	1183 [702]	7.35 [0.272]
Admixtures	1	1 [1	0.02 [0.001]
Total Weight		3863 [2291]	
Total Volume (4% Air)			27.00 [1.000]

APPENDIX D: STRAIN COMPATABILITY

Compression field theory was used for design of the T-specimens. Therefore, strain compatibility was assumed. If plane sections remain plane, i.e. strain compatibility, strains will vary linearly based on the depth of the section. For ultimate strength design, the concrete strain at the top most fiber of the section is set to crushing (0.003 strain). To have the concrete and steel exhibit the same strain at a given depth, the reinforcing steel must be fully bonded. Thus, strain compatibility is no longer valid after significant cracking. Strains in the reinforcing materials were measured at several loads and displayed in Fig. D.Fig. D.1 through Fig. D.11. To achieve strain compatibility, the strains should be linearly decreasing from the lowest point up to the highest point on the plot.

At low loads, it was more likely for the strains to be linear. Section 2 at midspan shows the best trend of strain compatibility. Due to the nature of strain gage application, the section over which the strain is being measured is already un-bonded from the concrete creating some variability in measurements. At high loads strain gages may have been damaged and show unreasonably high or low strains. Specimens T.45.Ld3(10).Ti and T.45.Ld3(6).SS show similar trends of strain in the section.

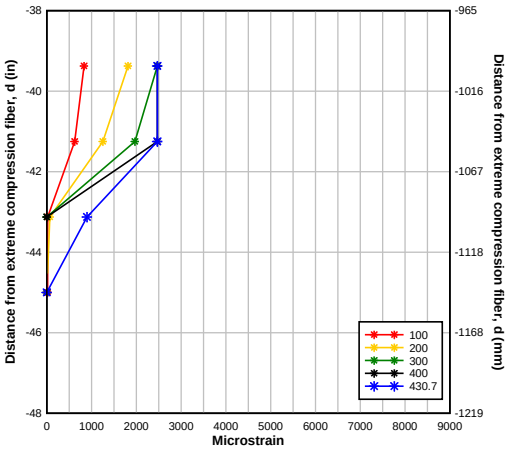

Fig. D.1 - T.45.Ld3(6).Ti Section 1

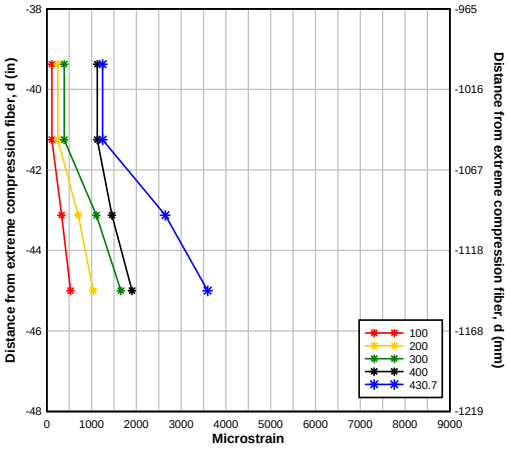

Fig. D.2 - T.45.Ld3(6).Ti Section 2

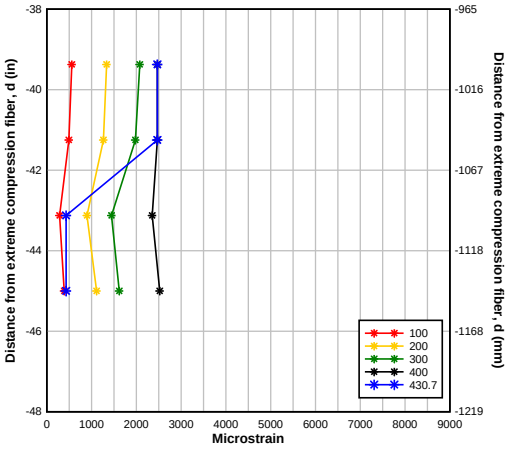

Fig. D.3 - T.45.Ld3(6).Ti Section 3

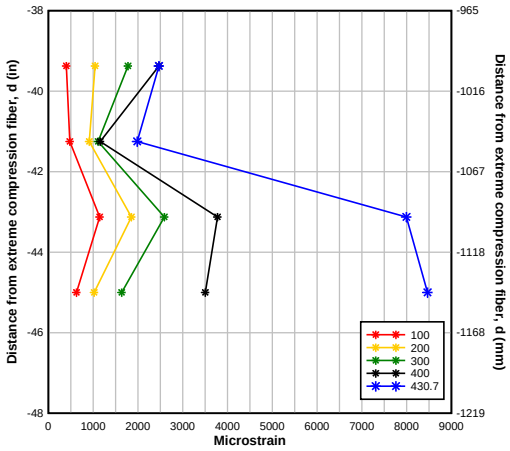

Fig. D.4 - T.45.Ld3(6).Ti Section 4

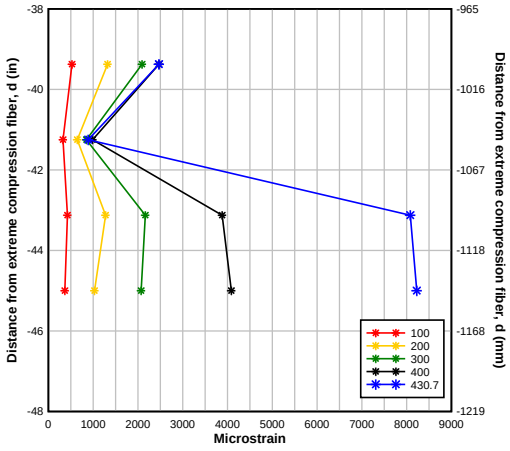

Fig. D.5 - T.45.Ld3(6).Ti Section 5

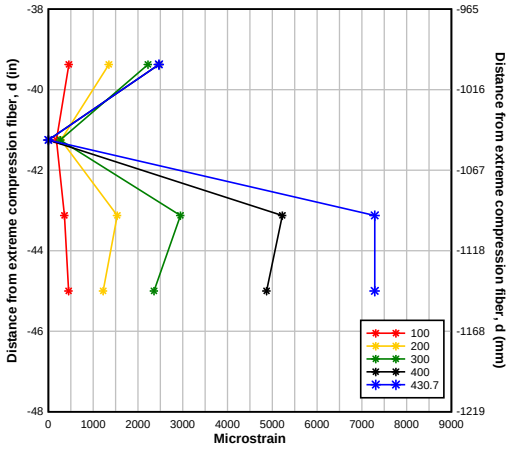

Fig. D.6 - T.45.Ld3(6).Ti Section 6

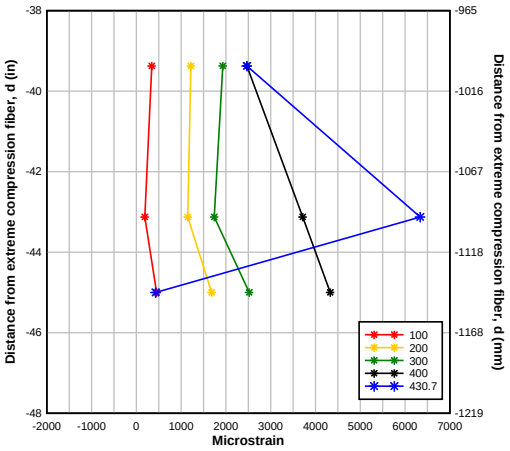

Fig. D.7 - T.45.Ld3(6).Ti Section 7

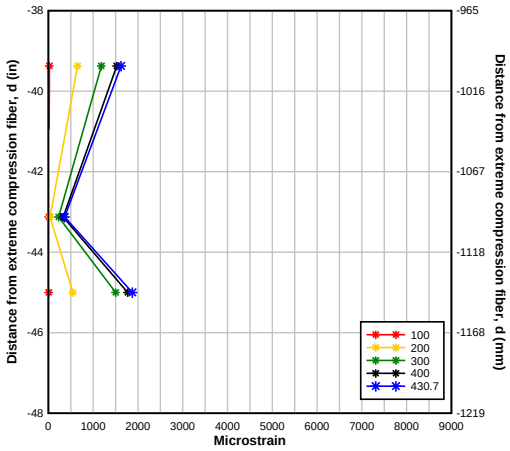

Fig. D.8 - T.45.Ld3(6).Ti Section 8

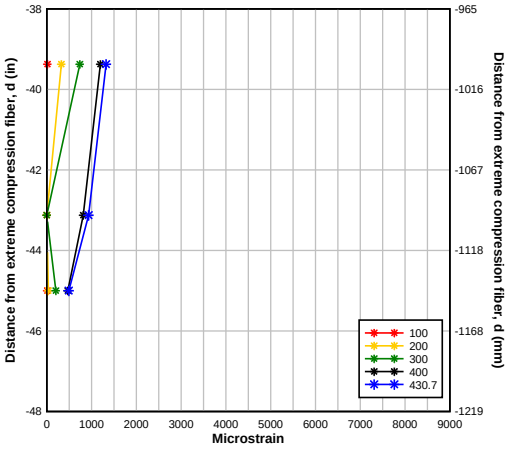

Fig. D.9 - T.45.Ld3(6).Ti Section 9

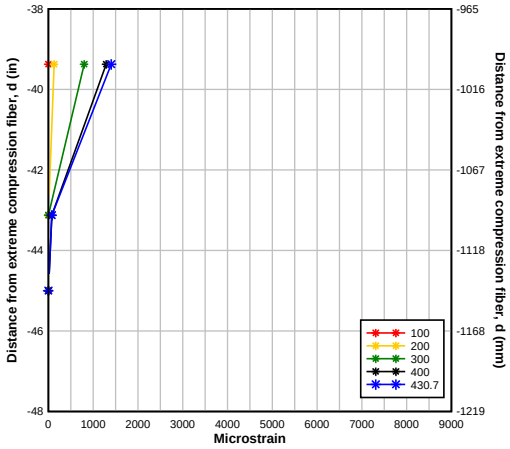

Fig. D.10 - T.45.Ld3(6).Ti Section 10

APPENDIX E: DESIGN SHEAR CAPACITY CALCULATIONS

This appendix provides design equations for calculating the shear capacity using ACI 318-11 and AASHTO-LRFD specifications.

E.1 ACI 318-11 Building Code Requirements for Structural Concrete

As determined in Chapter 11 of ACI 318-11, the nominal shear capacity of the section V_n, is:

$$V_n = V_c + V_s \qquad \text{ACI 318-11 (11-1)} \quad [E.1]$$

where V_c is the nominal shear strength provided by the concrete and V_s is the nominal shear strength provided by the shear reinforcement. The concrete subject to shear and flexure only, the nominal concrete shear strength V_c is:

$$V_c = 2\lambda\sqrt{f'_c} + b_w d \qquad \text{ACI 318-11 (11-3)} \quad [E.2]$$

where λ is the lightweight concrete factor, f'_c is the concrete compressive strength in psi, b_w is the web width, and d is the distance from the extreme compression fiber to the center of the longitudinal reinforcement. The contribution of the shear reinforcement, V_s, is calculated as:

$$V_s = \frac{A_v f_{yt} d}{s} \qquad \text{ACI 318-11 (11-15)} \quad [E.3]$$

where A_v is the area of the shear reinforcement within the stirrup spacing, s. And f_{yv} is the yield stress of the transverse reinforcement. For non-prestressed members, the area of transverse steel reinforcing shall be no less than:

$$A_{v,min} = 0.75\sqrt{f'_c}\,\frac{b_w s}{f_{yt}} \qquad \text{ACI 318-11 (11-14)} \quad [E.4]$$

E.2 AASHTO-LRFD Bridge Design Specifications

For non-prestressed sections, the AASHTO-LRFD nominal shear capacity, V_n, is calculated as:

$$V_n = V_c + V_s \qquad \text{AASHTO-LRFD (5.8.3.3-1) [E.6]}$$

where V_c is the nominal shear capacity of the concrete and V_s is the nominal shear capacity of the shear reinforcement. Typically, the AASHTO shear strength equation includes the shear capacity provided by the prestressing strands, V_p, but the term was neglected due to the existing details.

The AAHSTO-LRFD shear capacity equations incorporate modified compression field theory (MFCT). MFCT is a behavioral model that accounts for diagonally cracked sections that induce additional forces on the flexural steel due to moment and shear interactions. The shear capacity of the concrete $\underline{V_c}$ can be calculated as:

$$V_c = 0.0316\beta\sqrt{f'_c}b_v d_v \qquad \text{AASHTO-LRFD (5.8.3.3-3) [E.7]}$$

where b_v is the width of the web, and d_v is the distance from the centroid of the compression zone to the centroid of the tension zone. β relates transverse reinforcing bar strain to the shear capacity of concrete an is found by:

$$\beta = \frac{4.8}{1+750\varepsilon_s} \qquad \text{AASHTO-LRFD (5.8.3.4.2-1) [E.8]}$$

where ε_s is the strain in the transverse reinforcement. The crack angle, θ, is computed by the following equation:

$$\theta = 29 + 3500\varepsilon_s \qquad \text{AASHTO-LRFD (5.8.3.4.2-3) [E.9]}$$

After β and θ are calculated the nominal shear strength of the shear reinforcing steel can be calculated as:

$$V_s = \frac{A_{sv} f_{yv} d_v \cot(\theta)}{S}$$ AASHTO-LRFD (5.8.3.3-4) [E.10]

Where A_{sv} is the area of the shear reinforcing, f_{yv} is the yield stress of the stirrups, and S is the stirrup spacing. The minimum area of transverse reinforcement is found using the following equation:

$$A_v \geq 0.0316 \sqrt{f'_c} \frac{b_v s}{f_y}$$ AASHTO-LRFD (5.8.2.5-1) [E.11]

APPENDIX F: DESIGN MOMENT CAPACITY CALCULATIONS

Hand calculations of nominal flexural moment capacity reported in this thesis were calculated using AASHTO-LRFD specifications. Real material properties were used in calculations. All NSM materials were assumed to be yielding. To calculate the distance from the extreme compression fiber to the centroid of the tension reinforcement, $d_{s,}$ the internal reinforcing steel and NSM materials were lumped into one centroid. When calculating the flexural moment capacity with and without the NSM materials, the contribution of the compression steel was incorporated. The stress in the compression steel was found assuming a balanced strain condition and the strain diagram. The nominal moment calculations included the NSM materials by adding an additional NSM tension force multiplied by the combined moment arm.

F.1 ACI 318-11 Building Code Requirements for Structural Concrete

The provisions in ACI Chapter 10 outline the flexural design assumptions for reinforced concrete sections. ACI assumes plane sections remain plane, concrete compression strain is limited to 0.003, and strain in the steel is limited to yield. Assuming a rectangular concrete stress block, the length of the block, *a*, is calculated as:

$$a = \frac{A_s f_y}{0.85 f'_c b} \qquad \text{[F.1]}$$

where A_s is the area of flexural steel, f_y is the stress of the steel at yield, f'_c is the compressive stress of the concrete, and *b* is the width of the web. The distance to the neutral axis, *c*, is calculated as:

$$c = \frac{a}{\beta_1} \qquad \text{ACI 318-11 Sec. 10.2.7.1 [F.2]}$$

where β_1 is the concrete strength factor was taken as 0.85 for concrete between 2500 and 4000 psi. Before calculating the flexural moment capacity of the section, the assumption that the steel is at yield must be checked. The tensile strain in the reinforcement closest to the tension face, ε_t is calculated as:

$$\varepsilon_t = \frac{d_t - c}{c} \qquad \text{[F.3]}$$

where d_t is the distance from the extreme compression fiber to the extreme tension fiber in the reinforcing steel. A section is tension controlled if ε_t is greater than 0.005. If the strain in tension steel is at yield the nominal moment capacity M_n is:

$$M_n = A_s f_y \left(d - \frac{a}{2}\right) \qquad \text{[F.4]}$$

Section 10.5 of ACI 318-11 requires a minimum reinforcement of flexural members to be calculated as:

$$A_{s,min} = \frac{3\sqrt{f'_c}}{f_y} b_w d \qquad \text{ACI 318-11 (10-3) [F.5]}$$

But not less than $(200 b_w d)/f_y$. This equation applies to large cross sections to balance the tension and compression forces.

F.2 AASHTO-LRFD Bridge Design Specification

AASHTO-LRFD section 5.7.3.1 and 5.7.3.2.2 outlines provisions for calculating flexural resistance in flanged sections. The nominal moment capacity in a flanged section neglecting prestressing steel is calculated as:

$$M_n = A_s f_s \left(d_s - \frac{a}{2}\right) - A'_s f'_s \left(d'_s - \frac{a}{2}\right) + 0.85 f'_c (b - b_w) h_f \left(\frac{a}{2} - \frac{h_f}{2}\right)$$

AASHTO-LRFD (5.7.3.2.2-1) [F.6]

Where A_s and A'_s is the area of the flexural and compression reinforcing steel. f_s and f'_s is stress in flexural and compression reinforcing steel. The stress in the compression steel was found by strain compatibility. The strain in the tension steel was limited to yield while the strain in the concrete was 0.003 (crushing); the compression steel strain was determined from the depth of the compression steel. d_s is the distance from the extreme compression fiber to the centroid of the tension force. The height of the rectangular stress block, *a*, can be calculated as:

$$a = c\beta_1$$

AASHTO-LRFD Sec 5.7.3.2.2 [F.7]

Where β_1 is the stress block factor was taken as 0.85. The depth to the neutral axis, *c*, is calculated neglecting the prestressing forces as:

$$c = \frac{A_s f_s - A'_s f'_s - 0.85 f'_c (b - b_w) h_f}{0.85 f'_c \beta_1 b}$$

AASHTO-LRFD Sec 5.7.3.2.2 [F.7]

Where *b* is the effective flange width and h_f is the height of the flange.

APPENDIX G: FLEXURAL TENSION FORCE CALCULATION

Flexural tension capacity and demand were used to determine the likelihood of an anchorage failure. Flexural tension capacity of a section is determined from the nominal moment capacity as:

$$T_n = \frac{M_n}{d_v} \quad \text{[G.1]}$$

where M_n is calculated from the AASHTO flexural moment capacity, and d_v is from the center of the compression block to the centroid of steel.

The AASHTO flexural tension demand, T_u incorporates the additional force from shear on the longitudinal reinforcement. Neglecting the contribution of axial and prestressing forces the flexural tension demand is calculated as:

$$T_u = \frac{M_u}{d_v} + (V_u - 0.5V_s) * cot\theta \quad \text{AASHTO Eq. 5.8.3.5-1} \quad \text{[G.2]}$$

where M_u is the factored moment demand, V_s is the shear resistance provided by the transverse reinforcement, and θ is the crack angle. For each specimen, the maximum M_u value was set to equal the nominal moment capacity at midspan (without contribution of NSM).

The experimentally calculated flexural tension force used the following equation:

$$T_{exp} = A_x E_x \varepsilon_x \quad \text{[G.3]}$$

where A_s the area of longitudinal reinforcement, E_s is the modulus of elasticity of the material, and ε_s is the strain in the bar collected from testing.

APPENDIX H: RESPONSE 2000 SECTIONAL ANALYSIS

Response 2000 (R2K) is an open source reinforced concrete sectional analysis tool (see http://www.ecf.utoronto.ca/~bentz/r2k.htm). It was developed by Evan Bentz and Michael Collins at the University of Toronto in 2000. R2K has a simple windows based input and graphical and numerical output. The program uses modified compression field theory (MCFT) to analyze a two dimensional non-linear sectional analysis of beams and columns. R2K calculates the strength and ductility of a user-defined cross-section subject to shear, flexure, and axial load. R2K provided both shear and moment capacity predictions in this project. In addition to calculating capacities, longitudinal strains, and transverse strain based on MFCT, R2K also determines the AASHTO 99 shear and moment interaction diagrams. R2K inputs include cross-sectional shape, longitudinal steel arrangement, stirrup type, stirrup spacing, material properties, and shear to moment ratios.

All specimens used their unique stirrup spacing, material properties. NSM material was incorporated and longitudinal reinforcement and was considered to be fully bonded to the concrete section. Shear and moment ratios were chosen based on the distance from the support to the section considered. The area of steel in the cutoff bar was a function of the specified development length, and maintained the same yield stress. The shear and moment outputs were transformed into corresponding load capacities at each section. Longitudinal strains were recorded at each sectional analysis and transformed into flexural tension force. Critical sections were d_v away from the loading points, the end of the cutoff reinforcing bar, the preformed diagonal crack, and at midspan. The location of the 45° preformed crack was similar to d_v and therefore controlled the analysis. The shear and moment ratios for the critical cross sections are listed in Table H.1

Table H.1- Moment to shear ratio for sections of analysis in R2K

Specimen	Moment to Shear ratio (M/V) (ft) [m]		
	Midspan	45 preformed diagonal crack	End of cutoff reinforcing bar
T.45.Ld3(10)	40 [12.2]	7.52 [2.29]	5.67 [1.73]
T.45.Ld3(10).Ti	42.5 [13.0]	7.41 [2.26]	5.67 [1.73]
T.45.Ld3(6).Ti	25 [7.6]	7.11 [2.17]	5.67 [1.73]
T.45.Ld3(6).SS	25.5 [7.8]	7.25 [2.21]	5.67 [1.73]

Fig. H.1 displays a typical output screen for a T-specimen. The shear and moment capacities are on the left with longitudinal reinforcing bar strains mid figure.

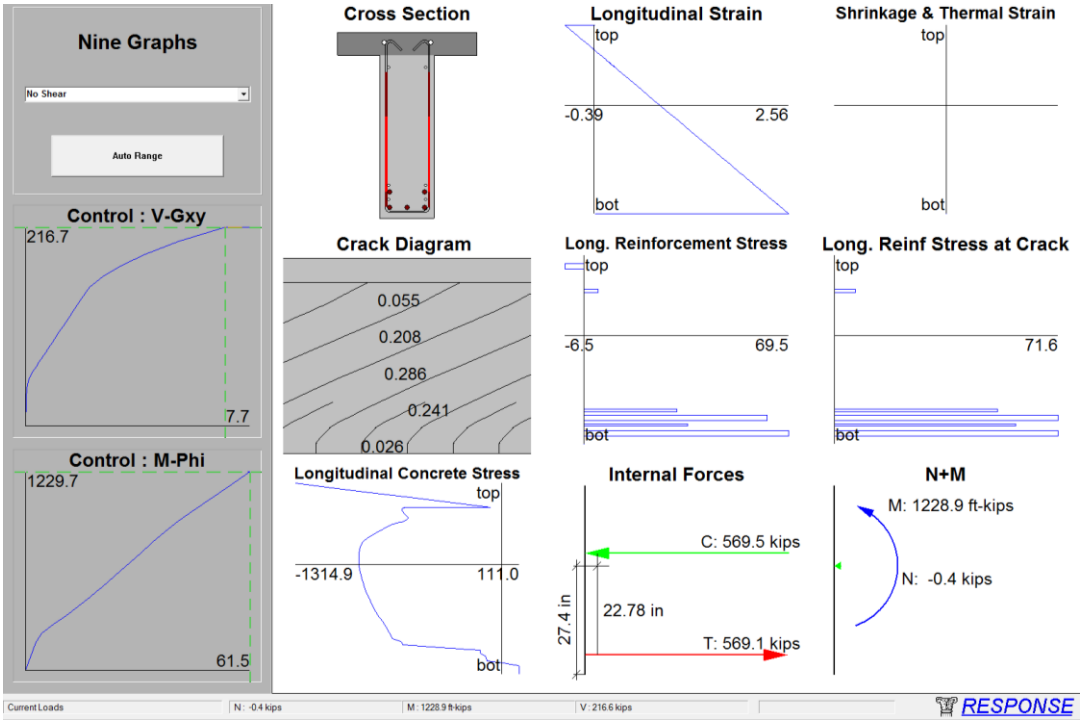

Fig. H.1 - Typical R2K output screen for T-specimen

APPENDIX I: MOSIER BRIDGE CASE STUDY

I.1 Introduction

The Mosier bridge case study was performed at the request of the Oregon Department of Transportation (ODOT). The bridge is an overcrossing of the Columbia River highway (I-84) in the state of Oregon. The Mosier connection serves a nearby quarry and was built in 1953. Typical of practices in the 1950s, the bridge was tapered and haunched to a smaller section at midspan than at the supports. During an annual bridge inspection in 2013, large vertical cracks were observed around known cutoff locations of longitudinal reinforcing steel in an interior girder. The cracks observed had a unique vertical offset and confirmed the need for further investigation. Fig. I.1 illustrates the location of the Mosier Bridge over the Columbia River Highway and Fig. I.2 shows an elevation view of the bridge and span under question.

Fig. I.1- Areal view of Mosier Bridge (Google Maps, 2014)

Fig. I.2 - Mosier bridge with highlighted span 1 (Google Maps, 2014)

The Mosier Bridge is a four span reinforced concrete deck girder (RCDG) bridge. The original three spans were built in 1953 and was lengthened in 1959 (ODOT, 2013). After the bridge inspection identified a 0.03 in. (0.762 mm) wide crack in the North span interior girder, the bridge was shored. Fig. I.3 below pictures the crack with vertical offset.

Fig. I.3 – View of haunch transition on interior girder of span 1 (right) and crack with vertical offset on interior girder of span 1(left) (ODOT 2013)

The load resistance factor rating found that other spans had shear deficiencies, but not the span with identified cracking. Upon completion of the bridge rating, shear, positive moment, and anchorage strengthening was deemed necessary. The bridge was shored immediately to maintain traffic and the strengthening was completed in the summer of 2014. The anchorage strengthening was dependent on the results of experimental testing by Higgins. Near-surface mounted (NSM) titanium, stainless steel, and CFRP were considered for the strengthening of the Mosier Bridge. However, due to geometric constraints, the titanium alloy bar was determined as the most cost effective retrofitting material.

I.2 Experimental Program

An experimental program was developed to strengthen anchorage deficiencies and flexural strength in a full-scale positive moment T-specimen to simulate a strengthening procedure on the Mosier Bridge. The specimens will be constructed, strengthened, and tested to failure to evaluate the effectiveness of the NSM titanium strengthening. The experimental program contains specimen design, details, material properties, instrumentation, and test protocol of the Mosier specimens.

I.2.1 Specimen Design

Mosier specimen design was based the as-built details from the Mosier bridge. The girder evaluated and strengthened in this program was the interior girder of span 1 shown in Fig. I.2. Similar to the Mosier Bridge girders, the specimens included a slight taper and haunch detail at midspan. Analysis of the span in consideration determined that the dead load produced negative moments, and live load produced positive moments at the haunch location. To simulate this, a unique test protocol was created described in Section *I.2.5 Test Protocols.* The clear span of the Mosier specimens was selected to match similar shear and moment demands at the haunch location in the Mosier Bridge. To further simulate conditions of the existing bridge similar concrete strengths and reinforcing steel strengths were selected. Specimen strengthening methodology was similar to the NSM titanium strengthening techniques used in the test program described in Chapter 4.

Three specimens were constructed in the Mosier Bridge experimental program: Mosier 1, the as-built specimen, Mosier 2, the NSM titanium strengthened specimen after failing reinforcing steel anchorage, and Mosier 3, the NSM titanium strengthened specimen with

reinforcing steel anchorage fully intact. Since the reinforcing steel cutoff details are detailed poorly, the designer would assume zero anchorage from the end of the reinforcing bars to the cracks evident in the Mosier Bridge. Mosier 2 would verify the strengthening process with the assumption that the ends of the flexural steel at midspan are not anchored.

I.2.2 Specimen Details

Simulating in-situ conditions required several unique details when constructing and testing the Mosier specimens. All specimens were 18 ft (5.49m) long and had a 6.5 x 36 in. (165 x 914 mm) deck. The stem was 9 x 29.5 in. (229 x 749 mm) in half of the specimen then transitioned to a cross section of 12.63 x 41.25 in (321 x 1048 mm) through horizontal and vertical tapering after midspan. The reinforcing steel selection and configuration was unique to the Mosier bridge and described in detail in Section *I.2.2.1 Reinforcing Steel.* Construction and NSM strengthening methods were similar to the process in Chapter 4.

I.2.2.1 Reinforcing Steel

Reinforcing steel configurations were determined by the as built drawings from 1953. The drawings indicated the reinforcing steel bars were square and also had lower yield strengths than steel commonly used today. Therefore, lower yield, smaller bars were used for construction of the Mosier specimens. Anchorage lengths and dimensions of the flexural steel from the as-built drawing were used to detail the Mosier specimens. Fig. I.4 and Fig. I.5 display the elevation and cross sections from the 1953 drawings of the girder being considered.

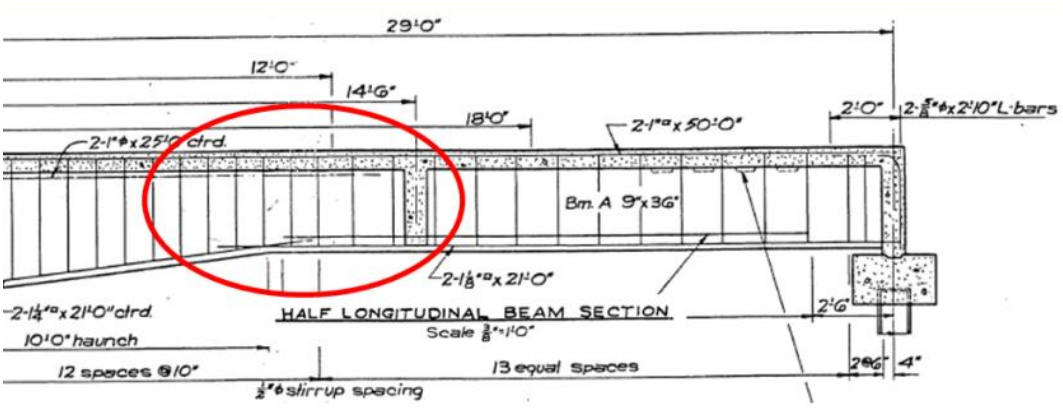

Fig. I.4 – As-built elevation drawing of Mosier Bridge with highlighted critical section (ODOT, 2014)

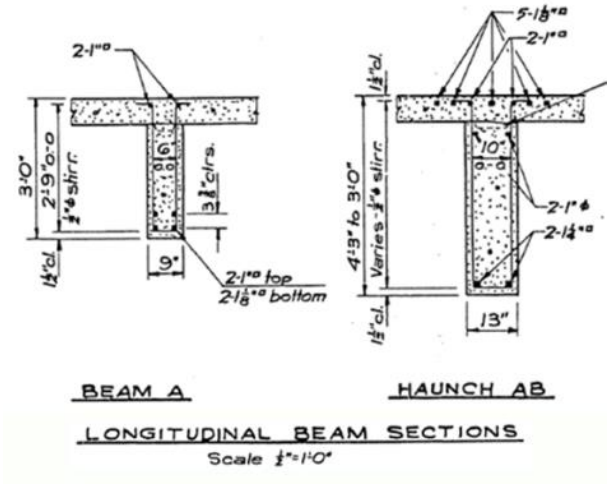

Fig. I.5 – As-built cross section of Mosier Bridge span 1 interior girder (ODOT, 2014)

The haunch intersection with vertical offset cracks in the Mosier Bridge is highlighted in Fig. I.4. Beam A in Fig. I.5 is the smaller, constant cross section in Mosier specimens for 9 ft (2.74 m). The Mosier specimen transitions to Haunch AB in the remaining 9 ft (2.74 m).

All specimens have identical longitudinal reinforcing steel. Longitudinal reinforcing steel in the web consisted of two #7 (22M) and two #8 (25M) bars on the South half and two #9

(29M) bars through the North half. Two #6 (19M) steel reinforcing bars were located in the upper stem on the north end. All longitudinal reinforcing steel bars were adequately anchored past the support locations. To resist negative moments, the Mosier specimens had two #7 (22M) and five #8 (25M) steel reinforcing bars in the flange terminating at various lengths. Double-legged, open #4 (13M) stirrups were spaced 12 in. (305 mm) on center throughout midspan in Mosier 1 and Mosier 2. Mosier 3 decreased the stirrup spacing before the NSM titanium strengthening initiated. Fig. I.6 through Fig. I.11 display the cross section and elevation drawings for the Mosier specimens built in this experimental program.

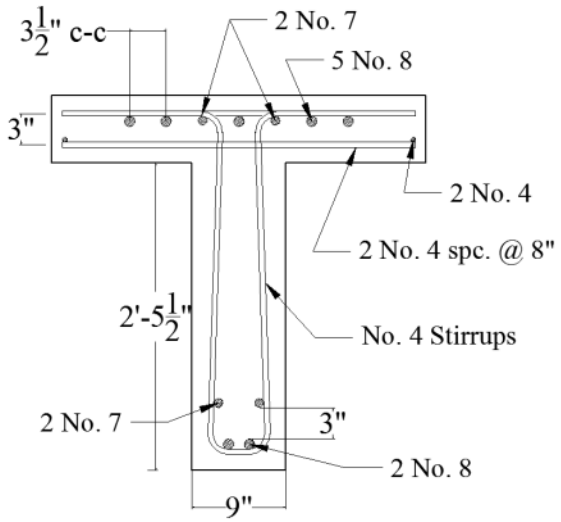

Fig. I.6 – Cross section at South end of Mosier specimen

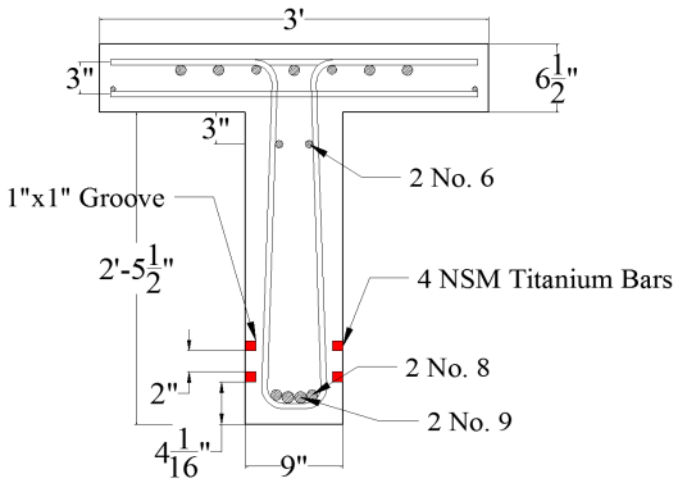

Fig. I.7 - Cross section at midspan of Mosier specimen with NSM Titanium

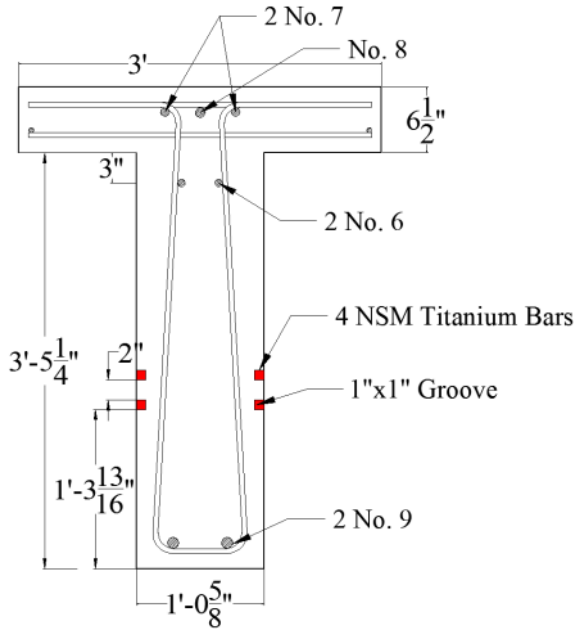

Fig. I.8 - Cross section at North end of Mosier specimen with NSM Titanium

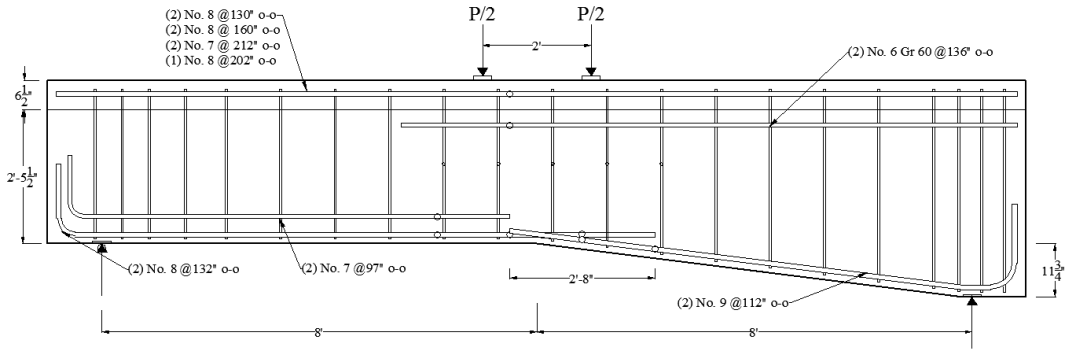

Fig. I.9 - Elevation of Mosier 1

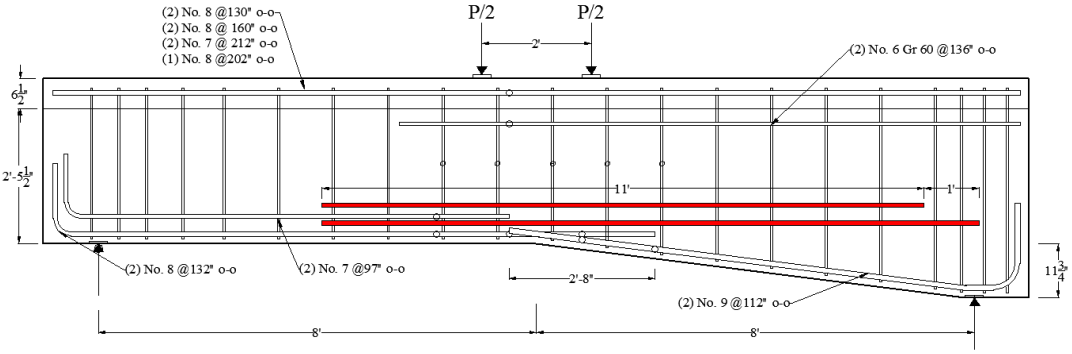

Fig. I.10 - Elevation of Mosier 2 with NSM titanium

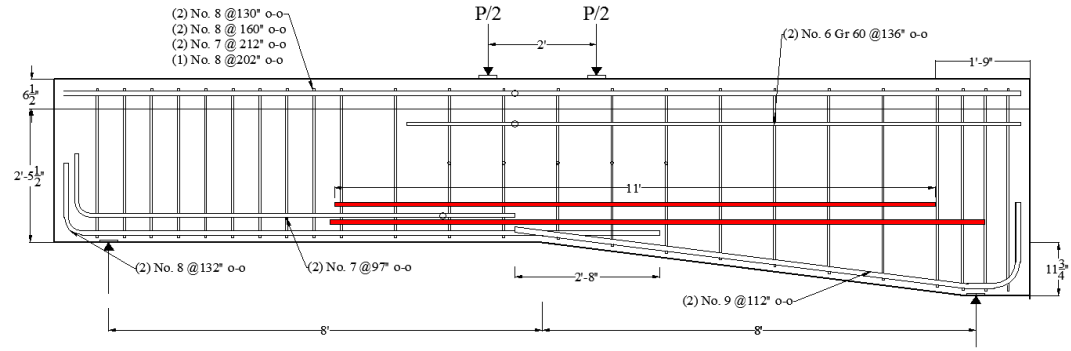

Fig. I.11 - Elevation of Mosier 3 with NSM titanium

The cross section drawings show the longitudinal reinforcing steel and NSM titanium for applicable specimens. The cross section at midspan was congested with four steel reinforcing bars in close proximity. The most deficient detail in the Mosier specimens was the overlapping of the #8 (25M) and #9 (29M) bars at midspan. While the as-built drawing suggested more overlap, in reality the two bars are developing simultaneously at the point of maximum moment. Mosier 3 decreased stirrup spacing and terminated the NSM titanium bars at slightly different locations than Mosier 2. The upper and lower NSM titanium bars were shifted 1 in. (25.4 mm) relative to each other.

I.2.2.2 Construction

The construction of the Mosier specimens initiated after strain gage sensors were applied to the internal reinforcing steel as described in Section *I.2.4.2 Internal Sensor Array.* This section describes the cage construction, the preformed crack details, and the concrete casting process.

The longitudinal bars were cut to length and bent on site using a bar bending machine. Stirrups of increasing height were ordered from a local reinforcing bar fabricator. To create the steel reinforcing cage, stirrups spaced 12 in. (305 mm) apart or tighter were hung from the steel reinforcing bars in the deck. Two #8 (25M) steel reinforcing bars were tied to the stirrups for the lower layer of flexural reinforcement on the south half of the Mosier specimens. Similarly, two #9 (29M) steel reinforcing bars were tied to the tapered stirrups as the flexural reinforcement on the north half. At midspan the two #9 (29M) steel reinforcing bars intersected the two #8 (25M) steel reinforcing bars as shown in Fig. I.12. The cutoff layer of #7 (22M) steel reinforcing bars were spaced 3 in. (76.2 mm) clear from

the top of the #7 (22M) layer. Several 1.5 in. (38 mm) wide spacers were attached to the stirrup legs and longitudinal steel to provide sufficient cover. Fig. I.13 pictures the completed reinforcing steel cage for Mosier 1.

Fig. I.12 - Midspan reinforcing steel terminations for Mosier specimens

Fig. I.13 - Mosier 1 reinforcing steel cage

In Mosier 1, a block-out was placed around the ends of the #7 (22M) steel reinforcing bars to measure the bar end slip. Mosier 2 did not measure the #7 (22M) reinforcing bar end slip because the anchorage was failed prior to testing. Mosier 3 did not include a block-out around the #7 (22M) reinforcing bar ends.

To achieve the specified dimensions, the Mosier formwork was tapered and haunched using falsework in a larger T-specimen form. Once the specimens were fully instrumented and constructed, the reinforcing cages were placed in the formwork. Concrete was supplied

by a local ready-mix provider. Concrete was placed into a bucket then placed into the forms using an overhead crane. Care was taken to avoid the internal instrumentation while the concrete was consolidated with a mechanical vibrator. The specimens were finished and cured for seven days. After initial curing, the specimens were removed from the formwork and placed in a stable configuration for the saw-cutting the grooves for the NSM retrofit.

I.2.2.3 NSM Details and Installation

The design intent of NSM material strengthening procedure is to retrofit anchorage deficiencies and provide additional flexural capacity in the Mosier Bridge. To accomplish this, the reduction in flexural strength where the #8 (25M) and #9 (29M) steel reinforcing bars are developing must be bridged. To increase the Mosier Bridge capacity and maintain posted ratings, the flexural reinforcing must be fully developed at midspan through the addition of the NSM material. NSM strengthening design methodologies from Chapter 3 were utilized in this case study.

The NSM titanium bar selected had a 0.61 in. (15.5 mm) diameter with a nominal yield stress of 145 ksi (1000 MPa). Using nominal tensile properties, the predicted addition to flexural capacity was found. To increase the positive moment ultimate strength, four NSM titanium bars were required. A 6 in. (152.4 mm) hooked development length was assumed for the titanium NSM materials. The extent of the NSM reinforcing was determined by the existing Mosier Bridge elements. A diaphragm was present at the south end of the interior girder, approximately 5 ft (1.5 m) from the south end of the Mosier specimen; therefore, the NSM titanium was terminated at least 2 in. (51 mm) before the diaphragm to allow for

drilling clearances. The NSM titanium on the north end of the Mosier 2 and Mosier 3 specimens was terminated after the exiting the flexural tension zone. The upper layer of NSM titanium bars was terminated prior to the lower layer to minimize a stress concentration. In summary, the strengthening required two NSM titanium bars at a length of 11 ft (3.35 m) out-to-out, and two NSM titanium bars at a length of 12 ft (3.65 m) out-to-out.

NSM groove depth and spacing requirements were determined by ACI 440.2R-08. The groove depth and width was 15/16 in. (23.8 mm) using a #5 (16M) NSM bar. The clear distance between grooves was approximately 3 in. (76.2 mm). The elevation of the NSM titanium was determined by the optimizing the effectiveness of the titanium (providing a large lever arm) and being spaced over the #7 (22M) reinforcing steel bar.

After initial curing, the Mosier 2 and Mosier 3 specimens were placed in a stable configuration for saw-cutting the NSM grooves. Three longitudinal passes made with a concrete saw. A roto-hammer was used to chip the grooves to their intended depth, and then holes for the hook were drilled using a 3/4 in. (19 mm) diameter drill. The corner between the NSM groove and circular hole was chiseled to allow for the bend radius of the hook. The NSM titanium was anchored using a 2 in. (51 mm) diameter 90° hook. Due to the width of the stem, the 6 in. (152 mm) hook could not be used if the NSM titanium bars terminated at the same location on each side of the stem. Mosier 2 used a smaller length of hook in the thinner South stem and the 6 in. (152 mm) hook length in the North stem. Mosier 3 used 6 in. (152 mm) long hooks on all ends of the NSM titanium. To allow for the increased hook length in Mosier 3, the NSM titanium bars were offset 1 in. (25.4 mm)

on each side of the stem so the hooks would not intersect. The NSM titanium hooks were fabricated in a bar bending machine around a 2 in. (51 mm) diameter pin. Prior to bending, the NSM titanium was heated to a maximum of 900 °F with an acetylene torch for all Mosier 2 hooks. The NSM titanium hooks of Mosier 3 were heated to at least 1250 °F.

Installation of the Mosier specimens NSM titanium was unique. The dead load of the Mosier Bridge produced negative moments in the section, therefore, the Mosier specimens must experience negative moments prior to and during the NSM titanium installation. A description of this unique loading scheme is described in Section *I.2.5 Test Protocols.* After the specimen was at the specified load to produce negative moments, the load was held. Grooves were cleaned and the epoxy was extruded into the groove before the bar was installed. The bars were held flush within the groove at the haunch transition by a clamp at midspan. The groove was filled with epoxy and finished. Epoxy was cured for a minimum of seven days before unloading the dead load and applying the actuator load.

To fulfill the design intent of the Mosier 2 specimen, the anchorage of the reinforcing steel at midspan was failed prior to installing the NSM titanium. A dynamic actuator load of over 40 kips was applied the Mosier 2 specimen through four point loading. The applied load brought the Mosier 2 specimen near to a flexural failure. The cracking around the anchorage was similar to the cracks seen in the Mosier Bridge. Cracked, unbonded concrete was removed from the anchorage region of the intersecting reinforcing steel bars at midspan. To ensure a monolithic response of the strengthened specimen, the cracks from pre-failing the anchorage were epoxy injected. Once the epoxy injection was cured the Mosier 2 specimen followed the testing protocols of Mosier 1 and Mosier 3.

The design intent of the Mosier 3 specimen was to test the NSM titanium strengthened specimen with all reinforcing bars fully embedded in the concrete. Additionally, the NSM titanium was confined at the haunch transition at midspan with two steel plates. A confinement plate would resist the outward force induced on the NSM titanium bars from the haunch transition geometry. The outward force on the NSM titanium could be approximately 1 kip (4.89 kN). The dimensions of the steel confining plates were 1/2 x 3 x 15 in. (13 x 76 x 381 mm). The plate was attached with two 1/2 in. (13 mm) diameter steel bolts. A hole was drilled through the stem above the NSM titanium groove at midspan for the steel bolt.

I.2.3 Material Properties

The concrete mixture for strengthened T-specimens described in Chapter 4 was used in the Mosier specimens. The concrete mixture design had a 28-day compressive strength of 3000 psi (20.68 MPa) and was designed to simulate vintage mixture proportions and materials. Test day concrete strengths for the Mosier specimens are listed in Table I.1 below.

Table I.1 - Concrete properties for Mosier specimens

Specimen	**f'_c (psi) [MPa]**	**Standard Deviation (psi) [MPa]**	**f_{ct} (psi) [MPa]**	**Standard Deviation (psi) [MPa]**	**Concrete Age (days)**
Mosier 1	3038 [21.0]	76.9 [0.53]	348 [2.40]	25.2 [0.17]	33
Mosier 2	3629 [25.0]	244 [1.68]	275 [1.90]	216 [1.49]	63
Mosier 3	3344 [23.1]	426 [2.94]	353 [2.43]	16.1 [0.11]	58

Test day compressive strengths were determined using the standard test method ASTM C39-12a. Cylinders for split tensile strengths were also crushed on the test date according to ASTM C496-11.

Lower grade, larger diameter steel was typically used in mid-century bridge construction. For the Mosier specimens, smaller Gr. 60 (Gr.420) reinforcing steel was used to follow development length of the intermediate grade steel used in the Mosier Bridge. To best match the actual strength curves of the Mosier bridge, the longitudinal steel was selected based on mill certifications from the reinforcing steel supplier. The longitudinal reinforcement consisted of Gr. 60 (Gr. 420) steel reinforcing bars that conformed to ASTM A706-09. The transverse reinforcement consisted of Gr. 40 (Gr. 280) stirrups and conformed to ASTM A615-09. Table I.2 lists the reinforcing steel material properties for the Mosier specimens.

Table I.2 - Reinforcing steel bar properties for Mosier specimens

Material	**Bar Diameter (in.) [mm]**	**Bar Area ($in.^2$) [mm^2]**	**Grade (ksi) [MPa]**	**Actual f_y (ksi) [MPa]**	**Actual f_u (ksi) [MPa]**
Transverse #4 [13M]	0.500 [12.7]	0.20 [12.7]	40 [280]	50.2 [346]	79.6 [549]
Longitudinal #6 [19M]	0.750 [19.1]	0.44 [248]	60 [420]	63.0 [434]	106.3 [733]
Longitudinal #7 [22M]	0.875 [22.2]	0.60 [387]	60 [420]	65.3 [450]	104.6 [721]
Longitudinal #8 [25M]	1.000 [25.4]	0.79 [509]	60 [420]	63.6 [438]	112.1 [773]
Longitudinal #9 [29M]	1.128 [28.7]	1.00 [645]	60 [420]	62.6 [432]	102.0 [703]

Procedures from ASTM E8-13a were used to find yield, ultimate, and elongation values for all samples. To measure strain in the coupon, an extensometer with a 2 in. (50.8 mm) gage length was used. The universal testing machine held an initial loading rate of 0.001 in/sec (0.025 mm/sec) until yield, and then increased subsequently afterward.

The titanium NSM reinforcing material has several unique properties. Seen in Fig. I.14, titanium was chosen because of its high strength, ductility, environmental durability and ability to bend around a tight radius.

Fig. I.14 - Deformation patterns on titanium

The titanium alloy used for the strengthening for the Mosier specimen was used in strengthening the T-specimens in Chapter 3. The titanium alloy has 6% aluminum and 4% vanadium (Ti-6Al-4V), and meets ASTM B348 specifications. An in-depth description of the titanium alloy used for the NSM strengthening is in Chapter 3. Titanium is an elasto-plastic material without a well-defined yield plateau. Material properties of titanium are contained in Table I.3. A custom deformation pattern was created for the titanium to increase bond with the epoxy interface.

Table I.3 - NSM titanium material properties

Material	**Bar Diameter (in.) [mm]**	**Bar Area ($in.^2$) [mm^2]**	**Grade (ksi) [MPa]**	**Actual f_y (ksi) [MPa]**	**Actual f_u (ksi) [MPa]**	**Elongation e_u (%)**
Titanium	0.625 [15.9]	0.2975 [7.6]	N/A	145.4 [1002]	158.1 [1090]	11.2

I.2.4 Instrumentation

To collect data necessary for analysis, internal and external sensors were applied prior to testing. Data from all sensors was sampled at 5 Hz or 0.20 sec intervals.

I.2.4.1 Internal Sensor Array

Bondable foil strain gages were used for the internal sensor array. Because of the sensitivity of the strain gages, the output of the collected data was in units of microstrain, an amplified in/in (mm/mm) value.

The internal steel reinforcing bars were instrumented with strain gages prior to tying the reinforcing bar cage. Strain gages were at several locations along the length of the Mosier specimens. All specimens had identical strain gage locations to enable an accurate comparison between the control and strengthened specimens. A total of six strain gages were applied to the flexural tension steel. Four strain gages were applied to different reinforcing steel bars in the deck. One strain gage was applied to the #6 (19M) reinforcing steel bar at midspan.

Five strain gages were applied to one leg of the transverse reinforcing steel at mid height to measure the shear force at midspan. Strain gages were applied to the NSM titanium at

coincident locations as the internal reinforcing steel and the end of the NSM titanium bars. Locations of the strain gages on the internal reinforcing steel and NSM titanium are shown in Fig. I.14 through Fig. I.17.

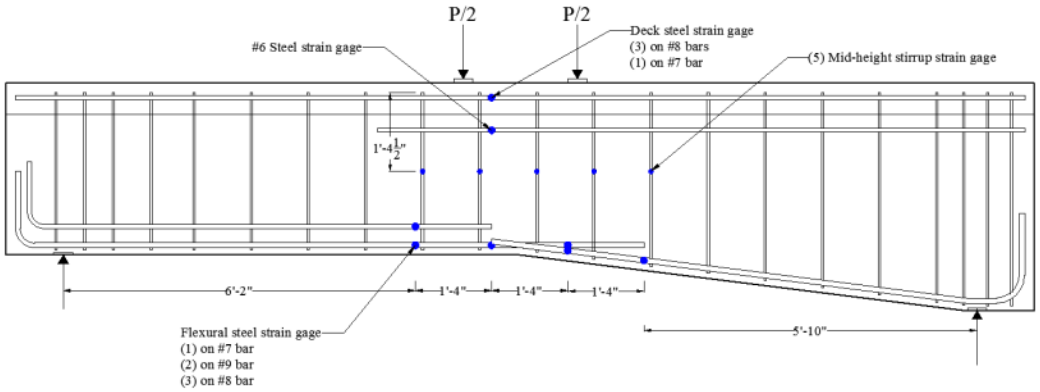

Fig. I.15 - Internal sensor array of Mosier 1

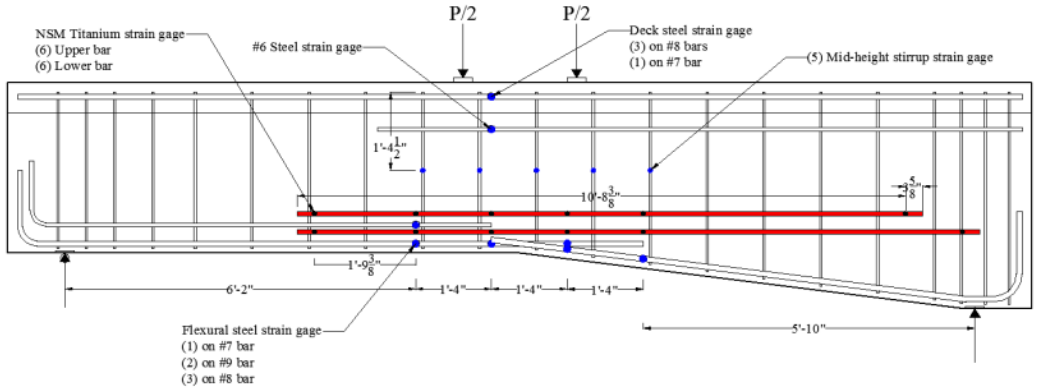

Fig. I.16 - Internal sensor array of Mosier 2

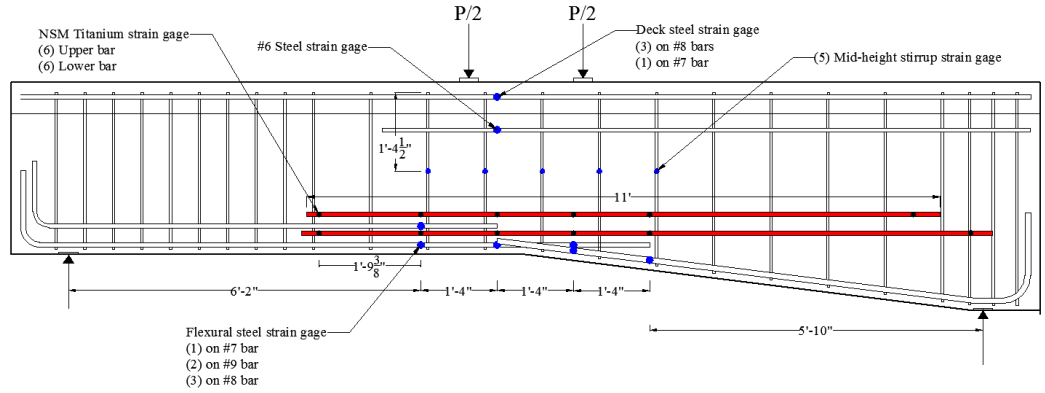

Fig. I.17 - Internal sensor array of Mosier 3

I.2.4.2 External Sensor Array

Three types of sensors were used to monitor the external response of the beam: string potentiometers, displacement sensors, and tilt sensors. All displacement sensors had units of inches and the tilt sensors measured in units of degrees.

The midspan displacement was monitored with two 10 in. (254 mm) stroke string potentiometers. Measuring displacement on each side of the web enabled the calculation of average midspan displacement. Each string potentiometer was attached to a steel dowel that was epoxied into the web.

Support settlements were measured with two 1.5 in. (38.1 mm) displacement sensors. The sensor was clamped to a metal stand and reacted off of an aluminum angle glued to the web of the beam. Measured North and South settlements were averaged and subtracted from the measured midspan displacement for the true midspan displacement.

The Mosier 1 specimen had a block-out around the end of the #8 (25M) bars. A 1 in. (25.4 mm) long stroke displacement sensor measured the slip of the #8 (25M) bar end relative to the concrete. Bar end slip was not measured for Mosier 2 or Mosier 3.

Tilt sensors were attached to one side of the web over each support. The sensors measured the rotation of each side of the specimen while loading.

Pairs of diagonal displacement sensors were used to measure crack width over regions of the beam. Each displacement sensor had a calibrated range of 1 in. (25.4 mm). The sensors were attached to small threaded rods epoxied in the web. The configuration of a typical diagonal displacement setup for the Mosier specimens is shown in Fig. I.18.

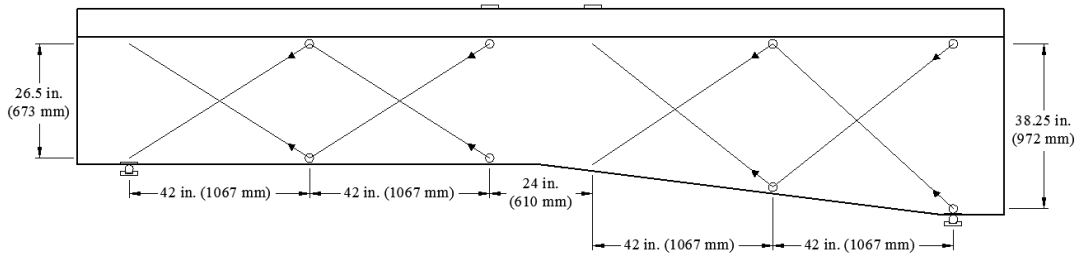

Fig. I.18 - Typical specimen diagonal displacement sensor layout (Barker, 2014)

I.2.5 Test Protocols

All Mosier T-specimens were tested at the Oregon State University Structural Engineering Research Laboratory. The simply supported Mosier specimens had a span length of 18 ft (5.48 m) from centerline of supports. Due to the abnormal geometry, a load cell was used under the South support as a spacer to level the flange. To simulate the dead load stresses in the Mosier Bridge, the specimen first required negative bending to be induced. A 100

kip (445 kN) hydraulic jack was placed under the soffit of the stem at midspan. An upward force of 34.5 kips (153 kN) was applied. To counteract this force, two steel tubes were placed on top of the deck and were tied into the strong floor with threaded rods shown in Fig. I.18. Mosier 1 held the dead load forces for three days then was unloaded. Mosier 2 and Mosier 3 induced and held the force for at least seven days while the NSM titanium epoxy was curing. The hydraulic jack was unloaded and removed before applying the positive bending loads.

To induce positive four-point bending, a reaction frame was anchored into the strong floor and held the servo-hydraulic load-controlled actuator. The actuator had a 500 kip (2224 kN) capacity and a 30 in. (762 mm) stroke. The actuator force was distributed through a spreader beam creating a 2 ft (610 mm) constant moment region at midspan shown in Fig. I.18. All reaction points distributed the load from a 4 in. (101.6 mm) plate on a 2 in. (50.8 mm) diameter captive roller. Loading plates at midspan were leveled with a high strength grout. Prior to testing, the actuator was plumbed, and loading plates were shimmed if necessary.

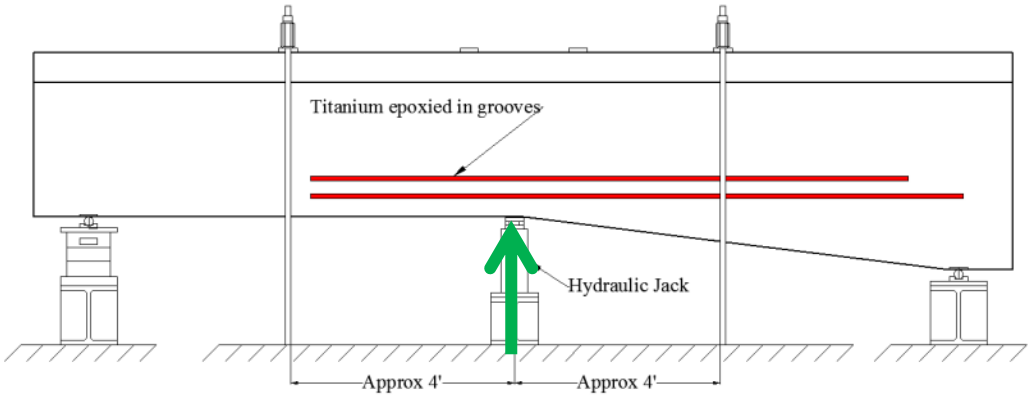

Fig. I.18 - Configuration for inducing dead load stresses and NSM installation

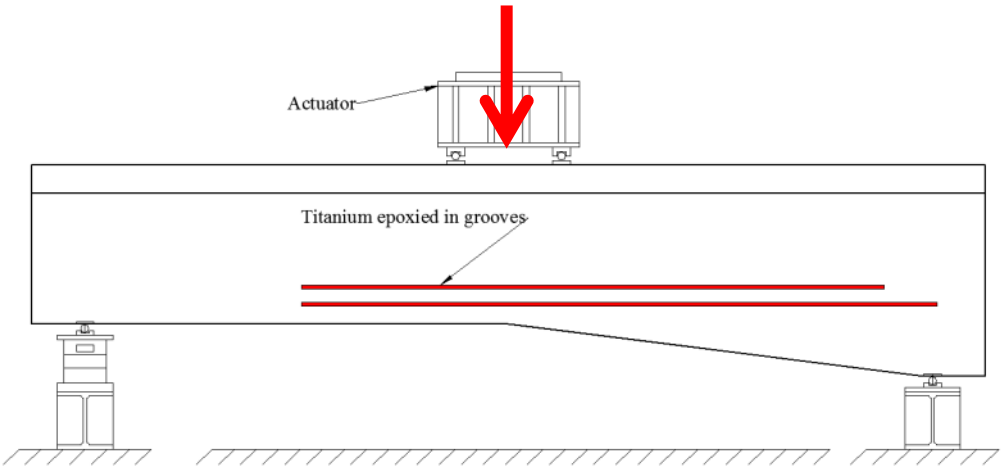

Fig. I.19 - Configuration for applying actuator loads

The positive bending load was applied at 10 kips (44 kN) increasing increments and unloaded to 5 kips (22.2 kN) between each cycle until failure in Mosier 1. The titanium strengthened specimens increased the applied load by increments of 25 kips (111 kN). The loading rate was pseudostatic at 0.15 kip/sec (0.67 kN/sec) without load reversals. After reaching each target load step, the load was reduced by at least 5 kips (22 kN) then held to minimize creep while cracks were identified. If the specimen was close to failure the load cycle was extended until the maximum capacity was reached.

I.3 Experimental Results

This section describes the experimental results of the three Mosier specimens tested in this research program. The tested specimens were identified as Mosier 1, Mosier 2, and Mosier 3. The reported responses include the load deformation, anchorage slip, material strains, and strain along the section.

I.3.1 Overall Specimen Response

The NSM titanium strengthened Mosier specimens were tested to failure and achieved greater loads than the baseline specimen, Mosier 1. The NSM strengthened specimens experienced ductile flexural failures and displayed distributed cracking and signs of distress prior to failure. The applied load, shear, V_{APP}, dead load shear, $V_{DL,}$ total shear, $V_{EXP,}$ midspan displacement, and observed failure crack angle are reported in Table I.4. The reported midspan displacement corresponds to the peak load. The total shear is the applied shear from the actuator plus the dead load shear. Dead load shear was calculated from the weight of concrete acting across the failure plane.

Table I.4- Summary of specimen capacity and midspan displacement

Specimen	Applied Load kips [MN]	Applied Shear (V_{APP}) kips [kN]	DL Shear (V_{DL}) kips [kN]	Total Shear (V_{EXP}) kips [kN]	Midspan Disp. in. [cm]	Failure Crack Angle deg.
Mosier 1	63.7 [0.283]	31.9 [141.6]	0.27 [1.2]	31.1 [142.8]	0.258 [6.55]	68
Mosier 2	138.4 [0.615]	69.2 [307.8]	0 [0]	69.2 [307.8]	1.02 [25.9]	90
Mosier 3	131.5 [0.585]	65.8 [292.5]	0 [0]	65.8 [292.5]	1.01 [25.7]	90

I.3.1.1 Load Deformation Response

The load and displacement response describes the overall behavior of the specimens. Load deformation responses for the NSM-retrofitted and baseline Mosier specimens are shown in Fig. I.20. Mosier 1 was loaded in 10 kip (44.5 kN) increments, then unloaded, and then proceeded to the next load step until eventual failure. Mosier 2 and Mosier 3, the NSM titanium specimens, had a larger predicted capacity and was loaded in 25 kip (111 kN) increments, unloaded to 5 kips (22.2 kN), and then proceeded to the next load step until failure.

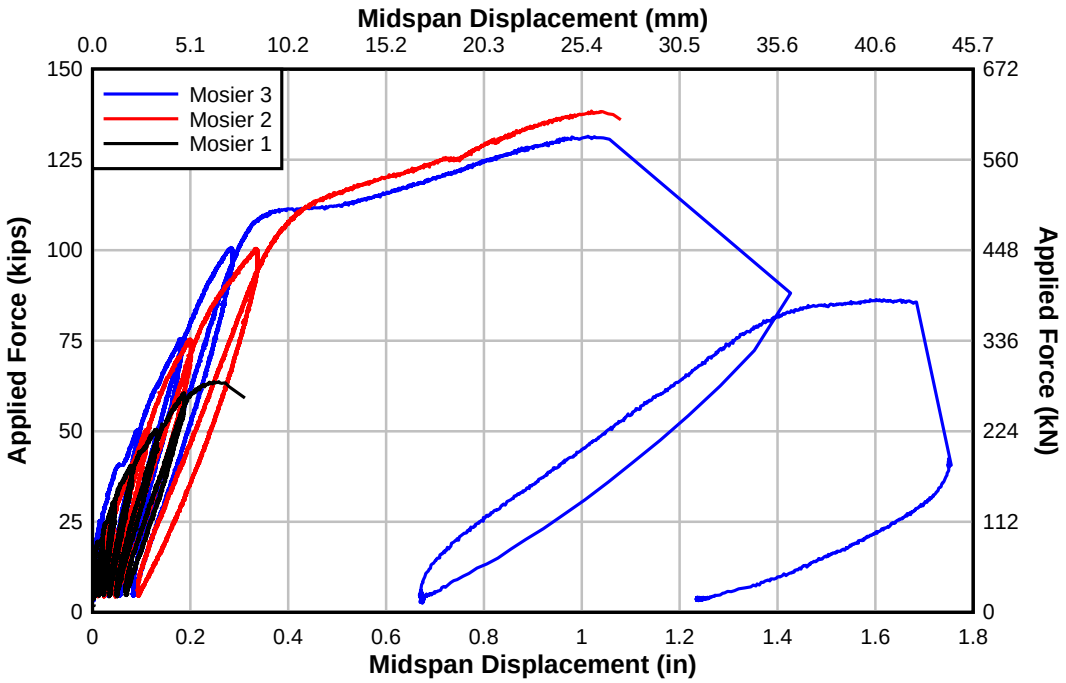

Fig. I.20 - Mosier specimens applied load and measured displacement response

Mosier 2 and Mosier 3 specimens increased the baseline specimen load capacity by 74.7 kip (332 kN) and 67.8 kip (302 kN) respectively. The ductility of the strengthened specimens increased by 0.762 in. (19.3 mm) and 0.752 in. (19.1 mm) compared to the

baseline for Mosier 2 and Mosier 3 respectively. Mosier 2 had a slightly lower stiffness than Mosier 3 because initial cracking of the concrete and slip of the cutoff reinforcing steel bars occurred prior to testing. The load was being carried by the NSM titanium that had a much lower modulus of elasticity. Mosier 3 maintained a composite section which lead to a stiffer response until the specimen became inelastic. Once inelastic, at approximately 109 kips (484 kN), Mosier 3 experienced a significant slip of the internal reinforcing which damaged the bond of the NSM titanium alloy bars. The damaged bond of the NSM titanium bars contributed to the slight decrease in ultimate capacity compared to Mosier 2.

Mosier 3 exhibited a significant amount of reserve capacity after failure. This reserve capacity is seen as the last load cycle upon which Mosier 3 achieved a load of 88 kips (391 kN). The reserve capacity indicates that the NSM titanium strengthening performs well at post ultimate conditions.

I.3.1.2 Crack Propagation

Concrete crack initiation and propagation was monitored throughout the test. After each load cycle, the load was decreased and then held to minimize creep effects. During this time, the specimens were inspected and cracks were measured and highlighted. Digital pictures were taken at each load step to record the cracked condition. The crack patterns at failure are shown in for each specimen in Fig. I.21. Digital photographs at failure are shown in Fig. I.22 through Fig. I.25.

Mosier 1

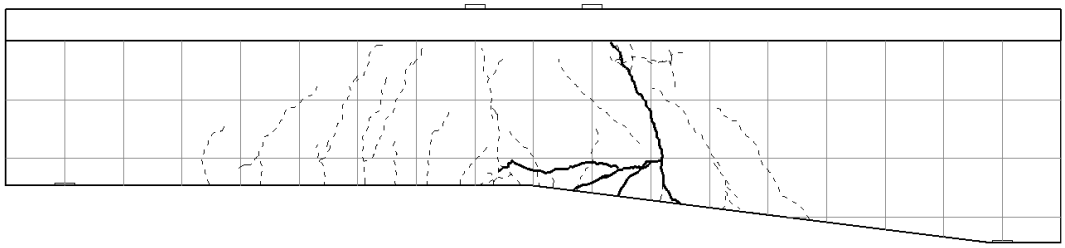

Mosier 2

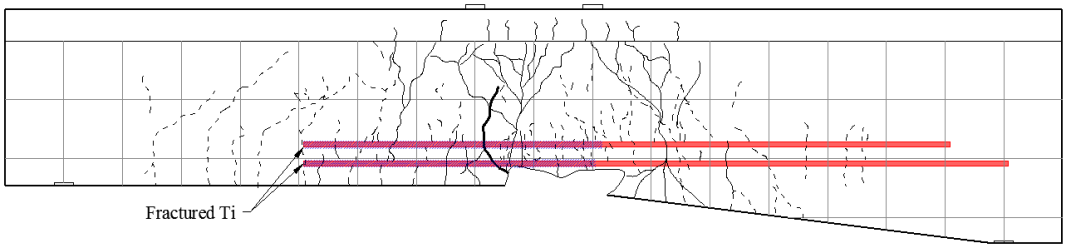

Mosier 3

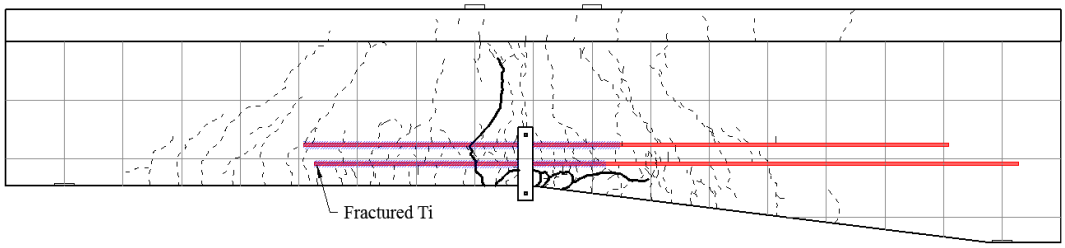

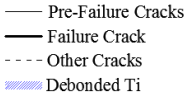

Fig. I.217 - Crack propagation of Mosier specimens

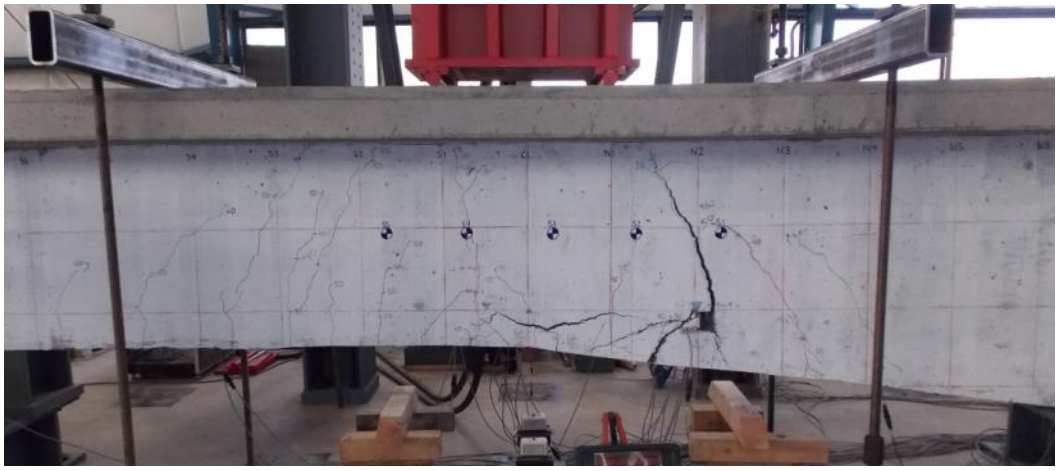

Fig. I.22 - Mosier 1 failure photograph

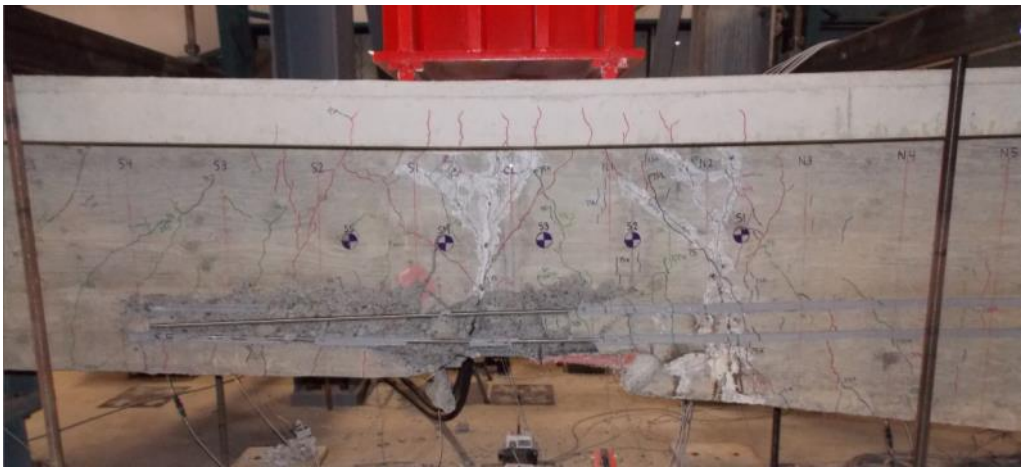

Fig. I.23 - Mosier 2 failure photograph

Fig. I.24 - Mosier 3 primary failure photograph

Fig. I.25 - Mosier 3 reserve capacity failure photograph

The Mosier 1 specimen failed in flexure and exhibited similar cracking patterns to the cracks observed in the Mosier Bridge. Mosier 2 and Mosier 3 specimens failed in flexure after debonding of the NSM titanium bars. The debonding, or delamination, of the NSM titanium bars initiated at midspan and propagated to the embedded NSM hook ends. After delamination of the NSM titanium bars, three out of the four titanium hooks fractured on the South end of Mosier 2. During failure of Mosier 3, all NSM titanium hooks remained intact at initial failure. After reloading and achieving the reserve capacity, one hook fractured and one hook was dislodged on the south end of Mosier 3. Chevron cracks, typical of anchorage failures, appeared near failure in all specimens. The chevron cracks were constrained by the NSM titanium. The NSM titanium strengthened specimens experienced distributed cracking over the constant moment region to the end of the NSM titanium bars in the south end of the specimen. Longitudinal cracks along the epoxy-concrete interface coincided with the abrupt debonding failure of specimens Mosier 2 and Mosier 3. The widespread extent of macro cracking in the concrete and around the epoxy provided visual indication of distress prior to failure.

I.3.1.3 Anchorage Slip Response

As the applied load increased, the internal reinforcing steel bars slipped regardless of the failure mode or location. Cutoff reinforcing bar slip sensors installed near the block-out on the #8 (25M) bars measured the reinforcing bar slip with respect to load in Fig. I.25.

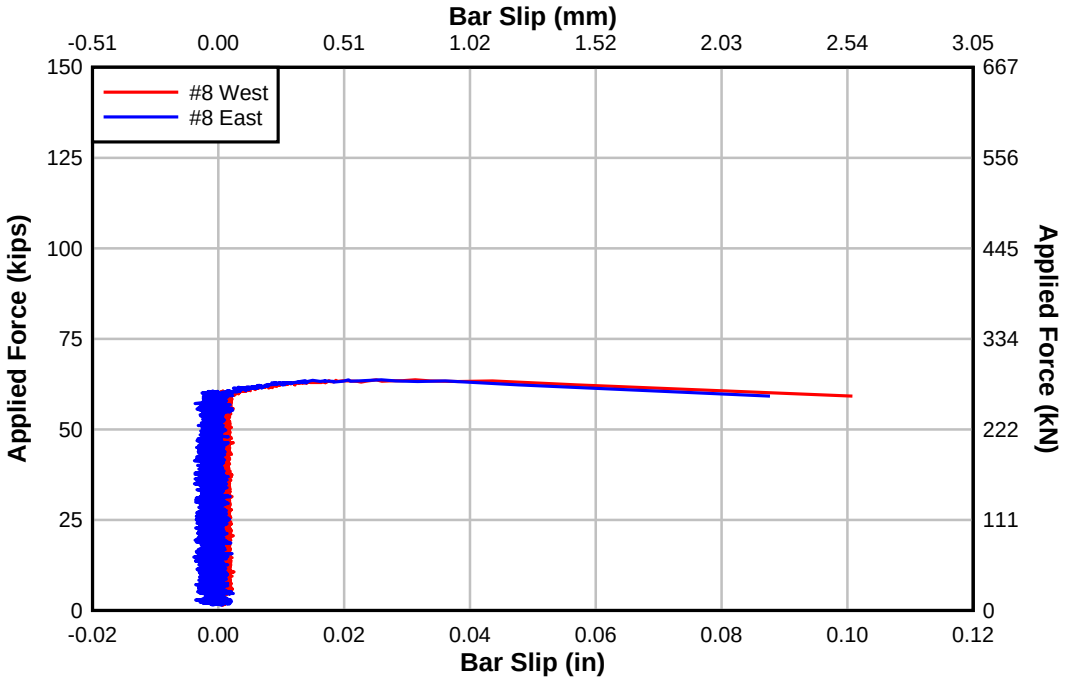

Fig. I.25 – Slip response of #8 Steel reinforcing bars in Mosier 1

The East and West #8 (25M) steel reinforcing bars had similar rates of slip throughout the test. Significant slips did not occur in the #8 (25M) steel reinforcing bar until near failure loads. Near the failure load, chevron cracking developed around the #8 (25M) bar.

Slip of the #8 (25M) steel reinforcing bar was not recorded in the Mosier 2 and Mosier 3 specimens. However, apparent slip of the #9 (29M) steel reinforcing bars is shown Fig. I.26 for Mosier 2 and Fig. I.27 for Mosier 3.

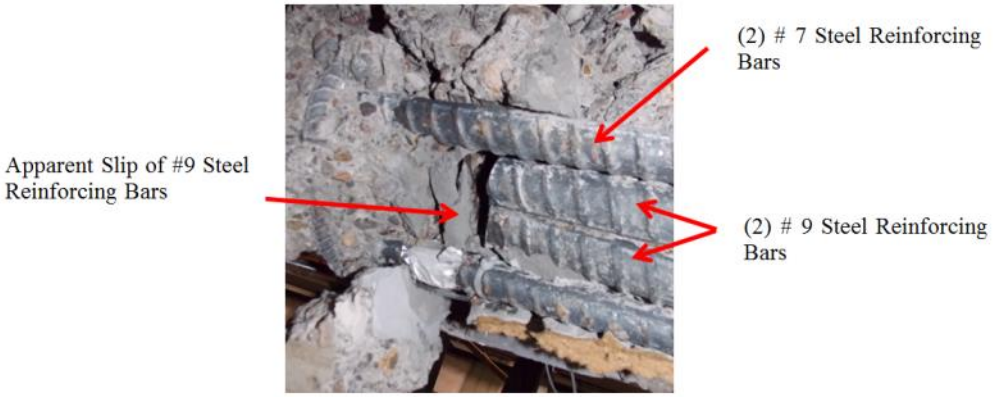

Fig. I.26 - Apparent slip of # 9 Steel Reinforcing Bars in Mosier 2

Fig. I.27 - Apparent slip of #9 Steel Reinforcing Bars in Mosier 3

The digital images also illustrate the lack of concrete cover and reinforcing steel congestion surrounding the #8 (25M) and #9 (29M) steel reinforcing bars.

I.3.1.4 Material Strains

Top, bottom, and NSM bar strains were plotted at each instrumented cross section. This comparison illustrates the interaction between the NSM bar and developing cutoff bar. The section labels start from the southernmost strain gage location on the NSM titanium bar. Therefore, section 1 on Mosier 1 does not exist. Strains for materials at cross sections

along the length of the specimen are found for Mosier 1 in Fig. I.29 through Fig. I.32. A guide for the sections can be found in the drawing Fig. I.28.

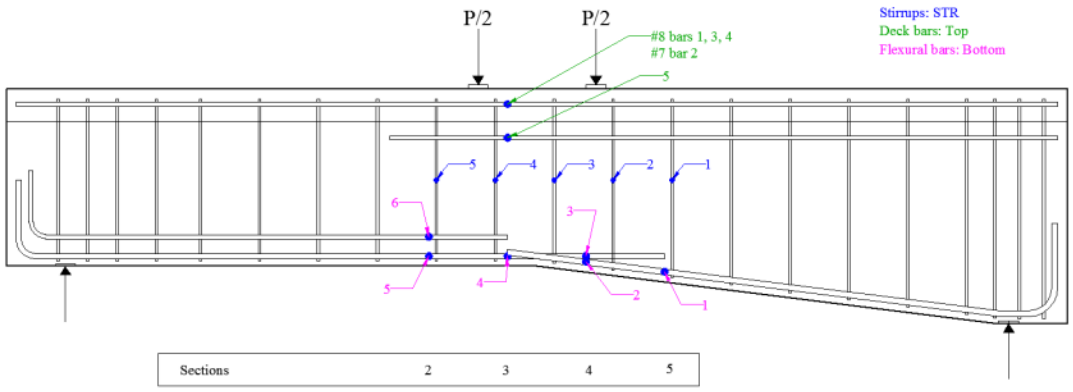

Fig. I.28 - Strain gage configuration for Mosier 1

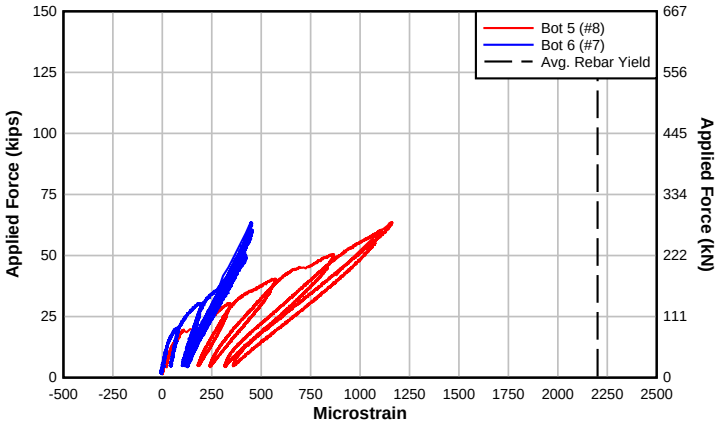

Fig. I.29 - Mosier 1 Section 2

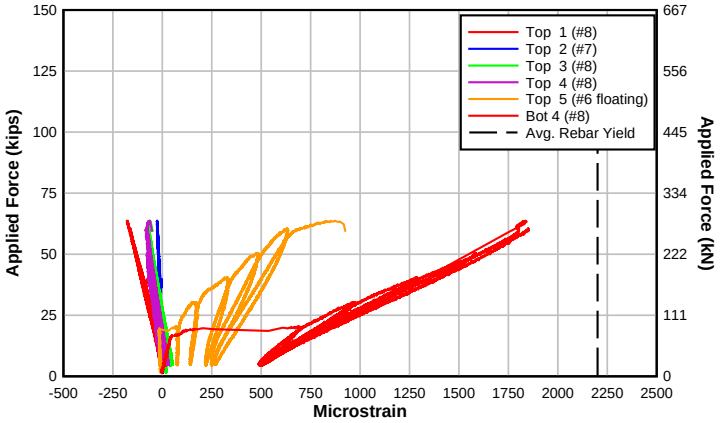

Fig. I.30 - Mosier 1 Section 3

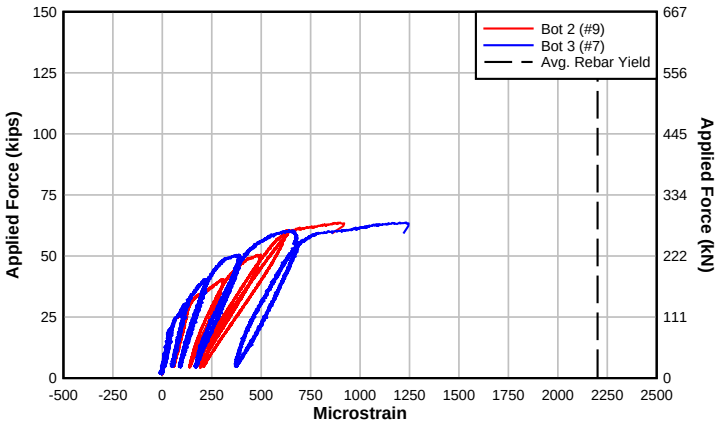

Fig. I.31 - Mosier 1 Section 4

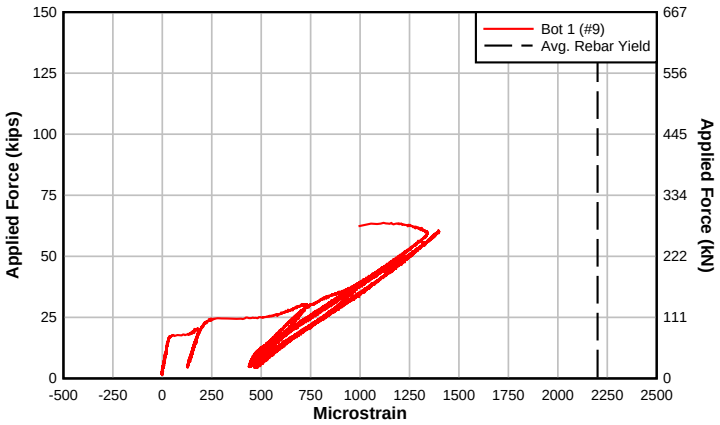

Fig. I.32 - Mosier 1 Section 5

Sectional strains for Mosier 2 are shown in Fig. I.34 through Fig. I.39. A guide for the sections can be found in the drawing Fig. I.33.

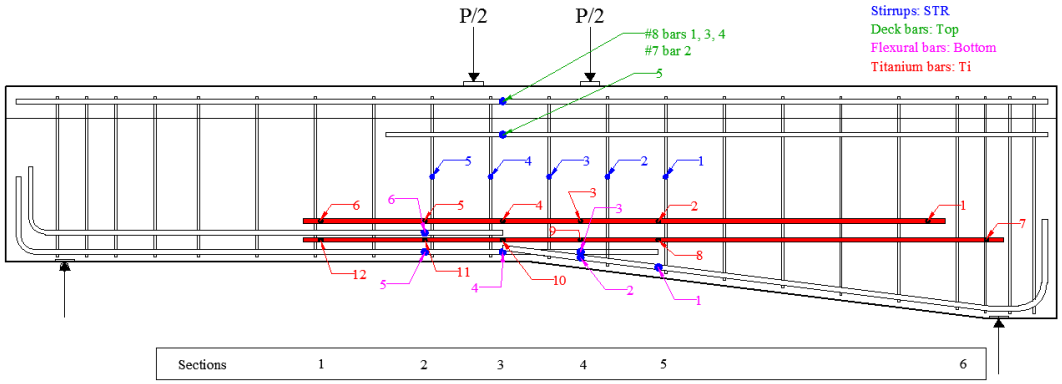

Fig. I.33 - Strain gage configuration for Mosier 2 and Mosier 3

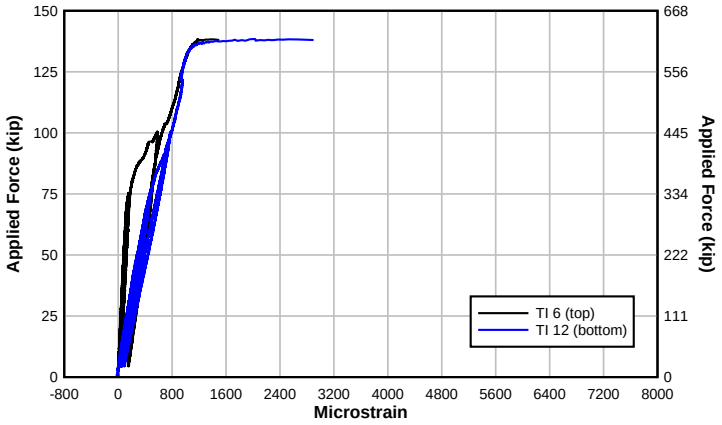

Fig. I.34 - Mosier 2 Section 1

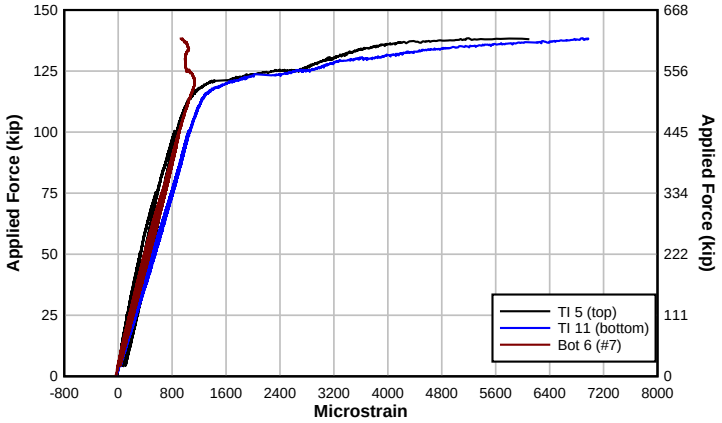

Fig. I.35 - Mosier 2 Section 2

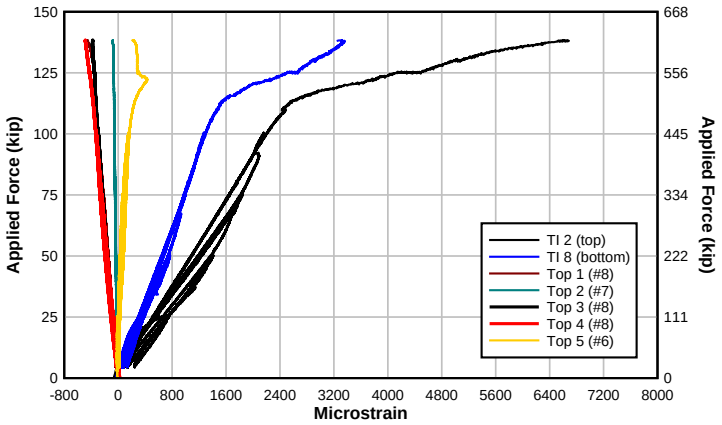

Fig. I.36 - Mosier 2 Section 3

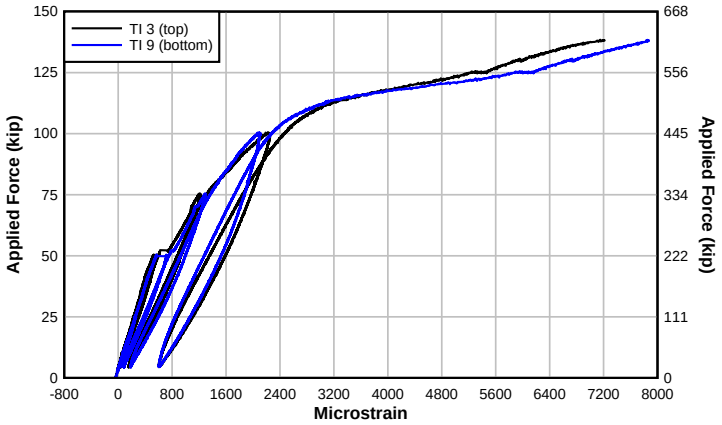

Fig. I.37 - Mosier 2 Section 4

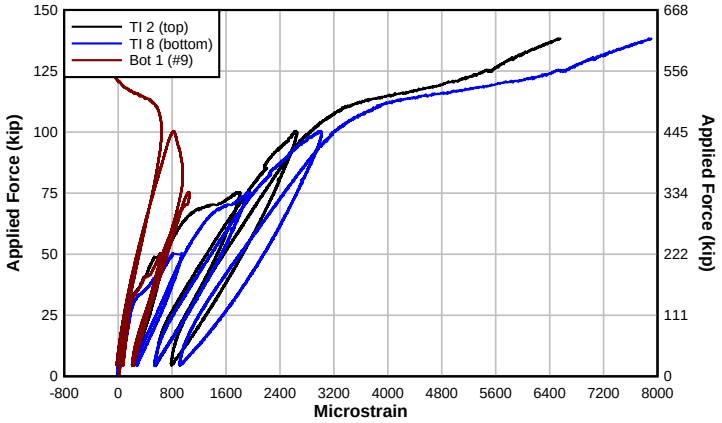

Fig. I.38 - Mosier 2 Section 5

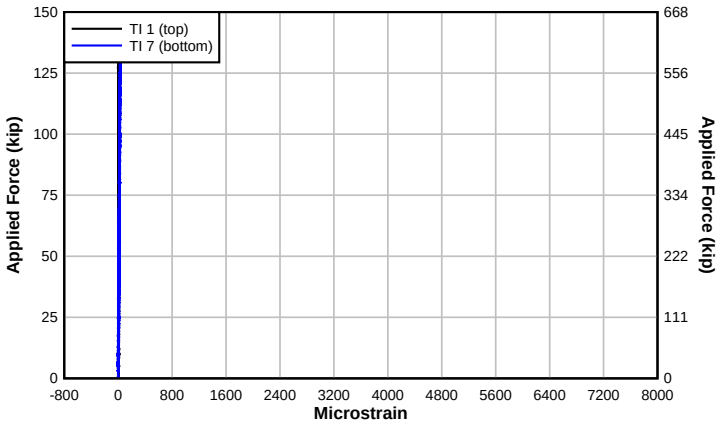

Fig. I.39 - Mosier 2 Section 6

Strains at each section are shown for Mosier 3 in Fig. I.40 through Fig. I.45.

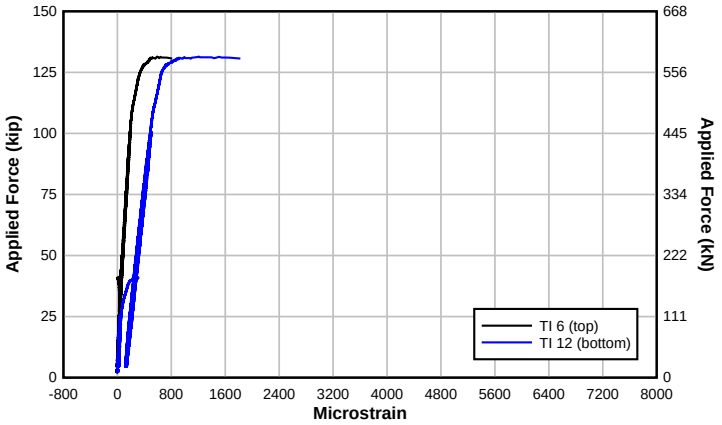

Fig. I.40 - Mosier 3 Section 1

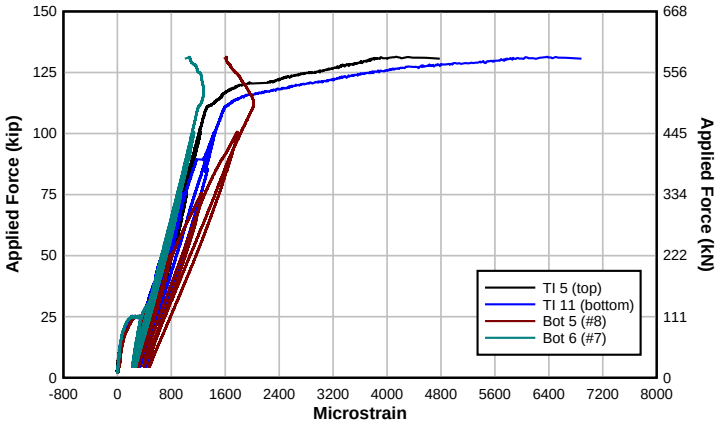

Fig. I.41 - Mosier 3 Section 2

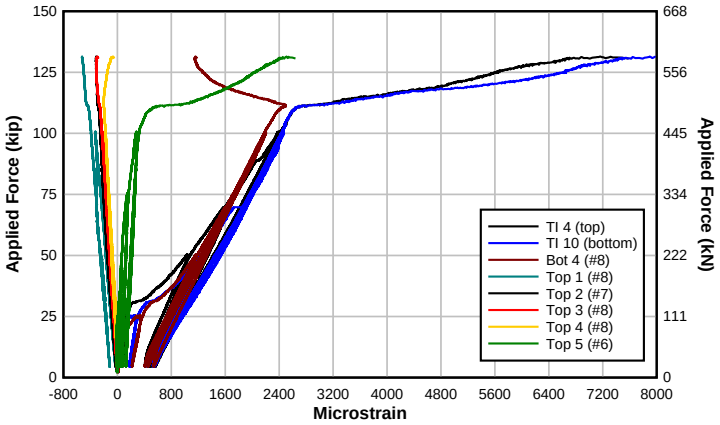

Fig. I.42 - Mosier 3 Section 3

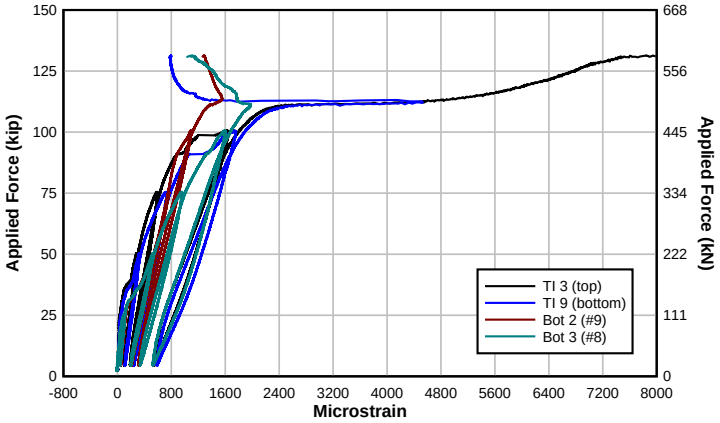

Fig. I.43 - Mosier 3 Section 4

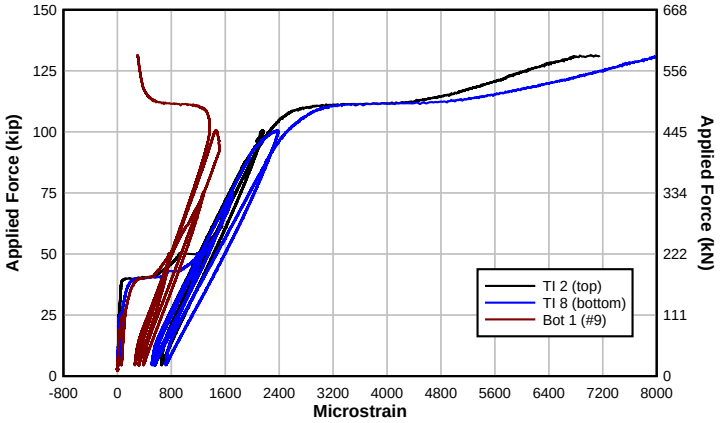

Fig. I.44 - Mosier 3 Section 5

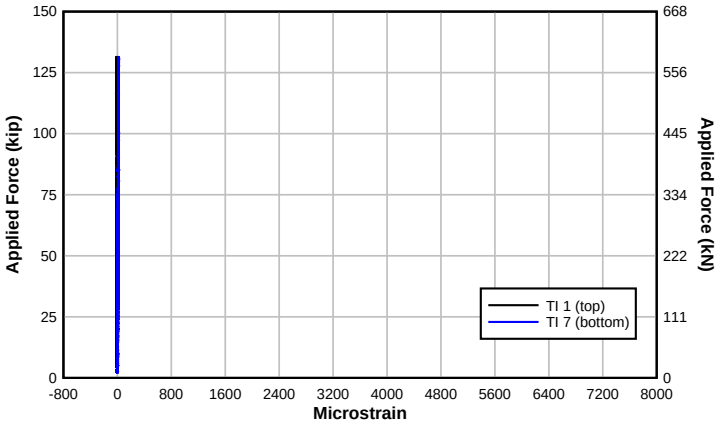

Fig. I.45 - Mosier 3 Section 6

Strains in the NSM titanium are negligible at the North end hook locations. The south end of the NSM titanium hooks had very linear strain until failure. Strain reversal in the #9 (29M) steel reinforcing bars indicates bar slip in the NSM titanium specimens. The strain reversal in the #7 (25M) is due to bar slip and neighboring bar slip of the #9 (29M) steel reinforcing bar.

Mid height stirrup strains are shown in Fig. I.46 through Fig. I.48 for the Mosier specimens. The NSM titanium strengthened specimens exhibit much larger strains that Mosier 1 due to the increased flexural strength provided by the NSM titanium bars. Yield strain for the stirrups was around 1731 microstrain, which means that none of the stirrups reached yield.

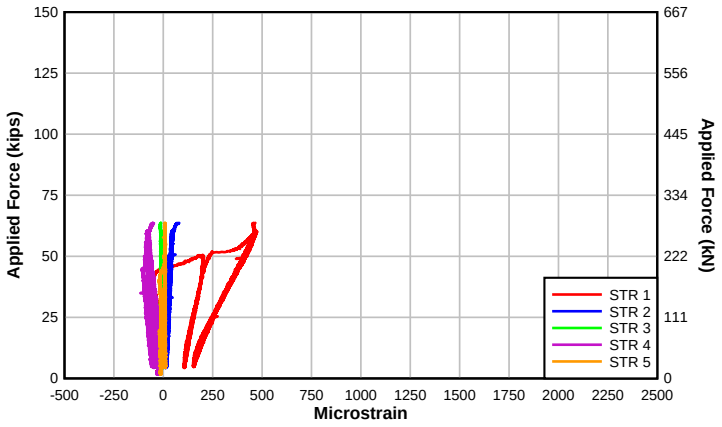

Fig. I.46 - Mosier 1 Stirrup strains

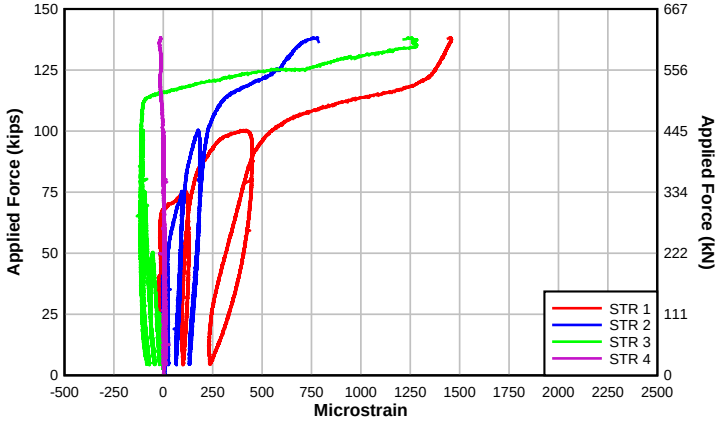

Fig. I.47 - Mosier 2 Stirrup strains

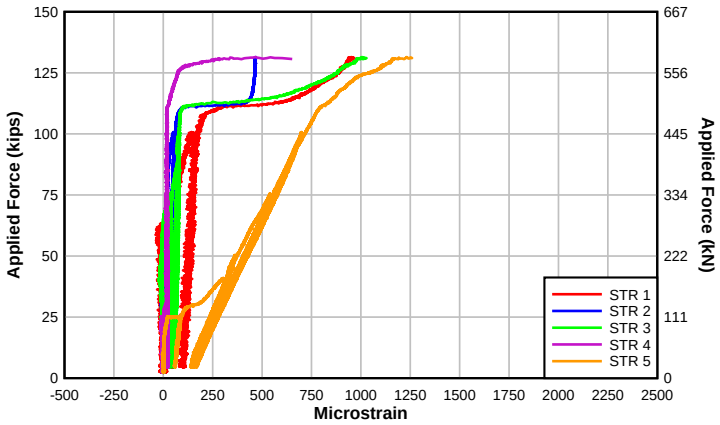

Fig. I.48 - Mosier 3 Stirrup strains

I.4 Design and Analytical Predictions

The design intent of the Mosier specimens was to strengthen the baseline specimen, Mosier 1, to an acceptable level above the design strength, M_u. The maximum nominal moment was found using AASHTO-LRFD and Response 2000 as shown in Fig. I.49.

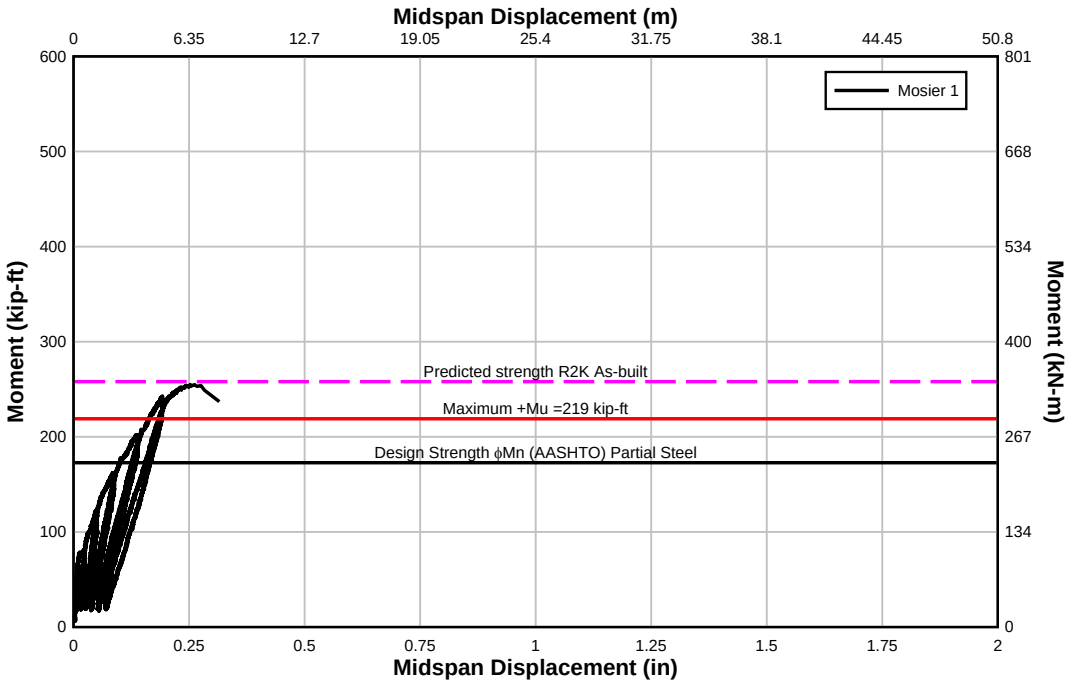

Fig. I.49 - Mosier 1 predicted and experimental capacities

The Mosier bridge design truck induces a moment demand of 219 kip-ft (297 kN-m) at the midspan of the Mosier 1 specimen. The calculated moment demand is 46 kip-ft (63 kN-m) over the AASHTO nominal moment capacity. This confirms the need for the NSM strengthening. Furthermore, R2K closely predicted the flexural capacity of Mosier 1 within 3 kip-ft (4 kN-m) using partial contribution of the reinforcing steel at midspan. The NSM titanium strengthened specimens are shown with their relative predictions in Fig. I.50. The solid lines are the AASHTO predictions with and without the partial contribution of reinforcing steel at midspan. The dashed lines represent the R2K flexural capacities with and without partial contribution of reinforcing steel at midspan.

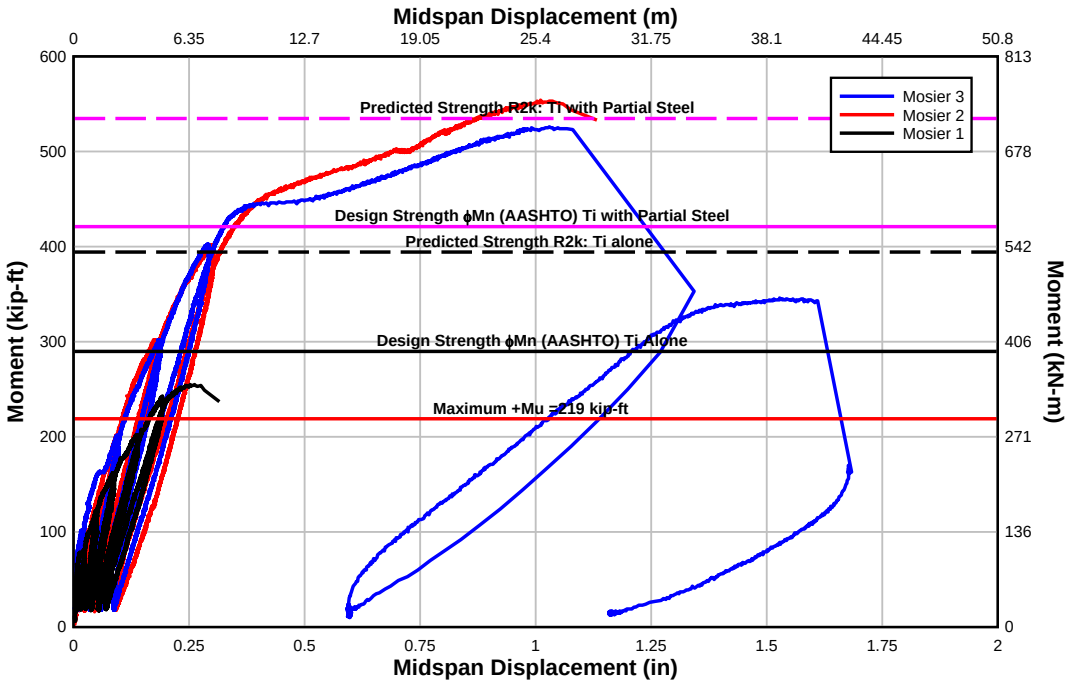

Fig. I.50 - Mosier specimens predicted and experimental capacities

The most conservative prediction, the AASHTO nominal moment capacity with NSM titanium, still exceeded the moment demand. This plot confirms that inclusion of the partially embedded or developed reinforcing steel at midspan will increase the accuracy of the results. Furthermore, R2K provides fairly accurate predictions of a NSM strengthened specimen with anchorage failures at midspan.

I.5 Discussion of Results

Experimental testing of T-specimens designed based off of the Mosier Bridge was performed. The control specimen exhibited very similar cracking as observed in the Mosier Bridge, confirming the validity of the model. The control specimen, Mosier 1, did not meet AASHTO requirements for moment capacity at midspan. The R2K predicted capacity of Mosier 1 was in very good agreement with the experimental results.

The NSM titanium strengthening of Mosier 2 and Mosier 3 was based of the NSM strengthening design discussed in Chapter 3. Both specimens had four titanium alloy bars epoxied into a groove cut into the concrete cover of the specimen. The bars were terminated with 2 in. (51 mm) diameter, 90° hooks. The lengths of the hooks were determined by the width of the web in Mosier 2 and Mosier 3. Mosier 3 offset the terminations of the south end NSM titanium bars to minimize stress concentrations. Mosier 3 also confined the NSM titanium material at midspan with a steel plate attached through the web.

The NSM titanium strengthened specimen, Mosier 2, pre-failed the anchorage of the reinforcing steel bars at midspan and achieved a slightly higher capacity than the Mosier 3 specimen. Since the ends of the reinforcing steel were not confined at midspan, dilatation of concrete and disturbance of the NSM epoxy concrete bond did not occur in Mosier 2. Mosier 3 followed a similar midspan moment and displacement curve as Mosier 2, validating the NSM retrofitting method. Chevron cracks were observed over the cutoff reinforcing steel bars prior to failure. The titanium alloy bars helped delay the cutoff bar slip and increased the ductility and capacity of the specimen.

All specimens had fairly accurate predictions from the R2K sectional analysis. The addition of the partially embedded reinforcing bars at midspan increased the accuracy of the predictions.

The Oregon Department of Transportation witnessed testing performed at Oregon State University and designed the NSM titanium strengthening based on ACI 440 specifications.

Construction on the Mosier Bridge began in April 2014 and was completed in May 2014. The NSM titanium retrofit was installed at critical locations in need of flexural or anchorage strengthening. Negative moment capacities were increased by installing NSM titanium in the deck. Other deficient members were strengthened with an external post tensioning system and all cracks greater than 0.015 in. (0.381 mm) were sealed. After construction was completed, the bridge was reopened and all load postings were removed.